

UCSF

UC San Francisco Electronic Theses and Dissertations

Title

Cellular heterogeneity and lineage dynamics of the developing, adult, and diseased murine pancreas

Permalink

<https://escholarship.org/uc/item/9dd66818>

Author

Byrnes, Lauren

Publication Date

2018

Peer reviewed|Thesis/dissertation

Cellular heterogeneity and lineage dynamics of the
developing, adult, and diseased murine pancreas

by

Lauren Byrnes

DISSERTATION

Submitted in partial satisfaction of the requirements for the degree of

DOCTOR OF PHILOSOPHY

in

Developmental and Stem Cell Biology

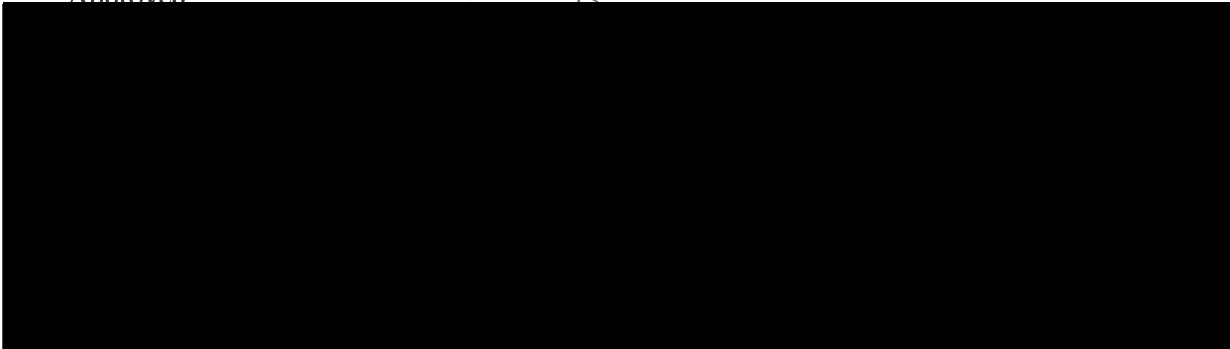
in the

GRADUATE DIVISION

of the

UNIVERSITY OF CALIFORNIA, SAN FRANCISCO

Approved:



Committee in Charge

To my family

Acknowledgements

This work would not have been possible without the support of many individuals. I would first like to thank my mentor, Julie Sneddon, for her guidance and support throughout my PhD. Julie's steadfast confidence in my capabilities were instrumental to my growth as a scientist, and I am very grateful for her insights and advocacy. I'd also like to thank all the members of the Sneddon lab – past and present – that offered their help and encouragement at every stage and made the lab environment an enjoyable place to share ideas and discuss science. In particular, I feel very lucky to have embarked on a collaborative project with another graduate student in the lab, Daniel Wong. Daniel is an excellent scientist and wonderful person, and I learned a great deal from him during my time in the lab. I'm also grateful to have worked with Sophie Patzek, a very talented clinical fellow in the lab. Thank you both, Daniel and Sophie, for the fruitful and enjoyable collaborations.

My trek into bioinformatics was facilitated by excellent mentorship from Jimmie Ye and Meena Subramaniam. I thank them for their insightful feedback and for the numerous discussions that were critical to the success of my work. I would also like to thank my thesis committee, Susan Fisher, Matthias Hebrok, and Tien Peng, for their helpful comments and support throughout my PhD. To my

fellow DSCB graduate students, thank you for being such an amazing community of intelligent, driven, and supportive individuals.

Outside the lab, I am very lucky to have an amazing group of friends and family. Dianna, Steve, Greg, Mary, and Emily – thank you for all the pizza nights, wine nights, SF Bootie nights, ice cream runs, 90s parties, hikes, and pick-me-up beers that kept me grounded during all the ups and downs of a PhD. To my long-distance friends, Ana and Jacquie, we never managed to visit each other or even set up a Skype date during my PhD, but the constant voice messages and texts were the most enjoyable part of my commute to lab. To my partner, Steven, thank you for your patience, support, and love. You are the best listener I've ever met, and I'm deeply grateful for all our scientific and non-scientific conversations that have and continue to inspire me. Finally, to the people that have been rooting for me since the beginning – Mom, Dad, Michael, Erica, and Ashley. Thank you for your endless support and love.

Cellular heterogeneity and lineage dynamics of the developing, adult, and diseased murine pancreas

Lauren Byrnes

Abstract

Organogenesis requires the complex interactions of multiple cell lineages that coordinate their expansion, differentiation, and maturation over time. In Chapters 2 and 3, we utilize a combination of single-cell RNA-sequencing, immunofluorescence, *in situ* hybridization, and genetic lineage tracing, to profile the cell types within the epithelial and mesenchymal compartments of the murine pancreas across developmental time. We find a previously undescribed endocrine progenitor population, as well as an analogous population in both human fetal tissue and human embryonic stem cells differentiating towards a pancreatic beta cell fate. Further, we identify candidate transcriptional regulators along the differentiation trajectory of this population towards the alpha or beta cell lineages. Within the mesenchyme, we identify previously underappreciated cellular heterogeneity and reconstruct potential lineage relationships among the pancreatic mesothelium and mesenchymal cell types. In Chapter 4, we further characterize the pancreatic mesothelium, identifying novel markers and secreted factors expressed within this population. Knockout of the secreted factor specifically expressed by the mesothelium, *Fgf9*, reveals a hypoplastic pancreas by late gestation. We find a disrupted ratio of epithelial and mesenchymal cells that suggests *Fgf9* regulates the epithelial-mesenchymal interactions critical for pancreatic development. In Chapter 5, we extend our single-cell RNA-sequencing approach to adult pancreatic homeostasis and disease, describing multiple subtypes of mesenchymal and mesothelial populations in both conditions. Comparison of diseased and

healthy pancreata reveal shifts in mesenchymal cell types, highlighting populations and transcriptional targets that may regulate the development of disease. In summary, this work reveals transcriptional and cellular heterogeneity of the developing, adult, and diseased pancreas, and identifies lineage relationships among novel populations within both the epithelial and mesenchymal compartments.

Contributions

The research for this thesis was conducted under the supervision of Dr. Julie Sneddon in the Diabetes Center at the University of California, San Francisco. Chapter 2 and 3 describes work published in a co-first authored manuscript in *Nature Communications* with co-authors Daniel M. Wong, Meena Subramaniam, Nathaniel P. Meyer, Caroline L. Gilchrist, Sarah M. Knox, Aaron D. Tward, Chun J. Ye, and Julie B. Sneddon. Daniel M. Wong performed the *in vivo* immunostaining validation and lineage tracing experiments. Meena Subramaniam assisted with the downsampling analysis of the single-cell RNA-sequencing dataset. Nathaniel P. Meyer performed hESC differentiation to a beta cell fate. Caroline L. Gilchrist performed immunofluorescence for the *Fev-Cre; Rosa26^{mTmG}* lineage tracing. Dr. Sarah M. Knox assisted in obtaining human fetal pancreas. Drs. Aaron D. Tward and Chun J. Ye provided bioinformatic expertise and edited the manuscript. I performed all single-cell capture, library preparation, and bioinformatic analyses, as well as the qRT-PCR experiments on hESC-derived beta cell stages. I assisted in the collection of *Fev-Cre; Rosa26^{mTmG}* cells for single-cell RNA-sequencing by FACS and the quantification of the *Ngn3-Cre; Rosa26^{mTmG}* lineage trace. I wrote the manuscript together with Daniel M. Wong and Dr. Julie B. Sneddon. Chapters 4 and 5 describes unpublished work. Dr. Sophie Patzek performed the quantification of epithelial and mesenchymal cells and assisted in the whole mount imaging of Fgf9 pancreata in Chapter 4. Jackie Bouza assisted in the preparation of PBS- and caerulein-treated animals for single-cell RNA-sequencing and imaged the H&E stained PBS- and caerulein-treated pancreata in Chapter 5. I performed all other experiments in these chapters. All the writing in this thesis is my own.

Table of Contents

Chapter 1: Introduction.....	1
Chapter 2: Identification of a novel endocrine progenitor population.....	20
Chapter 3: Mesenchymal heterogeneity and lineage relationships in the developing pancreas.	54
Chapter 4: Characterization of the pancreatic mesothelium and role of Fgf9 in pancreatic development.....	69
Chapter 5: Mesenchymal heterogeneity in adult homeostasis and fibrotic disease.....	105
Chapter 6: Conclusions and future directions.....	149
Materials and Methods.....	158
References.....	177

List of Figures

Figure 1. Single-cell sequencing identifies broad patterns of cellular heterogeneity in E14.5 murine pancreas	35
Figure 2. Quality control for single-cell RNA-sequencing runs.....	36
Figure 3. Single-cell RNA-sequencing batch information from E14.5 pancreata.....	37
Figure 4. Identification of epithelial cell populations in E14.5 mouse pancreas.....	39
Figure 5. Identification of known and novel epithelial cell populations in E14.5 pancreas.....	40
Figure 6. Fev^{Hi} cells are endocrine progenitors	42
Figure 7. Epithelial populations over developmental time	44
Figure 8. Differentiated, hormone ⁺ endocrine cells transit through a <i>Fev</i> -expressing stage during pancreatic development	46
Figure 9. <i>In vivo</i> <i>Fev</i> lineage tracing of E17.5 mouse pancreata.....	48
Figure 10. <i>In vivo</i> <i>Fev</i> lineage tracing of adult mouse pancreata	49
Figure 11. Identification of candidate regulators of beta and alpha cell fate decisions.....	50
Figure 12. Identification of candidate genes and pathways enriched along beta and alpha cell lineages	52
Figure 13. Expression of candidate regulators within the endocrine lineage prior to alpha or beta cell identity.....	53
Figure 14. Identification of multiple uncharacterized mesenchymal populations.....	63
Figure 15. Transcriptomic signatures and lineage dynamics among mesenchymal populations ..	65
Figure 16. Mesothelial cells are dynamic over developmental time and are predicted to give rise to vascular smooth muscle populations	67
Figure 17. Expression of <i>Wt1</i> during pancreatic development.....	94

Figure 18. Identification of pancreatic mesothelial markers	94
Figure 19. Unsuitable Cre drivers for mesothelial lineage tracing	95
Figure 20. Lineage tracing <i>Wt1</i> ⁺ cells in the embryonic pancreas.....	96
Figure 21. Expression of FGF signaling pathway components in E14.5 pancreata	97
Figure 22. Expression of WNT signaling pathway components in E14.5 pancreata.	98
Figure 23. Expression of BMP signaling pathway components in E14.5 pancreata	99
Figure 24. Loss of <i>Fgf9</i> results in a hypoplastic pancreas.....	100
Figure 25. Major lineages of the pancreas are present in E17.5 <i>Fgf9</i> ^{-/-} pancreata	101
Figure 26. E13.5 <i>Fgf9</i> ^{-/-} pancreata have a shifted ratio of mesenchymal to epithelial cells.....	103
Figure 27. Acute pancreatitis model and potential alterations in cellular and transcriptional heterogeneity.....	138
Figure 28. Caerulein injections result in acute pancreatitis in mice	139
Figure 29. Optimization of adult pancreatic dissociation	140
Figure 30. Dissociation of pancreata from PBS and caerulein injected animals	141
Figure 31. Single-cell RNA-sequencing of adult pancreata from PBS- and caerulein-treated animals	142
Figure 32. Mesenchymal and mesothelial heterogeneity during adult homeostasis.....	144
Figure 33. Mesenchymal and mesothelial heterogeneity during pancreatitis.....	146
Figure 34. Merging PBS and caerulein single-cell RNA-sequencing datasets.....	148

List of Tables

Table 1. Mouse lines used for mesothelial lineage tracing.....	93
--	----

Chapter 1

Introduction

Diabetes mellitus

Diabetes mellitus is a disease caused by deficient insulin production, resulting in abnormally high blood glucose levels. Currently, 425 million people across the globe are diagnosed with diabetes and that number is projected to rise to 642 million by 2040, highlighting the urgent need to understand, treat, and prevent this disease. (International Diabetes Federation: <http://www.diabetesatlas.org/>). Within the pancreas, groups of aggregated endocrine cells termed the islets of Langerhans secrete hormones in response to fluctuations in blood glucose levels. One of these endocrine cells within the islet, the beta cell, secretes insulin, the hormone responsible for initiating the uptake of glucose from the blood into cells throughout the body. The insulin-secreting function of beta cells is disrupted in individuals with both type 1 and type 2 diabetes. In type 1 diabetes, auto-immune destruction of beta cells results in their absence within the pancreas, leading to inadequate insulin secretion to regulate blood glucose. In type 2 diabetes, peripheral tissue resistance to uptake glucose requires increased production of insulin from beta cells. Over time, the beta cells are not able to increase the production of insulin and become dysfunctional, leading to dysregulated blood glucose levels. Therefore, the beta cells are a critical cell type for the maintenance of the body's blood glucose levels.

For individuals with Type 1 diabetes, who lack beta cells, restoring insulin to the body in order to regulate blood glucose levels has been a major focus of the last century. The isolation of insulin from pancreata of dogs, and later synthesis of human insulin, allowed for delivery of exogenous insulin to individuals with type 1 diabetes. Although insulin injections greatly reduced mortality associated with diabetes mellitus, secondary complications arising from the reduced glycemic control, such as diabetic nephropathy, neuropathy, and retinopathy, continue to affect individuals with the disease. Transplantation approaches, using either the whole pancreas

or only the pancreatic islet fraction, have continued to improve and can provide long-term tight regulation of blood glucose levels and slowed progression of secondary complications in individuals with diabetes (A. C. Gruessner & Gruessner, 2016; Posselt et al., 2010; Shapiro et al., 2000; Shapiro, Pokrywczynska, & Ricordi, 2016). Transplantation approaches demonstrate the success of restoring insulin production to cure type 1 diabetes. However, a severe lack of supply for transplantation makes this treatment unavailable for the large majority of individuals with diabetes mellitus.

There exists a great need for a renewable source of transplantation material to provide relief for individuals suffering from diabetes mellitus and its secondary complications. Stem cell differentiation platforms are a promising approach to produce a nearly unlimited supply of transplantation material (Pagliuca & Melton, 2013; Sneddon et al., 2018). These approaches take advantage of the ability of human embryonic stem cells (hESCs) to develop into any cell type of the body by guiding these pluripotent cells through a directed differentiation protocol to a particular cellular fate *in vitro*. Transplantation of hESC-derived oligodendrocyte precursors, for instance, has restored locomotion after spinal cord injury in an adult rat model (Keirstead et al., 2005). Similarly, hESC-derived cardiomyocytes have improved heart regeneration after infarction in guinea pigs (Shiba et al., 2012). Given the lack or dysfunction of one particular cell type in diabetes, the beta cell, directed differentiation of hESCs to a beta cell fate *in vitro* can produce theoretically limitless transplantation material for individuals with diabetes. A challenge, therefore, is developing differentiation protocols that can produce a beta cell *in vitro* with the same functionality as beta cells *in vivo*. Mouse studies of *in vivo* pancreatic development have facilitated significant progress in the development of differentiation protocols for hESC-derived beta cells.

Pancreatic epithelial development

Development of the pancreas results in a highly-branched, mature organ composed of multiple cell types that are organized into two separate compartments with distinct functions. The exocrine compartment, consisting of acinar and ductal cells, forms the network that shuttles acinar cell-produced digestive enzymes to the duodenum to aid in food digestion. The endocrine compartment, consisting of the islets of Langerhans, secrete multiple hormones to regulate blood glucose levels. The islets of Langerhans are composed of four different endocrine cell types that each secrete a different hormone, including beta (insulin), alpha (glucagon), gamma (pancreatic polypeptide), and delta (somatostatin) cells. During development, a fifth endocrine cell, the ghrelin-producing epsilon cell, is also present. Decades of work have sought to understand the developmental steps that produce the mature pancreatic organ, with a specific emphasis on the development of the beta cell.

Pancreas development begins with the specification of the endoderm and endoderm-derived gut tube, which is facilitated and marked by expression of the transcription factors *Sox17* and *FoxA2* (Ang & Rossant, 1994; Kanai-Azuma et al., 2002; Weinstein et al., 1994). The regulation of endoderm differentiation by Nodal signaling is conserved across multiple vertebrates, including mice (Tremblay, 2010). Within the endoderm, pancreas specification is marked by expression of the transcription factor *Pdx1* in two groups of cells along the dorsal and ventral primitive foregut by embryonic day 8.5 (E8.5) (Ohlsson, Karlsson, & Edlund, 1993). All epithelial cells in the pancreas are derived from this pool of Pdx1+ progenitors (G. Gu, Dubauskaite, & Melton, 2002). Expression of *Pdx1* requires the inhibition of hedgehog signaling and activation of retinoic acid signaling by secretion of signals from the notochord (Hebrok, Kim, & Melton, 1998) and mesenchymal cells (Martín et al., 2005; Molotkov, Molotkova, &

Duester, 2005), respectively. Around E9, the Pdx1⁺ cells evaginate into a cap of surrounding mesenchymal cells, proliferate to form a stratified epithelium, and begin to undergo branching morphogenesis (Fig. 1a). The proliferation and branching of Pdx1⁺ progenitors is supported by the secretion of FGF10 from the surrounding mesenchymal cap (Bhushan et al., 2001).

Coinciding with branching morphogenesis, subtypes of Pdx1⁺ progenitors form tip and trunk domains by E12.5. Cross-antagonistic interaction between two transcription factors, *Ptf1a* and *Nkx6-1*, delineate the tip and trunk regions (Schaffer, Freude, Nelson, & Sander, 2010). Tip cells, characterized by expression of *Ptf1a*, *Cpa1*, and *c-Myc*, act as multipotent progenitors for the three major cell types of the pancreas up until E13.5, when their cellular fate becomes restricted to the acinar cell (Q. Zhou et al., 2007). The trunk cells, marked by *Sox9*, *Hnf1b*, *Hnf6*, *Glis3*, and *Nkx6-1*, are restricted to either a ductal cell or endocrine cell fate (Kang et al., 2009; Y.-S. Kim et al., 2012; Schaffer et al., 2010; Seymour et al., 2008; Solar et al., 2009). The fate of a trunk cell toward the ductal or endocrine lineage is regulated by differential levels of Notch signaling (Apelqvist et al., 1999; Jensen et al., 2000; Shih et al., 2012). High levels of Notch result in a ductal fate, while lower levels lead to an endocrine cell fate (Shih et al., 2012).

The endocrine lineage begins with the expression of a transcription factor, *Neurogenin3* (*Ngn3*) in trunk cells with low levels of Notch (Fig. 1a). *Ngn3* expression defines the endocrine progenitor cells that will differentiate into the main endocrine lineages of the pancreas: alpha, beta, delta, and gamma cells (Gradwohl, Dierich, LeMeur, & Guillemot, 2000; G. Gu et al., 2002). Epsilon cells are partially derived from *Ngn3*⁺ progenitors, although an *Ngn3*-independent differentiation trajectory has also been described for this endocrine cell type (Arnes, Hill, Gross, Magnuson, & Sussel, 2012). In the mouse, *Ngn3* is expressed in two waves during development (Villasenor, Chong, & Cleaver, 2008). The first wave, termed the primary

transition, occurs from E9.5 – E12.5 and generates mostly alpha cells (Herrera, 2000; Pan & Wright, 2011). Only a minority of primary transition alpha cells are maintained in the adult pancreatic islet (G. Gu et al., 2002; Herrera, 2000). The second transition occurs from E12.5 to birth and generates the large majority of endocrine cells in the mature pancreas (Pan & Wright, 2011). In a divergence from mice, human pancreatic development consists of only one wave of *NGN3* expression and endocrine differentiation (Nair & Hebrok, 2015).

A critical function of *Ngn3* expression is to facilitate cell cycle exit in order to promote differentiation towards an endocrine cell fate (Miyatsuka, Kosaka, Kim, & German, 2011). Shortly after induction of *Ngn3* expression, cells exit the cell cycle, and only reenter after downregulation of *Ngn3* (Miyatsuka et al., 2011). The exit from the cell cycle and subsequent differentiation is facilitated by *Ngn3* induction of both negative regulators of the cell cycle, such as *Cdkn1a*, and endocrine differentiation genes, such as *Pax4*, *Neurod1*, *Nkx2-2*, and *Rfx6*. *Pak3*, a transcription factor downstream of *Ngn3*, also contributes to endocrine progenitor cell cycle exit, as *Pak3* deficient mice show increased proliferation of *Ngn3*⁺ endocrine progenitors (Piccand et al., 2014). Therefore, the coupling of cell cycle exit and differentiation is facilitated by the transient expression of *Ngn3* in endocrine progenitors.

The production of the different endocrine cell types by *Ngn3*⁺ endocrine progenitors is temporally regulated (K. A. Johansson et al., 2007). For example, *Ngn3*⁺ cells become competent to make beta cells after E10.5, while delta cells are not produced until after E14.5 (K. A. Johansson et al., 2007). This results in different proportions of endocrine cells during development. Prior to E14.5, alpha cells make up the majority of endocrine cells being produced (K. A. Johansson et al., 2007). The production of gamma cells peaks around E14.5, while beta cells are produced in the highest proportion beginning around E14.5 until birth (K. A. Johansson

et al., 2007). These competency windows create waves of endocrine differentiation throughout development, where most endocrine cells are being produced but in varying proportions.

The trajectory of a Ngn3^+ endocrine progenitor to one of the hormone-producing cell lineages is dependent on multiple transcription factors with dynamic roles throughout pancreatic development. *Pdx1*, *Nkx6-1*, *Nkx2-2*, and *Pax4* have been demonstrated to be important factors in beta cell differentiation, while *Arx* is critical for alpha cell differentiation. However, many of these factors are critical for more than one endocrine lineage and interact with other factors to regulate lineage allocation. In *Pax4*^{-/-} mice, loss of beta and delta cells is accompanied by an increase in alpha and epsilon cells, suggesting that *Pax4* regulates the decision toward a beta/delta or alpha/epsilon cell fate (Prado, Pugh-Bernard, Elghazi, Sosa-Pineda, & Sussel, 2004; Sosa-Pineda, Chowdhury, Torres, Oliver, & Gruss, 1997). *Arx* has been shown to oppose the action of *Pax4* in order to promote the development of alpha cells at the expense of beta and delta cells (Collombat et al., 2003). Double knockout mice for *Arx* and *Pax4* result in an absence of both alpha and beta cells, and replacement with delta cells, highlighting the complex interactions of transcription factors to regulate endocrine lineage allocation (Collombat, 2005). *Nkx2-2*^{-/-} mice have reduced numbers of beta, alpha, and gamma cells, and instead show increased numbers of epsilon cells (Prado et al., 2004; Sussel et al., 1998). Downstream of *Nkx2-2*, *Nkx6-1* is required for production of proper numbers of beta cells through the maintenance and/or expansion of beta cell precursors following *Ngn3* expression but prior to the production of insulin (Sander et al., 2000). *Pdx1*, required for early specification of pancreatic progenitors and expansion, is also critical for beta cell proliferation and survival (Gannon et al., 2008). Loss of *Pdx1* in beta cells results in decreased numbers of beta cells and a concomitant increase of alpha and delta cells. The increase of alpha and delta cells is a result of increased proliferation rates of

these cell types, rather than conversion of lineages, suggesting that communication between inter-islet cell types is also important for endocrine lineage allocation (Gannon et al., 2008). Given the complex interactions between multiple factors, endocrine lineage allocation remains incompletely understood, including the timing and coordination of these events during the progression from a Ngn3⁺ endocrine progenitor to a fully differentiated hormone-producing cell.

Pancreatic mesenchymal development

Although prior work has focused extensively on the development of the pancreatic epithelial compartment, the epithelium does not develop in isolation. Multiple non-epithelial cells are in close proximity to the epithelium and are critical for proper epithelial development. At E8, secretion of factors from the neighboring mesoderm and notochord specifies the region of endoderm that will ultimately give rise to the pancreas (Hebrok et al., 1998; S. K. Kim, Hebrok, & Melton, 1997; Kumar, Jordan, Melton, & Grapin-Botton, 2003). Fusion of the dorsal aortae by E8.5 displaces the notochord, and brings the dorsal aorta in close proximity to the dorsal pancreatic primordium (Lammert, Cleaver, & Melton, 2001). Vitelline veins remain in close proximity to the ventral pancreatic primordium. These endothelial structures induce expression of key transcription factors required for proper pancreatic differentiation and insulin expression (Lammert et al., 2001; Yoshitomi, 2004). Around E9, a group of mesenchymal cells, collectively termed the mesenchyme, condense around the dorsal gut, and facilitate the growth of the budding epithelium (Bhushan et al., 2001; Golosow & Grobstein, 1962; Landsman et al., 2011; Slack, 1995). As epithelial proliferation and branching morphogenesis proceeds, the epithelium protrudes into the surrounding cap of mesenchymal cells. The rapid growth of the epithelium results in a decreasing ratio of mesenchymal to epithelial cells during development, with rare

mesenchymal cells in the adult pancreas (Erkan et al., 2011; Landsman et al., 2011). Therefore, non-epithelial cell types are in constant contact with the pancreatic epithelium throughout development.

Many of the mesoderm-derived structures involved in early pancreatic development are relatively well defined, such as the notochord and dorsal aorta. However, the cells that migrate to condense around the dorsal pancreatic primordium and persist into adulthood are broadly termed mesenchymal cells. The term mesenchymal implies that these cells originate from the mesodermal germ layer, although this has not been definitively demonstrated for the mesenchymal cells surrounding the pancreas. Indeed, in some regions of the embryo, such as the head, mesenchymal cells and structures are derived from the ectodermal neural crest (Gilbert, 2000). Therefore, the assumption that all mesenchymal cells are derived from the mesoderm may not be correct for other areas of the embryo as well. In addition to their assumed mesodermal origin, these cells are annotated as mesenchymal based on morphological characteristics, such as an elongated, spindle shape, and *in vitro* behavior, such as attachment to plastic. There are a limited number of molecular markers that are used to identify mesenchymal cells, including collagens, *vimentin*, *desmin*, and *platelet-derived growth factor receptor alpha*. However, these markers may not always be specific to mesenchymal cells. For example, in E14.5 pancreas, Ngn3⁺ cells upregulate expression of *vimentin* transcripts and differentiated endocrine cells express the vimentin protein (Gouzi, Kim, Katsumoto, Johansson, & Grapin-Botton, 2011). There is a need for more specific molecular markers that can unambiguously identify mesenchymal cells in different organ systems.

Although poorly defined, the importance of the mesenchyme in pancreatic development has been demonstrated by both physical and genetic ablation approaches. Experiments in the

1960s dissected E11 pancreatic epithelial buds and cultured the buds *ex vivo* (Golosow & Grobstein, 1962). Without the mesenchyme, the epithelial bud failed to undergo the growth and morphogenetic processes that occur *in vivo*. Addition of the dissected pancreatic mesenchyme back to the epithelial bud *ex vivo* rescued both growth and branching morphogenesis, demonstrating the requirement of this compartment for epithelial development. Adding back mesenchyme from other organs, such as retina or kidney, could also restore epithelial growth, suggesting that multiple organs may share features of the mesenchyme to facilitate epithelial processes. Additionally, the mesenchyme was able to support epithelial development across a porous filter, indicating that mesenchymal-secreted factors may mediate the growth and morphogenesis of the epithelium. Later *ex vivo* culture experiments demonstrated that while the mesenchyme supports exocrine development, it repressed endocrine development (Duvillié et al., 2006; Miralles, Czernichow, & Scharfmann, 1998). Exocrine development was supported by close proximity to the mesenchyme, while endocrine development was supported with increased distance from the mesenchyme (Zhixing Li et al., 2004).

The importance of the mesenchyme in epithelial development was further supported by genetic ablation approaches, removing the mesenchyme during development *in vivo* (Landsman et al., 2011). Unlike prior *ex vivo* culture experiments, however, the mesenchyme was found to support both exocrine and endocrine development, by inducing the proliferation of pancreatic progenitors that contribute to both exocrine and endocrine lineages. The differences between the *ex vivo* and *in vivo* studies could be due to the artificial environment of the culture system. It is also possible that additional factors or structures present *in vivo* but missing *ex vivo* play an important role in differentiation processes. Nonetheless, these studies demonstrate the critical role of the mesenchyme in facilitating the development of the pancreatic epithelium.

In addition to cellular ablation studies, which physically remove the mesenchymal cells, ablation of mesenchymal-expressed genes has also resulted in impaired epithelial development. Expression of *Fgf10* within the mesenchyme is required for proper proliferation of Pdx1+ pancreatic progenitors (Bhushan et al., 2001). Depletion of *Fgf10* results in hypoplastic pancreata that fail to undergo branching morphogenesis. Loss of *Hox6*, a gene expressed in the pancreatic mesenchyme, results in decreased *Wnt5a* signaling in the mesenchyme. The loss of *Wnt5a* signaling leads to a subsequent downregulation of WNT inhibitors, *Dkk1* and *Sfrp3*, in Ngn3+ endocrine progenitors, impairing the differentiation of Ngn3+ cells towards an endocrine cell fate (Larsen, Hrycaj, Newman, Li, & Wellik, 2015). Finally, BMP signaling within the mesenchyme has been shown to regulate endocrine differentiation in both chick and mice (Ahnfelt-Rønne, Ravassard, Pardanaud-Glavieux, Scharfmann, & Serup, 2010). Mesenchyme-specific inhibition of BMP signaling in mouse pancreatic explants led to increased numbers of endocrine cells and reduced numbers of exocrine cells. These studies highlight mesenchymal-derived signals that function specifically to support endocrine differentiation. The application of these secreted signals to *in vitro* differentiation platforms has been of high interest, and has helped improve the derivation of beta cells (Pagliuca & Melton, 2013). Indeed, bulk proteomic analyses have identified mesenchymal secreted factors that can enhance hESC differentiation towards a beta cell fate (Russ et al., 2016). Therefore, at least one important mechanism of mesenchymal-supported epithelial development is the secretion of growth factors.

The ablation and genetic loss of function approaches described above treat mesenchymal cells as a single entity, by removing the entire mesenchyme or using whole body genetic knockouts. However, it remains unclear whether this compartment is truly composed of one homogeneous cell type or whether it contains multiple cell types with varying functions. It is

possible that different mesenchymal subtypes perform different functions to support either exocrine or endocrine differentiation and development. This may be reflected by contradictory evidence for the role of the mesenchyme in endocrine cell differentiation, with some studies suggesting an inhibitory role (Miralles et al., 1998), while others suggesting a supportive role. Perhaps a more definitive example of mesenchymal heterogeneity is the formation of the spleen, an entire organ, from a subgroup of cells within the pancreatic mesenchyme marked by *Nkx2-5*, *Tlx1* and *Wt1* (Hecksher-Sørensen et al., 2004). Therefore, there is evidence of functional differences between subtypes of mesenchymal cells during development. The use of bulk approaches, combined with the poor definition of mesenchymal cells, has hindered our ability to identify these mesenchymal subtypes and understand their potential differing functions.

Without clear definitions of the various subtypes within the pancreatic mesenchyme, studying the lineage dynamics of this compartment has been even more challenging. The mesenchymal cells of the pancreatic epithelium have been assumed to be derived from the neighboring splanchnic mesoderm (Hecksher-Sørensen et al., 2004). An outer columnar layer of the splanchnic mesoderm, termed the splanchnic mesodermal plate, has also been hypothesized to give rise to the underlying mesenchymal cells detected in E10.5 pancreata (Hecksher-Sørensen et al., 2004). Recently a study challenged these long-held assumptions (Angelo & Tremblay, 2018). By dye labeling various mesenchymal structures and tracing their cellular derivative, Angelo and Tremblay identified the coelomic mesothelium, the lining of the abdominal cavity, rather than the splanchnic mesoderm, to act as a source of pancreatic mesenchymal cells. Beyond these early stages of development, very little is known about the lineage dynamics of the pancreatic mesenchyme.

The need for further studies on mesenchymal heterogeneity, function, and lineage is becoming more recognized in other organ systems. Studies of the lung mesenchyme have begun to characterize distinct mesenchymal cell types, their impact on epithelial development, and their lineage relationships (McCulley, Wienhold, & Sun, 2015). Similar to the pancreas, the mesenchyme surrounding developing epithelial lung buds are a critical source of signals that facilitate epithelial growth, morphogenesis, and differentiation processes (McCulley et al., 2015). Early tissue recombination studies revealed the presence of distal and tracheal mesenchymal compartments that direct the differentiation of the epithelium to either a distal or tracheal phenotype, highlighting the heterogeneity within the mesenchymal compartment (Shannon, Nielsen, Gebb, & Randell, 1998). Additionally, specific mesenchymal cell types with distinct markers have been noted to perform functions critical for proper epithelial development. For example, the migration and differentiation of alveolar smooth muscle cells, a mesenchymal cell type marked by PDGFR-alpha, is required for the process of alveologenesis, where the epithelium undergoes shape and differentiation processes to support efficient gas exchange within the lung (Lindahl et al., 1997). Finally, studies have begun to examine the origin and lineage dynamics of the different mesenchymal cell types (Agha et al., 2014; Kumar et al., 2014; Peng et al., 2013). They have revealed the presence of local mesenchymal progenitor niches that utilize a variety of mechanisms to produce diverse mesenchymal cell types (Kumar et al., 2014). The lung mesenchyme, once thought of as a homogenous, growth-factor secreting group of cells, is becoming recognized as a group of diverse, functionally relevant cell types with lineage dynamics as intricate and sophisticated as those of the epithelium (Kumar et al., 2014). The deeper understanding of mesenchymal development is critical to understanding lung development as a whole.

The similarities between lung and pancreas development, including their endoderm origin and branched epithelial structure, suggest that the pancreatic mesenchyme also contains functionally diverse cell types derived via various lineage trajectories. Understanding mesenchymal development and subsequently the epithelial-mesenchymal interactions that guide pancreatic development, will require the ability to study the function of individual cell types within each compartment.

***In vitro* recapitulation of beta cell development**

Information about how the pancreas develops *in vivo* has been crucial for building differentiation protocols to derive beta cells from hESCs. By mimicking key steps of development with the addition of cocktails of exogenous signaling or growth factors, *in vitro* differentiation protocols aim to mimic the progression of pancreatic development *in vivo* towards a beta cell fate (Pagliuca & Melton, 2013). Recapitulation of developmental steps can be assessed by expression of the key transcription factors detected *in vivo* (Pagliuca & Melton, 2013). The *in vitro* derivation of endoderm and Pdx1+ pancreatic progenitors from hESCs was accomplished by the addition of activin A, a TGF-beta family member with similar binding partners to Nodal, inhibitors of hedgehog signaling, retinoic acid, and FGF10, all signaling pathways involved in early endoderm and pancreatic differentiation (D'Amour et al., 2005; 2006; Pagliuca & Melton, 2013). From these hESC-derived Pdx1+ progenitors, Ngn3+ endocrine progenitors were produced by modulation of Notch signaling, and additional factors that were determined empirically (D'Amour et al., 2006). Since then, numerous protocols have generated pancreatic islet cells (Guo, Landsman, Li, & Hebrok, 2013; Kroon et al., 2008) and subsequently, insulin-producing beta cells capable of sensing and responding to glucose from

hESCs (Pagliuca et al., 2014; Reznica et al., 2014; Russ et al., 2015)². Therefore, the information from developmental processes was critical for the development of these stem cell differentiation protocols.

While there has been great progress in the production of beta cells *in vitro*, the resulting hESC-derived beta cells do not fully recapitulate their *in vivo* counterparts. Although recent protocols have produced functional hESC-derived beta cells that respond appropriately to fluctuating glucose levels (Pagliuca et al., 2014; Reznica et al., 2014; Russ et al., 2015; Zhu et al., 2016)², their glucose-sensing function is not maintained long-term *in vitro*. This phenotypic instability of hESC-derived beta cells greatly hinders transplantation, drug screening efforts, and studies of human beta cell physiology. Additionally, the efficiency of most stem cell platforms remains problematic for therapeutic applications, with the final product of most published protocols containing around 30% beta cells. These limitations to the current *in vitro* protocols suggest that additional optimization is required to produce stable, functional beta cells in large numbers.

There are multiple reasons why hESC-derived beta cells may not fully recapitulate *in vivo* beta cells. First, cellular intrinsic defects may be present. For example, cells may fail to express genes required for proper differentiation and function during *in vitro* differentiation. Although many genes required for beta cell differentiation, function, and stability have been identified, there may be additional unknown factors that are present *in vivo* but absent *in vitro*. On the other hand, hESC-derived cells may misexpress genes that are not normally expressed within the beta cell lineage *in vivo*. This concept is demonstrated by identification of adult beta cell “disallowed” genes. Disallowed genes are specifically downregulated in beta cells and disrupt beta cell function when improperly expressed (K. Lemaire, Thorrez, & Schuit, 2016).

Disallowed genes may also be present during beta cell differentiation processes *in vivo* and require inhibition during *in vitro* differentiation. Besides the absence or presence of particular genes, proper differentiation and function may require tight regulation of gene levels. Levels of Notch signaling dictate the differentiation of a pancreatic progenitor towards a ductal or endocrine fate (Shih et al., 2012). The dosage of *Pdx1* is also critical for pancreatic development. The creation of hypomorphic *Pdx1* alleles demonstrated a requirement for high levels of *Pdx1* for pancreatic development but lower levels for gut and stomach development (Fujitani et al., 2006). If proper levels of critical genes are not replicated *in vitro*, the differentiation trajectory may be disrupted. Finally, as a third layer of regulation, the timing of gene expression may be dysregulated *in vitro*. Coordinated cascades of gene expression may be required to fully recapitulate *in vivo* processes (M. E. Wilson, Scheel, & German, 2003). These intrinsic defects related to gene expression may hinder the full maturation and stability of the hESC-derived beta cell.

A second reason for the inability of current differentiation protocols to produce stable beta cells may relate to missing extrinsic signals. It is possible that the current emphasis on the production of a single cell type, the beta cell, has missed the importance of exogenous signals from other cell types. *In vivo*, beta cells develop within a complex structure that contains multiple cell types. The absence of these cell types in the *in vitro* platform, therefore, remains a stark difference to *in vivo* development. Focusing efforts on *in vivo* cellular interactions and tissue development as a whole can provide insight into crucial exogenous signals needed for proper beta cell function, maturation, and stability. Indeed, addition of mesenchymal cell types to the *in vitro* platform increased proliferation of pancreatic progenitor cells, greatly increasing the efficiency of the platform (Sneddon, Borowiak, & Melton, 2012). This effect could not be

replicated by addition of 16 different exogenous growth factors, suggesting that the increased progenitor proliferation by the mesenchyme is likely multifactorial (Sneddon et al., 2012). A clearer understanding of the various cell types, and their function, during pancreatic development can allow for the addition of missing signals to the *in vitro* platform and solve the remaining challenges of deriving beta cells from hESCs.

Approaches to studying cellular heterogeneity of the developing pancreas

Prior approaches to understand cellular heterogeneity within a tissue have relied on the identification of individual genes to define or mark a group of cells. These approaches, including gene knockout and Cre-based lineage tracing, require prior knowledge of marker genes, and rely on that marker being specific to a particular population of cells. Cellular populations with distinct functions may be defined by sets of genes, rather than one individual gene, making their study by traditional approaches challenging. Identification of populations defined by multiple genes or novel genes can be done by screening assays, such as *in situ* or immunohistochemistry for a library of probes (Q. Zhou et al., 2007). However, these approaches require large investment of time and effort, and are still limited to the probes contained in the library. Genome-wide, unbiased methods, such as bulk RNA-sequencing have been used to overcome these limitations. By pooling together cells of interest, bulk RNA-sequencing can identify sets of genes expressed in specific populations without any prior knowledge of those genes. However, this approach requires the ability to separate a cell population of interest, either by physical dissection or fluorescence-activated cell sorting (FACS), which requires known cell surface markers.

Recent advances in molecular biology and microfluidics have allowed for development of methods to sequence whole genome or transcriptomes in thousands of individual cells in parallel (Macosko et al., 2015; Zheng et al., 2017). Bioinformatic analyses can then classify cells into groups based on whole transcriptomic information, simultaneously identifying novel populations and the whole set of genes that define them. Single-cell RNA-sequencing has been used to assess cellular and transcriptional heterogeneity and identify novel populations in a variety of organs during development, adult homeostasis, and disease states (Potter, 2018). Recent studies of late embryonic, postnatal, and adult alpha and beta cells have demonstrated the power of single-cell transcriptomic profiling for unraveling endocrine lineage heterogeneity and revealing distinct transcriptional states of beta cell maturation (Dorrell et al., 2016; W.-L. Qiu et al., 2017a; Zeng et al., 2017). However, the application of this technology to the pancreas across early developmental time (before E17) has not been performed, and these studies focused solely on the epithelial compartment of the pancreas.

Contribution to the field

This work uses single-cell RNA-sequencing to identify and characterize a novel endocrine population within the epithelium and multiple subtypes of mesenchymal populations. *In silico* lineage modeling approaches predict the novel endocrine population to be derived from Ngn3⁺ progenitors and to give rise to alpha and beta cells during development. This approach also allowed for identification of candidate transcriptional regulators of the alpha or beta cell fate from the newly characterized endocrine progenitors. This work, therefore, enhances our knowledge of endocrine development, and specifically highlights an additional unknown cellular stage towards beta cell development. Transcriptional profiling of thousands of mesenchymal

cells identified, for the first time, distinct cell types of the pancreatic mesenchyme. This dataset also highlights a particular mesenchymal cell type, the mesothelium, that has been characterized as a critical regulator of mesenchymal cell development in multiple other organs but remains largely unstudied in the pancreas. Our *in silico* modeling predicts the lineage relationships among the pancreatic mesothelium and mesenchymal subtypes that can now be validated *in vivo* utilizing the transcriptional markers identified in our dataset. Additionally, we identify a role for the mesothelial-expressed factor, *Fgf9*, in regulating mesenchymal and epithelial compartment sizes, which ultimately regulates pancreatic size as a whole. Finally, we build single-cell RNA-sequencing datasets for mesenchymal populations during adult homeostasis and fibrosis, which will facilitate studies on the mesenchymal cellular dynamics during disease. Therefore, this work identifies and describes pancreatic cellular heterogeneity in both the epithelial and mesenchymal compartments with implications for endocrine differentiation, and mesenchymal regulation of development and disease.

Chapter 2

Identification of a novel endocrine progenitor population

Introduction

The derivation of hormone-producing cells from Pdx1⁺ pancreatic progenitors has been an area of intense research in the last few decades. Identification of distinct cellular stages during pancreatic progenitor differentiation has clarified the cellular origin of the major cell types of the adult pancreas. *Neurogenin3* (*Ngn3*) marks a cellular stage that ultimately gives rise to all four endocrine cell types in the mature pancreas. The intervening steps between *Ngn3* and hormone expression, however, remain unclear. A better mechanistic understanding of how Ngn3⁺ endocrine progenitors differentiate into multiple cellular fates is critical for informing *in vitro* beta cell differentiation protocols.

The derivation of multiple cell types from one progenitor suggests that the Ngn3⁺ population may represent a heterogeneous group of progenitors already specified towards one particular endocrine cell fate. One study used clonal lineage tracing to show that each Ngn3⁺ progenitor gave rise to exactly one endocrine cell, supporting the hypothesis that Ngn3 is a broad marker for a heterogeneous group of pre-specified unipotent cells (Desgraz & Herrera, 2009). However, this conclusion is complicated by the fact that Ngn3⁺ progenitors are post-mitotic; thus, it is possible that they are not pre-specified, but rather, have the capability to produce any endocrine cell type. Internal or external signals, downstream of Ngn3 expression, may then push the progenitor towards one particular cell fate. In the case of either Ngn3⁺ progenitor pre-specification or post-specification of endocrine cell fates, a clonal lineage trace would result in the production of only a single endocrine cell. The heterogeneity within the Ngn3⁺ progenitor population, and whether this heterogeneity reflects a bias towards a particular endocrine cell fate remains an important unanswered question.

Attempts to isolate and study the Ngn3⁺ population have relied on a Ngn3-eGFP reporter mouse line and fluorescence-assisted cell sorting (FACS) to separate Ngn3⁺ progenitors from their downstream progeny (G. Gu et al., 2004; P. White, May, Lamounier, Brestelli, & Kaestner, 2008). The transient expression of *Ngn3* and extended half-life of eGFP (Corish & Tyler-Smith, 1999), however, resulted in collection of more fully differentiated endocrine cells that no longer express *Ngn3*. Inclusion of these Ngn3-negative cell types was masked by downstream bulk analysis, confounding the expression profiles of Ngn3⁺ endocrine progenitors. To overcome the limitations of the eGFP reporter, one study identified cell surface markers to isolate Ngn3⁺ progenitors by fluorescence-assisted cellular sorting (FACS) (Sugiyama, Rodriguez, McLean, & Kim, 2007). Two markers were used to isolate Ngn3⁺ cells: CD133, which separated Ngn3⁺ cells from insulin⁺ and glucagon⁺ cells, and CD49f, which separated Ngn3⁺ cells from CarbA⁺ exocrine cells. While this technique could successfully isolate fully differentiated hormone⁺ cells from Ngn3⁺ cells, it does not account for cellular stages that may be both Ngn3-negative and hormone-negative. The cellular stages immediately following *Ngn3* expression may be critical for determining the ultimate fate of a Ngn3⁺ endocrine progenitor. Therefore, there is a great need for specific isolation of Ngn3⁺ endocrine progenitors from their immediate descendants.

To better segregate Ngn3⁺ progenitors from downstream progeny, a Ngn3 “timer” mouse line was developed (Miyatsuka, Li, & German, 2009). In this line, a fluorescence protein that shifts its emission peak from green to red over time is expressed under the *Ngn3* promoter. Collection of distinct green, green/red (yellow), and red populations allows for increased temporal isolation of Ngn3⁺ progenitors and downstream progeny that recently expressed *Ngn3* but no longer do so. Gene expression analysis of these collected populations has allowed for increased resolution of gene expression cascades downstream of *Ngn3*, but the temporal

resolution is based on the timing of the fluorescent protein emission shifts, rather than alterations in cellular gene expression. The shift from green to yellow occurred within 6 hours of *Ngn3* expression, while yellow shifted to red within 12 hours. *Ngn3* has been shown to be expressed for around 24 hours (Beucher et al., 2012), indicating that the timer mouse may not exactly match endogenous *Ngn3* expression. Therefore, even with these improved tools, the distinct stages of *Ngn3*⁺ progenitor differentiation towards a particular endocrine cell fate has remained elusive.

The advent of single-cell RNA-sequencing allows for the identification of novel cell populations or cellular states, independent of known markers. Here, we use this technology to identify an additional endocrine progenitor stage downstream of *Ngn3* expression, marked by expression of the gene *Fev*. By ordering thousands of individual cells by their transcriptomic similarity along a pseudotime differentiation trajectory, we identify candidate regulators of alpha and beta cell fates. The *Fev*⁺ progenitor population is likely relevant to human endocrine biology, as we find this population in both human fetal pancreas and hESC-derived endocrine progenitors *in vitro*.

Results

Cellular heterogeneity in the murine pancreas

We first characterized the major sources of cellular heterogeneity in the developing pancreas. Two batches of mouse pancreata at E14.5, a particularly active time of expansion, morphogenesis, and diversification (Pan & Wright, 2011) (Fig. 1a), were dissected from individual litters, dissociated into single-cell suspensions, sorted for live cells, and sequenced using the 10X Chromium Single-Cell version 1 (v1) kits (Fig. 1b and Fig. 2a-e). We performed

filtering, normalization, variable gene identification, linear regression for batch, and Principal Component Analysis (PCA) with the R package, Seurat (Fig. 2d,e and 3a,b). Graph-based clustering (Satija, Farrell, Gennert, Schier, & Regev, 2015) of batch-adjusted, merged data identified 19 distinct cell populations, classified as epithelial, mesenchymal, immune, or vascular populations based on the expression of known markers (Fig. 1c,d and Supplementary Data 1). We identified expected populations, including endocrine, exocrine (acinar and ductal), and endothelial cells (Fig. 1e). The proportions of endocrine, mesenchymal, immune, and vascular populations were similar between E14.5 batches (Fig. 3b-d). Downsampling analysis confirmed that sufficient sequencing depth had been reached for calling clusters (Fig. 3e-g). These results reveal the power of single-cell RNA-sequencing to identify a broad range of cell types during development.

A previously undescribed endocrine progenitor population

We first sub-clustered the 2,049 cells from our E14.5 dataset that comprised just the epithelial populations (Fig. 4a and Fig. 5a). We identified 10 clusters, including acinar, ductal, beta, alpha, and Ngn3⁺ progenitor populations, as revealed by differential expression of known markers (Fig. 4a-b and Fig. 5b). Our analysis highlighted previously uncharacterized markers of acinar, Ngn3⁺, beta, and alpha cell populations, such as *Reep5*, *Btbd17*, *Gng12*, and *Peg10*, respectively (Fig. 4b). We also found *Sst*- and *pancreatic polypeptide (Ppy)*-expressing cells, but they did not cluster into their own populations (Fig. 5c).

After the ductal, acinar, Ngn3⁺, and hormone⁺ populations had been accounted for, there still remained one population that eluded classification based on known marker genes. This population was distinguished from all other epithelial populations by high-level expression of the

E26 transformation-specific (ETS) transcription factor *Fev*, previously shown to be expressed within the developing pancreas but not described as a marker of a distinct epithelial population (Ohta et al., 2011) (Fig. 4a,b). This *Fev*⁺ population expressed genes marking endocrine lineage cells, such as *paired box 4 (Pax4)*, *chromogranins A/B (Chga/b)* and *Neurod1* (Shih, Wang, & Sander, 2013) (Fig. 5d), but not mature endocrine markers, such as *insulin1 (Ins1)* or *Gcg*, or the transitory early endocrine lineage marker, *Ngn3* (Fig. 4b,c). Pairwise comparison between the *Fev*⁺ and *Ngn3*⁺ clusters identified 99 genes more highly expressed in *Fev*⁺ and 87 more highly expressed in *Ngn3*⁺ cells, suggesting that they are distinct populations (Fig. 4d). This *Fev*⁺, *Ngn3*⁻, hormone- cluster will henceforth be referred to as the *Fev*^{Hi} population. Pathway analysis of the *Ngn3*⁺ and *Fev*^{Hi} populations revealed enrichment of cell cycle and Notch signaling pathways in *Ngn3*⁺ cells (Fig. 4e), likely reflecting the exit of *Ngn3*⁺ progenitors from the cell cycle (Miyatsuka et al., 2011) and the role of *Ngn3* in Notch signaling (Shih et al., 2012). The *Fev*^{Hi} cluster expressed genes in pathways related to serotonin and insulin signaling, Activating Transcriptional Factor 2 (ATF-2) signaling, and sphingosine-1-phosphate signaling, which have been reported to regulate endocrine differentiation^{29,30}. This relationship to serotonin is consistent with prior work establishing *Fev* as a critical transcription factor in serotonergic neurons (Ohta et al., 2011; Spencer & Deneris, 2017).

Further sub-clustering of all 661 cells within the endocrine lineage revealed additional sub-groups of *Fev*-expressing cells. The first was marked by high expression of *Pax4* and *runx1 translocation partner 1 (Runx1t1)* and lower levels of *Ngn3*. The second was marked by *Chgb* and *vimentin (Vim)* (Fig. 4f and Fig. 5e,f). Therefore, our analysis proposed the existence of multiple intermediate states, marked by *Fev*, within the endocrine lineage. The *Fev* gene was

also expressed at lower levels in a subset of the hormone-producing alpha, beta, and epsilon cell populations, which will collectively be referred to as hormone⁺/Fev^{Lo} populations (Fig. 4b).

Given that the Fev⁺ populations expressed endocrine lineage genes, we utilized pseudotime ordering (X. Qiu et al., 2017b) to test the hypothesis that both Fev⁺ populations were lineage-related to the Ngn3⁺ progenitors that give rise to the endocrine compartment of the pancreas (G. Gu et al., 2002). This *de novo* reconstruction of the developmental trajectory placed both the Fev⁺/Pax4⁺ and Fev^{Hi}/Chgb⁺ cells between Ngn3⁺ endocrine progenitors and alpha and beta cells (Fig. 4g and Fig. 5g), suggesting that Fev^{Hi} cells comprise a progenitor stage following *Ngn3* expression and before hormone acquisition. The Fev⁺/Pax4⁺ population was placed closer in pseudotime to the Ngn3⁺ population and was followed by the Fev^{Hi}/Chgb⁺ population (Fig. 4g), indicating that the former represents an earlier cell state. Unlike alpha and beta cells, epsilon cells were found throughout the trajectory populated by the Fev⁺/Pax4⁺ and Fev^{Hi}/Chgb⁺ populations (Fig. 4g), possibly reflecting their function as multipotent progenitor cells for alpha and gamma lineages during development (Arnes et al., 2012).

To validate these lineage relationships, we performed an *in vivo* lineage trace of Ngn3⁺ cells. In E14.5 *Ngn3-Cre; ROSA26^{mTmG}* mouse pancreata, where lineage-traced cells are membrane-GFP⁺ (Muzumdar, Tasic, Miyamichi, Li, & Luo, 2007), approximately 20% of all *Ngn3*-lineage traced cells were identified as the Fev^{Hi} population by the presence of *Fev* and the absence of both *Ngn3* and the pan-differentiated endocrine cell marker *Islet1* (*Isl1*) (Fig. 6a,e, yellow arrows and bar, and Fig. 5h). We also detected the hormone⁺/Fev^{Lo} population identified by our single-cell data (Fig. 6a, purple arrows) and cells that co-expressed *Fev* and *Ngn3* (blue arrows), consistent with a model in which Fev^{Hi} cells represent an intermediate progenitor state following Ngn3⁺ cells but prior to differentiated endocrine cells (Fig. 6g).

We next tested if the Fev^{Hi} population was also present in developing human pancreatic tissue. In human fetal pancreas at 23 weeks post conception, we observed cells that expressed only *NGN3* (Fig. 6b, grey arrows), only *CHGA* (magenta arrows), a marker of all hormone-expressing endocrine cells, and both *FEV* and *CHGA* (purple arrows). We also detected cells that expressed *FEV* but not *NGN3* or *CHGA* (Fig. 6c, yellow arrows), analogous to the murine Fev^{Hi} population. The existence of these cellular states in human development suggests that the lineage relationships we identified generalize beyond murine pancreatic organogenesis to that of human, as well.

We then probed hESCs undergoing directed differentiation towards the pancreatic beta cell lineage *in vitro* (Pagliuca et al., 2014). *FEV* was detected in endocrine progenitor-stage cells and beta-like cells (BLCs) at levels comparable to adult human islets, but not in undifferentiated hESCs (Fig. 5i). Further, we observed *FEV+* (*NGN3-/ISL1-*) (yellow arrows), *FEV+/ISL1+* (*NGN3-*) (purple arrows), and *NGN3+/FEV+* (*ISL1-*) (blue arrows) populations in differentiating hESC-derived cells mid-way through the endocrine progenitor stage (Fig. 6d,f). While endocrine differentiation progresses as a wave throughout development (K. A. Johansson et al., 2007) *in vivo*, it is more synchronized in the hESC differentiation platform *in vitro* (Pagliuca et al., 2014). At a timepoint directly preceding beta cell differentiation, we found that nearly 70% of hESC-derived cells were either *NGN3+/FEV+* or *FEV+* (Figure 6f, blue and yellow bars). These data place the *FEV+* population at a timepoint consistent with an endocrine progenitor population during human beta cell differentiation *in vitro*.

Endocrine dynamics over developmental time

Although we had captured comparatively fewer epithelial cells at E12.5 and E17.5 than at E14.5, we could still identify the Fev^{Hi} cells at both timepoints (Fig. 7a). To capture more epithelial cells and account for those that were missing from E12.5 and E17.5 version 1 (v1) runs, we re-performed an entirely new (version 2) set of single-cell RNA-sequencing experiments at E12.5, E14.5, and E17.5 after depletion of CD140a+ mesenchymal cells in order to enrich for epithelial cells (Fig. 7b,c). Given the high numbers of red blood cells at E17.5, we ran two wells of E17.5 cells (replicates 1 and 2) to increase our capture of epithelial cells and then aggregated the datasets. We first analyzed the exocrine compartment and identified acinar, ductal, and proliferating populations of both at all timepoints (Fig. 7). We then focused on the endocrine compartment, where we captured 584, 1,267, and 1,837 endocrine cells at E12.5, E14.5, and E17.5, respectively. We found similar gene expression topologies as in our v1 dataset but gained additional resolution with increased cell numbers and transcriptomic coverage (Fig. 7e).

To analyze how endocrine populations change over time, we merged all three v2 timepoints into one dataset using canonical correlation analysis (A. Butler, Hoffman, Smibert, Papalexi, & Satija, 2018). We correlated the v2 dataset to the v1 dataset and could identify all populations present in the v1 dataset (Fig. 7f). We also found additional populations, including a cluster characterized by decreased expression of *Fev* and increased expression of *Pdx1* and *Mafb*, genes with known roles in endocrine lineage decisions (Fig. 6h and Fig. 7g). This $Pdx1^{+}/Mafb^{+}$ population correlates most strongly with the $Fev^{Hi}/Chgb^{+}$ population, as well as both the alpha and beta cell populations in the v1 dataset (Fig. 7f). We also found a second beta cell population characterized by increasing expression of *Ins1* and *Ins2* and lower expression of *Pdx1*, perhaps

representing more mature beta cells (Fig. 7g). Indeed, this second beta cell group is almost entirely comprised of cells from the E17.5 timepoint (Fig. 6i). To examine how these populations shift over developmental time, we calculated the proportion of these populations at each timepoint (Fig. 6j). We found shifts in cell proportions that match those reported in literature, such as a high proportion of alpha cells early in development at E12.5 and increasing proportions of beta and delta cells at later timepoints (K. A. Johansson et al., 2007). The *Ngn3*⁺ population decreased over time, while the *Fev*⁺/*Pax4*⁺, *Fev*^{Hi}/*Chgb*⁺, and *Pdx1*⁺/*Mafb*⁺ populations peaked at E14.5, consistent with previous studies that reported peak *Ngn3* expression at approximately E14.5 and its subsequent downregulation as differentiation into endocrine lineage ensues (Villasenor et al., 2008). At E17.5, we also found an increasing proportion of proliferating endocrine cells, presumably those responsible for the expansion of endocrine cell mass in later embryonic development (Bonner-Weir, Aguayo-Mazzucato, & Weir, 2016). These results from the larger v2 dataset confirm our initial findings from the v1 dataset and add additional resolution to the endocrine populations during pancreatic development.

Lineage decisions within the endocrine compartment

As the *in vivo* lineage tracing data had revealed that the *Fev*^{Hi} population is derived from the *Ngn3*⁺ population, we hypothesized that the *Fev*^{Hi} population could then function as a progenitor for the endocrine populations of the developing pancreas. We utilized a *Fev-Cre*; *ROSA26*^{mTmG} lineage tracing strategy to label *Fev*-expressing cells and their progeny. We found that 100% of alpha, beta, and delta cells, 90.1% of gamma cells, and 23.2% of epsilon cells were lineage-traced in E14.5 pancreas (Fig. 8a-e). These proportions of lineage labeling held true later in development (E17.5) and in adulthood (6 weeks) (Fig. 9 and 10). Epsilon cells are rare in the

adult pancreas (Arnes et al., 2012) and still exhibited only partial lineage tracing in E17.5 pancreas (47.8% traced) (Fig. 9e). These results demonstrate that the majority of endocrine cells pass through a *Fev*-expressing stage during development.

We next combined this lineage tracing approach with single-cell RNA-sequencing to identify transcriptional regulators of endocrine differentiation. FACS sorting was used to enrich for *Fev*-expressing cells and their progeny (membrane-GFP+) from *Fev-Cre; ROSA26^{mTmG}* pancreata at E14.5 (Fig. 8f,g). All expected endocrine populations were identified in the resulting single-cell dataset (Fig. 8h,i). In addition, we found that *eGFP* reads mapped to all endocrine populations except the *Ngn3*⁺ population (Fig. 8i), further confirming that *Fev* expression turns on after *Ngn3*.

We next set out to model the lineage relationships among the endocrine cells and identify transcriptional regulators of differentiation. Pseudotime ordering identified a trajectory that began with *Ngn3*⁺ cells, transitioned into *Fev*⁺ cells, and then split into two main branches (Fig. 11a; see similar branching pattern in analysis of our first v1 dataset, Fig. 12a). The termini of the branches were populated by differentiated beta and alpha cells, suggesting that the branches represent a transition from a progenitor to fully differentiated hormone⁺ cell (Fig. 11a).

We next used Monocle's branched expression analysis modeling (BEAM) to identify the genes that distinguish the paths along the two branches to either alpha or beta cells. We found gene clusters that were upregulated along different segments of the pseudotime trajectory (Fig. 11b) and performed pathway analysis to identify pathways enriched at each stage of pseudotime (Fig. 12c). Genes upregulated at the beginning of pseudotime in gene cluster 2 included early markers of endocrine differentiation, such as *Sox4* and *Ngn3* (Fig. 11b). *Fev* was in gene cluster 6 and increased in both branches before ultimately decreasing in expression at the branch termini

(Fig. 11b,c). Gene cluster 6 also included other genes expressed within the Fev^{Hi} population, including *Cldn4*, *Vim*, and *Chgb* (Fig. 11b,c and Fig. 12b). We found branch-specific clusters that included known markers of beta (*Ins1*) and alpha (*Gcg*) cells and known differentiation regulators of alpha (*Arx*, *Pou3f4*, *Irx1*, *Slc38a5*, and *Tmem27*) and beta (*Pdx1*, *Pak3*, and *Nkx6-1*) cells (Fig. 11c and Fig. 12b) (Pan & Wright, 2011; Petri et al., 2006; Piccand et al., 2014; Scott Heller et al., 2004; Stanescu, Yu, Won, & Stoffers, 2017). These clusters also contained genes that were enriched in either the alpha or beta branch but were expressed before acquisition of hormone expression (Fig. 12b). Within the alpha cell branch, *Peg10*, *Smarca1*, *Auts2*, and *Wnk3* increased in expression before upregulation of *Gcg* occurred (Fig. 12b). *Peg10* and *Auts2* have roles in differentiation (Dekel et al., 2006; Hishida, Naito, Osada, Nishizuka, & Imagawa, 2007) and migration (Hori et al., 2014), but a role in endocrine differentiation has not been described. As a regulator of chromatin states and an adult human alpha cell marker (Muraro et al., 2016), *Smarca1* may be involved in the epigenetic regulation of alpha cell differentiation. Within the beta cell branch, *Gng12*, *Tssc4*, *Ece1*, *Tmem108*, *Wipi1* and *Papss2* increased in expression before upregulation of *Ins1* (Fig. 12b). To our knowledge, a role in endocrine lineage decisions have not been described for these beta branch-specific genes. We found a similar endocrine differentiation trajectory by an orthogonal method that uses force-directed layouts to visualize gene topologies and infer lineage relationships within single-cell data (Tusi et al., 2018; Weinreb, Wolock, & Klein, 2018) (Fig. 12d). We hypothesize that the genes identified by the analysis above may represent regulators of the differentiation of an endocrine progenitor to a fully differentiated hormone-expressing cell.

To validate our pseudotime results, we performed ISH for markers that defined each branch of the trajectory. First, we confirmed the expression of *Peg10* and *Gng12* within the Fev^{Hi}

population (Fig. 11d,e, indigo and teal gradient arrows), validating the expression of these genes in a stage before hormone acquisition. We also validated the enrichment of *Peg10* and *Gng12* in alpha and beta cells, respectively (Fig. 11f,g, solid indigo and teal arrows). First, 95.8% of beta cells expressed *Gng12* (n=46 cells, 6 pancreata), while 30.5% expressed *Peg10* (n=71 cells, 7 pancreata) (Fig. 11f and Fig. 13a). Additionally, 100% of alpha cells expressed *Peg10* (n=31 cells, 6 pancreata), while only 5.4% expressed *Gng12* (n=32 cells, 4 pancreata) (Fig. 11g and Fig. 13b). The lineage relationships generated by pseudotime ordering, combined with the validation *in vivo*, lead us to hypothesize that the *Fev*⁺/*Peg10*⁺ cells are fated towards an alpha cell identity and *Fev*⁺/*Gng12*⁺ cells towards a beta cell identity (Fig. 11h). These results suggest that lineage allocation of endocrine progenitors towards alpha or beta cell fates may occur after the onset of *Fev* expression.

Discussion

Our identification of a *Fev*^{Hi} endocrine progenitor population provides increased resolution of endocrine differentiation. The relative timing of expression of canonical endocrine lineage genes can now be mapped onto these additional differentiation stages. Several lines of evidence suggest that the gene *Fev* may be a direct target of *Ngn3*: *Fev* is the transcription factor most strongly expressed in *Ngn3*⁺ endocrine progenitors (Miyatsuka et al., 2009), and *Ngn3* knockout embryos do not express *Fev* in the developing pancreas (Ohta et al., 2011). Known target genes of *Ngn3*, such as *Pax4* (Collombat et al., 2003) and *Runx1t1i* (Benitez et al., 2014), are expressed by the early-stage *Fev*⁺/*Pax4*⁺ population. Additionally, *Pax6* is upregulated within the *Fev*^{Hi} population. Although *Chga* and *Chgb* are often utilized as markers of differentiated endocrine lineages, we found that both are expressed in the *Fev*^{Hi} population prior

to hormone acquisition. This result is consistent with previous work that identified Chga⁺, hormone- cells in rodent pancreatic development (A. E. Butler et al., 2016). The Fev^{Hi} cell stage likely represents the cell stage during endocrine differentiation preceding specialized hormone production and may now serve as a cellular landmark for understanding endocrine lineage gene expression dynamics.

The gene *Fev* has been previously studied mainly in serotonergic neurons, where it is a master transcriptional regulator required for cellular differentiation, maturation, and serotonin synthesis (Spencer & Deneris, 2017). *Fev* switches transcriptional targets from differentiation genes during development to maturation genes postnatally in serotonergic neurons (Wyler et al., 2016). In an insulinoma cell line, *Fev* directly binds to the regulatory regions of serotonergic genes, such as *Tph1*, *Tph2*, *Ddc*, *Slc18a2*, and *Slc6a4*, as well as the *Ins1* promoter itself (Ohta et al., 2011). Future ChIP-seq studies of embryonic pancreas will globally identify direct targets of *Fev* and *Fev*-regulated transcriptional networks in developing endocrine cells.

Using genetic lineage tracing *in vivo*, we have demonstrated that the majority of endocrine cells in the developing pancreas transit through a *Fev*-expressing stage, and that *Fev*-lineage cells contribute not only to embryonic, but also to adult pancreatic endocrine cells. The fraction of epsilon cells not derived from a *Fev*-lineage may represent the subset of Ghrl⁺ cells previously reported to give rise to the ductal and exocrine lineages (Arnes et al., 2012). As all adult gamma cells are *Fev*-lineage labeled, the small subset of gamma cells not lineage traced during pancreatic development may represent those that do not persist in the adult pancreas.

Further highlighting the relevance of Fev^{Hi} progenitors during pancreatic development, our pseudotime analysis revealed that *Fev*-expressing cells may be pre-specified towards an alpha or beta cell fate. As expected, we found expression of *Ins1* and *Gcg* at the termini of the

beta and alpha branches, and upregulation of *Pdx1* and *Arx*, which are known regulators of endocrine cell fate decisions, earlier in pseudotime. In addition, our pseudotime analysis identified genes enriched along the alpha or beta branch and expressed prior to upregulation of hormones. These genes warrant further study as potential regulators of the acquisition of alpha or beta cell identity.

For the eventual application of this knowledge to human therapeutics, the findings in the murine model must be validated in human pancreatic development. Our staining of human fetal pancreas identified the analogous FEV^{Hi} population, consistent with our findings in murine pancreata. Directed differentiation of hESCs towards endocrine cell fates will provide a platform for modeling and manipulating the putative lineage regulators found in this study. Indeed, we have identified a FEV⁺ population within hESC-derived endocrine progenitor cells. Deeper knowledge of these lineage decisions may substantially improve directed differentiation efforts to efficiently generate functional beta cells for cellular replacement therapy for people with diabetes. This study highlights the power of combining single-cell transcriptomic information with *in vivo* lineage tracing to reconstruct developmental trajectories within cellular compartments. Discovery of populations and their lineage relationships will promote identification of the mechanisms that drive lineage decisions and commitment.

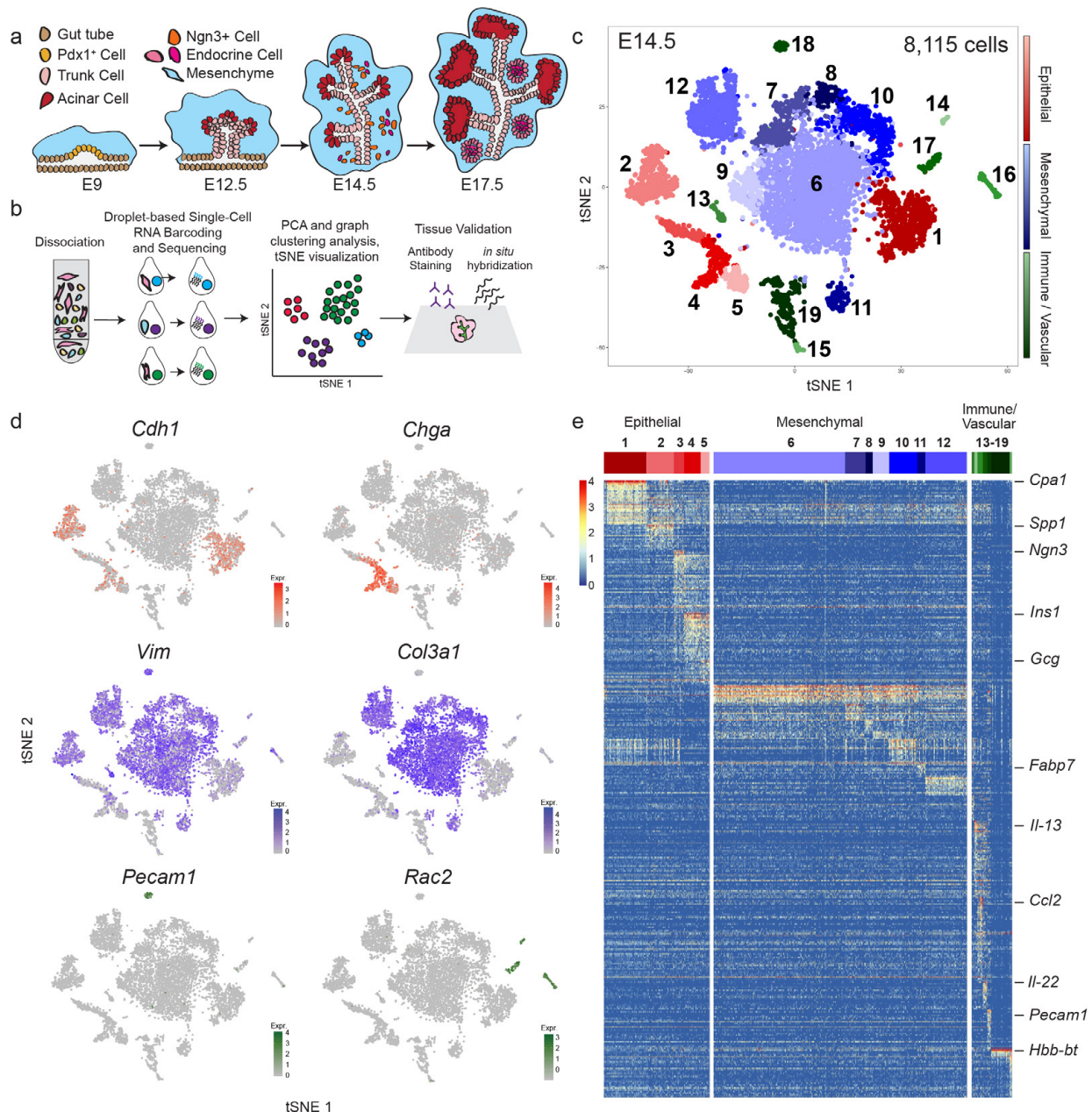


Figure 1. Single-cell sequencing identifies broad patterns of cellular heterogeneity in E14.5 murine pancreas. (a) Overview of murine pancreatic development. (b) Schematic of experimental approach. (c) t-Distributed Stochastic Neighbor Embedding (t-SNE) visualization of populations from pooled E14.5 mouse pancreata (n=14). Each dot represents the transcriptome of a single cell, color-coded according to its cellular identity (epithelial, mesenchymal, or immune/vascular). Each cell compartment contains multiple sub-populations, represented by varying degrees of color shading. (d) Established marker genes identify epithelial cells (*Cdh1*+), endocrine cells (*Chga*+), mesenchymal cells (*Vim*+ and *Col3a1*+), endothelial cells (*Pecam1*+), and immune cells (*Rac2*+). (e) Heatmap depicting greater than 2-fold differentially expressed genes in each cluster compared to all other clusters. Cells are represented in columns, and genes in rows. Specific genes used to annotate clusters are indicated to the right of the heatmap.

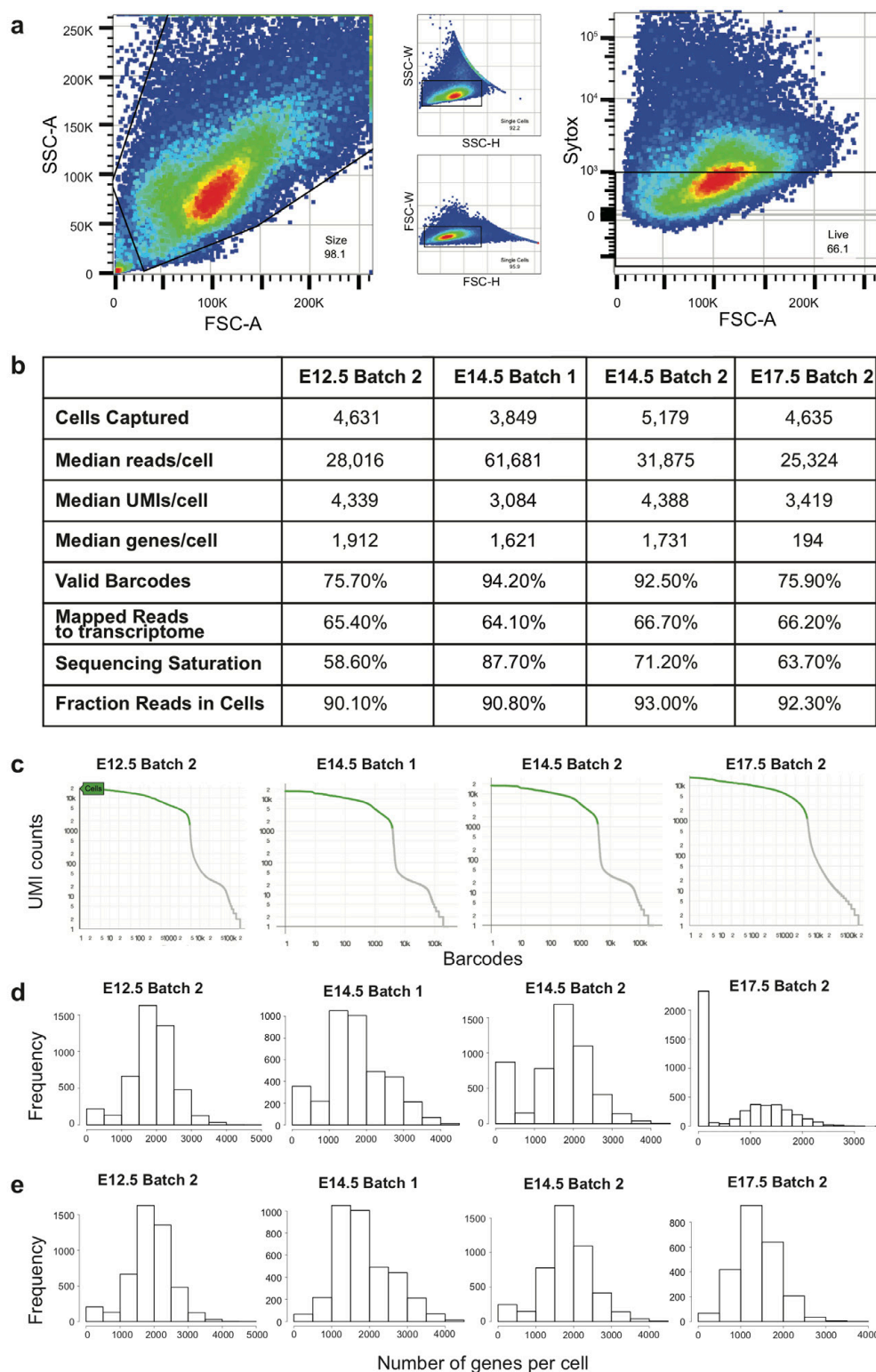


Figure 2. Quality Control for Single-cell RNA-sequencing Runs. (a) Representative FACS plot of single, live cells sorted from dissociated Swiss Webster embryonic pancreata and used for

single-cell sequencing. (b) Quality control statistics for all single-cell sequencing runs prepared with the Chromium Single Cell 3' Reagent Version 1 Kit. The “valid barcodes” metric indicates the percentage of cells with barcodes that match a known barcode contained on a bead. “Mapped reads to transcriptome” refers to the percentage of reads that confidently map to a unique gene in the reference transcriptome. “Fraction Reads in Cells” is the percentage of reads that contain a cell-associated barcode. (c) Cellranger cell calls based on the number of UMIs. The dropoff indicates the threshold for the number of UMIs required for a barcode to be considered a cell. (d) Histogram of the number of genes per cell in all single-cell runs pre-filtering steps. (e) Histogram of the number of genes per cell in all single-cell runs post-filtering steps. E17.5 Batch 2 contained a large number of red blood cells, which expressed fewer than 200 genes, resulting in their removal during minimum gene threshold filtering (see Methods).

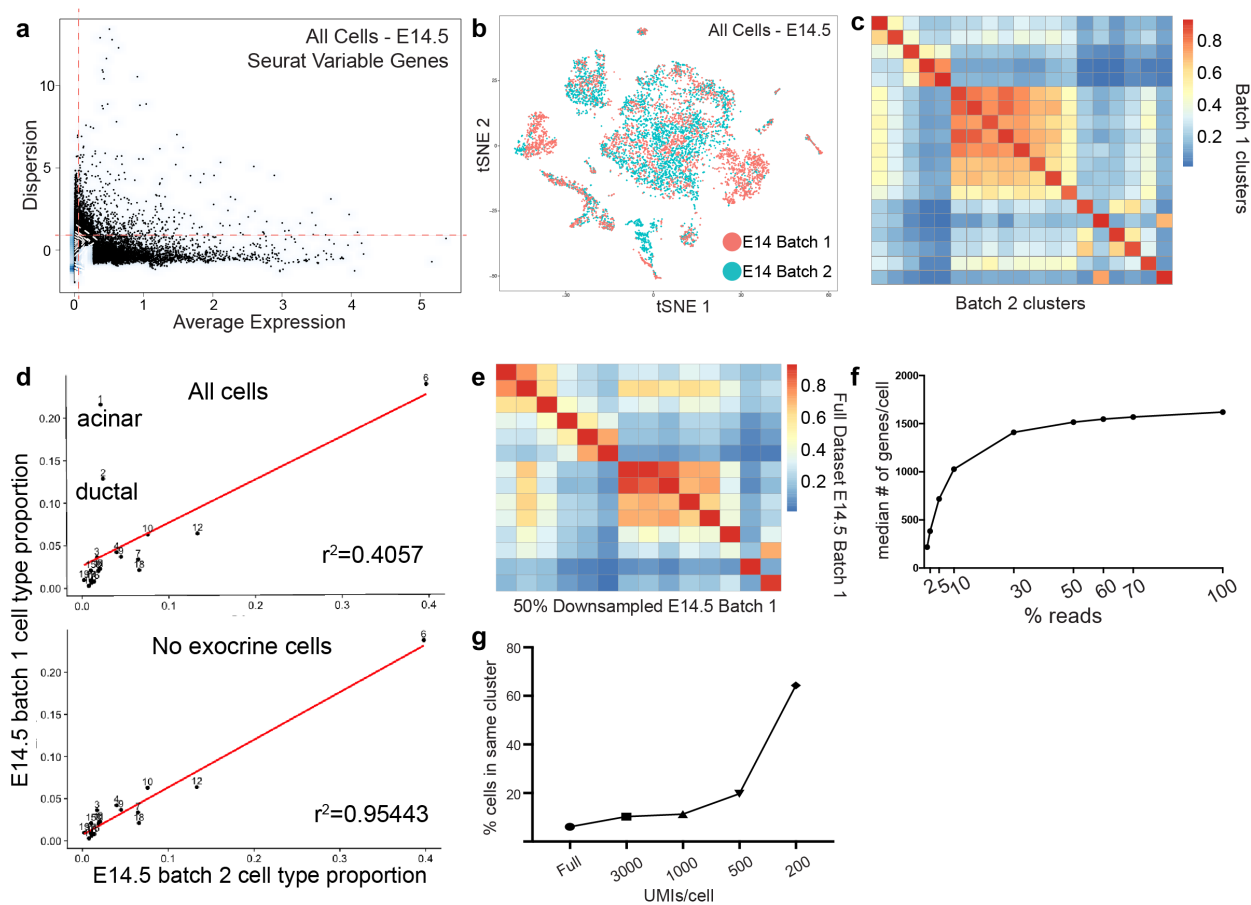


Figure 3. Single-cell RNA-sequencing Batch Information from E14.5 Pancreata. (a) Selection of variable genes in the E14.5 dataset (all cells) by Seurat’s MeanVarPlot function. (b) t-SNE visualization of merged E14.5 batches, color-coded by batch. Batch 1 and 2 contribute to all clusters, reflecting a successful batch correction. (c) Pearson’s correlation of E14.5 batch 1 cells with E14.5 batch 2 cells within each cluster based on average expression of variable genes. Batch 1 cells correlate most highly with batch 2 cells within the same cluster, indicating proper merging of the two batches. (d) Cell type proportions in E14.5 batch 1 and 2 with exocrine

(acinar and ductal) clusters included (top panel) and excluded (bottom panel). All cell types except the exocrine compartment show high correlation between the two batches. (e) Pearson's correlation between clusters from the E14.5 batch 1 full dataset and those from the E14.5 batch 1 dataset downsampled to 50% of the reads, based on average expression of shared variable genes. (f) Maintenance of the number of median genes/cell after random downsampling of reads, indicating sufficient sequencing depth. (g) Maintenance of cluster structure after random downsampling of UMIs is reflected by the similar percentage of cells found within the same cluster with fewer UMIs.

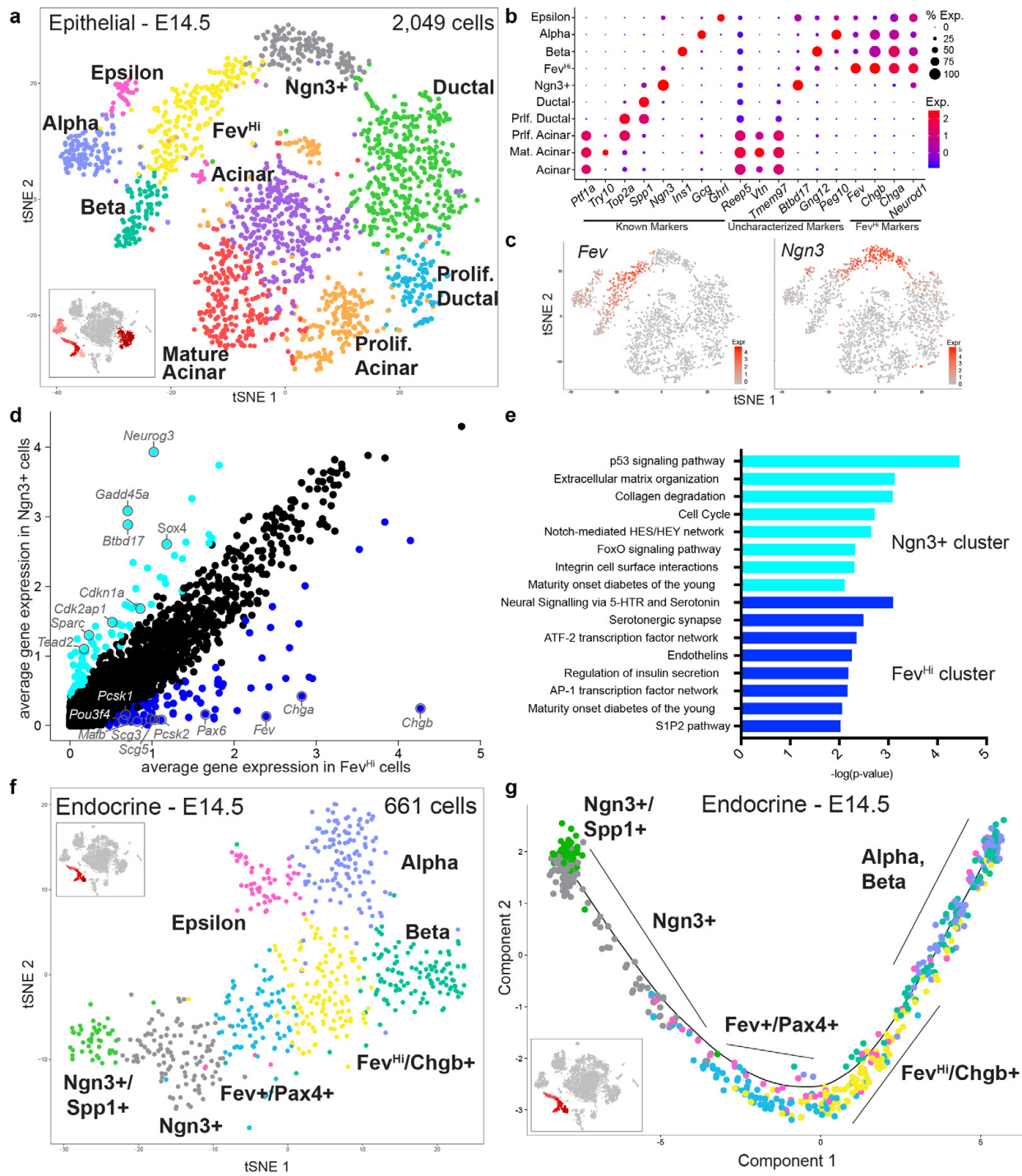


Figure 4: Identification of epithelial cell populations in E14.5 mouse pancreas. (a) t-SNE visualization of epithelial groups only, as defined in Figure 1. (b) Dot plot depicting known and uncharacterized markers of epithelial populations, as well as markers specific to the Fev^{Hi} population. Size of the dot represents proportion of the population that expresses each specified marker. Color indicates level of expression. (c) Expression of *Fev* and *Ngn3* within epithelial cells. Color indicates level of expression. (d) Gene expression comparison between the Ngn3⁺

and Fev^{Hi} population. Genes greater than 2-fold differentially-expressed are highlighted in dark blue (higher in Fev^{Hi} cells) or light blue (higher in $Ngn3^+$ cells). (e) Pathway analysis of genes greater than 2-fold differentially-expressed in $Ngn3^+$ and Fev^{Hi} populations (f) t-SNE visualization of the 661 cells of the endocrine lineage ($Ngn3^+$, Fev^{Hi} , alpha, beta, and epsilon populations). (g) Pseudotime ordering of $Ngn3^+$, Fev^+ / $Pax4^+$, Fev^{Hi} , alpha, and beta cell populations place Fev^+ cells between $Ngn3^+$ and hormone+ populations.

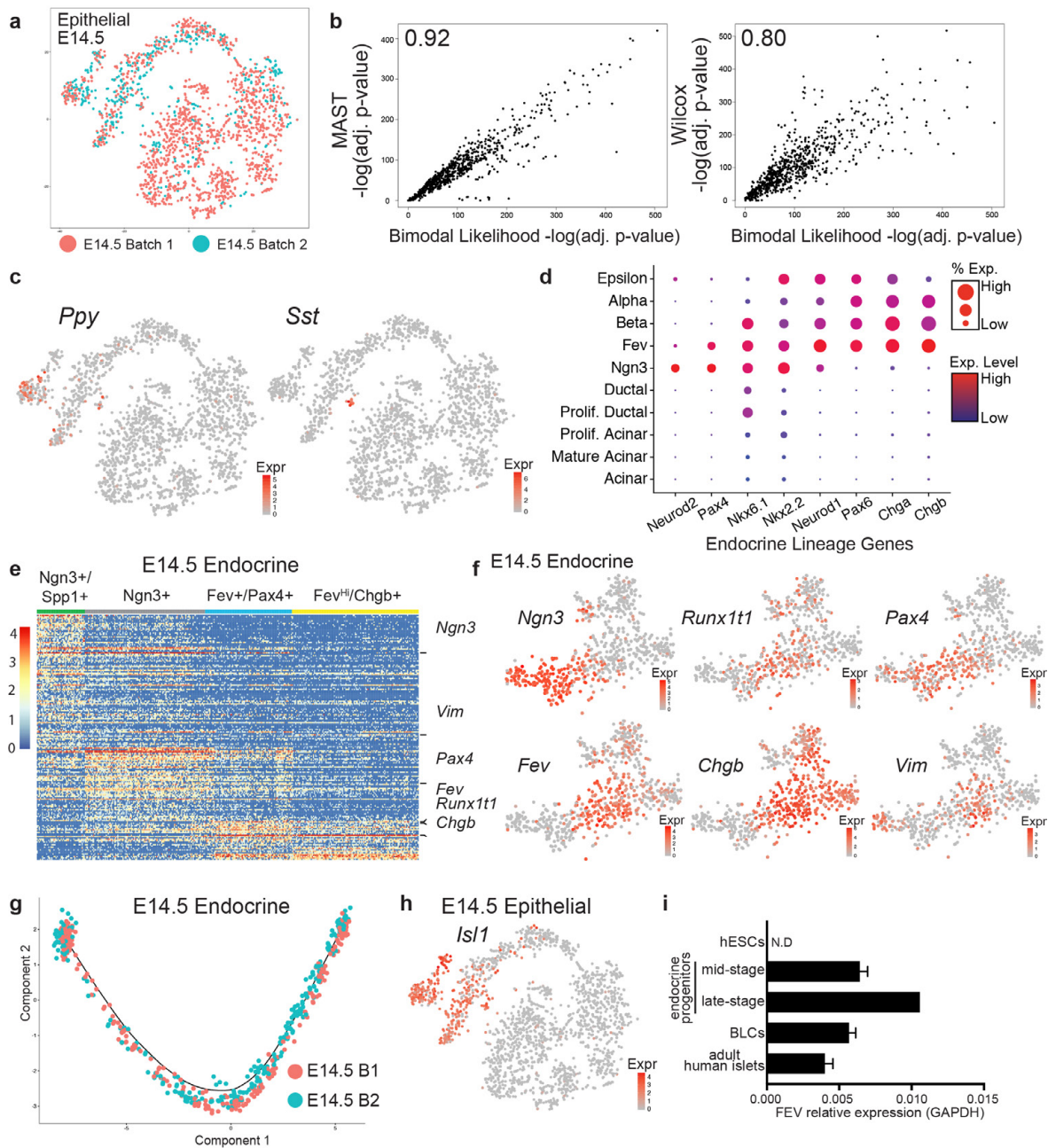


Figure 5. Identification of Known and Novel Epithelial Cell Populations in E14.5 Pancreas. (a) t-SNE visualization of E14.5 epithelial batches, colored by batch. Significant overlap and

most importantly, clusters that include cells from both batches, reflects successful batch correction. (b) Comparison of bimodal likelihood ratio test adjusted p-values to adjusted p-values calculated by either MAST (left panel) or Wilcoxon rank sum (right panel) tests for all greater than 2-fold differentially-expressed genes. Pearson's correlation value is shown in top left corner. (c) Expression maps of *Ppy* and *Sst* hormones within E14.5 epithelial dataset. (d) Dot plot of endocrine lineage genes across the epithelial populations. (e) Heatmap depicting genes over 2-fold differentially-expressed in Ngn3⁺ and Fev⁺ populations. Differentially-expressed genes were determined from the endocrine dataset depicted in Fig. 4f and only Ngn3⁺ and Fev⁺ populations were shown in the heatmap. (f) Expression of selected markers of early- and late-Fev⁺ populations in all endocrine cell lineages. (g) Pseudotime ordering of Ngn3⁺, Fev⁺/Pax4⁺, Fev^{Hi}, alpha, and beta cell populations, colored by batch. (h) Expression of *Islet1* (*Isl1*) in E14.5 epithelial cells is largely confined to hormone⁺ populations. (i) Quantification of *FEV* expression by quantitative RT-PCR in pluripotent hESCs, mid- and late-stage endocrine progenitor cells, beta-like cells (BLCs), and adult human islets. *FEV* expression is normalized to *GAPDH*. Error bars represent standard deviation. N.D = not detected.

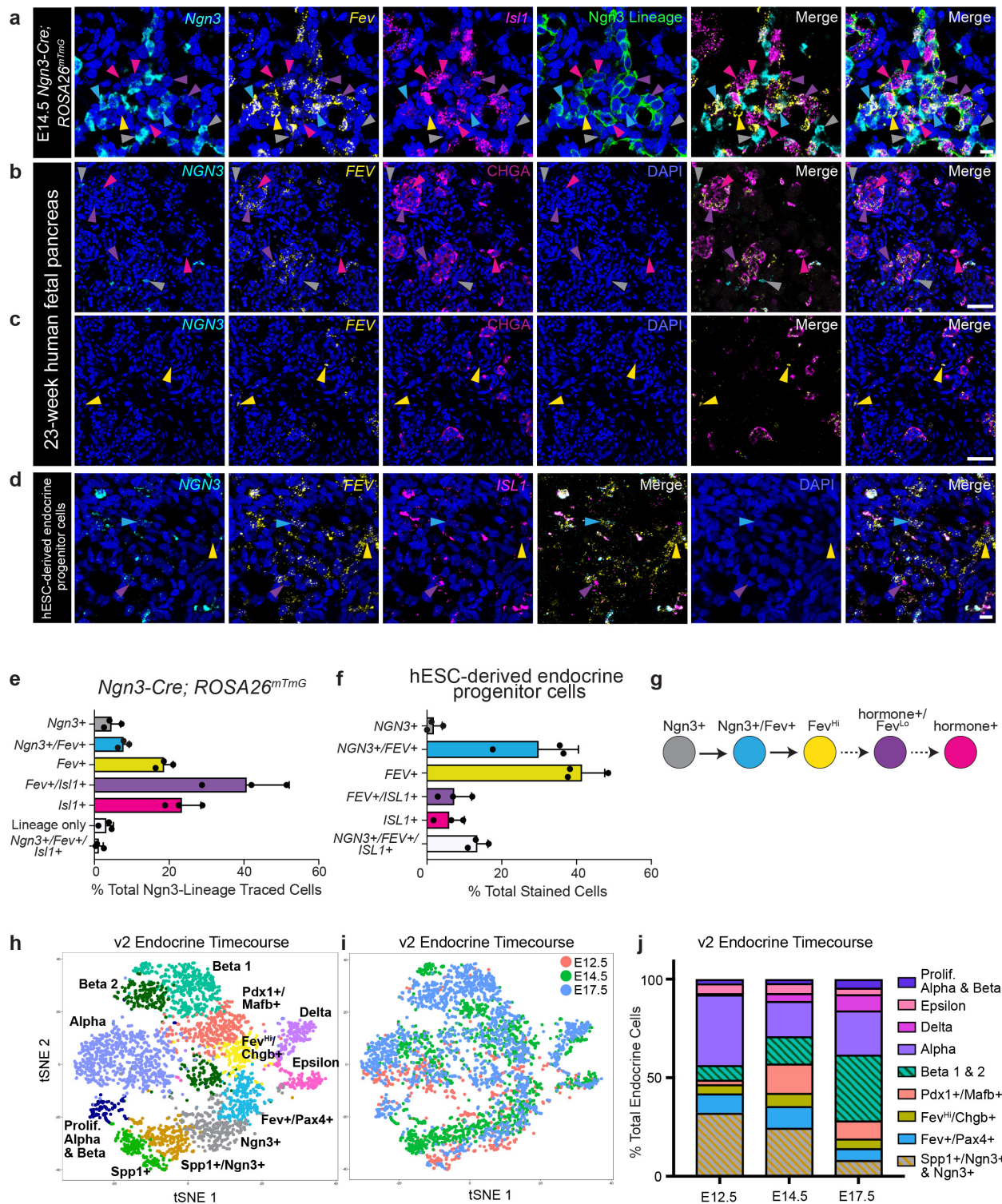


Figure 6. *Fev^{Hi}* cells are endocrine progenitors. (a) *In situ* hybridization (ISH) for *Ngn3*, *Fev*, and *Isl1* in lineage-traced *Ngn3-Cre*; *Rosa26^{mTmG}* E14.5 pancreata where *Ngn3*-lineage traced cells are mGFP+. Grey arrowheads identify *Ngn3*+ cells, presumably not yet *Ngn3*-lineage labeled due to the transient nature of *Ngn3* expression and the delay of Cre-mediated recombination that permits expression of mGFP. Blue arrowheads identify *Ngn3*+/*Fev*+ cells

that are *Ngn3*-lineage traced. Yellow arrowheads identify *Ngn3*-lineage traced cells that are *Fev*⁺ but do not express *Ngn3* or *Isl1*. Purple arrowheads identify *Fev*⁺/*Isl1*⁺ cells that are *Ngn3*-lineage traced. Magenta arrowheads identify *Isl1*⁺ cells that are *Ngn3*-lineage-traced. (b-c) Dual ISH/immunofluorescence (IF) for *NGN3* and *FEV* mRNA and CHGA protein in human fetal pancreas at 23 weeks of gestation (n=1 pancreas). Grey arrowheads identify *NGN3*⁺ cells. Yellow arrowheads identify *FEV*⁺ cells. Purple arrowheads identify *FEV*⁺/CHGA⁺ cells. Magenta arrowheads identify CHGA⁺ cells. (d) Multiplexed fluorescent ISH for *NGN3*, *FEV*, and *ISL1* mRNA in hESC-derived endocrine progenitor cells. Blue arrowheads identify *NGN3*⁺/*FEV*⁺ cells. Yellow arrowheads identify *FEV*⁺ cells. Purple arrowheads identify *FEV*⁺/*ISL1*⁺ cells. (e) Quantification of each population detected in *Ngn3*-lineage traced pancreata as a percentage of *Ngn3*-lineage traced cells (n=464 cells, 6 pancreata). Data are represented as mean + standard deviation (SD). (f) Quantification of each population detected in hESC-derived progenitor cells as a percentage of total stained cells (n=418 cells, 3 clusters representing technical replicates from one hESC differentiation). Data are represented as mean + SD (g) Proposed model for the derivation of *Fev*^{Hi} endocrine cells from *Ngn3*⁺ cells, and their differentiation into hormone⁺/*Fev*^{Lo} endocrine cells. Colors of arrowheads and bars in a-f correspond to cell identity in g. (a and d) Scale bar: 10 μ m. (b and c) Scale bar: 20 μ m. (h) t-SNE visualization of v2 merged endocrine timecourse (E12.5, E14.5, aggregated E17.5). Clusters are annotated based on correlation with v1 dataset or top differentially-expressed genes. (i) Timepoint labels for v2 merged endocrine timecourse data. t-SNE is the same as Fig. 5h. (j) Cell type proportions at each timepoint, calculated from the clusters depicted in Fig. 5h.

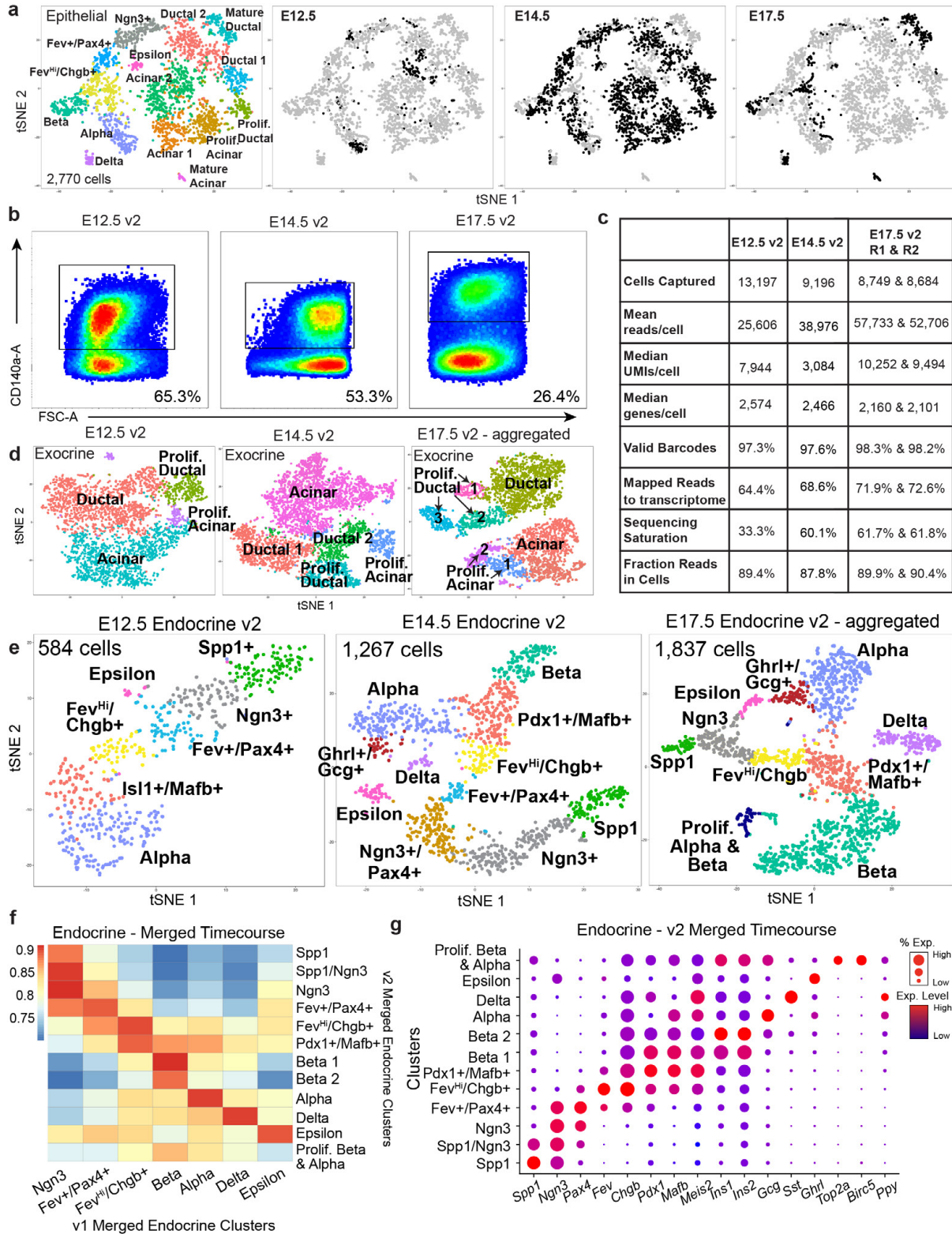


Figure 7. Epithelial Populations over Developmental Time. (a) t-SNE visualization of merged version 1 epithelial clusters from E12.5 (n=18 pancreata), E14.5 (n=14 pancreata for batch 1; n=11 for batch 2), and E17.5 (n=8 pancreata). All panels depict the same t-SNE plot. In the far-

left panel, cluster identity is denoted by different colors. Throughout figure, cells are color-coded by cluster identity. In the three remaining panels, cells from the indicated timepoint are represented by black dots; all cells from the other timepoints are gray. (b) FACS plots depicting CD140a negative selection from E12.5 (n=14), E14.5 (n=13), and E17.5 (n=13) pancreata. CD140a-negative cells were used for single-cell sequencing. (c) Quality control statistics for 10X Chromium version 2 single-cell RNA-sequencing runs. These datasets are referred to as v2 datasets. Two technical replicates of E17.5 cells were run from the same pancreata on two separate wells on the 10X Chromium machine. The two E17.5 runs were aggregated and analyzed as one dataset. (d) Individual t-SNE plots of v2 E12.5, E14.5, and E17.5 (aggregated) exocrine dataset. Clusters are annotated based on gene expression. (e) Individual t-SNE plots of v2 E12.5, E14.5, and E17.5 (aggregated) endocrine dataset. Clusters are annotated based on correlation with v1 datasets and differentially-expressed genes. (f) Pearson's correlation among clusters from v1 merged endocrine timecourse and v2 merged endocrine timecourse. (g) Dot plot of top differentially-expressed genes for clusters in the v2 merged endocrine dataset. Clusters correspond to those depicted in t-SNE in Fig. 6h.

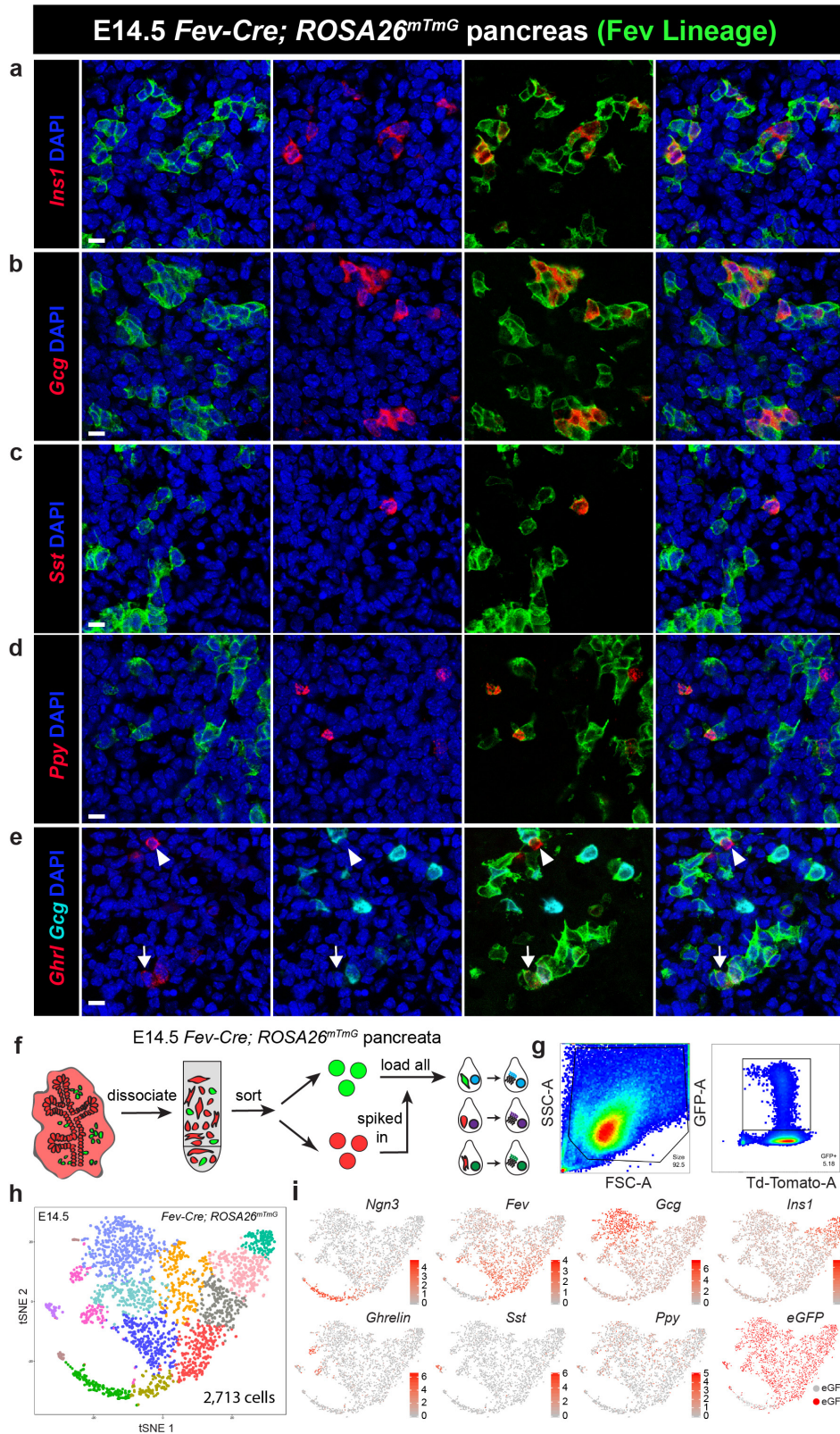


Figure 8. Differentiated, hormone+ endocrine cells transit through a *Fev*-expressing stage during pancreatic development. (a-e) Dual IF (for membrane GFP) and fluorescent ISH for

hormones in *Fev-Cre; ROSA26^{mTmG}* lineage traced animals at E14.5. n=46 cells of 4 pancreata for *Ins1* (100% labeled-lineage); n=103 of 4 pancreata cells for *Gcg* (100% lineage-labeled); n=6 cells of 2 pancreata for *Sst* (100% lineage-labeled); n=26 cells of 2 pancreata for *Ghrl/Gcg* (23.2% lineage-labeled); n=71 cells of 8 pancreata for *Ppy* (90.1% lineage-labeled). Scale bar represents 10um. (f) Schematic of E14.5 *Fev-Cre; ROSA26^{mTmG}* FACS sorting and single-cell RNA-sequencing. (g) Representative FACS plots of sorted single, live GFP+ and TdTomato+/GFP- cells from dissociated pancreata used for single-cell sequencing. (h) t-SNE visualization of endocrine cells in *Fev*-lineage traced E14.5 mouse pancreata (n=3). (i) Expression of major markers of endocrine cell types. Color indicates level of expression, except for the *eGFP* plot, which indicates presence or absence of *eGFP* counts.

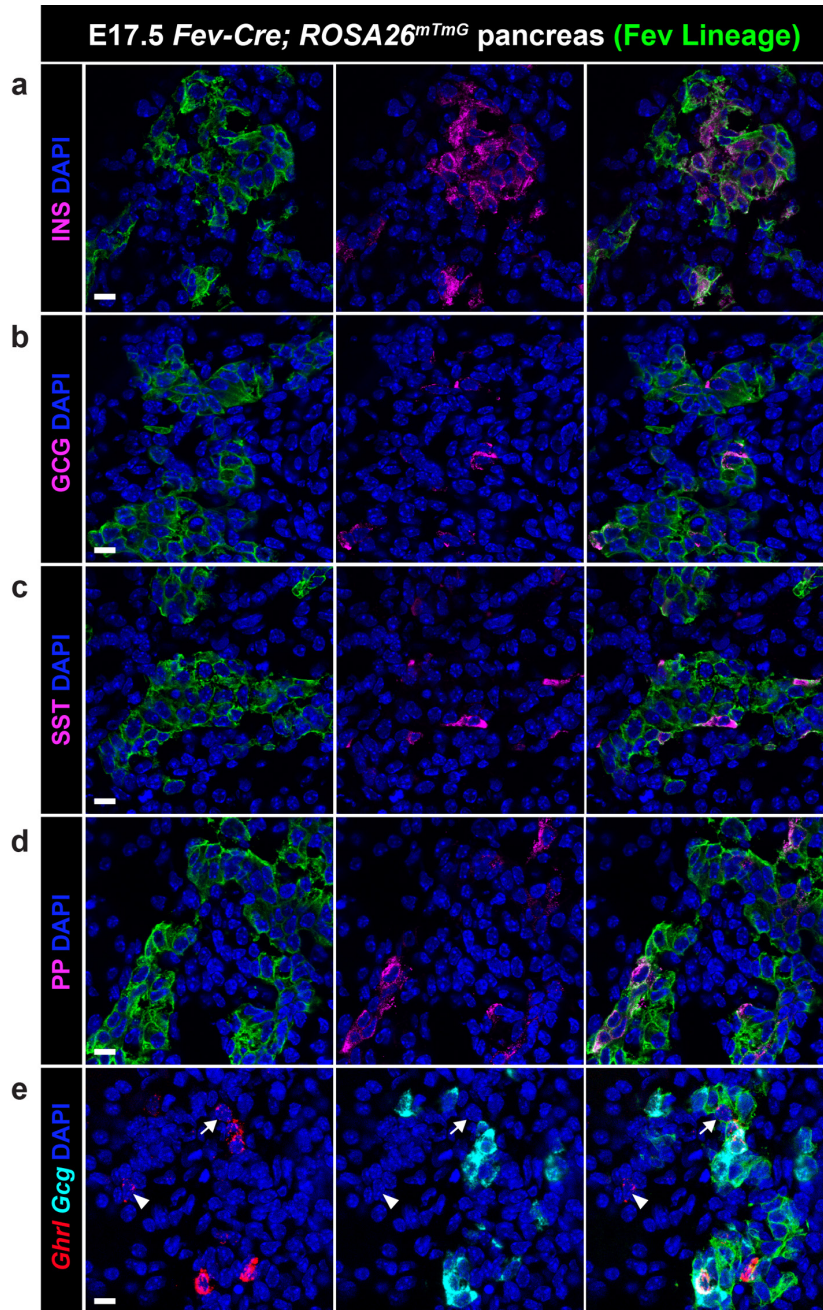


Figure 9. *In vivo* Fev lineage tracing of E17.5 mouse pancreata. (a-d) Immunofluorescence (IF) for hormones INS (100% lineage-labeled), GCG (100% lineage-labeled), SST (96.7% lineage-labeled), and PP (100% lineage-labeled) in embryonic pancreatic hormones in *Fev-Cre*; *ROSA26^{mTmG}* lineage traced animals at E17.5 (n=86 cells of 5 pancreata for INS; n=57 cells of 5 pancreata for GCG; n=30 cells of 5 pancreata for SST; n=47 cells of 5 pancreata for PP). (e) Dual IF (for membrane-GFP) and multiplexed fluorescent ISH for *Ghrl* and *Gcg* in *Fev-Cre*; *ROSA26^{mTmG}* lineage traced animals at E17.5 (n=23 cells of 2 pancreata for *Ghrl*/*Gcg*). *Ghrl*⁺/*Gcg*⁻ cells (47.8% lineage-labeled) represent the epsilon population. Non-lineage labeled epsilon cells are denoted by the arrowheads, and lineage-labeled epsilon cells are denoted by the arrows. Scale bar represents 10um in a-e.

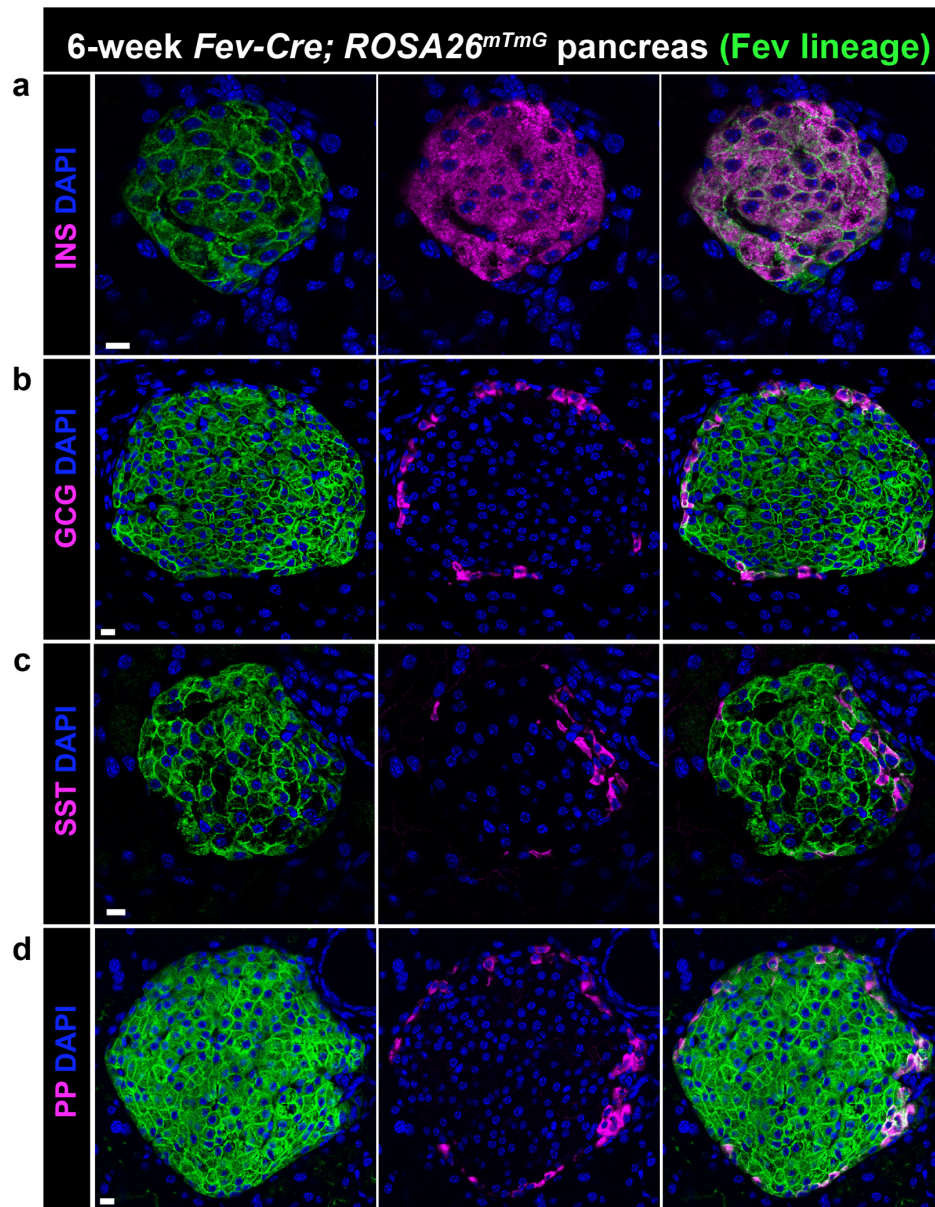


Figure 10. *In vivo* Fev lineage tracing of adult mouse pancreata. (a-d) IF for adult hormones in 6-week *Fev-Cre*; *ROSA26^{mTmG}* lineage-traced pancreas. From one animal: n=172 cells for INS (100% lineage-labeled); n=65 cells for GCG (100% lineage-labeled); n=86 cells for SST (97.7% lineage-labeled); n=30 cells for PP (100% lineage-labeled). Scale bar represents 10um in a-d.

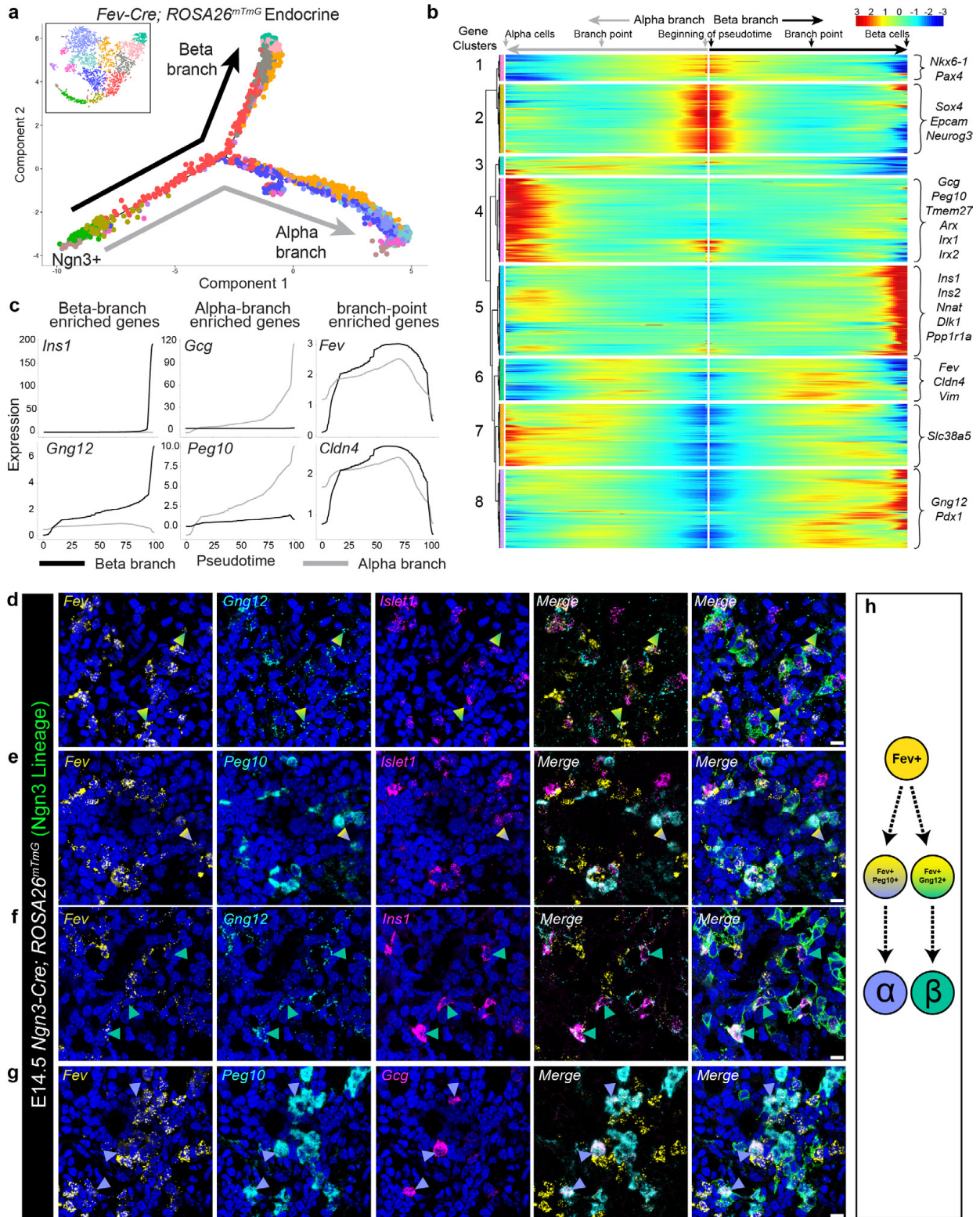
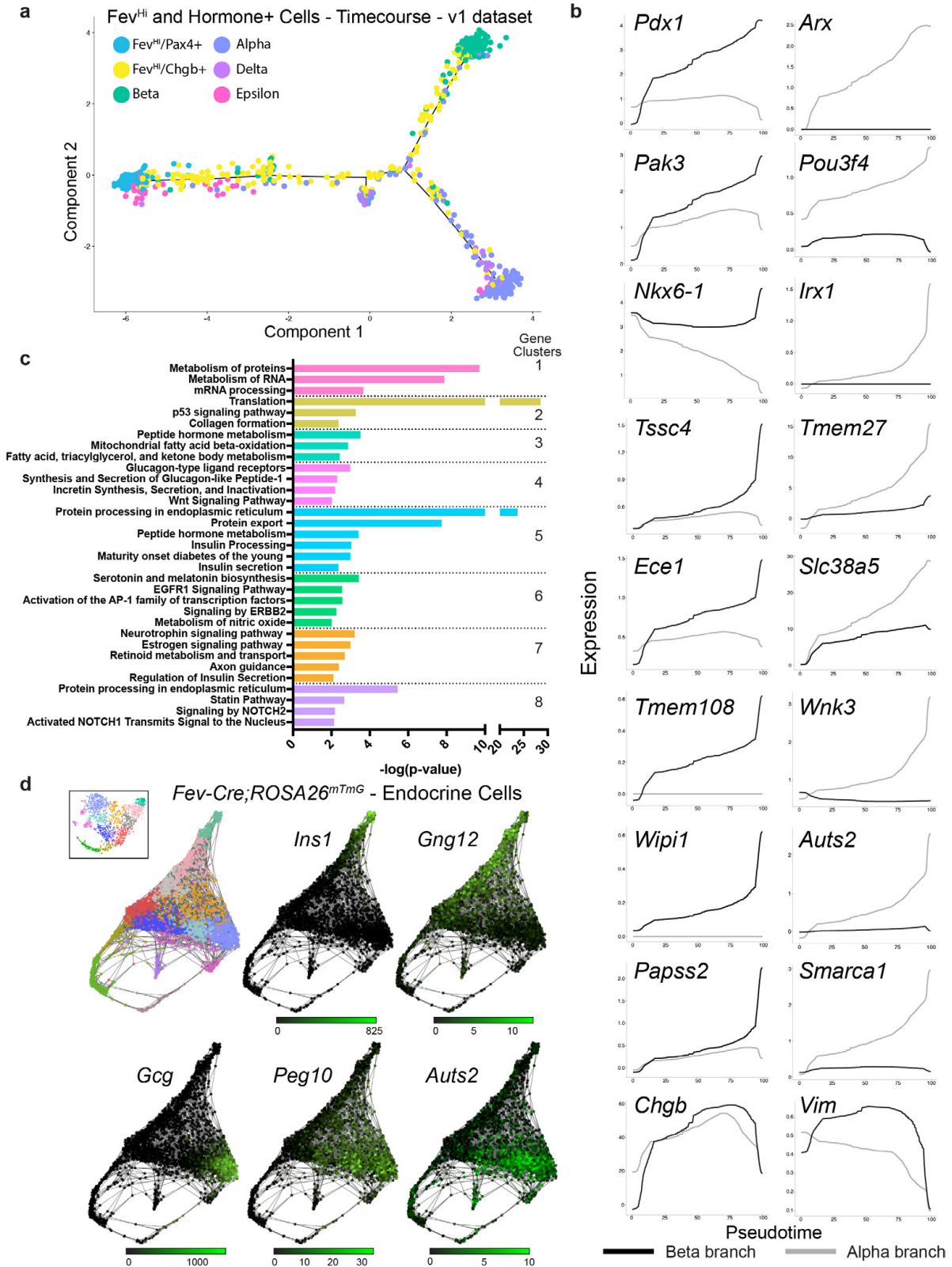


Figure 11. Identification of candidate regulators of beta and alpha cell fate decisions. (a) Pseudotime ordering of the endocrine cells at E14.5 depicted in Fig. 6h yields a bifurcated tree in which the two main branches terminate in cells that highly express *Ins1* (beta cell branch) or *Gcg*

(alpha cell branch). (b) Heatmap depicting the expression of genes along each branch, in pseudotime. An independent expression pattern is calculated across the entire pseudotime trajectory for each branch. Therefore, the portion of the trajectory before the branch point is displayed for each branch separately. Genes are clustered based on expression pattern across pseudotime; selected genes with differential expression along the branches are highlighted to the right. (c) Gene expression plots depicting the kinetic trends along each branch. (d-e) Multiplexed fluorescent ISH for *Fev*, *Gng12*, and *Islet1* (d) or *Fev*, *Peg10*, and *Islet1* (e) in lineage-traced E14.5 *Ngn3-Cre; ROSA26^{mTmG}* pancreas. Arrowheads identify lineage-traced *Fev*⁺/*Islet1*⁻ cells with *Gng12* (d, teal gradient arrowheads) or *Peg10* (e, indigo gradient arrowheads) expression. (f) Multiplexed fluorescent ISH for *Fev*, *Gng12*, and *Ins1*. Teal arrowheads identify lineage-traced *Ins1*⁺ beta cells that express *Gng12*. (g) Multiplexed fluorescent ISH for *Fev*, *Peg10*, and *Gcg*. Indigo arrowheads identify lineage-traced *Gcg*⁺ alpha cells that express *Peg10*. (h) Model for *Fev*^{Hi} (yellow) cell differentiation into distinct alpha or beta cells. *Peg10* and *Gng12* expression in *Fev*^{Hi} cells may represent progenitors pre-fated towards the alpha and beta lineages, respectively, during endocrine lineage allocation. (d-g) Scale bars represent 10 μ m. Blue staining represents DAPI-labeled nuclei. Colors of arrowheads match colors of cells represented in (h).



E12.5, E14.5 (batch 1 and batch 2), and E17.5 datasets. (b) Gene expression plots depicting the kinetic curves of individual genes (from Fig. 7b) across pseudotime in the alpha or beta branches. (c) Pathway analysis for clusters of genes from the BEAM analysis. Gene clusters correspond to Figure 7b. (d) SPRING plots for *Fev*-lineage traced dataset, including all endocrine cells. Colors match those in Fig. 6h and 7a. Expression of selected genes predicted from monocle BEAM analysis.

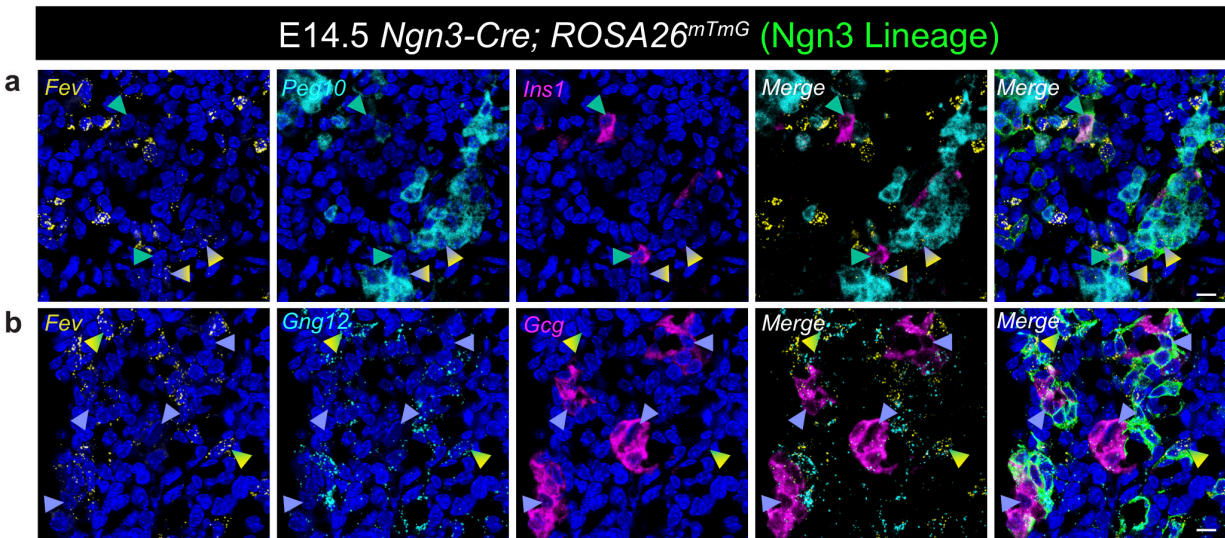


Figure 13. Expression of Candidate Regulators within the Endocrine Lineage Prior to Alpha or Beta Cell Identity. (a) Multiplex fluorescent ISH for *Fev* (yellow), *Peg10* (cyan), and *Ins1* (magenta) in lineage-traced E14.5 *Ngn3-Cre; ROSA26^{mTmG}* pancreas. Indigo-graded arrows highlight lineage-traced *Fev*⁺/*Peg10*⁺ cells that do not express *Ins1*. Teal arrows highlight *Ins1*⁺ beta cells that do not express *Peg10*. (b) Multiplex fluorescent ISH for *Fev* (yellow), *Gng12* (cyan), and *Gcg* (magenta) in lineage-traced E14.5 *Ngn3-Cre; ROSA26^{mTmG}* pancreas. Teal-graded arrows highlight lineage-traced *Fev*⁺/*Gng12*⁺ cells that do not express *Gcg*. Indigo arrows highlight *Gcg*⁺ alpha cells that are not enriched for *Gng12*.

Chapter 3

Mesenchymal heterogeneity and lineage relationships in the developing pancreas

Introduction

While previous studies have identified numerous markers of pancreatic epithelial populations (Pan & Wright, 2011), comparatively little is known about heterogeneity among pancreatic mesenchymal cells. Across the body, mesenchymal cells continue to be a poorly understood cell type. The definition of a mesenchymal cell is based on their cellular origin, morphology and organization, and aspects of their behavior. First, mesenchymal cells are generally derived from the mesoderm germ layer, although mesenchymal cell types of the craniofacial region are neuroectoderm-derived (Gilbert, 2000). Mesenchymal cells are often described as “spindle-shaped”, with long, thin processes and display a loosely packed organization. While the organization of epithelial cells in adherent sheets limits their mobility, mesenchymal cells are highly migratory. Finally, upon isolation and culture, mesenchymal cells attach to plastic. These relatively undefined characteristics of mesenchymal cells have led to ambiguity in their identification and study across the body.

The pancreatic mesenchyme refers to the cells that condense around the budding epithelium by E9. Endothelial cells and nerves, although important non-epithelial cells involved in pancreatic development, are not considered to be a part of the pancreatic mesenchyme. Both the dorsal and ventral pancreatic bud are surrounded by mesenchymal cells, and few studies have attempted to describe the similarities or differences of these groups. The gene *islet1* (*Isl1*) has been shown to mark mesenchymal cells of the dorsal bud, but not the ventral bud (Ahlgren, Pfaff, Jessell, Edlund, & Edlund, 1997). Similarly, *N-Cadherin* is expressed in a dorsal-ventral gradient within the pancreatic mesenchyme, with highest expression in dorsal mesenchyme (Esni, Johansson, Radice, & Semb, 2001). Functionally, *Isl1* and *N-Cadherin* are only required for dorsal pancreatic development. Upon fusion of the dorsal and ventral bud, whether this

mesenchymal heterogeneity is maintained is unknown. Indeed, most studies have utilized techniques that treat the mesenchymal cells as one homogenous entity, resulting in very little information about the heterogeneity within this compartment during pancreatic development.

One approach to uncovering cellular heterogeneity within a group of cells is by fluorescence-activated cell sorting (FACS). This methodology uses fluorescence-activated antibodies to cell surface markers to sort individual cells into separate tubes. Once separated, distinct populations of cells can be analyzed for specific characterized or analyzed by unbiased methods such as bulk RNA-sequencing. Although commonly applied to other systems, the limited number of cell surface markers that are expressed in subpopulations of the pancreatic mesenchyme has hindered the success of this approach in the pancreas. Screening of genes by *in situ* hybridization has been employed to identify subtypes of pancreatic epithelial cells (Q. Zhou et al., 2007). Extensive time and labor are required for screening all the genes within the genome by staining approaches. Therefore, most staining approaches select a subset of genes to test, such as transcription factors, potentially biasing the ability to discover novel heterogeneity in some cellular compartments. These challenges have resulted in very little knowledge of pancreatic mesenchyme subtypes.

To overcome the challenges of prior approaches, we utilized single-cell RNA-sequencing to assess the cellular and transcriptional heterogeneity of the developing pancreatic mesenchyme. A major benefit of this approach is that it does not rely on known markers to capture and identify cell types. Rather, all cells of the pancreas can be captured and sequenced, and bioinformatically sorted into individual populations. Additionally, compared to staining-based screening approaches, single-cell RNA-Sequencing is a transcriptome-wide technique and thus does not require the selection of subsets of genes to test.

Using an unbiased, single-cell RNA-sequencing approach, we are able to identify multiple distinct mesenchymal subpopulations and define their transcriptomic signatures across developmental time. We find that a particular mesenchymal population, the mesothelium, displays timepoint-specific transcriptomic signatures, suggesting that it may have multiple functions throughout pancreatic development. *In silico* lineage modeling of a subset of the identified mesenchymal populations predicts the derivation of vascular smooth muscle-related populations from the pancreatic mesothelium. Furthermore, the *in silico* model highlights multiple putative progenitor stages that mesothelial cells transit through during differentiation towards a vascular smooth muscle fate. These results begin to divide the mesenchyme into distinct cellular populations and assemble potential lineage relationships among them, allowing for future studies to more easily target and manipulate mesenchymal subpopulations.

Results

Characterization of mesenchymal heterogeneity

We characterized the mesenchymal compartment by sub-clustering only mesenchymal cells (5,069 cells) from the original E14.5 dataset (see Chapter 2) and re-performing the clustering analysis (Fig. 14a and Fig. 15a). Despite being less divergent from one another than were cells in the epithelial compartment (Fig. 14b and Fig. 15b), mesenchymal cells could still be sub-divided into 10 transcriptionally distinct mesenchymal clusters (Fig. 14a,c). We verified the differential gene expression analysis with three tests: bimodal likelihood ratio test (McDavid et al., 2012), Wilcoxon rank sum, and MAST (Finak et al., 2015) (Fig. 15c). We annotated two clusters based on the expression of known marker genes: cluster 1 is pancreatic mesothelial cells (*Wt1*, *Krt19*, and *Upk3b*) (Kanamori-Katayama et al., 2011; Winters & Bader, 2013) and cluster

3 represents vascular smooth muscle (VSM) cells (*Acta2*, *Tagln*, and *Myl9*) (Fig. 14c) (Majesky, Dong, Regan, Hoglund, & Schneider, 2011). Indeed, in E14.5 pancreas, WT1 expression was restricted to the tissue edge, as expected for mesothelial cells, while ACTA2 expression was localized to cells surrounding vessels, as expected for VSM cells (Fig. 15d,e). Cells in the mesothelial cluster also expressed the secreted factors *Fgf9*, *Pdgfc*, *Rspo1*, and *Igfbp5* (Fig. 15f) and genes regulating prostaglandin hormone signaling and tight junctions (Fig. 14d).

The remaining mesenchymal clusters included proliferating cells (clusters 6, 7, and 8), a large cluster (10) expressing pan-mesenchymal markers, and four clusters (2, 4, 5, and 9) each expressing a signature distinct from that of cluster 10 (Fig. 14a,c). Cluster 2 was defined by differential expression of *stathmin 2* (*Stmn2*), a gene involved in neurite outgrowth and osteogenesis (Chiellini et al., 2008; Grenningloh, Soehrman, Bondallaz, Ruchti, & Cadas, 2003). We also found two populations, clusters 4 and 5, that differentially expressed multiple secreted factors. Cluster 4 expressed *Ace2*, the chemokines *Cxcl12* and *Cxcl13*, and *Vegfd*, while cluster 5 expressed high levels of the WNT antagonists *secreted frizzled-related protein 1 and 2* (*Sfrp1* and *Sfrp2*) (Fig. 14c-e). Cluster 5 also expressed the transcription factor *barH-like homeobox 1 1* (*Barx1*) and members of the Id DNA-binding protein family (Fig. 14c-e). Cluster 9 expressed *Nk2 homeobox 5* (*Nkx2-5*) and *Tlx1*, transcription factors reported to contribute to splenic development during a window in which the embryonic pancreas and spleen share a mesenchymal compartment (Fig. 14c) (Hecksher-Sørensen et al., 2004). Pathway analysis identifies multiple signaling pathways that may be functionally relevant in these populations (Fig. 14d). We validated a subset of these distinct clusters using dual *in situ* hybridization/immunofluorescence (ISH/IF) on E14.5 pancreas for differentially-expressed markers of clusters 1 (*Cav1* and *Barx1*), 2 (*Stmn2*), and 5 (*Barx1*) (Fig. 14e-h). These gene expression profiles demonstrate a previously

underappreciated level of heterogeneity in the mesenchymal compartment of the developing pancreas.

Mesothelial cells undergo changes across developmental time

During organogenesis, the dynamics of each lineage are defined by the expansion, differentiation, and maturation of its constituent cells. To address how these processes change across chronological time within the developing pancreas, we performed single-cell sequencing at two additional timepoints, E12.5 and E17.5 (Fig. 16a). We identified mesenchymal cells from E12.5, E14.5, and E17.5 timepoints, merged them into one dataset, and re-performed the clustering analysis. We identified the clusters detected in our E14.5 analysis (clusters 1-10) along with seven new clusters (11-17) (Fig. 16a and Fig. 15g-i). The addition of E12.5 and E17.5 cells revealed further sub-division of the mesothelium into timepoint-specific clusters (1, 11, and 17), each with unique transcriptomic signatures (Fig. 16a,b). Within the mesothelium, we verified *paired-like homeodomain transcription factor 2 (Pitx2)* expression at E12.5 and its absence at E17.5 and *mesothelin (Msln)* expression at E17.5 and its absence at E12.5 (Fig. 16c), consistent with the single-cell data. These data provide evidence of transcriptional maturation over developmental time within the mesothelial compartment.

While the mesothelium is a well-established mesenchymal progenitor cell population for VSM and fibroblasts in multiple other organs, both the role of the mesothelium and the origin of the mesenchymal cell types within the pancreas remain uncharacterized (Asahina, Zhou, Pu, & Tsukamoto, 2011; Bin Zhou et al., 2008; Que et al., 2008; Wilm, Ipenberg, Hastie, Burch, & Bader, 2005). We utilized our single-cell mesenchymal dataset to determine whether the pancreatic mesothelium may function as a mesenchymal progenitor cell population during

development. We found six populations (clusters 2, 3, 4, 5, 12, and 13) that expressed VSM cell genes, such as *Acta2* and *Tagln*, or genes known to regulate VSM development, such as *Mgp* (Speer et al., 2009), *Fhl1* (Kwapiszewska et al., 2008; L.-L. Wang et al., n.d.), *Barx1* (Jayewickreme & Shivdasani, 2015), and *Pitx2* (Shang, Yoshida, Amendt, Martin, & Owens, 2008) (Fig. 16d). Based on these VSM-related gene expression profiles, we hypothesized that these populations could represent VSM progenitors derived from the pancreatic mesothelium. To test the lineage relationships among these populations, we ordered cells in pseudotime based on their transcriptional similarity (X. Qiu et al., 2017b). This analysis placed mesothelial cells on one side of the pseudotime trajectory (Fig. 16e). Mesothelial branches corresponded to either a maturation process, based on placement of E17.5 cells at the branch terminus, or proliferating mesothelium, based on expression of proliferation genes (Fig. 16e and Fig. 15j). VSM-related populations were placed on the other side of the trajectory (Fig. 16e and Fig. 15j). We calculated the proportion of each population over pseudotime and found a transition from the E12.5 mesothelial population (cluster 11) to cluster 12, both of which share expression of the gene *Pitx2* (Fig. 16e-g). Cluster 12 then transitioned into the *Stmn2*-expressing cluster 2, which split into a branch composed of VSM populations, clusters 3 and 13 (Branch 1), and a branch composed of clusters 4 and 5 (Branch 2) (Fig. 16e-g). Thus, this analysis proposes clusters 2 and 12 as potential mesothelial-derived mesenchymal progenitor populations that can contribute to the VSM lineages (Fig. 16g). Our analysis has identified and validated multiple mesenchymal subtypes and possible lineage relationships among them.

Discussion

The mesenchyme is critical for epithelial specification and proliferation throughout pancreatic development (Bhushan et al., 2001; Golosow & Grobstein, 1962; Landsman et al., 2011), yet the individual cell types responsible for these processes remain unidentified. Our single-cell dataset has enabled the identification of multiple mesenchymal subpopulations and gene candidates for regulating epithelial-mesenchymal interactions. Secreted factors, such as mesothelial-derived FGF9, may play a similar role in the pancreas as in the lung (see Chapter 4), where it regulates mesenchymal cell proliferation and vascular formation (Yin, Wang, & Ornitz, 2011). Additionally, secretion of WNT antagonists by cluster 5 may regulate WNT signaling in the developing pancreas, influencing processes such as epithelial specification, expansion, and exocrine development (Murtaugh, 2008). Future work can focus on uncovering the functions of these individual mesenchymal populations in development, physiology, and pathology of the pancreas.

With the cell types of the mesenchyme now enumerated and their markers identified, we can begin to elucidate the maturation and lineage relationships across the pancreatic mesenchymal compartment. Our timecourse data have provided evidence of maturation within the mesothelial population. Genes such as *Pitx2*, *kallikren 13 (Klk13)* and 8 (*Klk8*), were differentially expressed in younger, E12.5 mesothelial cells. *Pitx2* regulates differentiation in multiple systems (Cao et al., 2013; Hernandez-Torres, Rodríguez-Outeiriño, Franco, & Aranega, 2017; Shang et al., 2008), and the kallikren family are serine proteases involved in extracellular matrix and adhesive molecule degradation (Kapadia, Ghosh, Grass, & Diamandis, 2004). Expression of these genes suggests that the E12.5 mesothelial population may be primed for migration and differentiation. In contrast, the E17.5 mesothelial population expressed genes

related to barrier or immune function, such as *dermokine (Dmkn)* (Hasegawa et al., 2013; Huang et al., 2017), *bone marrow stromal antigen 2 (Bst2)*, and *retinoic acid receptor responder 2 (Rarres2)* (Ernst & Sinal, 2010). These results suggest stage-dependent roles for the mesothelium throughout development.

The different roles for the mesothelium across time are also evident from our pseudotime analysis, which proposes that the mesothelium serves as a progenitor for other mesenchymal cell types during development. The mesothelium is a critical mesenchymal progenitor population in other organs, such as the heart, intestine, lung, and liver (Asahina et al., 2011; Bin Zhou et al., 2008; Que et al., 2008; Wilm et al., 2005). Our data suggest that mesothelial progenitor activity occurs at E12.5 or earlier during pancreatic development, consistent with other organ systems (Bin Zhou et al., 2008; Que et al., 2008; Winters & Bader, 2013). Indeed, a recent study identified that parietal mesothelial cells can function as progenitor cells prior to pancreatic specification (Angelo & Tremblay, 2018). The transcriptomic information obtained by this study will allow the development of tools to target individual populations within the mesenchyme and perform lineage tracing, ablation, and expression studies *in vivo*. Furthermore, this developmental dataset can be compared to mesenchymal population dynamics during adult disease progression, where aberrant recapitulation of developmental pathways can lead to disease states in the pancreas (Jensen et al., 2005; Rhim & Stanger, 2010). Thus, this dataset is a broad resource for the implementation of future studies in pancreatic mesenchymal biology.

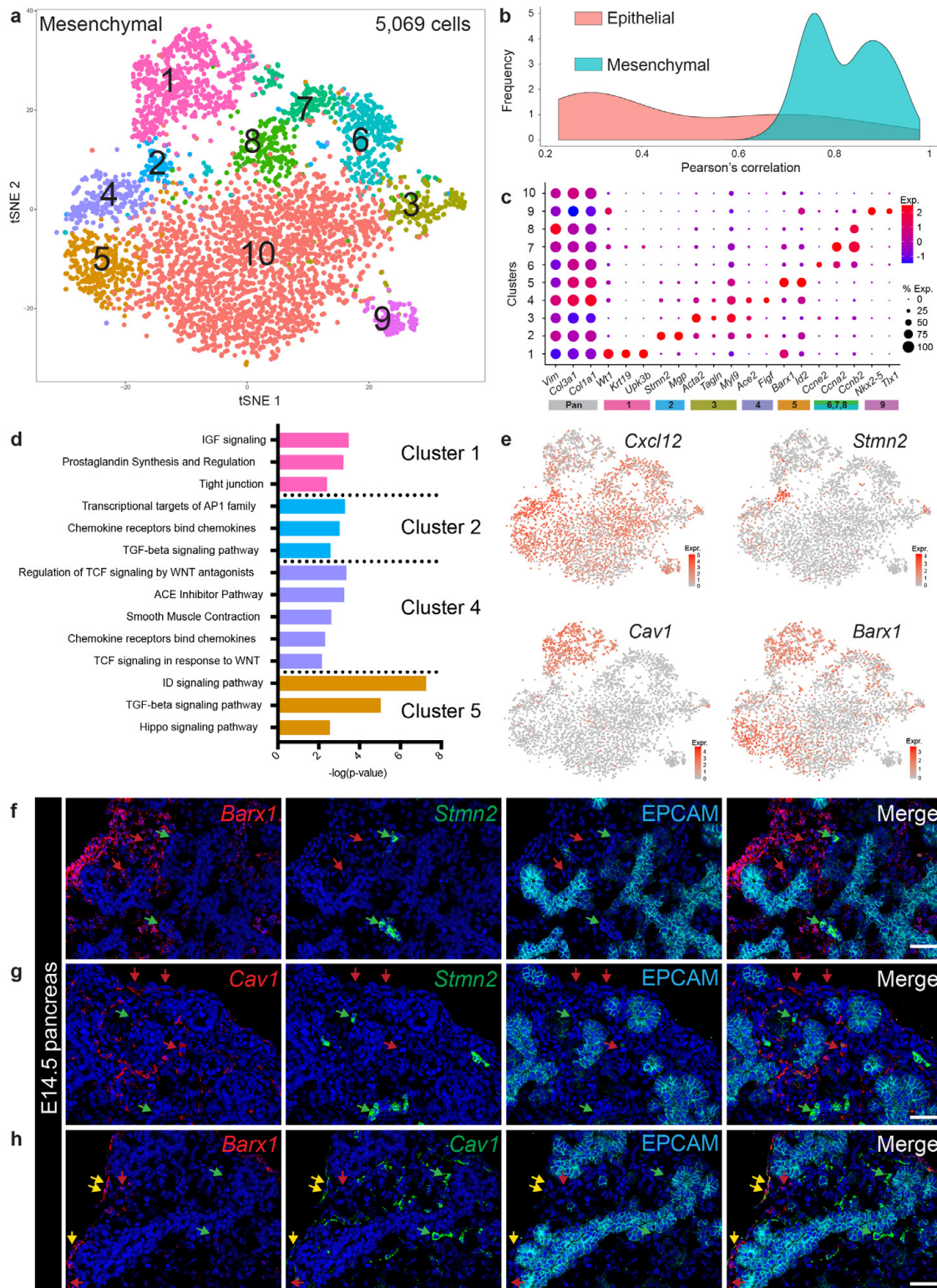


Figure 14: Identification of multiple uncharacterized mesenchymal populations. (a) t-SNE visualization of subclustered E14.5 mesenchymal clusters (from n=14 pancreata). (b) Density plot depicting Pearson's correlation values (depicted in heatmap in Fig. 15b) within the epithelial

and mesenchymal populations based on average gene expression in each cluster. (c) Dot plot of top differentially-expressed markers of each mesenchymal population. Bars are color-coded by cluster identity in (a). The grey bar represents pan-mesenchymal markers. The size of each dot represents the proportion of cells within a given population that expresses the gene; the intensity of color indicates the average level of expression. (d) Pathway analysis of genes greater than 2-fold differentially-expressed by cells in clusters 1, 2, 4, and 5. (e) Expression of genes marking clusters 1 (*Cav1*), 2 (*Stmn2*), 4 (*Cxcl12*), and 5 (*Barx1*) in all E14.5 mesenchymal cells. Color intensity indicates level of expression. (f-h) Multiplexed fluorescent ISH combined with EPCAM IF validates clusters 2 and 5 (e) and cluster 1 (f-g). EPCAM marks pancreatic epithelium. In (f), *Barx1*⁺ cells (red arrows, cluster 5) are distinct from *Stmn2*⁺ cells (green arrows, cluster 2), validating the single-cell data. In (g), *Cav1*⁺ cells (red arrows, cluster 1) are distinct from *Stmn2*⁺ cells (green arrows, cluster 2). In (h), *Barx1*⁺ cells that do not express *Cav1* (red arrows) represent cluster 5, whereas *Barx1*⁺/*Cav1*⁺ cells (yellow arrows) represent cluster 1. *Cav1*⁺ cells that do not express *Barx1* are also identified (green arrows), likely representing endothelial cells (Frank, 2003). Scale bar represents 50 μ m in f-h.

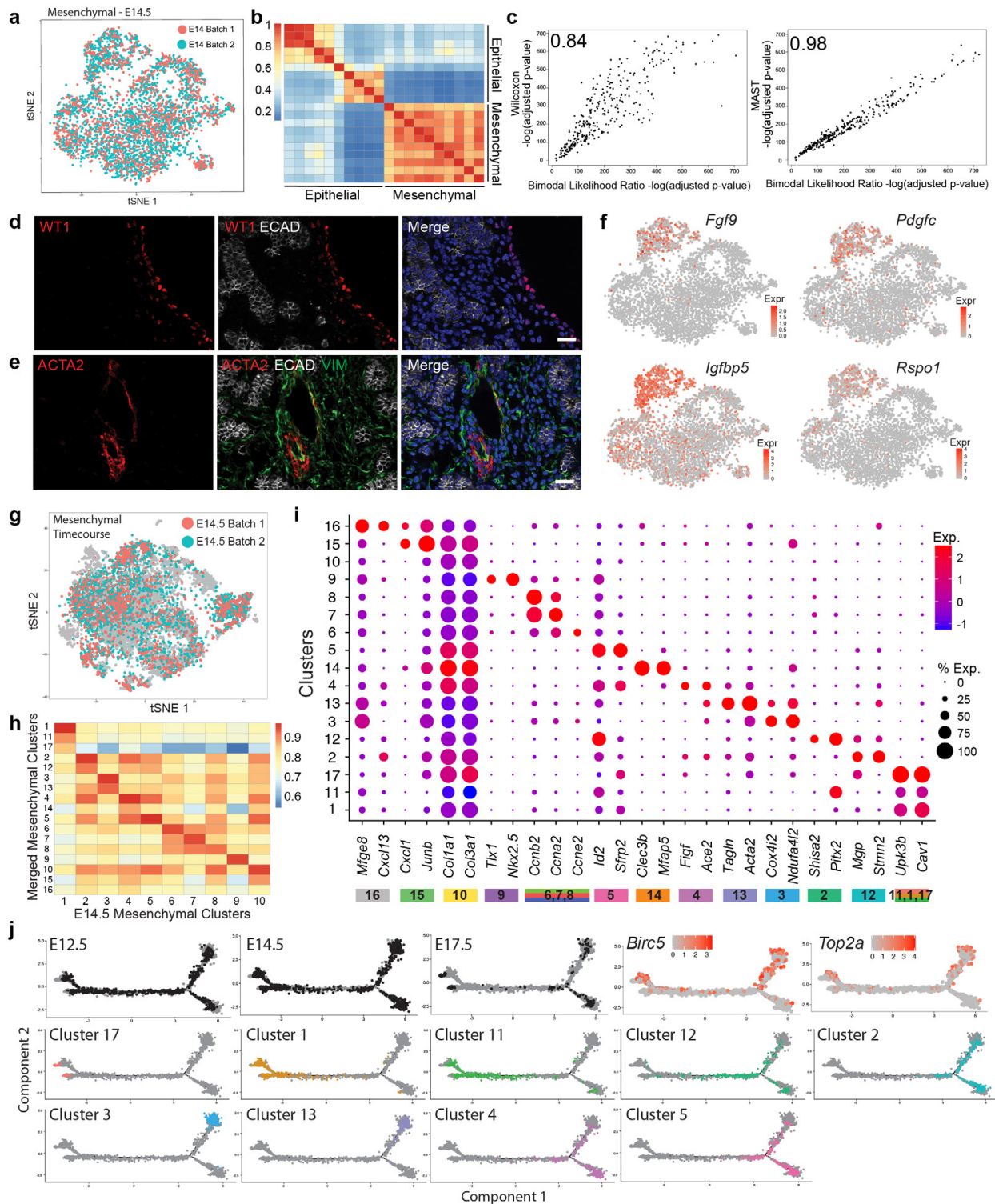


Figure 15. Transcriptomic Signatures and Lineage Dynamics among Mesenchymal Populations. (a) t-SNE visualization of E14.5 biological replicates, colored by batch, demonstrating effectiveness of batch correction. (b) Pearson's correlation of E14.5 epithelial and mesenchymal clusters based on average expression of variable genes. (c) Comparison of bimodal likelihood ratio test adjusted p-values to adjusted p-values calculated by either MAST (left

panel) or Wilcoxon rank sum (right panel) tests for all greater than 2-fold differentially-expressed genes. Pearson's correlation value is shown in top left corner. (d,e) IF validation of (d) mesothelium (Wt1+) and (e) vascular smooth muscle (Acta2+) cells in E14.5 pancreata. ECADHERIN (ECAD) marks epithelium, and VIMENTIN (VIM) marks mesenchyme. Scale bar: 50 μ m. (f) Expression of secreted factors within the mesothelium. Color indicates level of expression. (g) t-SNE visualization of merged mesenchymal timecourse dataset. E14.5 biological replicates are colored, serving as a measure of batch correction effectiveness within the merged mesenchymal timecourse dataset. Grey dots represent both E12.5 and E17.5 cells. (h) Correlation of E14.5 mesenchymal populations with merged (E12.5, E14.5 and E17.5) mesenchymal clusters based on average expression of the variable genes from all datasets. Merged populations were matched with E14.5 (Fig. 2) by highest correlation and assigned the same cluster identity (cluster 1-10). Remaining merged clusters were assigned cluster identities 11-17. (i) Dot plot of differentially-expressed genes from each merged mesenchymal cluster. Colored bars correspond to t-SNE in Fig. 14a (j) Contribution of cells from each timepoint is mapped onto pseudotime plots. Expression of proliferation markers, *Birc5* and *Top2a*, in the pseudotime trajectory. Color indicates level of expression. Contribution of cells from each timepoint is broken down by individual cluster and mapped onto pseudotime plots. Colors correspond to cell clusters in Fig. 14a,e.

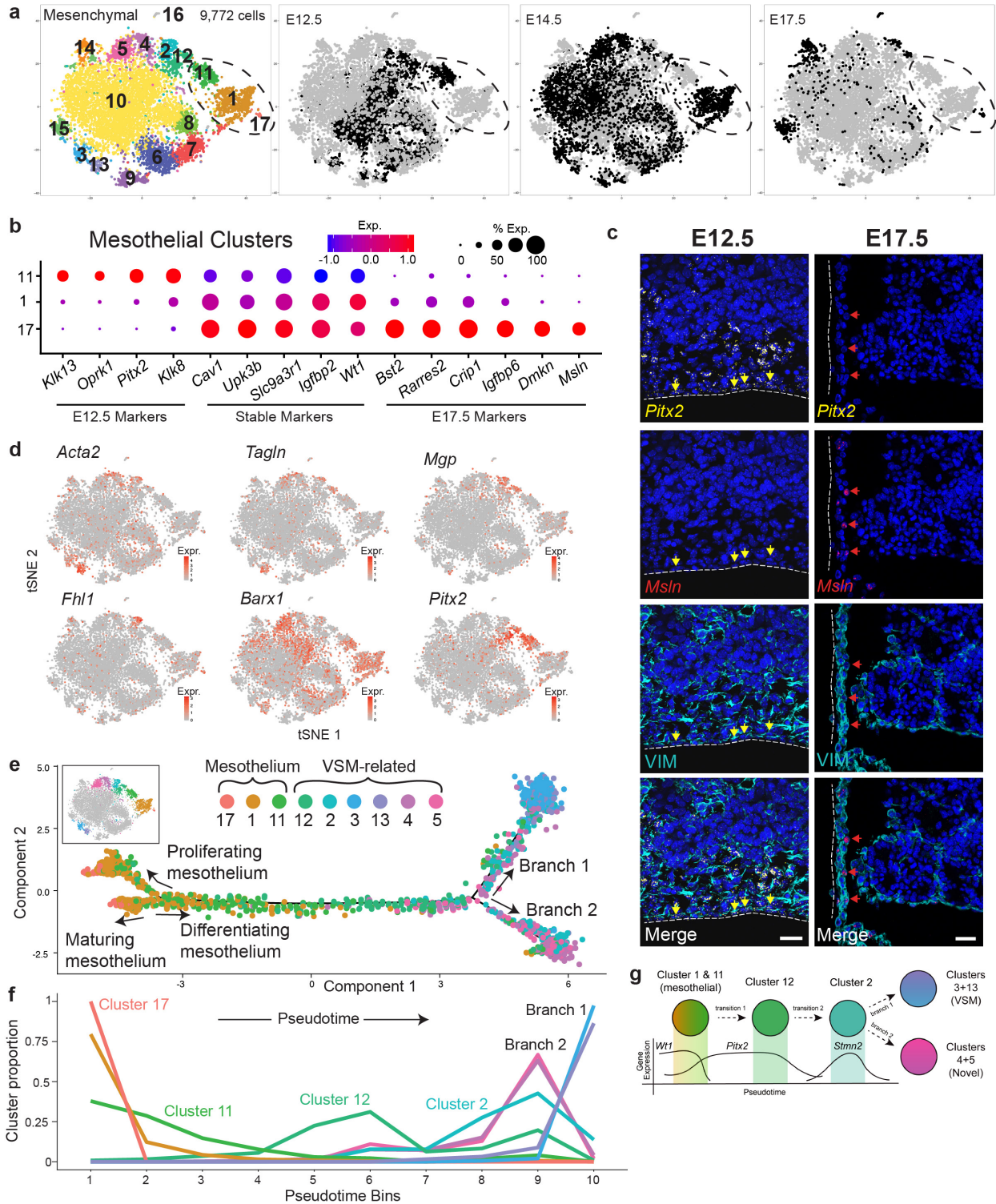


Figure 16. Mesothelial cells are dynamic over developmental time and are predicted to give rise to vascular smooth muscle populations. (a) t-SNE visualization of merged mesenchymal clusters from E12.5 (n=18 pancreata), E14.5 (n=14 pancreata for batch 1; n=11 for batch 2), and E17.5 (n=8 pancreata) tissue. Mesenchymal clusters were identified at each timepoint,

subclustered, merged together, and reanalyzed. Cells are colored by cluster or timepoint. Dotted circle highlights timepoint-segregated mesothelial clusters. (b) Dot plot of top differentially-expressed genes in timepoint-specific mesothelial clusters (clusters 1, 11, and 17). Size of the dot represents proportion of the population that expresses each specified marker. Color indicates level of expression. (c) ISH for *Pitx2* and *Msln* in E12.5 and E17.5 pancreata. *Pitx2* expression was detected in E12.5 but not E17.5 mesothelium, whereas *Msln* was detected in E17.5 but not E12.5 mesothelium. VIMENTIN (VIM) IF staining depicts pancreatic mesenchyme. Dotted line indicates tissue boundary. Yellow arrows identify *Pitx2*⁺ mesothelial cells. Red arrows identify *Msln*⁺ mesothelial cells. Scale bar represents 50 μ m. (d) Expression levels of VSM-related genes in merged mesenchymal clusters. Color intensity indicates level of expression. (e) Pseudotime ordering of mesothelial and VSM-related merged mesenchymal clusters. Colors correspond to t-SNE in (a). All clusters are individually plotted in Fig. 15j. (f) Cluster proportions over pseudotime. Pseudotime was binned into 10 groups and the proportion of each cluster within that bin of pseudotime was calculated. (g) Model of lineage relationships among mesothelial, vascular smooth muscle, and VSM-related mesenchymal populations based on pseudotime ordering in (e).

Chapter 4

Characterization of the pancreatic mesothelium and role of Fgf9 in pancreatic development

Introduction

The mesothelium is a single-cell layer of mesoderm-derived epithelial-like cells that line the body's internal organs and body cavities (Mutsaers & Wilkosz, 2007; Winters & Bader, 2013). The parietal mesothelial cells lining the three body cavities—pleura (lungs and diaphragm), peritoneal (abdomen and pelvis), and pericardial (heart)—form a continuous lining with the visceral mesothelial cells lining the internal organs. The diverse functions of mesothelial cells during development and in adult tissues has increased the attention to these cellular layers.

Although located in association with different organs and cavities throughout the body, mesothelial cells share multiple common characteristics: cellular shape, unique intermediate filament expression pattern, cellular polarity, cell/cell adhesion, and production of a basement membrane (Michailova & Usunoff, 2006; Winters & Bader, 2013). Most mesothelial cells have a flattened squamous-like shape, although cuboidal mesothelial cells have been noted in certain areas of the pleura and viscera of the liver and spleen (Mutsaers & Wilkosz, 2007). As an epithelial-like mesoderm-derived cell, mesothelial cells express intermediate filaments characteristic of both mesenchymal cells, such as *vimentin* (*Vim*) and *desmin* (*Des*), and epithelial cells, such as *cytokeratins* (LaRocca & Rheinwald, 1984). The apical surface of mesothelial cells may be covered by microvilli and cilia and face towards the coelomic space (Gaudio, Rendina, Pannarale, Ricci, & Marinozzi, 1988; Michailova & Usunoff, 2006), while the lateral side is identified by localization of tight junction proteins (Andrée et al., 2000; Reese, Zavaljevski, Streiff, & Bader, 1999). In addition to tight junctions, mesothelial cells form numerous cell-cell junction complexes, including adherens, gap junctions, and desmosomes, helping facilitate their barrier formation (Michailova & Usunoff, 2006; Mutsaers & Wilkosz, 2007). Finally, the mesothelium produces and rests on a basement membrane (Mutsaers &

Wilkosz, 2007; Winters, Thomason, & Bader, 2012). These characteristics are used to identify mesothelial cells throughout the body and across organisms.

In the adult, the mesothelium functions as a protective barrier and source of surfactant to facilitate intra-organ movement (Michailova, 2004). As the barrier between the organ parenchyma and body cavity, mesothelial cells regulate the passage of fluids and cells, including immune cells, across the mesothelial monolayer (Mutsaers & Wilkosz, 2007). Additionally, mesothelial cells protect organs from foreign pathogens by the secretion of chemokines and cytokines and the presentation of antigens to recruit and activate immune cells (Valle et al., 1995). Mesothelial cells are also critical during injury and repair processes, where they participate in regulating inflammation, coagulation, and fibrinolysis (Mutsaers et al., 2015). Therefore, the mesothelium plays an active role during both adult homeostasis and injury conditions.

A major focus of mesothelial biology has been on its function as a mesenchymal progenitor cell during development. Mesothelial cells undergo a process similar to epithelial-to-mesenchymal transition (EMT), often termed a mesothelial-to-mesenchymal transition (MMT), in which they leave the mesothelial layer, migrate into the organ parenchyma, and differentiate into various mesenchymal cell types (Ariza, Carmona, Cañete, Cano, & Chapuli, 2016). Studies of mesothelial progenitor function have utilized dye labeling and more recently, genetic Cre-lox technology, to label and trace migrating mesothelial cells (see table 1 for overview of genetic mouse lines used to study the mesothelium and their references). An understanding of the mesenchymal cell types derived from mesothelial layers has started to unravel the complex lineage relationships among mesenchymal cells in different organs.

The epicardium, the mesothelial layer lining the heart, has been shown to give rise to vascular smooth muscle, fibroblasts, endothelial, and myocardial cells (Bin Zhou et al., 2008; Dettman, Denetclaw, Ordahl, & Bristow, 1998). While studies have agreed that the majority of smooth muscle cells surrounding the coronary vessels and a portion of fibroblasts are derived from the epicardium (Dettman et al., 1998; Wessels et al., 2012), the derivation of endothelial cells from the epicardium remains controversial. Experiments utilizing quail-chick transplantations demonstrated an epicardial origin of coronary vascular cells, but these findings were not supported by lineage tracing in mice (Bin Zhou et al., 2008; Cai et al., 2008; Perez-Pomares et al., 2002). The mouse studies utilized two different genetic lines with Cre expression driven by either *Wt1* or *Tbx18*. These genes were shown to be expressed within the epicardium, as well as the progenitor cells that give rise to the epicardium, the proepicardium. A later study found that WT1 and TBX18 expression was heterogenous within the proepicardium (Katz et al., 2012). A proepicardial domain that did not express WT1 nor TBX18, but instead expressed *Semaphorin 3D* (*Sema3D*) and *Scleraxis* (*Scx*), was demonstrated to give rise to endothelial cells of the coronary vasculature. This study proposed that these distinct proepicardial domains could explain the divergent results from prior studies.

The origin of myocardial cells, the muscle cells that compose the heart, has also remained controversial. Evidence for an epicardial origin of myocardial cells was provided by lineage tracing with *Wt1*-Cre, *Wt1*-CreER, and *Tbx18*-Cre driver lines (Bin Zhou et al., 2008; Cai et al., 2008). The validity of these lines, however, has been called into question (Christoffels et al., 2009; Rudat & Kispert, 2012). Rudat and Kispert reported sporadic and ectopic recombination of the *Wt1*-Cre allele throughout the embryo, suggesting that lineage tracing may lead to erroneous conclusions. Additionally, the recombination efficiency of the *Wt1*-CreER line in the

epicardium was both low and highly variable. These authors also found *Wt1* and *Tbx18* expression in non-epicardial cells, suggesting that these markers are not specific to the epicardium (Christoffels et al., 2009; Rudat & Kispert, 2012). Whether myocardial cells are derived from the epicardium remains to be solved.

Although the epicardium is the best studied mesothelial layer, studies in other organs have also provided evidence for a mesenchymal progenitor function. The majority of vascular smooth muscles of the gut and around 30% in the lung, have been shown to be derived from mesothelial layers of the respective organs by utilizing different *Wt1*-Cre lines than the line developed by Zhou and colleagues (E. Cano, Carmona, & Munoz-Chapuli, 2013; del Monte et al., 2011; Dixit, Ai, & Fine, 2013; Que et al., 2008; Wilm et al., 2005). These findings were also supported by a mesothelin-CreER line (Rinkevich et al., 2012). Both a portion of interstitial fibroblasts within the lung and interstitial cells of Cajal in the gut have been shown to be derived from mesothelial layers of the lung and gut, respectively (E. Cano et al., 2013; Carmona, Cano, Mattiotti, Gaztambide, & Munoz-Chapuli, 2013; Dixit et al., 2013). Cano et al. also demonstrated that a portion of lung endothelial cells is derived from *Wt1*⁺ pleural mesothelium. Dye labeling of the chick coelomic mesothelium demonstrated a mesothelial contribution to the liver sinusoidal endothelium (Pérez Pomares et al., 2004). A later study utilizing a *Wt1*-CreER mouse line found the liver mesothelium contributed to the stellate cells, a type of fibroblast, and perivascular cells (Asahina et al., 2011). Finally, cells from the coelomic epithelium on both sides of the gonad primordia migrate and differentiate into Sertoli and Leydig cells, which form the stroma of the developing gonads (Kusaka et al., 2010). These studies demonstrate the wide range of cell types derived from mesothelial layers throughout the body.

In addition to its progenitor function, mesothelial layers also act as a source of secreted factors to regulate organ development. FGFs, in particular, have been shown to be mesothelial-secreted factors that influence organ development. A study by Lavine and colleagues showed that retinoic acid (RA)-regulated expression of *Fgf9* within the epicardium, the mesothelial layer of the heart, induced myocardial proliferation (Lavine et al., 2005). Furthermore, the authors found that FGF signaling induced epicardial expression of *sonic hedgehog* (*Shh*), which subsequently induced myocardial expression of *vascular endothelial growth factor* (*Vegf*) ligands and *angiopoietin-2* (*Ang-2*). *Vegf* and *Ang-2* then regulated coronary vascular development (Lavine, 2006; Lavine & Ornitz, 2008).

Similar to the heart, studies have identified a pro-proliferative role of *Fgf9* during lung development (Colvin, White, Pratt, & Ornitz, 2001). A study utilizing Cre drivers for epithelial and mesenchymal compartments found a specific role for epithelial-expressed *Fgf9* in epithelial branching and mesothelial-expressed *Fgf9* in mesenchymal proliferation (Yin et al., 2011). FGF9 has also been shown to regulate differentiation processes, specifically the inhibition of vascular smooth muscle cells (Weaver, Batts, & Hogan, 2003). The authors hypothesized that the localized secretion of FGF9 from the mesothelium maintains mesenchymal cells along the outer edge of the lung in an undifferentiated state. These studies suggest multi-faceted roles for FGF9 during lung development.

Intestinal development is also dependent on *Fgf9*, as the small intestines of *Fgf9* ^{-/-} mice were shorter than wild-type controls, due to reduced mesenchymal proliferation and premature differentiation (Geske, Zhang, Patel, Ornitz, & Stappenbeck, 2008). However, expression of *Fgf9* in both epithelial and mesothelial cells suggests that some of these defects could be due to

epithelial-expression of *Fgf9*, as found in the lung. Finally, *Fgf9* is also expressed in the hepatic mesothelium, but its function during development has not been determined (Colvin et al., 2001).

In addition to FGF signaling, the epicardium also expresses the secreted factor, *insulin growth factor 2 (Igf-2)* (Peng Li et al., 2011). *Igf-2* was found to regulate the proliferation of the myocardium, identifying an additional mesothelial-derived mitogen that acts on underlying mesenchymal cells. Further work identified a relay system of signals that results in proliferation of myocardial cells; RA signaling induced the expression of *erythropoietin (Epo)* in the liver, which traveled to the heart and induced expression of *Igf-2* in the epicardium, ultimately resulting in IGF-2 secretion and proliferation of underlying myocardial cells (Brade et al., 2010).

RA signaling has been shown to regulate upstream processes that lead to expression of *Fgf9* and *Igf-2* in the epicardium. In the liver, however, RA has been proposed as a mesothelial-secreted mitogen that regulates hepatoblast proliferation (Ijpenberg et al., 2007). In *Wt1* knockout embryos, expression of the *retinoic acid synthesizing enzyme (Raldh2)*, is downregulated in the hepatic mesothelium. These animals displayed decreased hepatoblast proliferation and increased differentiation of vascular smooth muscle cells. Inhibition of RA synthesis in chick embryos also resulted in decreased hepatoblast proliferation and a smaller liver (Ijpenberg et al., 2007), suggesting that the proliferation defects are a direct effect of RA signaling. Therefore, mesothelial layers have been shown to secrete multiple mitogenic factors in order to regulate organ size during development.

While mesothelial layers have been well-studied in organs such as the lung and heart, the development and function of the pancreatic mesothelium is unknown. One study examined the origin of the pancreatic mesothelium by chick-quail transplantation of dorsal pancreatic buds (Winters, Williams, & Bader, 2014). These experiments suggested that the pancreatic

mesothelium was derived from resident progenitors within the transplanted pancreatic tissue, rather than an exogenous source from the host. However, this study only transplanted the dorsal pancreatic bud, and has yet to be verified in other organisms or by more defined lineage tracing experiments. The timing and mechanism of pancreatic mesothelial formation has not been reported.

Studies have only just begun to identify the downstream progeny of mesothelial layers in the pancreas. Angelo and Trembley found that the condensed dorsal mesenchymal cells are derived from the coelomic mesothelial layer from E9.5 – E10.5 (Angelo & Tremblay, 2018). The ventral coelomic mesothelial layer contributed to the ventral pancreatic mesenchyme, suggesting that both the dorsal and ventral buds may share a source of mesenchymal cells. As this study utilized dye labeling of early mesodermal structures, it is possible that the coelomic mesothelium gives rise to the visceral pancreatic mesothelium, which subsequently produces the mesenchymal cells of the developing pancreas. Additional studies that can specifically label the visceral mesothelial layer of the pancreas will clarify the downstream progeny of pancreatic mesothelium.

Finally, whether mesothelial-derived secreted factors regulate pancreatic development is unknown. FGF signaling has been shown to be a mesothelial-regulated pathway important for the development of multiple organs. While secretion of FGF ligands by the pancreatic mesothelium has not been demonstrated, expression of multiple FGF ligands and receptors has been detected during pancreatic development. Utilizing quantitative real-time PCR, expression of FGF ligands, including *Fgf1*, *Fgf7*, *Fgf9*, *Fgf11*, and *Fgf18*, was found throughout pancreatic development (Dichmann, Miller, Jensen, Scott Heller, & Serup, 2003). This study also analyzed expression of the various FGF receptor isoforms, which include the “b” and “c” isoforms. “b”

isoforms have been shown to be expressed in epithelial cells, while “c” isoforms are expressed in mesenchymal cells (Ornitz & Itoh, 2015). *Fgfr1b*, *Fgfr1c*, *Fgfr2b*, *Fgfr2c*, *Fgfr3b*, and *Fgfr4* were found to be expressed in varying patterns during pancreatic development. *Fgfr1b* and *Fgfr2b* showed a similar pattern of expression, which peaked at E14 and remained at lower levels until birth. *Fgfr1c*, *Fgfr2c*, and *Fgfr4* were most highly expressed at E12, and subsequently downregulated at later gestational ages. *Fgfr3b* increased in expression over developmental time. While this study did not distinguish expression between the epithelium and mesenchyme, another study determined the expression FGF receptors at E11.5 within each of these compartments (Sylvestersen, Herrera, Serup, & Rescan, 2011). *Fgfr2b* and *Fgfr4* were found to be expressed specifically within the epithelium, *Fgfr2c* and *Fgfr1c* were enriched in the mesenchyme, and *Fgfr3c* was expressed in both the epithelium and mesenchyme by quantitative PCR measurements. This study detected very low expression of *Fgfr1b* and *Fgfr3b* in both compartments, which fits with the patterns of expression detected by Dichmann and colleagues (Sylvestersen et al., 2011). The varying expression patterns of both FGF ligands and receptors indicates that they may have distinct roles in regulating pancreatic development.

Indeed, a functional role for FGF signaling has been noted by multiple studies. Mesenchymal-derived *Fgf10* has been identified as a critical mitogen for early pancreatic progenitors, regulating the size of the developing pancreatic organ (Bhushan et al., 2001; Ohuchi et al., 2000). *Fgf10* is thought to function through *Fgfr2b*, an epithelial-expressed receptor, in order to maintain Notch expression, enhance proliferation, and block differentiation in pancreatic progenitor cells (Hart, Papadopoulou, & Edlund, 2003). FGF10, therefore, directly acts on epithelial cells to influence pancreatic development. It is also possible that FGF signaling can influence mesenchymal cell development. Misexpression of *Fgf4*, a ligand not normally found to

be expressed in the developing pancreas, under the *Pdx1*-promoter (*Pdx1-Fgf4*) led to defects within both the epithelial and mesenchymal compartment (Dichmann et al., 2003). *Pdx1-Fgf4* pancreata displayed large fluid-filled cysts, with interspersed groups of cells resembling acini and increased number of disorganized ductal structures. By E19, when wild type pancreata have already formed large clusters of endocrine cells that will become the islets of Langerhans, *Pdx1-Fgf4* pancreata showed dispersed endocrine cells that failed to aggregate and were reduced in total number. Instead, the majority of the pancreas was composed of mesenchymal cells, a large number of which were proliferating. FGF4 binds preferentially to the FGFR “c” isoforms, which are expressed in the mesenchyme (Ornitz & Itoh, 2015). The authors of the study, therefore, suggest the effects of FGF4 may function directly on mesenchymal cell development, which in turn effects epithelial development. Additionally, they hypothesize that FGF9 may mimic the role of FGF4, as FGF9 also preferentially binds FGFR “c” isoforms (Ornitz & Itoh, 2015) and is endogenously expressed during pancreatic development. FGF4 also binds with lower affinity to FGFR “b” isoforms and FGFR4, and so it is also formally possible that some of these effects are a result of direct actions on epithelial cells. These studies highlight the role of FGF signaling in regulating epithelial-mesenchymal interactions and overall pancreatic development.

Work in this chapter validates the gene expression profile of the pancreatic mesothelium detected in our single-cell RNA-sequencing datasets (see Chapter 3), highlights the need for new tools for lineage tracing the mesothelium, and identifies a novel role for *Fgf9* in pancreatic development. We first validate expression of multiple markers of the mesothelium detected in our single-cell RNA-sequencing by performing immunohistochemistry *in vivo*. Many of these markers are known mesothelial markers in other organ systems, but we also identify two

additional markers not previously associated with mesothelial layers. Next, we perform experiments to lineage trace the pancreatic mesothelium during development. These experiments highlight the limitations of the current set of tools for accurately studying the lineage of this cell type. The novel markers identified, therefore, are candidates for future tools to more specifically label the pancreatic mesothelium. Our single-cell RNA-sequencing datasets also identify multiple secreted factors expressed within the pancreatic mesothelium. We find that embryos lacking *Fgf9* have hypoplastic pancreata, indicating a functional role for FGF9 in pancreatic development. This chapter, therefore, validates and begins to study the functional role of a specific mesenchymal subtype during pancreatic development.

Identification of pancreatic mesothelial markers

In chapter 3, we identified a mesothelial population present in E12.5, E14.5, and E17.5 pancreatic single-cell RNA-sequencing datasets. Therefore, we set out to validate the expression of markers identified within these datasets in pancreatic mesothelial cells. The most common marker used to identify the mesothelium in other organs is *wilms tumor 1 (Wt1)*. We also detected *Wt1* expression in our single-cell RNA-sequencing datasets (Fig. 17a-c). *Wt1* was enriched within the mesothelium, and also expressed in other mesenchymal cell types. We next stained for WT1 protein and detected expression in mesothelial layers and mesenchymal cells of E12.5, E14.5, and E17.5 pancreata, matching the expression data from the single-cell sequencing datasets (Fig. 17a-c). WT1 protein appeared to be more highly expressed in mesothelial cells than mesenchymal cells. Our findings contrast with other reports of WT1 as a specific marker of the mesothelium in other organs, as *Wt1* RNA and WT1 protein were detected in both

mesothelial (arrows) and non-mesothelial (arrowheads) mesenchymal cells during pancreatic development.

In addition to *Wt1*, we also validated other known and novel markers highly expressed in the mesothelium in our E14.5 single-cell RNA-sequencing dataset. Using immunohistochemistry on both tissue sections and in whole mount pancreata, we aimed to identify markers with high specificity to the mesothelium. Caveolin1 (CAV1) was expressed in the mesothelium, as well as endothelial cells, as predicted by our single-cell data and previously reported (Parton & Simons, 2007) (Fig. 18a). Additionally ezrin-radixin-moesin binding phosphoprotein-50 (EBP50) and crystalline alpha B (*CRYAB*) showed specific expression on the membrane of the mesothelium, with some weaker staining around the acini (Fig. 18b-c). These antibodies also successfully stained the mesothelium in a whole mount staining approach with a clearing step to allow for three-dimensional (3D) imaging (Fig. 18b-c). These results identify and validate two novel markers of the pancreatic mesothelium, EBP50 and CRYAB, that offer superior specificity than classical markers of mesothelial layers, such as WT1 and CAV1.

Lineage tracing the pancreatic mesothelium

The mesothelium has been demonstrated to give rise to multiple mesenchymal cell types during development of the liver, heart, lung, and intestine (Asahina et al., 2011; Bin Zhou et al., 2011; Que et al., 2008; Wilm et al., 2005). Predictions from our *in silico* lineage modeling suggest the pancreatic mesothelium gives rise to vascular smooth muscle cells (see Chapter 3). To validate these predictions *in vivo*, appropriate Cre driver lines are required to specifically label the pancreatic mesothelium. Prior studies have utilized the *Wt1*-EGFP-Cre mouse line to lineage trace mesothelial populations (see Table 1 for list of mouse lines and references). When

we crossed the *Wt1*-EGFP-Cre line to the *Rosa26^{mTmG}* reporter to lineage trace *Wt1*⁺ expressing cells, we found that a large number of epithelial cells were labeled in adult pancreata (Fig. 19a). Given the specificity of *Wt1* expression in mesothelial and mesenchymal populations (Fig. 17a-c), we suspect that this epithelial recombination may be a result of inappropriate recombination of the Cre allele. Indeed, there have been reports that this Cre line undergoes sporadic and ectopic recombination throughout the embryo (Rudat & Kispert, 2012). These results suggest that the *Wt1*-EGFP-Cre line is not suitable for lineage tracing the pancreatic mesothelium.

We next analyzed the recombination of two cytokeratin inducible Cre driver lines, *Krt19*-CreER and *Krt18*-CreER by crossing these lines to *Rosa26^{mTmG}* reporter mice (Table 1). Both *Krt19* and *Krt18* are expressed in the developing pancreatic mesothelium (Fig. 19b-c). We were unable to achieve high efficiency labeling of the mesothelium with either the *Krt19*-CreER or *Krt18*-CreER drivers (Fig. 19b-c). Although we occasionally identified lineage-labeled mesothelial cells with the *Krt19*-CreER driver, this required two 4.5 mg doses of tamoxifen injected at E12 and E13, often resulting in deformed embryos (Fig. 19b). Lineage-labeled mesothelial cells were even more rare with the *Krt18*-CreER driver, as most lineage-labeled cells were located within the pancreatic parenchyma and likely represented ductal cells (Fig. 18c). We conclude that these three lines are not suitable for high efficiency, specific labeling of the pancreatic mesothelium.

Although the constitutive *Wt1*-EGFP-Cre driver was determined to be unsuitable, we hypothesized that the inducible *Wt1*-CreER driver may show higher specificity for the pancreatic mesothelium (Table 1). To test this, we crossed the *Wt1*-CreER line to the *Rosa26^{mTmG}* reporter line and delivered two doses of 2.5 mg of tamoxifen 8 hours apart by oral gavage to pregnant dams at E12.5 (Fig. 20a). Pancreata were collected at E13.5 to assess the initial labeling

capability of the driver line. We found lineage-labeled mesothelial cells and more rarely, mesenchymal cells, but not epithelial cells (Fig. 20b). This matched the endogenous expression of WT1, which is highly expressed in the mesothelium, more lowly expressed in mesenchymal cells, and absent in the epithelium (Fig. 17a-c). Pancreata collected at E17.5 with the same tamoxifen dosing showed a similar lineage-labeling pattern, with mesothelial and mesenchymal lineage labeling (Fig. 20c). More mesothelial cells were labeled than at E13.5, perhaps due to proliferation of labeled cells during development. Similar to E13.5, mesenchymal cells were more rarely labeled (Fig. 20c). These results suggest that the *Wt1*-CreER line is a more suitable driver than the *Wt1*-EGFP-Cre. However, as demonstrated by both immunohistochemistry and the *Wt1*-CreER lineage tracing results, *Wt1*/WT1 is not specifically expressed within the mesothelium.

Expression of secreted factors by the pancreatic mesothelium

In addition to its described role as a mesenchymal progenitor cell, the mesothelium has also been shown to secrete factors that regulate organ development (A. C. White et al., 2006; Yin et al., 2011). Therefore, we looked for expression of secreted factors, their receptors, and downstream targets in three pathways known to have roles in pancreatic development. Of the 28 different FGF ligands, we only detected appreciable levels of *Fgf9* (Fig. 21a-d). Expression of this factor was largely restricted to the pancreatic mesothelium, with sparse expression in the ductal and endocrine populations (Fig. 21a-d). We also found expression of the *Fgfr1* expression in the mesenchyme and sparser expression of *Fgfr1-4* in the epithelium (Fig. 21a-d). *Fgfr2* was enriched within the ductal cells (Fig.21 c-d). Due to the 3' biased sequencing approach, we were not able to obtain isoform information for the receptors. Finally, we detected expression of FGF

downstream transcription targets, *Spry1* and *Spry4*, which overlapped to varying degrees with the expression of the FGF receptors (Fig. 21a-d). These results highlight the specific expression of *Fgf9* in the pancreatic mesothelium, and potential regulation of both the epithelial and mesenchymal compartments through their expression of various FGF receptors.

Within the WNT signaling pathway, multiple receptors were expression in both the E14.5 mesenchyme and epithelium (Fig. 22). Of the expressed receptors, most were widely expressed in the mesenchyme, such as *Fzd1*, *Fzd2*, *Fzd3*, *Fzd7*, *Lrp5*, and *Lrp6* (Fig. 22a-b). The exception was *Fzd4*, which was enriched within the mesothelial compartment (Fig. 22a-b). Overall, WNT receptors were expressed more sparsely in the epithelium, but some displayed differential expression in various populations. For example, *Fzd2* was largely absent from endocrine cells while *Fzd3* was more sparsely expressed in the ductal population (Fig. 22c-d). We also found expression of genes that are downstream of the WNT receptors, including *Dvl2*, *Axin2*, and the transcription factors *Lef1*, *Tcf3*, and *Tcf4*. *Lef1* was enriched in the mesothelium while *Tcf4* was enriched in the non-mesothelial mesenchymal populations (Fig. 22a-b). Finally, we identified expression of multiple WNT ligands that were enriched in the mesothelium, such as *Wnt2b* and *Wnt9a* (Fig. 22a-b). In the epithelium, *Wnt2b* was specifically expressed within the ductal cells (Fig. 22c-d). Prior studies have utilized qPCR and *in situ* hybridization to study WNT pathway expression, but focused on early (E10) and late (E17) gestational timepoints(Heller et al., 2002). Additionally, single-cell resolution now allows us to more accurately map on the expression of WNT members in a cell type specific manner.

In addition to FGF and WNT, we also found expression of components of the BMP signaling pathway. BMP ligands expressed by the mesenchyme include *Bmp1*, *Bmp7*, and at lower levels, *Gdf11* (Fig. 23a-b). *Bmp2* and *Bmp4* were highly enriched in the mesothelium, and

Gdf6 was enriched in both the mesothelium and cluster 2, the *Stmn2*⁺ population (Fig. 23a-b). These ligands also displayed cell-type specific expression patterns in the epithelium, where *Bmp1* was enriched in the *Ngn3*⁺ and beta cell populations, but largely absent from the *Fev*⁺ population (Fig. 23e-f). *Bmp7*, on the other hand, was restricted to ductal and acinar cell populations but was absent in the endocrine cells. Most BMP receptors were expressed at lower levels and did not display obvious enrichment in either the mesenchymal or epithelial compartments, although *Acvr2b* was slightly enriched in the mesothelium (Fig. 23a,c,e-f). Finally, the mesenchymal populations expressed *Smad1/4-7*, proteins that act as signal transducers for BMP signaling (Fig. 23a, d).

Fgf9 is required for proper pancreatic development

Our single-cell RNA-sequencing dataset identified numerous candidate mesothelial-secreted factors (Fig. 21-23, see Chapter 3). One of the factors most specifically expressed by the mesothelium was *Fgf9* (Fig. 24a). Although *Fgf9* has also been shown to regulate vascular development in the heart and lung (Olivey & Svensson, 2010; A. C. White, Lavine, & Ornitz, 2007; Yin et al., 2011), intestinal elongation (Geske et al., 2008), and cecum formation (Alam et al., 2012), the role of *Fgf9* in pancreatic development is unknown.

We next set out to determine the role of *Fgf9* during pancreatic development. E12.5, E14.5, and E17.5 single-cell RNA-sequencing datasets revealed a high specificity of *Fgf9* to the mesothelium, although there was low expression in some ductal and endocrine populations as well (Fig. 24a). We utilized a mouse line with a LacZ knock-in allele in the *Fgf9* locus (Huh, Warchol, & Ornitz, 2015). As mice lacking both alleles of *Fgf9* do not survive to adulthood, we crossed *Fgf9* heterozygous (*Fgf9* +/-) animals to obtain homozygous wild-type (*Fgf9* +/+),

heterozygous (*Fgf9* +/-) and homozygous null (*Fgf9* -/-) embryos. *Fgf9* -/- embryos were smaller in size than their *Fgf9* +/+ littermates (Fig. 24b), and dissection of the gut tube region containing the stomach, spleen, pancreas, and proximal intestine revealed multiple defects (Fig. 24c). *Fgf9* -/- embryos had a hypoplastic stomach and pancreas and lacked a discernable spleen (Fig. 24c-d). *Fgf9* +/- embryos and gut tube regions were indistinguishable from *Fgf9* +/+ littermate controls (data not shown). Whole mount staining for the epithelial marker, CD326 (Epcam), revealed that *Fgf9* -/- embryos had less branching than pancreata from littermate *Fgf9* +/+ embryos (Fig. 24e). Therefore, we concluded that *Fgf9* is required for the proper development of multiple gut tube-derived organs, including the pancreas.

The smaller size of *Fgf9* -/- pancreata may be due to the failure of particular cell types to develop in the absence of *Fgf9*. To determine whether the major cell lineages were present in *Fgf9* -/- pancreata, we performed immunohistochemistry on E17.5 pancreata from *Fgf9* +/+ and *Fgf9* -/- embryos (Fig. 25). We identified the major lineages of the pancreas in both *Fgf9* +/+ and *Fgf9* -/- pancreata, including acinar (*Cpa1*+), ductal (*Krt19*+), mesothelial (*Krt19*+, localized to tissue edge), alpha (*Gcg*+), beta (*Ins*+), mesenchymal (*Vim*+), vascular smooth muscle (*Sma*+), and endothelial cells (*CD31*+) and did not observe obvious differences between homozygous wild type and mutant pancreata at this stage. These results suggest that the diminished pancreatic size is not due to loss of a particular cell type.

We next analyzed whether the pancreatic lineages were also present at an earlier developmental stage, as *Fgf9* has been demonstrated to function at early stages and compensation effects may allow for recovery by late developmental stages. Similar to E17.5, the major pancreatic lineages were present at E13.5, including acinar, ductal, mesothelial, mesenchymal, endothelial, and low numbers of alpha and beta cells (Fig. 26a-f). We did not

detect Sma⁺ vascular smooth muscle in either Fgf9^{+/+} or Fgf9^{-/-} pancreata, although they are reported to be recruited to blood vessels by E13.5 in the pancreas (Azizoglu et al., 2016). Upon comparison of the epithelial and mesenchymal compartments, we observed a reduction of the mesenchymal compartment (Fig. 26g-h). Additionally, we found less space occupied by mesenchymal cells between the CD326⁺ epithelial branches, contributing to the compact phenotype identified in whole mount imaging (Fig. 24e). As prior studies in the lung have identified *Fgf9* as a mesothelial-secreted factor that regulates mesenchymal proliferation, we quantified the number of epithelial (CD326⁺) and non-epithelial (CD326⁻) cells in Fgf9^{+/+} and Fgf9^{-/-} pancreata. We found E13.5 Fgf9^{-/-} pancreata had differing proportions of epithelial and non-epithelial cells in comparison to Fgf9^{+/+} controls (Fig. 26g-i). In Fgf9^{-/-} embryos, 80.8% of the pancreas was CD326⁺ and 19.2% CD326⁻ while cells of the same organ of Fgf9^{+/+} littermates were nearly equally distributed, with 43.3% CD326⁺ and 56.7% CD326⁻ negative (Fig. 26i). The results of this molecular analysis reveal a bias in the size of the epithelial and non-epithelial compartment in E13.5 Fgf9^{-/-} pancreata.

Discussion

Lineage tracing the mesothelium remains challenging with existing markers and genetic tools. The utility of the *Wt1*-EGFP-Cre driver line has been called into question by other groups (Rudat & Kispert, 2012), due to sporadic and ectopic recombination of the Cre allele. The high degree of recombination within the epithelial compartment of the pancreas could be a result of early, ectopic recombination of this allele in the embryo, as reported by Rudat and Kispert. Another possibility, although unlikely, is that *Wt1* is endogenously expressed in pancreatic epithelial precursors at some point during development or adulthood, and the resulting lineage

labeled cells reflect true *Wt1* expression. In either case, these results suggest that the Wt1-EGFP-Cre line will be not be useful for specific lineage labeling of the pancreatic mesothelium.

To overcome the problems with the Wt1-EGFP-Cre line, we tested multiple other inducible Cre driver lines for mesothelial specificity. We found that the Wt1-CreER was the most successful in terms of efficiency. However, we also found recombination in non-mesothelial mesenchymal cells one day after tamoxifen injection. The labeling of non-mesothelial cells at E13.5 could be occurring by two mechanisms. First, the lower levels of WT1 expression in non-mesothelial mesenchymal cells may be enough to drive recombination. The second possibility is that these cells are truly derived from the mesothelium, and are in the process of downregulating WT1 expression during differentiation, as hypothesized in the lung (E. Cano et al., 2013). Although prior studies have assumed the low levels of WT1 in non-mesothelial mesenchymal cells represent recently delaminated mesothelial cells, this has not been formally demonstrated in the pancreas. These challenges highlight the need for improved tools to specifically label and trace the mesothelium.

Even with the uncertainty of the specificity of the Wt1-CreER, after pulsing with tamoxifen at E12.5, there were very few lineage-traced mesenchymal cells by E17.5. If all or only a proportion of these lineage-labeled cells are truly derived from the Wt1+ mesothelium, this represents a very small proportion of the pancreatic mesenchyme. The mesothelium may not actively give rise to mesenchymal cells at all stages of development. Indeed, most other organ systems show evidence of MMT and differentiation at earlier stages of development, typically between E10.5 – E12.5 (Asahina et al., 2011; Gise et al., 2016; Wilm et al., 2005). For example, in the lung, the mesothelium could be efficiently labeled from E10.5 – E11.5, and was shown to contribute to mesenchymal lineages (Dixit et al., 2013). However, the ability to label and trace

the mesothelium was reduced at later gestational stages, as the expression of *Wt1* decreased. Tracing the pancreatic mesothelium at earlier stages may allow for higher efficiency labeling. Additionally, the mesothelium may be most active during these earlier stages and subsequently contribute fewer cells to mesenchymal lineages at later stages in development.

Our hypothesis that the pancreatic mesothelium was active at earlier stages of development was supported by a recent study, published during the completion of this work, that traced the developing pancreatic mesothelium (Ariza, Cañete, Rojas, Chapuli, & Carmona, 2018). Utilizing the *Wt1*-CreER line, the authors found that the pancreatic mesothelium contributed to the developing mesenchyme when labeled between E9.5 and E11.5. Labeling the mesothelium at E9.5 only produced rare labeled parenchyma cells and the authors did not test later labeling of the mesothelium. In agreement with our findings, the authors noted the expression of low levels of WT1 protein in non-mesothelial mesenchymal cells in E12.5 and E13.5 embryos. The expression pattern of WT1 at earlier timepoints, when the tamoxifen pulsing was performed to label the mesothelium, was not shown. Additionally, the initial labeling immediately after pulsing with tamoxifen was not shown. Therefore, it is possible that WT1 and subsequent labeling with the *Wt1*-CreER line, was not specific to the mesothelium during this time, consistent with both this work and the author's own findings at E12.5 and later. The low levels of WT1 expression in non-mesothelial mesenchymal cells at E12.5 was attributed to delaminated mesothelial cells that are downregulating WT1 as they differentiate into mesenchymal cell types, as had been reported in other systems (E. Cano et al., 2013). Whether this assumption is true remains to be tested. Therefore, the results of these *Wt1*-CreER experiments should be interpreted with caution until the line's specificity to the mesothelium can be demonstrated.

The creation of additional Cre driver lines for the mesothelium to validate the findings from the *Wt1* lines would be of great value to the mesothelial field. One of the most specific markers from the single-cell RNA-sequencing data is *Uroplakin3b* (*Upk3b*). An inducible Cre line was created under this promoter, but did not induce the expression of Cre in mesothelial tissues (Rudat et al., 2014). Our identification of additional mesothelial markers, including *Ebp50* and *Cryab*, provide promising candidates for more specific markers of the mesothelium. The expression pattern of these genes should be extended to pre-E12.5 and post-E17.5 timepoints during pancreatic development to test their specificity throughout pancreatic development.

Besides its function as a possible mesenchymal progenitor cell, the mesothelium also secretes growth factors to regulate organ development (Olivey & Svensson, 2010; Yin et al., 2011). We find expression of multiple secreted factors in the pancreatic mesothelium and identify a role for *Fgf9* in the development of the pancreas. The hypoplastic phenotype of *Fgf9*^{-/-} pancreata is reminiscent of the proliferation defects within both the epithelial and mesenchymal compartments in the lung of *Fgf9*^{-/-} embryos (Colvin et al., 2001). Later work in the lung described distinct roles for mesothelial and epithelial-expressed *Fgf9* (Yin et al., 2011). *Fgf9* from the mesothelium regulated mesenchymal proliferation and WNT signaling while *Fgf9* from the epithelium regulated branching. The high expression of *Fgf9* in the pancreatic mesothelium and reduced size of the mesenchymal compartment, suggests that a similar mechanism may occur in pancreatic development. We find a potential branching phenotype, where the epithelium appears more compact with less extended branches than wild type pancreata. We also detect very low levels of *Fgf9* in ductal and endocrine cells in our single-cell RNA-sequencing datasets. The reduced size and branching of the epithelium, therefore, may be

an indirect effect of mesenchymal dysregulation, a direct effect of mesothelial-secreted FGF9 on the epithelial cells, or a direct effect of FGF9 from epithelial cells. Experiments using mesenchymal and epithelial Cre drivers with the *Fgf9* floxed allele line can clarify the function of *Fgf9* from the mesothelium or epithelium during development.

Our E13.5 and E17.5 immunohistochemistry experiments do not indicate that the major cellular lineages of the pancreas are absent in *Fgf9* ^{-/-} pancreata. However, this study remains incomplete and requires analysis of additional markers of both the epithelium and mesenchyme. Staining for the Ngn3⁺ endocrine progenitor population and the remaining hormone-producing cells (delta, gamma, and epsilon) will be important for verifying the proper differentiation of the epithelium. Additionally, we have not yet determined whether the reduction in the mesenchyme is due to the loss of a particular mesenchymal cell type or an overall reduction of all mesenchymal cell types. Now that we have cataloged the mesenchymal populations, and have sets of marker genes to identify them, we can look for the presence of these populations in developing *Fgf9* ^{-/-} pancreata. These experiments will establish whether *Fgf9* is required for differentiation of specific cellular lineages within the developing epithelium and mesenchyme.

Rather than an absence of cellular lineages, the reduced size of *Fgf9* ^{-/-} pancreata could be due to decreased proliferation of various cell types or increased cell death. Measuring the rates of proliferation and cell death across developmental time, therefore, will be conducted. Additionally, the ratios of specific cell types will be quantified in order to determine if the loss of *Fgf9* leads to biases in the production of particular cell types. These experiments will help determine the underlying mechanism of *Fgf9* function in pancreatic development.

Uncovering the signaling pathways affected by loss of *Fgf9* ^{-/-} will also be crucial for gaining a mechanistic understanding of *Fgf9* function. As a secreted factor, the localization of

the FGF9 receptors can give insight into the signaling pathway regulating pancreatic size. FGF9 binds to the “c” isoforms of FGF receptors 1, 2 and 3 (FGFR1c, FGFR2c, FGFR3c), the “b” isoform of FGF receptor 3 (FGFRb), and FGR receptor 4 (FGFR4) (Ornitz & Itoh, 2015). Studies have yet to determine the receptor through which FGF9 acts within the pancreas, although *Fgfr2c* and *Fgfr1c* were reported to be expressed in the pancreatic mesenchyme at E11.5 (Sylvestersen et al., 2011). FGF9 can also signal through FGFR4, which is expressed in the pancreatic epithelial (Sylvestersen et al., 2011). It is possible FGF9 functions through multiple receptors, in either a spatially or temporally regulated manner. Although we found expression of FGF receptors in our dataset, we were not able to identify the receptors isoforms. Determining the localization pattern of these FGF receptor isoforms, either by immunohistochemistry or *in situ* hybridization, will help shed light on the potential interactions with secreted FGF9 from the mesothelium.

Studies in the lung have identified key pathways regulated by *Fgf9* signaling. Loss of *Fgf9* within the entire lung results in decreased *Fgf10* expression, which is hypothesized to lead to a reduction in epithelial branching (Colvin et al., 2001; A. C. White et al., 2006). In contrast to this result, mesothelial specific loss of *Fgf9* did not affect *Fgf10* signaling in the lung. The discrepancy between the whole body *Fgf9* knockout and the mesothelial specific knockout implies that epithelial-expressed *Fgf9* may be important for *Fgf10* expression in the mesenchyme. During cecal bud formation in the gut, *Fgf9* signals via the transcription *Pitx2* to regulate *Fgf10* expression in the mesenchyme (Alam et al., 2012). A role for *Fgf10* in pancreatic proliferation is well established. A model where *Fgf9* signaling from the mesothelium regulates *Fgf10* expression in the mesenchyme to ultimately control organ size would fit the results described in this work. Detecting changes in *Fgf10* expression levels, either at the transcript or

protein level, in *Fgf9*^{-/-} pancreata can help clarify the effect of *Fgf9* on *Fgf10* signaling. If *Fgf10* is downregulated in *Fgf9*^{-/-} pancreata, rescuing the *Fgf9*^{-/-} phenotype by addition of exogenous FGF10 will solidify an upstream role for *Fgf9* in regulating *Fgf10* signaling.

Besides *Fgf10* signaling, WNT/Beta-catenin signaling was disrupted in the mesenchyme of lungs with a mesothelial specific loss of *Fgf9* (Yin et al., 2011). The authors suggest a model whereby *Fgf9* regulates *Wnt2a* expression in the mesenchyme, which in turn regulates mesenchymal WNT/Beta-catenin and mesenchymal *Fgfr* expression. Loss of either *Fgf9* or WNT/Beta-catenin signaling resulted in increased *Noggin* expression, a BMP inhibitor, suggesting that the BMP pathway is downstream of *Fgf9*-regulated WNT/Beta-catenin signaling. As BMP signaling is known to regulate epithelial proliferation of the lung (Eblaghie, Reedy, Oliver, Mishina, & Hogan, 2006), this may be the mechanistic link of *Fgf9* to epithelial development.

Both WNT and BMP signaling have been demonstrated to have important roles in pancreatic development (Ahnfelt-Rønne et al., 2010; Larsen et al., 2015). Multiple ligands and receptors from both the WNT and BMP pathways are expressed in the mesenchymal and epithelial populations of E14.5 pancreata. Expression of the BMP receptor, *Acvr2b*, was enriched in the mesothelial compartment, along with BMP ligands, *Bmp2* and *Bmp4*. It is possible that mesothelial-secreted factors function in an autocrine manner to regulate mesothelial cell function and development. Epithelial populations also display cell-type specific expression of *Bmp1* and *Bmp7*. Expression of these ligands may be regulated by upstream pathways originating in the mesothelium, analogous to findings in the lung (Yin et al., 2011). Alternatively, these pathways may function independently of each other to regulate discrete aspects of pancreatic development.

In either case, the expression patterns found in this work can inform future approaches to unravel the relationship between *Fgf9*, WNT, and BMP signaling.

Understanding how WNT, BMP, and *Fgf10* signaling pathways are affected upon loss of *Fgf9* in the pancreas will be informative for understanding how *Fgf9* regulates pancreatic epithelial size and branching. These pathways can be tested by qPCR experiments, immunohistochemistry or sequencing approaches in *Fgf9* $+/+$ and *Fgf9* $-/-$ pancreata. Temporal and spatial control over *Fgf9* knockout by use of the *Fgf9* floxed allele will help uncover the specific role of mesothelial-expressed *Fgf9* in regulating these pathways.

Creator	Additional Relevant References	Line	Gene Driver	Cre Expressed
Zhou et al. 2008	this study	<i>Wt1tm1(EGFP/cre)Wtp</i>	Wilms tumor 1	Cre
Wilm et al. 2005	Que et al. 2008	<i>Tg(WT1-cre)AG11Dbdr</i>	Wilms tumor 1	Cre
Del Monte et al. 2011	Cano et al. 2013, Carmona et al.	<i>mWt1/IRES/GFP-Cre</i>	Wilms tumor 1	Cre
Zhou et al. 2008	this study, Dixit et al. 2013, Asahina et al. 2011, von Gise et al. 2016	<i>Wt1tm2(cre/ERT2)Wtp</i>	Wilms tumor 1	CreER
Rinkevich et al. 2012		<i>MSLN-CreERT2-IRES-lacZ</i>	Mesothelin	CreER
Means et al. 2008	this study	<i>Krt19-CreER</i>	Cytokeratin 19	CreER
Van Keymeulen et al. 2009	this study	<i>Krt18-CreER</i>	Cytokeratin 18	CreER
Cai et al. 2008		<i>Tbx18-Cre</i>	<i>T-box transcription factor 18</i>	Cre

Table 1. Mouse lines used for mesothelial lineage tracing. Study that created line is noted in “Creator” and additional studies that utilize the line for mesothelial lineage tracing are listed in “Additional Relevant References”. Gene driver and specific line is shown along with whether the line expresses a constitutive or inducible Cre.

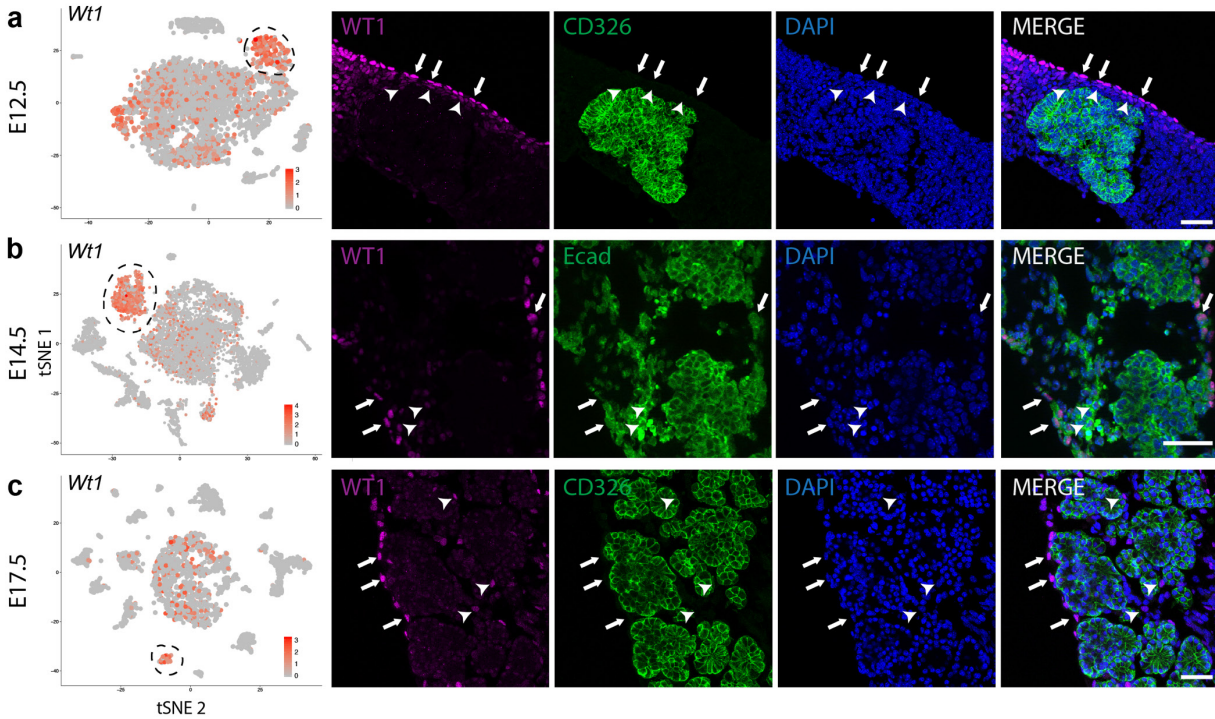


Figure 17. Expression of *Wt1* during pancreatic development. a-c) Expression of *Wt1* transcript in single-cell RNA-sequencing dataset from E14.5 pancreata (all cells) (left panel) and WT1 protein *in vivo* (four right panels) in E12.5 (a), E14.5 (b), and E17.5 (c) pancreata. Dotted circle highlights mesothelial populations in left panels. In right panels, arrows point to Wt1+ mesothelial cells and arrowheads point to Wt1+ non-mesothelial cells. Scale bars are 50 μ m.

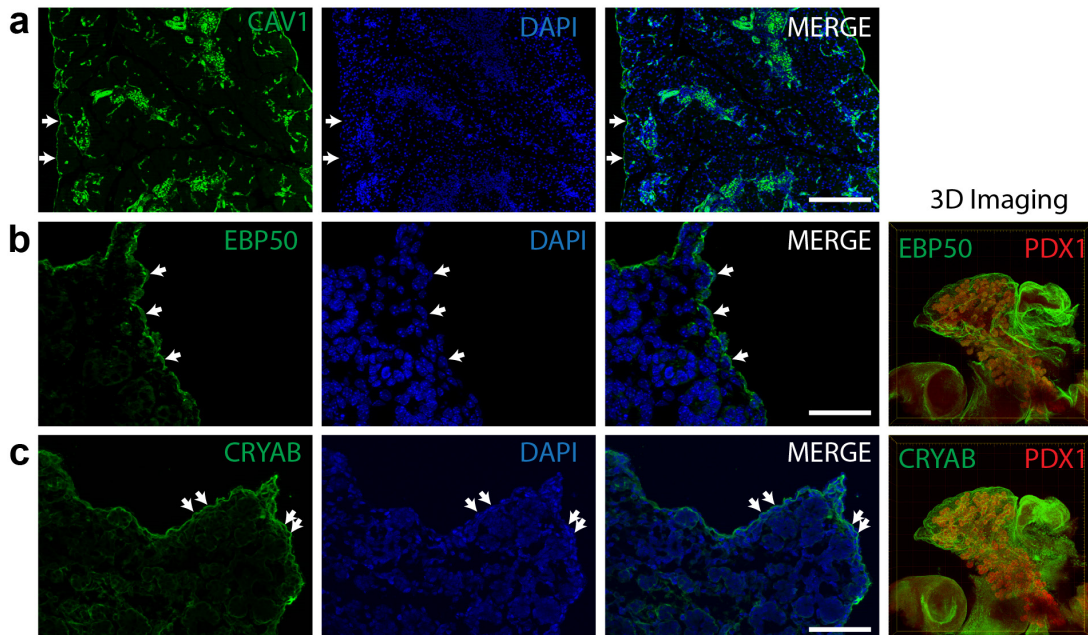


Figure 18. Identification of pancreatic mesothelial markers. (a) Immunohistochemistry for CAV1 in E17.5 pancreata. Positive signal in the internal tissue consists of Cav1+ endothelial

cells and auto-fluorescence from red blood cells. (b-c) Immunohistochemistry for novel markers, EPB50 (b) and CRYAB (c), in the mesothelium of E14.5 pancreata, as predicted by single-cell RNA-sequencing. Whole mount staining and 3D imaging for markers are depicted in right panels. (a-c) Arrows point to mesothelial cells. Scale bars represent 50 μ m.

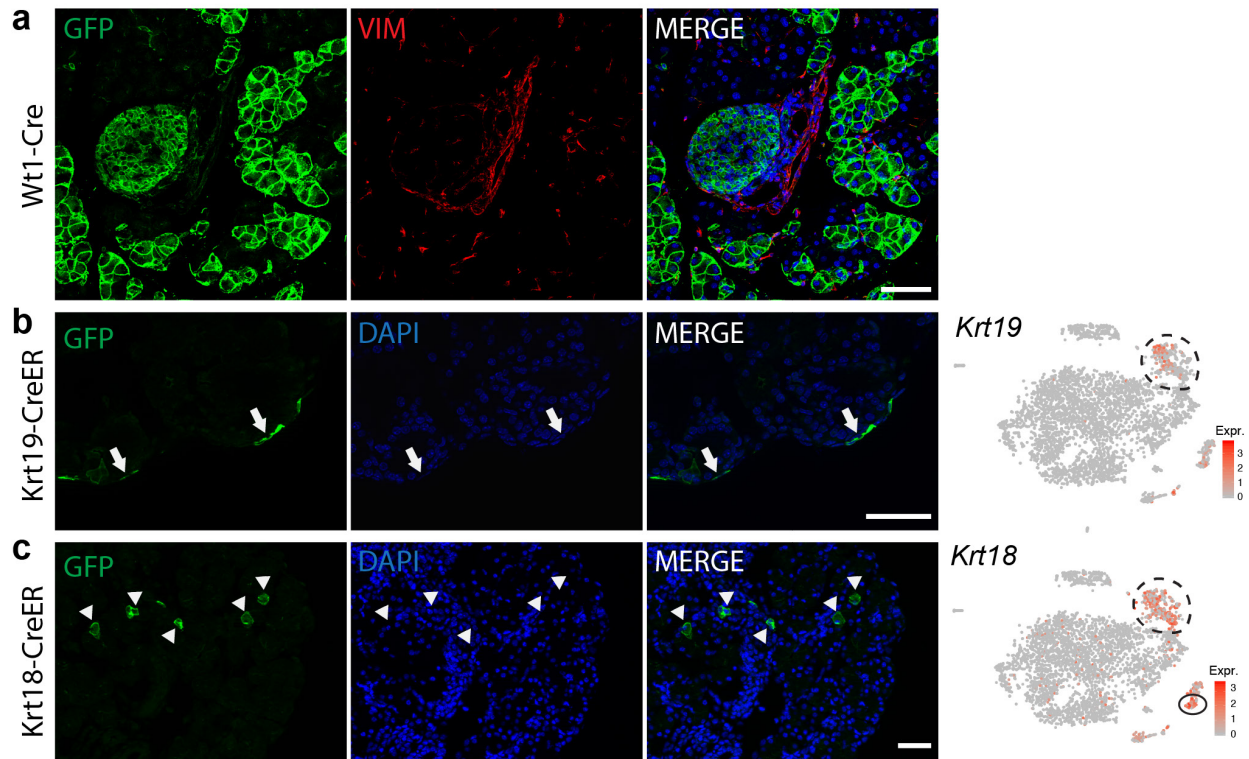


Figure 19. Unsuitable Cre drivers for mesothelial lineage tracing. (a) Immunohistochemistry for GFP (green), VIM (red) and DAPI in Wt1-Cre; Rosa26^{mTmG} adult pancreata. (b) Immunohistochemistry for GFP (green) and DAPI in Krt19-CreER; Rosa26^{mTmG} E17.5 pancreata. Pregnant dams were injected with 4.5 mg tamoxifen at E12.5 and E13.5. Arrows point to GFP⁺ mesothelial cells. Rightmost panel shows expression of *Krt19* in E12.5 single-cell RNA-sequencing dataset. Dotted circle highlights mesothelial population. (c) Immunohistochemistry for GFP (green) and DAPI in Krt18-CreER; Rosa26^{mTmG} E18.5 pancreata. Pregnant dams received 3 mg tamoxifen at E11.5 and E12.5 by oral gavage. Arrowheads point to GFP⁺ non-mesothelial cells. Rightmost panel shows expression of *Krt18* in E12.5 single-cell RNA-sequencing dataset. Dotted circle highlights mesothelial population. Solid circle highlights ductal population. (a-c) Scale bar represents 50 μ m.

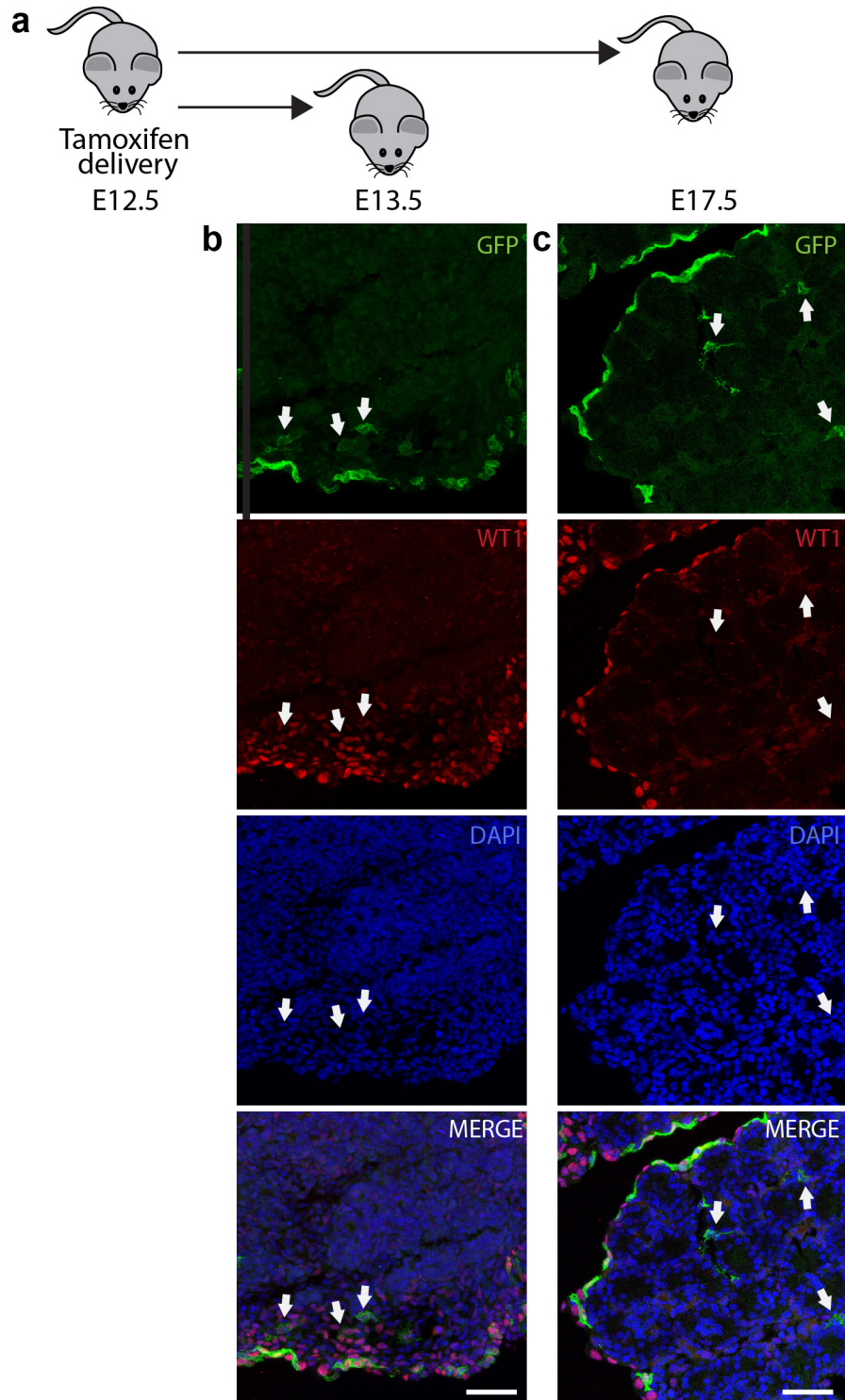


Figure 20. Lineage tracing Wt1+ cells in the embryonic pancreas. a) Tamoxifen delivery scheme for lineage tracing. Pregnant dams received two 2.5 mg doses of tamoxifen 8 hours apart at E12.5 and pancreata were collected at either E13.5 or E17.5. b-c) Immunohistochemistry for GFP (green), WT1 (red), and DAPI in lineage-traced pancreata collected at E13.5 (b) or E17.5 (c). (b-c) Scale bars represent 50 μ m. White arrows highlight GFP+ non-mesothelial cells.

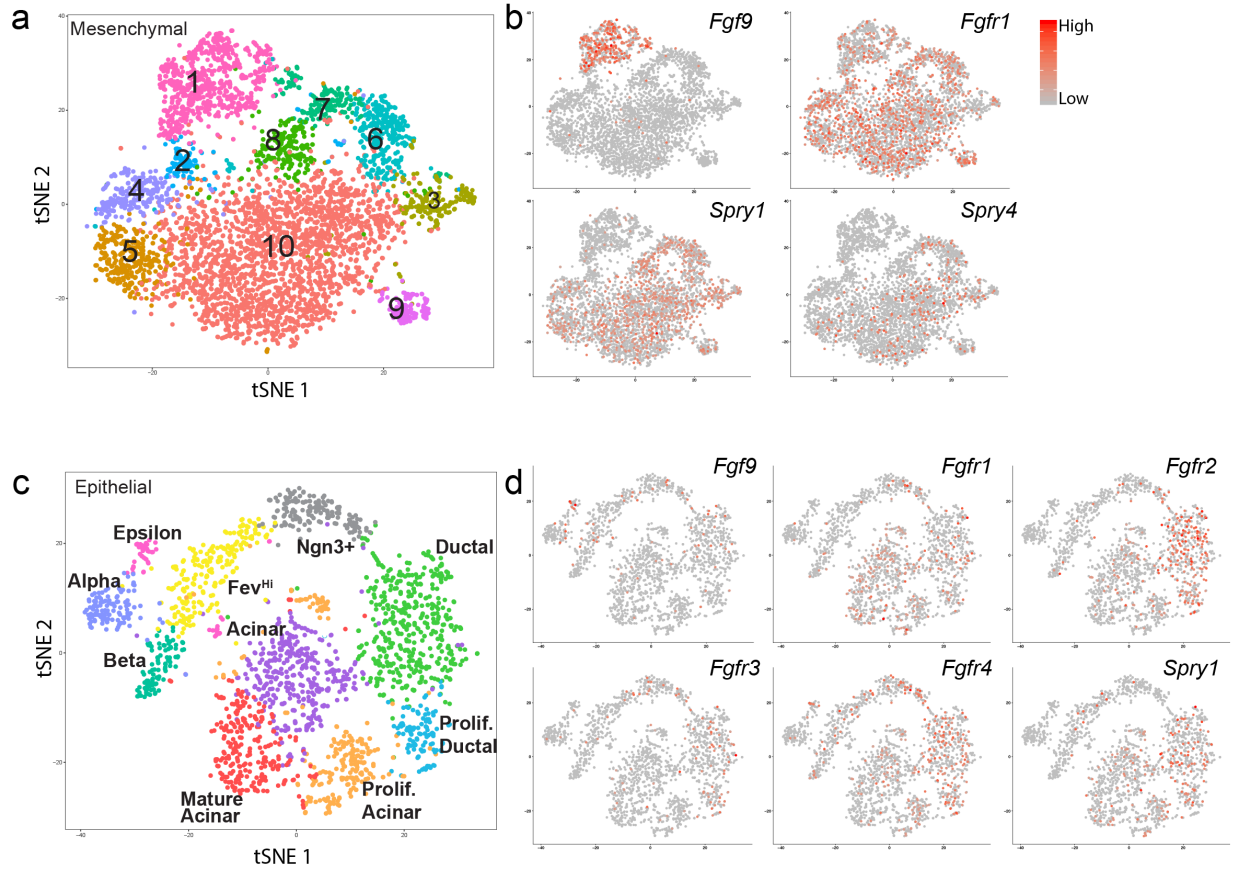


Figure 21. Expression of FGF signaling pathway components in E14.5 pancreata. (a-b) E14.5 pancreatic mesenchymal cells (from Chapter 3). a) t-SNE visualization of mesenchymal clusters, labeled by cluster ID. b) Expression of FGF ligands, receptors, and downstream targets. (c-d) E14.5 pancreatic epithelial cells (from Chapter 2). C) t-SNE visualization of epithelial clusters, labeled by cluster ID. d) Expression of FGF ligands, receptors, and downstream targets. (b, d) Color indicates level of expression, as depicted by legend in (b).

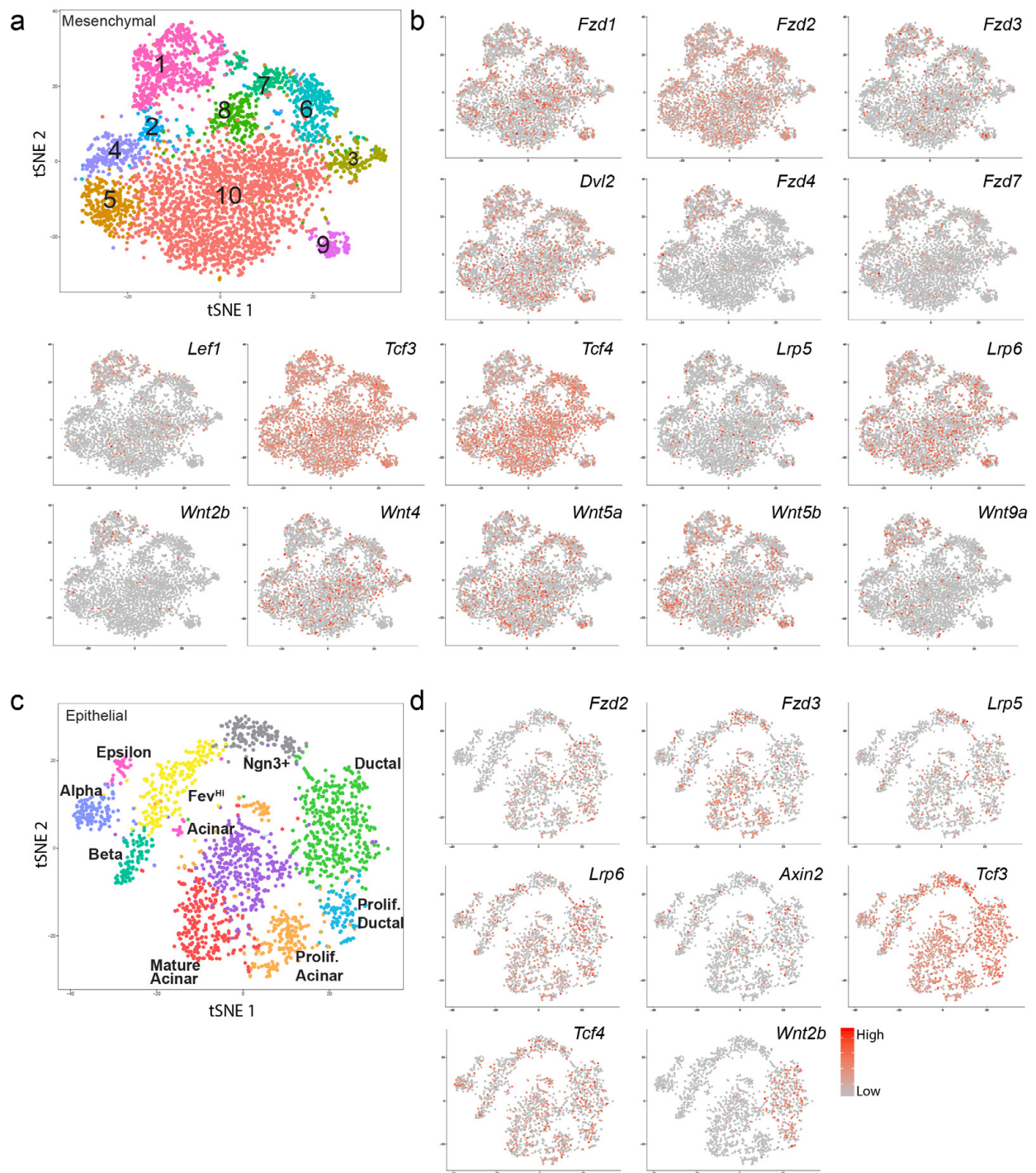


Figure 22. Expression of WNT signaling pathway components in E14.5 pancreata. (a-b) E14.5 pancreatic mesenchymal cells (from Chapter 3). a) t-SNE visualization of mesenchymal clusters, labeled by cluster ID. b) Expression of WNT ligands, receptors, and downstream targets. Color indicates level of expression. (c-d) E14.5 pancreatic epithelial cells (from Chapter 2). C) t-SNE visualization of epithelial clusters, labeled by cluster ID. d) Expression of WNT ligands, receptors, and downstream targets. (b,d) Color indicates level of expression, as indicated by legend in (d).

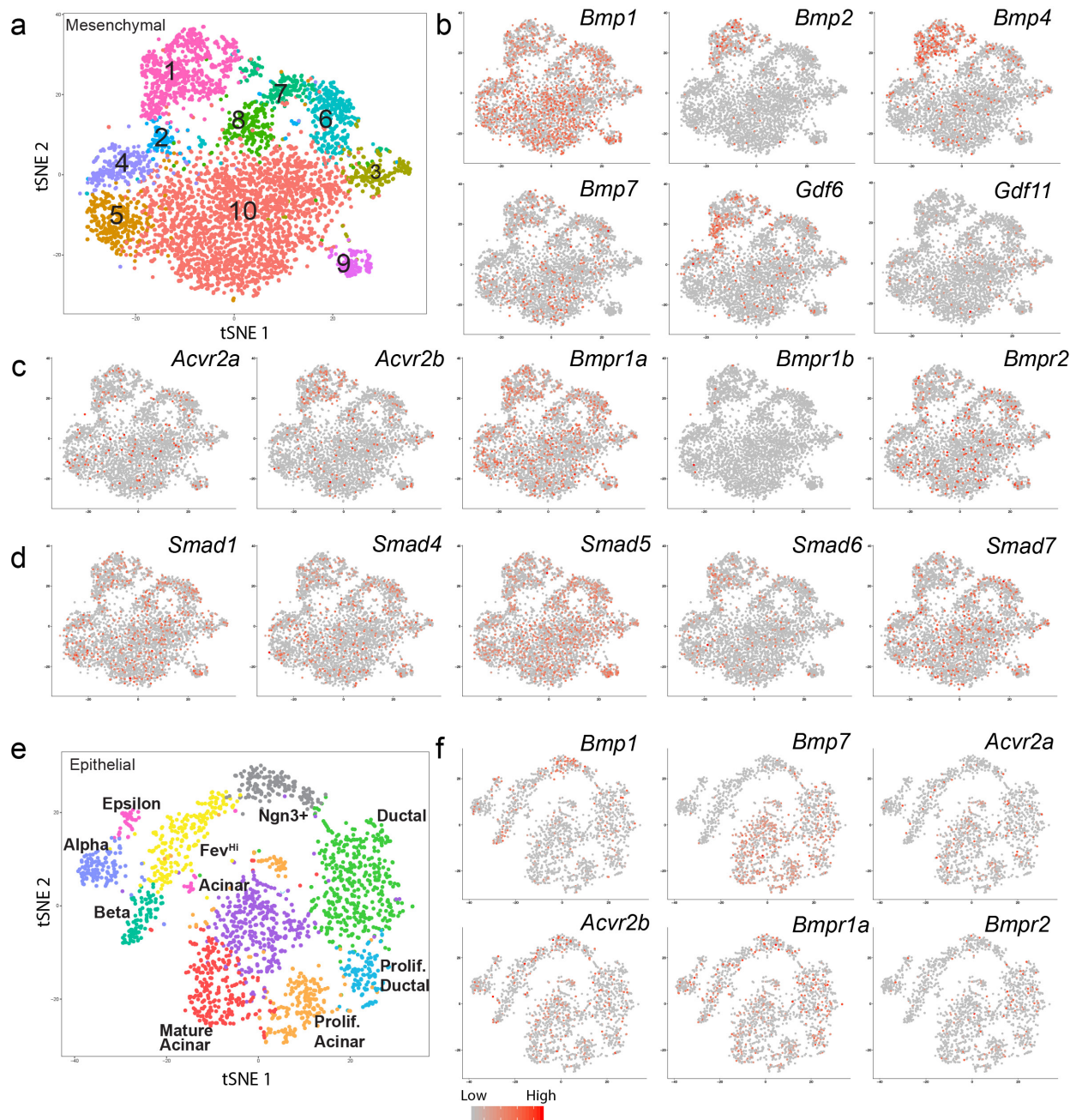


Figure 23. Expression of BMP signaling pathway components in E14.5 pancreata. (a-d) E14.5 pancreatic mesenchymal cells (from Chapter 3). a) t-SNE visualization of mesenchymal clusters, labeled by cluster ID. (b-d) Expression of BMP ligands (b), receptors (c), and downstream targets (d). (e-f) E14.5 pancreatic epithelial cells (from Chapter 2). e) t-SNE visualization of epithelial clusters, labeled by cluster ID. f) Expression of BMP ligands, receptors, and downstream targets. (b-d,f) Color indicates level of expression, as depicted in legend in (f).

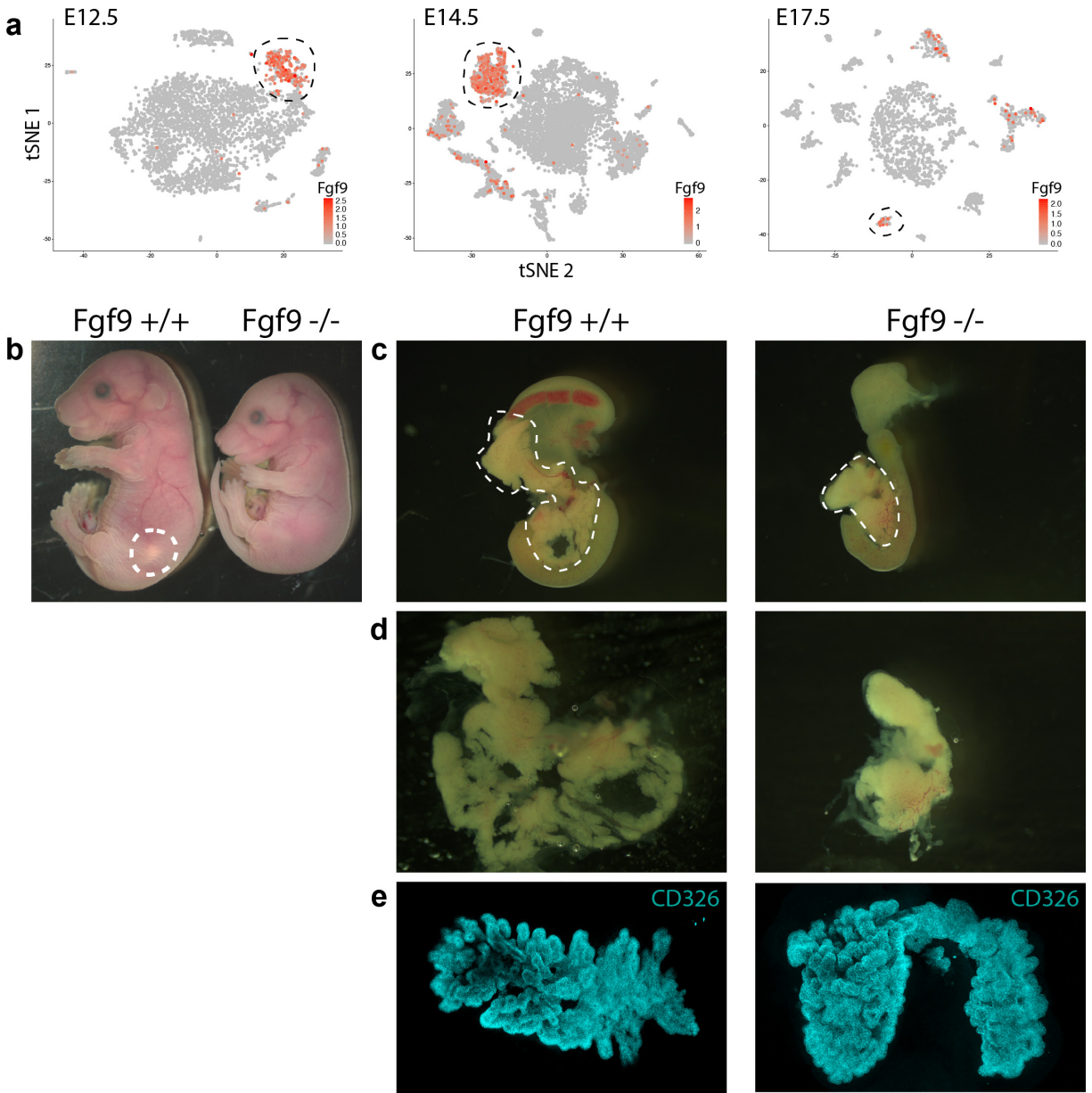


Figure 24. Loss of *Fgf9* results in a hypoplastic pancreas. a) Expression of *Fgf9* in single-cell RNA-sequencing datasets from E12.5, E14.5, and E17.5 pancreata. Expression level is indicated by red color. Dotted circle highlights mesothelial population. b) Littermate *Fgf9* $+/+$ and *Fgf9* $-/-$ embryos. Dotted circle highlights pancreas in *Fgf9* $+/+$ embryo. c) Dissected whole gut tube from *Fgf9* $+/+$ and *Fgf9* $-/-$ embryos, including stomach, spleen, pancreas, and proximal intestine. Dotted circle highlights pancreas. d) Dissected pancreata from *Fgf9* $+/+$ and *Fgf9* $-/-$ embryos. e) Whole mount imaging of pancreata stained with CD326. *Fgf9* $+/+$ image contains only dorsal pancreas. *Fgf9* $-/-$ pancreata includes both dorsal and ventral pancreas.

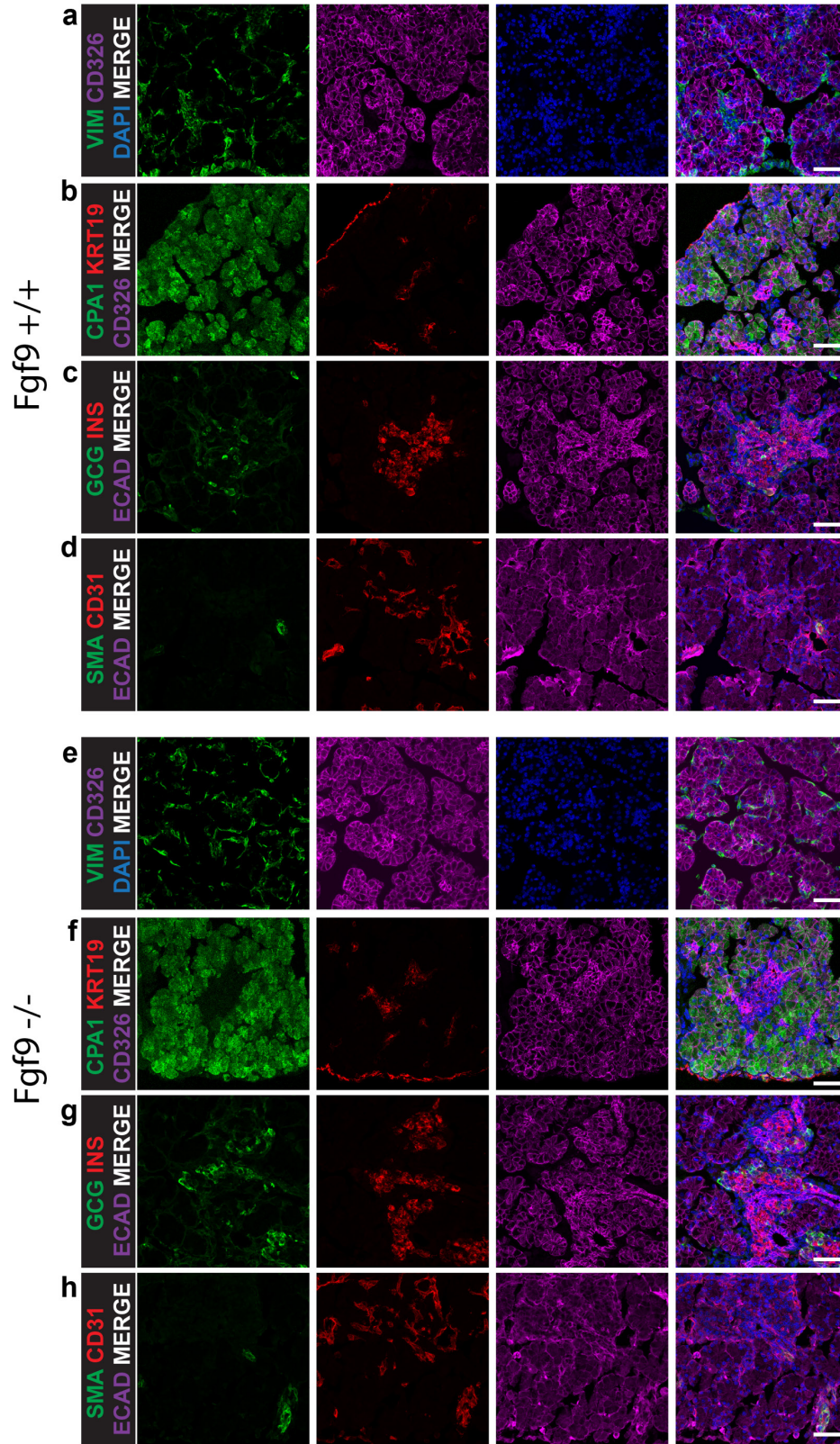


Figure 25. Major lineages of the pancreas are present in E17.5 *Fgf9*^{-/-} pancreata. (a-h) Immunofluorescence on E17.5 pancreata from *Fgf9*^{+/+} embryos (a-d) or *Fgf9*^{-/-} (e-h) embryos.

Expression of mesenchymal marker, VIM (green), and epithelial marker, CD326 (purple). (b,f) Expression of acinar cell marker, CPA1 (green), ductal and mesothelial cell marker, KRT19 (red) and epithelial marker, CD326 (purple). (c,g) Expression of alpha cell marker, GCG (green), beta cell marker, INS (red), and epithelial marker, CD326 (purple). (d,h) Expression of vascular smooth muscle cell marker, SMA (green), endothelial cell marker, CD31 (red), and epithelial marker, ECAD (purple). (a-h) Scale bars represent 50 um. DAPI is included in all merged images.

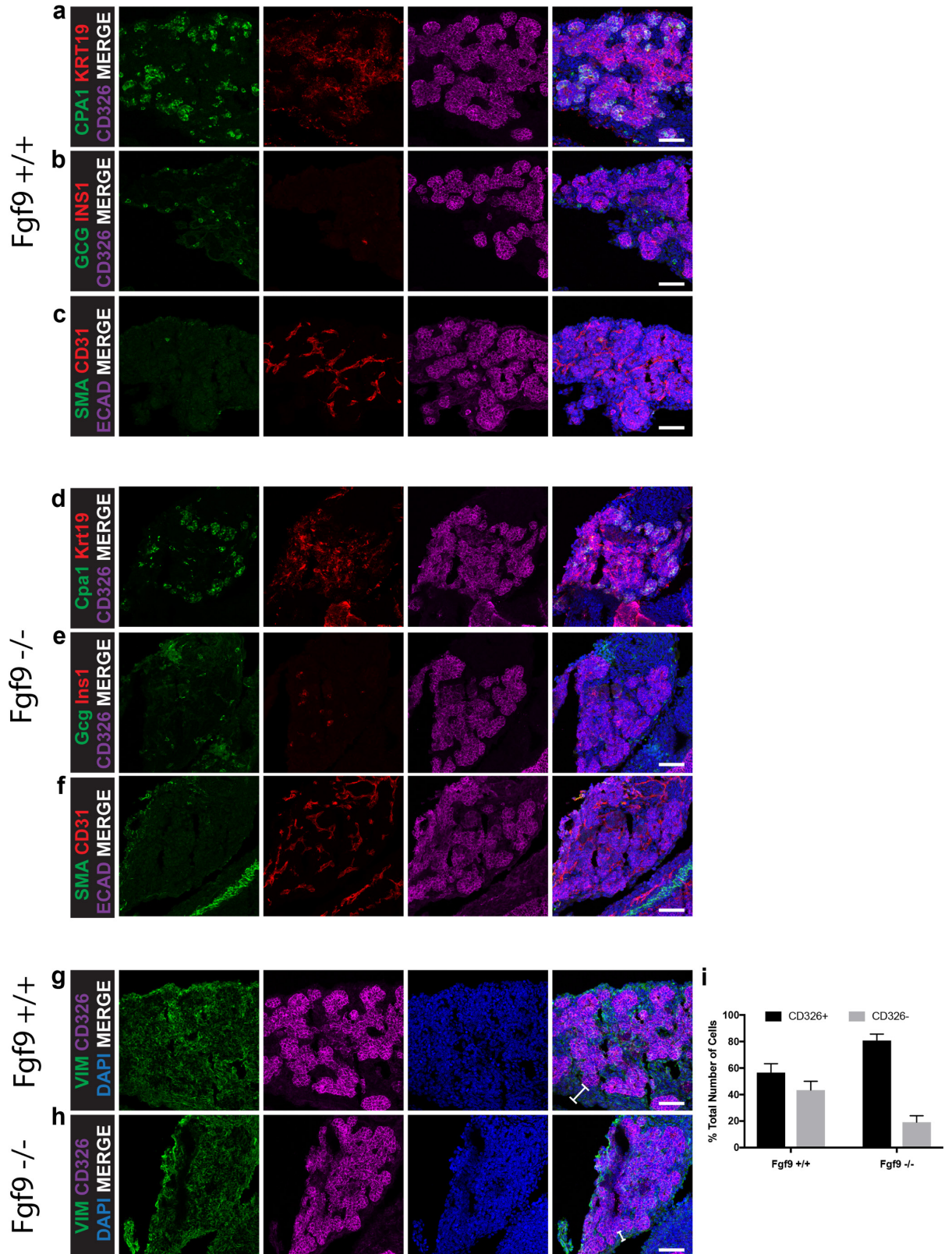


Figure 26. E13.5 Fgf9^{-/-} pancreata have a shifted ratio of mesenchymal to epithelial cells
 (a-h) Immunofluorescence on E13.5 pancreata from Fgf9^{+/+} (a-c, g) or Fgf9^{-/-} (d-f, h)

embryos. (a,d) Expression of acinar cell marker, CPA1 (green), ductal and mesothelial cell marker, KRT19 (red), and epithelial marker, CD326 (purple). (b,e) Expression of alpha cell marker, GCG (green), beta cell marker, INS (red), and epithelial marker, CD326 (purple). (c,f) Expression of vascular smooth muscle cell marker, SMA (green), endothelial cell marker, CD31 (red), and epithelial marker, ECAD (purple). (g,h) Expression of mesenchymal marker, VIM (green), and epithelial marker, CD326 (purple). Brackets indicate the size of surrounding mesenchymal compartment. i) Quantification of CD326⁺ and CD326⁻ cells in Fgf9^{-/-} and Fgf9^{+/+} pancreata. 3 fields of view from n=1 embryo was counted. Error bars represent standard deviation. (a-f) Scale bars represent 50 μ m. DAPI is included in all merged images.

Chapter 5

Mesenchymal heterogeneity in adult homeostasis and fibrotic disease

Introduction

Pancreatitis is a set of inflammatory diseases that result in degradation of the pancreas. Acute pancreatitis is characterized by infiltration of monocytes, leukocytes, and granulocytes, loss of acinar cells, and activation of a fibroblast population called pancreatic stellate cells (PSCs) (Manohar, Verma, Venkateshaiah, Sanders, & Mishra, 2017). Upon repeated insult to the pancreas, prolonged inflammation and activation of PSCs results in production and deposition of extracellular matrix, ultimately leading to fibrosis and development of chronic pancreatitis (Manohar et al., 2017). Globally, 13-45 per 100,000 persons are diagnosed with acute pancreatitis annually (Yadav & Lowenfels, 2013), and acute pancreatitis is the leading cause of hospitalizations for gastrointestinal disorders in the United States (Peery et al., 2012). 5-12 per 100,000 persons are diagnosed with chronic pancreatitis every year with a prevalence of about 50 per 100,000 persons globally (Yadav & Lowenfels, 2013). Multiple risk factors for the development of pancreatitis, including alcohol consumption, smoking, obesity, gallstones, and genetic susceptibility, suggest a multifactorial etiology of pancreatitis (Lee, Zhao, & Habtezion, 2017).

Individuals with acute pancreatitis suffer from severe abdominal pain and are at risk for persistent organ failure and death while those with chronic pancreatitis can develop pancreatic insufficiency and diabetes (Mandalia, Wamsteker, & DiMagno, 2018; Pham & Forsmark, 2018). Treatments include supportive care and lifestyle changes for acute pancreatitis and replacement of digestive enzymes and insulin by exogenous sources in the case of chronic pancreatitis. Currently, there are no treatments that can prevent or reverse the progression of chronic pancreatitis and fibrosis, highlighting a critical need for improved understanding of disease pathology and identification of disease targets.

Studying the pathology of pancreatitis requires the development of model systems that can replicate disease onset and progression. The complex etiology of pancreatitis has made the development of model systems challenging. Our current mechanistic understanding of pancreatitis has been derived from *in vitro* studies, animal models, and limited experiments with tissue from pancreatitis patients (Gorelick & Lerch, 2017; Lerch & Gorelick, 2013). While each model can provide key benefits for studying pancreatitis, no single model captures all aspects of disease development, progression, and regeneration. Nevertheless, multiple animal models of both acute and chronic pancreatitis display a disease phenotype that resembles the human condition, allowing for study of the mechanistic regulation of the disease.

One of the most common models of acute pancreatitis is the injection of supraphysiological levels of the drug caerulein, a peptide orthologue of cholecystokinin (CCK) (Lerch & Gorelick, 2013). CCK is a hormone that regulates the secretion of digestive enzyme from acinar cells (Smith & Solomon, 2014). Injection of caerulein at 10-100 times the physiological levels of CCK results in premature activation of pancreatic proteases that lead to autodigestion of the pancreas in rats and mice (Lampel & Kern, 1977; Niederau, Ferrell, & Grendell, 1985; Yamaguchi, Kimura, Mimura, & Nawata, 1989). The caerulein injections induce a phenotype that resembles acute pancreatitis, including edema, necrosis, and inflammation. Additionally, caerulein-injected pancreata recover within a few days, modeling the recovery of human patients from an acute attack. The caerulein model is relatively easy to perform and reproducible, and allows for the study of the intracellular mechanisms during disease progression, leading to its popularity as an acute pancreatitis model (Gorelick & Lerch, 2017). Additionally, this model can be combined with other methods, such as duct ligation (Sendler et al., 2015), or modified, such as performing repeated injections over multiple weeks, to induce

pancreatic fibrosis, resembling chronic pancreatitis (Neuschwander-Tetri et al., 2000). The induction of pancreatitis modeled by caerulein injections most closely resembles the induction caused by scorpion venom (Becerril, Marangoni, & Possani, 1997) or cholinergic toxins (Singh, Bhardwaj, Verma, Bhalla, & Gill, 2016), which does not represent the etiology for most pancreatitis patients. Additionally, disease progression differs between mice and rats, and the severity of disease depends on the strain of mice. Nevertheless, the caerulein model offers the advantages of reproducibility and ease of use for studying the cell biology of pancreatitis, and is thus the most popular model to date (Gorelick & Lerch, 2017; Su, Cuthbertson, & Christophi, 2006).

In contrast to the limited relevance of the caerulein-induced etiology, ethanol-induced pancreatitis aims to model the effects of alcohol, a major risk factor for pancreatitis, on the induction of the disease. However, treatment with ethanol alone has not produced pancreatitis in animals, and instead requires sensitization by co-treatment with CCK (Saluja & Bhagat, 2003) or the bacterial endotoxin lipopolysaccharide (LPS) (Vonlaufen et al., 2007). These models have been used to study the effects of ethanol metabolites on acinar cells and microcirculation during pancreatitis (Su et al., 2006). The model of ethanol-feeding with LPS stimulation is thought to be one of the most clinically relevant models, as patients with chronic alcoholism display increased serum levels of LPS (Urbaschek et al., 2001). The mechanisms by which LPS may contribute to acute pancreatitis development remain unclear, but LPS has been shown to evoke expression of inflammatory mediators in acinar cells, which was exacerbated by alcohol metabolites (H. Gu et al., 2013). Therefore, these combinatory models may help provide insight into the etiology of alcohol-associated acute pancreatitis.

Genetic mouse models of pancreatitis have also been developed based on discovery of human mutations that lead to the development of pancreatitis, termed hereditary pancreatitis (Aghdassi et al., 2011; Whitcomb et al., 1996). Individuals with mutations in the *serine protease inhibitor Kazal type 1 (SPINK1)*, *cystic fibrosis transmembrane conductance regulator (CFTR)*, *chymotrypsinogen C (CTRC)* and *calcium-sensing receptor (CASR)*, are at increased risk for chronic pancreatitis (Keim et al., 2001). Correspondingly, mutations in genes such as *trypsin 4 (Try4)*, *serine protease inhibitor Kazal type 3 (Spink3)*, and *Cftr* in mice result in the development of various characteristics of pancreatitis, such as enhanced trypsin activity, inflammation, and acinar cell necrosis (Dimagno et al., 2005; Ohmuraya, Hirota, Araki, Baba, & Yamamura, 2006; Ohmuraya et al., 2005; Selig et al., 2006). While these models allow for the study of individual gene function in pancreatitis, the constitutive loss of these genes throughout the body may induce systemic and secondary effects that confound our understanding of the gene's role within the pancreas.

Another model of pancreatitis entails the administration of L-arginine (Arg) (Mizunuma, Kawamura, & Kishino, 1984), which induces acinar cell necrosis in a dose-dependent manner in rats. Lower, repeated doses of Arg can lead to chronic pancreatitis in rats. The mechanism of action for Arg remains unclear, although it is hypothesized that the production of free radicals, Arg metabolites, and cytokines lead to disease development. The ability to regulate the severity of pancreatitis is an advantage of this model. However, Arg-induced pancreatitis in mice has been inconsistent with the findings in rats, and the relevance of this model to the development of pancreatitis in humans remains unknown (Su et al., 2006).

Besides treatment with exogenous inducers, surgical procedures have also been used to model pancreatitis in animals. Ligation of the pancreatic duct, infusion of bile salts into the

pancreatic duct, perfusion of the pancreatic duct, and closing the duodenal loop have all been performed to model different aspects of pancreatitis (Su et al., 2006). These models most closely resemble the etiology of gallstone-induced pancreatitis. Many of these techniques require surgical expertise, have limited reproducibility, or show incomplete development of pancreatitis.

The combination of multiple experimental models of pancreatitis, *in vitro* studies, and studies of human tissue have helped shed light on the underlying pathology of pancreatitis (Fig. 27a). Acute pancreatitis is characterized by improper activation and secretion of acinar-produced digestive enzymes, protease-induced injury to cellular membranes, infiltration of immune cells, and activation of PSCs (Lankisch, Apte, & Banks, 2015). Identification of a mutation in the trypsinogen gene, which produces a degradation-resistant protease, in patients with hereditary pancreatitis, suggested that improper activation of digestive enzymes could cause pancreatitis (Whitcomb et al., 1996). Further studies demonstrated that dysfunctional lysosomes led to an imbalance of lysosomal hydrolases, cathepsins, resulting in a failure to degrade trypsin and an accumulation of trypsin in autophagic vacuoles within acinar cells (Gukovsky & Gukovskaya, 2010; Gukovsky et al., 2012). The accumulation of trypsin activates digestive enzymes that can result in auto-digestive injury and improper release of active trypsin into the surrounding interstitial space (Gaisano et al., 2001; Lankisch et al., 2015). The injury wrought by the release of active trypsin stimulates an inflammatory response, with the infiltration of neutrophils, eosinophils, macrophages, and monocytes and secretion of multiple chemokines and cytokines (Manohar et al., 2017). These inflammatory signals can then activate PSCs, which themselves then secrete additional cytokines and chemokines. Ultimately, this cascade of events induces apoptosis and necrosis of the pancreatic parenchyma, which can result in additional damage to

surrounding tissue, such as the vasculature (Barge & Lopera, 2012; Gukovskaya & Pandol, 2004).

Upon clearing of the initial insult, the pancreas recovers from the damage of an acute pancreatitis attack within days to weeks (Murtaugh & Keefe, 2015). Studies have sought to understand the cellular mechanisms underlying the reduction of the inflammatory response and regenerative capacity of the exocrine pancreas after injury. In addition to immune cell infiltration, PSC activation, and cellular death, tubular structures, also termed acinar-to-ductal metaplasia (ADM), are a hallmark of pancreatitis in both human tissue and mouse models (Bockman, Boydston, & Anderson, 1982; Ebert et al., 1999; Zang et al., 2015). These structures are thought to be a result of acinar cell dedifferentiation, marked by upregulation of developmental genes *Pdx1* and *Hes1* (Jensen et al., 2005; Miyamoto et al., 2003), and ductal genes, such as the transcription factor *sex-determining region Y-Box 9* (*Sox9*), and intermediate filament *cytokeratin19* (*Krt19*) (Morris, Cano, Sekine, Wang, & Hebrok, 2010; Zhong et al., 2004; Zimmermann et al., 2002).

Successful regeneration has been linked to the resolution of these ADM structures and the dampening of the inflammatory response (Fendrich et al., 2008; Figura, Morris, Wright, & Hebrok, 2014; Siveke et al., 2008). The resolution of ADM and subsequent regeneration of exocrine tissue could be due to the redifferentiation of dedifferentiated acinar cells (Murtaugh & Keefe, 2015). This model is supported by lineage tracing experiments demonstrating that the majority of newly regenerated acinar cells after injury are produced by pre-existing acinar cells rather than neogenesis from a stem cell source (Desai et al., 2007; Strobel et al., 2007). The differentiation of ADM structures has been proposed to be regulated by opposing actions of prodifferentiation factors, such as *Nr5a2*, *Notch1*, and *Smo*, and factors involved in promoting

inflammation, acinar cell death, and acinar dedifferentiation, such as *Nf-kB* (Murtaugh & Keefe, 2015) Liou:2013dm}. In this model, the balance between these factors dictates whether acute pancreatitis is resolved or progresses to chronic pancreatitis (Murtaugh & Keefe, 2015).

Chronic pancreatitis is a disease characterized by consistent, low-grade inflammation, and fibrosis of the pancreas. Similar to acute pancreatitis, the etiology of chronic pancreatitis is not well understood, with multiple risk factors and potential origins of the disease, including duct obstruction, genetic factors, or repeated episodes of acute attacks (Majumder & Chari, 2016). Regardless of the initial insult, the death of pancreatic exocrine cells results in deposition of extracellular matrix (ECM) in the interstitial spaces once occupied by these exocrine cells. This expanded fibrosis disrupts the morphology and structural integrity of the pancreas, preventing the function of both the exocrine and endocrine compartments. Therefore, individuals with chronic pancreatitis suffer from malnutrition due to the failure to secrete enzymes for food digestion and diabetes (Brock, 2013).

The pathogenesis of both acute and chronic pancreatitis highlights the role of a variety of different cell types, including acinar, ductal, immune, and pancreatic stellate cells. While much emphasis has been placed on understanding the cascade of events within the acinar cell, the function of PSCs during disease progression and regeneration has also begun to receive attention. As their name implies, PSCs share many characteristics with hepatic stellate cells (HSCs), such as the star-shaped morphology (the original German name for HSCs was “sternzellen” or “star cells” (Kupffer, 1876)), and the presence of lipid droplets containing vitamin A (Apte, Pirola, & Wilson, 2012). These star-shaped, vitamin A storing PSCs are estimated to comprise 4-7% of pancreatic cell mass, and are localized at the base of the pancreatic acini as well as near blood vessels and pancreatic ducts (Apte et al., 1998; Bachem et al., 1998; Ikejiri, 1990; Watari, Hotta,

& Mabuchi, 1982). Transcriptional markers of quiescent PSCs include *desmin (Des)*, *vimentin (Vim)*, *nestin (Nes)*, and *glial fibrillar acidic protein (Gfap)*, although not all PSCs express all markers. For example, only 20-40% of cultured PSCs were shown to express *Des* (Bachem et al., 1998). During homeostasis, PSCs function to maintain ECM turnover (Phillips et al., 2003), and facilitate acinar cells' secretion of digestive enzymes in response to cholecystokinin (CCK) (Berna et al., 2010; Phillips et al., 2010).

During injury, PSCs undergo multiple morphological, transcriptional, and functional changes, often referred to as an “activation” process. Upon activation, PSCs no longer contain vitamin A lipid droplets, and begin to express genes associated with “myofibroblasts” such as *alpha smooth muscle actin (Acta2)* and ECM proteins, including *collagen I, II*, and *fibronectin (FnI)* (Apte et al., 1999; Omary, Lugea, Lowe, & Pandol, 2007). Activated PSCs also increase their expression of *Nes*, an intermediate filament expressed in neural stem cells (Lardon, Rooman, & Bouwens, 2002). *Acta2* is most commonly used to mark activated PSCs, but this marker is also expressed in other cell types, including myofibroblasts, vascular smooth muscle cells, and pericytes (Erkan et al., 2011). The expression profiles and functions of these various cell types remains poorly defined during homeostasis and disease conditions. PSCs can be activated indirectly after injury through the secretion of cytokines from infiltrating immune cells (Apte et al., 1999; Mews et al., 2002; E. Schneider et al., 2001) or directly by the insult itself, such as alcohol metabolites or oxidative stress (Apte et al., 2000). In particular, *transforming growth factor beta (Tgf-b)*, *platelet-derived growth factor (Pdgf)*, and *fibroblast growth factor (Fgf)* ligands have been demonstrated to activate PSCs (Apte et al., 1999; Luttenberger et al., 2000; Satoh, Shimosegawa, Hirota, Koizumi, & Toyota, 1998).

Functionally, PSCs increase their proliferation (Mews et al., 2002; E. Schneider et al., 2001), migration (McCarroll et al., 2004), and secretion of cytokine, chemokines, growth factors, and ECM proteins during activation (Andoh et al., 2000; Shek et al., 2002). Increased expression of *DES* was found in human tissue from chronic pancreatitis patients and in a rat model of chronic pancreatitis. The authors suggest that this could indicate increased replication of PSCs during disease *in vivo* (Haber et al., 1999), although another possibility is the appearance of a different disease-induced cell type that also expresses this protein. Evidence for both autocrine and paracrine effects of cytokine secretion have been documented, although most of this work has been *in vitro*. For example, treatment of PSCs with TGF- β 1 was shown to regulate expression of *matrix metalloproteinases (MMPs)* and *procollagen type 1* (Shek et al., 2002). Moreover, PSCs expressed *Tgf- β 1* and *Tgf- β* receptors, and inhibition of TGF- β 1 *in vitro* led to decreased *MMPs* and *procollagen type 1* expression, suggesting autocrine regulation of PSC behavior by TGF- β 1 (Shek et al., 2002). Another study found ethanol, acetaldehyde, IL-6 and TGF- β 1 upregulated expression of *MMPs* and *tissue inhibitor of metalloproteinases 2 (Timp2)* in PSCs, suggesting a role for PSCs in ECM turnover and subsequent fibrosis (Phillips et al., 2003). With a lack of markers specific for PSCs, these findings have yet to be verified *in vivo*.

Given the important contributions of PSCs to the development of fibrosis during injury, the cellular origin of these cells has become a major question in the field. Studies of the origin of hepatic stellate cells (HSCs), which share many morphological and transcriptional features with PSCs (Erkan et al., 2010), have provided clues for the potential origin of PSCs. Dual expression of mesenchymal markers, *Des* and *Vim*, and neuronal markers, *Nes* and *Gfap*, by HSCs suggested potential derivation from mesoderm or neural crest (Roskams, Cassiman, De Vos, & Libbrecht, 2004). Lineage tracing with the neural crest marker, Wnt1-Cre, did not support a

neural crest origin of HSCs (Cassiman, Barlow, Vander Borgh, Libbrecht, & Pachnis, 2006). In contrast, lineage tracing with the MesP1-Cre line, which marks early mesoderm cells during gastrulation, supported a mesoderm origin of HSCs (Asahina et al., 2008; Saga et al., 1999). Whether PSCs are also derived from mesodermal tissues remains to be tested.

Further studies have focused on the cell types within the mesoderm that give rise to HSCs in the liver and myofibroblasts during injury across multiple organs. As mesothelial layers have been demonstrated to give rise to mesenchymal cell types during organogenesis (see Chapter 4), studies have lineage traced these cells during adult liver homeostasis and disease. Utilizing the Wt1-CreER mouse line, Li and colleagues demonstrated that hepatic mesothelial cells underwent a mesothelial-to-mesenchymal transition (MMT), and contributed to HSCs and activated HSCs in two mouse models of liver fibrosis (Yuchang Li, Wang, & Asahina, 2013). Another study by the same group demonstrated that TGF- β signaling within hepatic mesothelial cells promoted their migration and differentiation towards an HSC fate (Yuchang Li, Lua, French, & Asahina, 2016). Similar to the liver, the adult epicardium has been demonstrated to undergo MMT and give rise to fibroblasts, myofibroblasts, and vascular smooth muscle cells after myocardial infarction (Bin Zhou et al., 2011). These epicardial-derived cell types did not contribute to the myocardial cell types of the regenerating heart, but secreted factors that supported the regeneration process (Bin Zhou et al., 2011; González-Rosa, Peralta, & Mercader, 2012; J. Wang, Karra, Dickson, & Poss, 2013). Finally, studies of human mesothelial cells have provided evidence of peritoneal MMT during peritoneal dialysis both *in vitro* and by *in vivo* staining of human tissue (Yáñez-Mó et al., 2003). Therefore, mesothelial layers may retain their differentiation capacity during adult injury conditions to give rise to activated fibroblasts.

Studies of the pleural mesothelial layer have also supported a mesothelial origin of myofibroblasts during lung injury, although the timing of MMT is debated. Lineage tracing of adult pleural mesothelial cells with the Wt1-CreER mouse line showed their MMT, migration and differentiation into lung myofibroblasts after TGF- β 1-induced injury (Karki et al., 2014). In contrast to an adult mesothelial origin, another study found only fetal pleural mesothelial cells contributed to myofibroblasts in two models of lung injury (Gise et al., 2016). The different conclusions of these studies may result from the short, 4 hour time window after injury examined by Karki et al. Von Gise et al. suggest that only the mesenchymal cells derived from fetal mesothelial cells make long-term contributions to the activated fibroblasts during injury. Therefore, whether adult or fetal mesothelial cells are the main contributors to myofibroblasts may vary across organ systems.

Evidence from these other organ systems suggest that the pancreatic mesothelium may act as a source of PSCs and activated PSCs during pancreatitis. The finding that epicardial-derived cells secrete factors critical for heart regeneration (Bin Zhou et al., 2011; González-Rosa et al., 2012; J. Wang et al., 2013) supports a model of mesothelial-derived activated PSCs, which are known to be a source of multiple cytokines, chemokines, and growth factors upon activation *in vitro*. Experiments that lineage trace the adult pancreatic mesothelium can help elucidate the derivation of different mesenchymal cell types present during pancreatitis.

The known importance of activated PSCs in pancreatitis warrants a better understanding of their heterogeneity, origin, and function. Similar to the mesenchymal compartment during development, very little is known about the heterogeneity of this compartment during adult homeostasis. While studies have attempted to differentiate PSCs from other mesenchymal cell types, such as fibroblasts, vascular smooth muscle, and pericytes, they have often relied on

broadly expressed, poor markers derived from *in vitro* experiments. It has been difficult to define sets of specific markers for each of these cell types *in vivo*. As different cell types may have distinct functions during homeostasis and injury, being able to non-ambiguously define these cell types is critical. Once the mesenchymal cell types are defined, the dynamics of these cellular populations during disease progression can then be assessed. For example, do new disease-specific populations arise during pancreatitis? Are there shifts in proportions of cell types during different stages of disease progression and recovery? Are there transcriptional changes within homeostatic populations upon injury? (Fig. 27). Answers to these questions will uncover how the pancreatic mesenchyme changes during pancreatitis and offer new cell types and transcriptional targets to prevent or reverse the progression of disease.

In this work, we utilize single-cell RNA-sequencing to profile the heterogeneity of the mesenchymal compartment during adult homeostasis and fibrotic disease. We first establish the caerulein model of acute pancreatitis in Swiss Webster mice and verify the induction of pancreatitis. Next, we optimize dissociation conditions for adult pancreata, and highlight multiple challenges that remain in deriving highly viable, representative single-cell suspensions from adult pancreata. Finally, we describe the transcriptional and cellular heterogeneity identified by single-cell RNA-sequencing of PBS- and caerulein-treated pancreata at three days post-injection, identifying multiple subtypes of mesenchymal and mesothelial populations. Shifting populations between PBS and caerulein pancreata reveal potential disease-driven transcriptional changes and biases in mesenchymal and mesothelial populations. This work begins to define individual mesenchymal cell types in the adult pancreas, and starts to unravel the changes induced by fibrosis within this compartment.

Results

Caerulein-induced acute pancreatitis timecourse

We first set out to establish the caerulein-induced mouse model of acute pancreatitis in our laboratory. We injected either 75 ug/kg caerulein or PBS once per hour for 8 hours on two consecutive days into the peritoneum of 6-8 week old Swiss Webster adult mice, as previously reported (Fukuda, Morris, & Hebrok, 2012; Jensen et al., 2005) (Fig. 28a). Pancreata were collected at 24 hr, 48 hr, 72 hr, and 5 days post-injection and stained with hematoxylin and eosin. In comparison to PBS injected controls, we found increased pancreatic edema, vacuolization, and ADM structures in caerulein injected animals, consistent with a pancreatitis phenotype (Fig. 28b-c). This was verified by a blinded pathologist at UCSF. Edema was reduced by 48 hrs. post-injection, and by 5 days post-injection caerulein treated animals displayed reduced vacuolization, edema and ADM structures, consistent with regeneration processes. These results demonstrate that caerulein injections are able to induce acute pancreatitis in Swiss Webster mice.

Dissociation of adult pancreas

Building transcriptional profiles of individual cells requires the dissociation of tissues into single cells. The pancreas is an especially challenging organ to dissociate, due to the high levels of digestive enzymes produced by the exocrine compartment. Therefore, we tested multiple dissociation protocols and measured their yield of viable, single cells by fluorescence-assisted cell sorting (FACS). Additionally, we measured the percentages of live cells expressing epithelial or mesenchymal cellular surface markers, CD326 (EPCAM) and CD140a (PDGFRA), respectively, to determine if the dissociation biased the proportions of these compartments.

Prior studies have reported successful dissociation of adult pancreata with an enzymatic approach, using Collagenase P (Epshtein, Sakhneny, & Landsman, 2017; Russ et al., 2016). Therefore, we first titrated the concentration of Collagenase P in the dissociation of adult pancreas using a dissociation buffer comprised of Collagenase P at 0.2, 0.4, or 0.8 mg/mL, 1 ng/mL DNase1 in PBS, 10% bovine serum albumin (BSA), and 0.2 mg/mL soybean trypsin inhibitor (STI) (Figure 29a). BSA is often used as a cellular nutrient and protectant during cell culture while STI inhibits the trypsin produced in large amounts by the exocrine compartment of the pancreas (Kurup & Bhonde, 2002). After dissociation, single-cells were stained with the live/dead dye sytox blue (which enters cells with damaged membranes), CD45 (a marker of immune cells), CD326 (an epithelial marker), and CD140a (a mesenchymal marker). We used FACS to determine the viability and ratio of epithelial and mesenchymal cells within the single-cell suspensions. All three concentrations of Collagenase P resulted in similar percentages of live cells after dissociation, although the 0.4 mg/mL concentration was slightly lower than either 0.2 mg/mL or 0.8 mg/mL (Figure 29a). The percentage of CD45⁺ and CD140a⁺ cells was increased when dissociation was performed with 0.4 mg/mL, while the percentage of CD326⁺ cells remained consistent across all three concentrations (Figure 29a). Given the increase in CD45⁺ and CD140a⁺ cells with 0.4 mg/mL Collagenase P, we thought this concentration may better facilitate release of single cells from the tissue, with minor effects on cell viability. This result, combined with the use of 0.4 mg/mL Collagenase P in prior literature (Epshtein et al., 2017; Russ et al., 2016), led us to use 0.4 mg/mL Collagenase P in further downstream experiments.

We next tested the inclusion of BSA and STI in the dissociation buffer. Adult pancreata were dissociated in three different buffers: 1) 0.4 mg/mL Collagenase P and 1 ng/mL DNase1, which we will now term the base buffer, 2) the base buffer plus 0.2 mg/mL STI (Base + STI), or

3) the base buffer plus 0.2 mg/mL STI and 10% BSA (Base + STI + BSA) (Figure 29b). We found that addition of BSA led to a decrease in the percentage of live cells, from around 47-48% in the Base and Base + STI buffers to 19% in the Base + STI + BSA buffer (Figure 29b). Therefore, we excluded BSA from further experiments. Between the Base and Base + STI buffers, we found a similar percentage of CD140a⁺ cells and a small increase in CD326⁺ cells in the Base condition (Figure 29b). As STI has been shown to support acinar cell cultivation (Kurup & Bhonde, 2002), and lead to relatively similar results as the Base buffer alone, we decided to conduct future experiments using the Base + STI buffer.

Finally, we tested three dissociation times to optimize the viability and yield of resulting single-cell suspensions. We found that a 20 minute dissociation time led to increased viability as compared to 10 or 15 minutes and resulted in a 5-7% decrease in CD326⁺ cells but similar percentage of CD140a⁺ cells (Figure 29c). After dissociation, large pieces of still intact tissue were observed in the 10 and 15 minutes dissociation tubes, while these pieces were reduced in the 20 minute dissociation. Therefore, in order to avoid biases of dissociating only cells on the surface of the tissue we decided to continue with a 20 minute dissociation protocol for future experiments. In summary, these optimization experiments led us to dissociate adult pancreata with a buffer consisting of 0.4 mg/mL Collagenase P, 1 ng/mL DNase1, and 0.2 mg/mL STI for 20 minutes for further experiments.

Single-cell RNA-sequencing of adult PBS and caerulein treated pancreata

Although mesenchymal cells are critical in disease onset and progression, these cells have been challenging to study *in vivo* due to their poor definition and lack of specific markers. To overcome these challenges and begin cataloguing the mesenchymal cell types present during

homeostasis and disease, we performed single-cell RNA-sequencing on dissociated pancreata from PBS- and caerulein-injected animals utilizing the optimized conditions described above. We chose to analyze animals on day 3 after the injection with either PBS or caerulein. This timepoint is after a large infiltration of immune cells and death of a large portion of the exocrine compartment, but prior to the onset of regeneration (Jensen et al., 2005). Therefore, we hypothesized that the exocrine tissue may be primed for regeneration processes. Additionally, the mesenchymal compartment is expanded at 3 days post injection (Jensen et al., 2005), allowing for identification of heterogeneity of newly formed mesenchymal cells.

FACS analysis of dissociated pancreata revealed biases in cell type proportions between PBS- and caerulein-treated pancreata (Figure 30). First, we found that the percentage of live cells varied between PBS- and caerulein-treated pancreata, as measured by the percentage of cells that were negative for both sytox blue and propidium iodide (PI) (Figure 30a). Dissociation of caerulein-treated pancreata resulted in 56.7% live cells, while PBS-treated single-cell suspensions contained only 21.5% live cells. We hypothesize that the digestive enzymes produced by acinar cells makes their dissociation particularly difficult, resulting in high amounts of cell death. Given that caerulein treatment induces acinar cell death at early stages (day 1) (Jensen et al., 2005), it's possible the higher viability of caerulein-treated pancreata is due to the presence of fewer acinar cells during the dissociation and sorting.

We next measured the percentage of immune cells, marked by CD45+, contained within the live fraction. Caerulein-treated pancreata contained more CD45+ cells (33.2%) than PBS-treated controls (19%), consistent with the infiltration of immune cells during pancreatitis (Boggs et al., 2018; Lankisch et al., 2015) (Figure 30b). Within the CD45-negative fraction, we found increased representation of mesenchymal cells, marked by CD140a+, in caerulein-treated

pancreata (81.8%) compared to PBS-treated pancreata (47.6%) (Figure 30c). This is also consistent with increased proliferation of the mesenchymal compartment at this stage (Jensen et al., 2005). These experiments suggest a shift in cellular proportions between PBS- and caerulein-treated pancreata.

We next sorted dissociated cells in preparation for single-cell RNA-sequencing. CD45+ and CD45-negative fractions of all live cells were sorted into two separate tubes. In order to enrich for epithelial and mesenchymal cell types, we combined the sorted tubes in a ratio consisting of 15% CD45+ and 85% CD45-negative cells for both the PBS and caerulein samples. We then loaded these cellular suspensions onto the 10X Chromium single-cell RNA-sequencing platform (10X Genomics) to build transcriptomic profiles of individual cells. Quality control, normalization, regression, and clustering led to identification of multiple distinct cellular populations in both PBS and caerulein samples (Fig. 31a-b). We first identified the major categories of cellular populations present within the samples by plotting the expression of key markers for each group: epithelial (*Ecad*), mesenchymal (*Pdgfra*), immune (*Rac2*), and vascular (*Pecam1*) (Fig. 31c-d). Within the PBS sample, we identified one epithelial population, five mesenchymal populations, two immune populations, and three endothelial populations. The remaining clusters were identified as mesothelial, based on expression of *Msln*, and proliferating cells, based on proliferation genes such as *Top2a*. One small cluster, named “Ambig” for “ambiguous” could not be annotated based on these broad markers (Fig. 31a, c, e). Within the Caerulein sample, we did not identify any epithelial populations. *Pdgfra* identified seven mesenchymal clusters, and *Msln* marked three mesothelial populations. We also found an immune, an endothelial, and a proliferating population. Finally, a small “ambiguous” population was identified (Fig. 31b, d, f).

To further refine these categories of cell types, we looked for known markers of various epithelial and mesenchymal cell types. The PBS epithelial population expressed high levels of the ductal markers *Spp1*, *Sox9*, and lower levels of *Krt19*, consistent with a ductal cell identity (Fig. 31e). A small percentage of cells also expressed *Cpa1*, indicating that some acinar cells may also be present within this population (Fig. 31e). We did not find expression of any hormones expressed by islet cells (Fig. 31e). As we could not detect epithelial cells in the caerulein sample, we did not find appreciable levels of *Spp1*, *Sox9*, *Cpa1*, or any hormone (Fig. 31f). We next probed broad mesenchymal markers, such as *Vim*, *Col3a1*, and *Colla1*. These markers were expressed in all mesenchymal and mesothelial clusters, and immune populations in both PBS and caerulein samples (Fig. 31e-f). *Vim* was expressed in ductal cells from the PBS sample as well, albeit at lower levels. *Desmin*, another common mesenchymal marker, was expressed at low levels in the mesenchymal population and in the PBS sample, and was most highly expressed in the third endothelial population (Fig. 31e-f). Mesothelial markers *Wt1*, *Upk3b*, and *Krt19*, were highly expressed in all mesothelial populations from both samples (Fig. 31e-f). Finally, we found low-level expression of *Acta2*, a vascular smooth muscle and activated PSC marker, in the mesothelial populations of both the PBS and caerulein sample (Fig. 31e-f). The ambiguous population detected in both samples displayed a similar expression pattern across these known markers, with a mixture of ductal- and mesenchymal-type (Fig. 31e-f). Therefore, we identified expression of multiple known markers within the epithelial and mesenchymal compartments.

To determine the transcriptional profiles that segregate the subgroups of mesenchymal and mesothelial cells, we subclustered the mesenchymal and mesothelial clusters and reperformed the analysis for both PBS and caerulein samples. The ambiguous populations were

included in both the PBS and caerulein samples, as these cells expressed both epithelial intermediate filaments (cytokeratins) and mesenchymal genes (*Vim*, *Coll1a1*), reminiscent of mesothelial layers. In the PBS sample, reanalysis identified six mesenchymal and three mesothelial populations, based on expression of *Pdgfra* and *Msln*, respectively (Fig. 32a). We also found a population expressing both endothelial and mesenchymal markers, which is denoted M/Endo, and an ambiguous population with a similar expression pattern to the ambiguous population before subclustering (Fig. 32a, c). Two genes with known expression and functional roles in adult pancreata homeostasis and injury are *Wt1* and *Acta2* (Apte et al., 2012; Zang et al., 2015). WT1 has been reported to be expressed in the adult pancreatic mesothelium and PSCs during homeostasis (Chau et al., 2011), while *Acta2* is a marker of vascular smooth muscle cells and activated PSCs during injury (Apte et al., 2012). In the PBS-treated pancreas, *Wt1* was highly expressed in the mesothelial, as well as in additional mesenchymal populations, most notably M5, matching prior reports (Fig. 32b). *Acta2* was only sparsely expressed within the mesothelium, perhaps reflecting the homeostatic conditions of the PBS-treated animal and a failure to capture vascular smooth muscle cells in this approach (Fig. 32b).

The ability to selectively study mesothelial cells separately from mesenchymal cells is critical for determining their lineage and function. Although numerous mesothelial markers have been identified in other organs, their expression patterns in adult pancreas have not been studied. Therefore, we grouped all mesenchymal populations and all mesothelial populations and determined the differentially-expressed genes between these two larger groups. We found 144 genes that were more than 2-fold more highly expressed in mesothelial cells, and 172 in mesenchymal cells (Fig. 32c). Many known mesothelial markers, such as *Upk3b*, *Gpm6a*, *Msln*, *Krt18*, and *Krt19* were identified as pancreatic mesothelial DE genes, consistent with literature in

other organs (Kanamori-Katayama et al., 2011; Mutsaers & Wilkosz, 2007; Rinkevich et al., 2012; Rudat et al., 2014). We also identified markers for the non-mesothelial mesenchymal cells, including the known marker *Pdgfra*, and less well-described markers, such as *lipoprotein lipase* (*Lpl*) or *lumican* (*Lum*) (Fig. 32c). These genes specific to the mesothelium or mesenchyme can be used in tool development to further study the function and lineage of these cell types.

Given the multiple populations of mesenchymal and mesothelial cells, we next assessed the transcriptomic signature of each population in contrast to all other populations within the subclustered dataset. The mesenchymal clusters, M1-M4, displayed overlapping signatures with varying expression levels of two groups of genes (Fig. 32d). M1 and M2 had high expression of the ECM-associated glycoproteins, *Fbn1* and *Mfap5* (Davis et al., 2016; Gibson, Finnis, Kumaratilake, & Cleary, 2016). M3 and M4 displayed differential expression of *Serpine2*, an ECM-associated serine protease that promotes the invasion of pancreatic cancer cells by remodeling the ECM (Buchholz et al., 2003), and *Cxcl14*, a chemokine upregulated in the stroma of tumors in multiple tissues, including the pancreas (Lu, Chatterjee, Schmid, Beck, & Gawaz, 2016). The M5 and M6 populations displayed more distinct transcriptomic signatures, with M5 defined by expression of the ECM-associated glycoprotein, *Mfap4* (Pilecki et al., 2016), and *Cxcl12*, a chemokine involved in pancreatic cancer development and progression (Sleightholm et al., 2017) (Fig. 32d). While M6 expressed distinct genes, such as *Cxcl13* and *Gatm*, this population also shared expression patterns within both the mesenchymal and mesothelial populations. For example, *Cd74* and *Csrp2* were expressed by both M6 and Meso1 while *Gsn* and *Col3a1* were expressed by both M6 and M1-M5. M6 also displayed lower levels of mesothelial markers, *Upk3b* and *Gpm6a*, suggesting that this population may be a transitory state between mesothelial and mesenchymal identity.

The transcriptomic signatures were weak for the mesothelial populations, with all three groups expressing the top markers at varying levels (Fig. 31d). Therefore, we isolated the three mesothelial populations and reformed the clustering analysis, which resulted in 5 populations (Fig. 32e). One of these populations, cluster 5, was defined by differential expression of acinar cell genes, such as *Cpal*, *Ctrb1*, and *Try4* (Fig. 32f). Likely, this small cluster represents doublets consisting of mesothelial and acinar cells. Similarly, cluster 4 expressed many of the mesenchymal-specific gene identified in Fig. 32c, such as *Lum*, *Dpep1*, and *Ddt*, indicating that this may be a cluster of doublets of mesenchymal and mesothelial cells (Fig. 32f). However, these may also represent real populations that express both sets of markers. The remaining three larger populations expressed varying levels of mesothelial markers and distinct transcriptomic signatures (Fig. 32e-f). Cluster 1 expressed lower levels of *Upk3b*, *Krt19*, and *Msln*, but the highest levels of *Wt1*, and expressed multiple secreted factors, such as *Enpp2*, *Igfbp3*, and *Igfbp2*. This cluster also differentially-expressed *Evt1*, a transcription factor that regulates stromal expansion and metastasis in pancreatic cancer (Heeg et al., 2016). Cluster 2 expressed *Tnsfr11b*, a secreted decoy TNF receptor that regulates beta cell insulin secretion during infection (Kuroda et al., 2016), and lipocalin, *Lcn2*, which encodes a secreted protein involved in the response to injury (Asimakopoulou, Weiskirchen, & Weiskirchen, 2016) (Fig. 32f). Finally, cluster 3 was defined by the secreted factor, *Sfrp1*, an inhibitor of WNT signaling (Jayewickreme & Shivdasani, 2015), and the laminin alpha5 receptor, *Bcam* (Moulson, Li, & Miner, 2001) (Fig. 32f). These gene expression profiles suggest multiple subtypes of mesothelial cells with potentially distinct function roles in regulating cellular processes.

Having catalogued the mesenchymal and mesothelial populations in the PBS-treated pancreata, we next turned our attention to the caerulein-treated pancreata. We first subclustered

the mesenchymal and mesothelial populations (M1-M7, Meso1-Meso3, and Ambig). *Pdgfra* expression identified six mesenchymal populations while *Msln* marked two mesothelial populations (Fig. 33a-b). We found wide-spread expression of the *Wt1* gene in the mesenchymal and mesothelial populations, in contrast to the more restricted expression pattern in the PBS sample (compare Fig. 32a-b with Fig. 33a-b). Although we also expected to see increased expression of *Acta2* in the caerulein-treated pancreata, we found only sparse expression (Fig. 33b). The near absence of *Acta2* in the dataset could indicate either a failure to capture *Acta2*⁺ cells or that the transcript is expressed at too low of a level to be captured by the shallow transcriptomic coverage of droplet-based approaches. In addition to the large groups of mesenchymal and mesothelial populations, we identified one population that expressed both *Pdgfra* and *Msln*, and therefore, was labeled M/Meso. We also identified two small “ambiguous” populations, which did not express either *Pdgfra* or *Msln*, but instead displayed distinct transcriptomic signatures (Fig. 33c). Expression of both ductal and acinar cell markers, *Spp1* and *Ctrb1*, in ambiguous 1 likely indicates a doublet identity for this population. Numerous cytokeratins (*Krt12*, *Krt15*) and low levels of mesenchymal and mesothelial markers could indicate a rare population with all these features, or a small group of mixed doublets.

Similar to the PBS sample, the mesenchymal groups in the caerulein sample displayed overlapping, but distinct transcriptomic signatures. These groups expressed secreted factors and ECM-related proteins that had been identified in the PBS mesenchymal populations, including *Mfap4*, *Fbn1*, *Serpine2*, *Cxcl12*, and *Cxcl13*. Similar to the PBS populations, we found one mesenchymal population, M6, that was closer transcriptionally to the mesothelial populations, with a low expression of mesothelial markers (Fig. 33c). The M/Meso population also displayed shared mesenchymal and mesothelial characteristics, but in contrast to M6, did not have an

additional distinct signature. This could indicate that M/Meso is a doublet population of mesenchymal and mesothelial cells, rather than a population of cells with characteristics of both cell types. The two mesothelial populations displayed weaker distinct signatures, but differed in expression of genes such as *Igfbp3*, *Msln*, and *Slpi* (Fig. 33c). These results suggest an overall similar transcriptomic similarity to the PBS sample, but indicates an expansion of *Wt1* expression in the caerulein sample.

To more directly compare the PBS and caerulein populations, we correlated each cluster from the caerulein sample to all the PBS clusters. We found that caerulein clusters M1-M5 correlate most highly with PBS clusters M1, M2, and M5 (Fig. 33d). Specifically, caerulein cluster M4 matched PBS cluster M1, while the M5 clusters from each sample correlated most highly. Additionally, the M6 populations from both groups not only correlated most highly to each other, but clustered with the mesothelial populations, highlighting their expression of mesothelial genes. Two PBS mesenchymal clusters, M3 and M4, did not correlate as highly with any caerulein mesenchymal cluster, suggesting perhaps an absence of this particular mesenchymal subtype during pancreatitis. The two caerulein mesothelial populations correlated most highly with the PBS mesothelial populations, as expected. These results suggest that multiple mesenchymal populations in both caerulein (M1-M3) and PBS (M3-M4) samples may possess distinct features that do not match in the other sample, resulting in their lower correlation.

As subclustering analysis of the PBS sample resulted in increased resolution of mesothelial populations, we next performed the same subclustering on the two identified caerulein mesothelial populations. We identified 6 populations and genes that define these populations (Fig. 33e, g). Comparisons to the PBS mesothelial populations (Fig. 32e) showed

correlation of 5 out of 6 populations to one or more PBS mesothelial populations (Fig. 33f). Cluster 6, which did not correlate well, was a small cluster that also expressed mesenchymal markers, suggesting that this population may be a small group of mesothelial and mesenchymal doublets. Caerulein mesothelial clusters 1 and 2 correlated mostly highly to PBS mesothelial cluster 1, while cluster 5 correlated well with PBS mesothelial clusters 2 and 3. Caerulein clusters 3 and 4 appeared to be the most distinct mesothelial clusters in comparison to PBS mesothelial cells, although these populations still had a spearman correlation coefficient > 0.85 . Therefore, we find highly similar transcriptional profiles of mesothelial populations between the PBS- and caerulein-treated pancreata.

Although correlation analysis can help uncover major differences between datasets, more subtle differences, such as in levels of gene expression within similar populations, require more sophisticated analyses. One method of analyzing changes between two datasets is to combine the cells into one large dataset that can undergo similar normalization, scaling, and regression processes (see Chapter 2 and Chapter 3). Therefore, we combined the PBS and caerulein datasets, and utilized two methods of batch correction in order to account for overall technical differences between the two datasets. First, we tried linear regression, which was successful in our developmental dataset to correct for batch effects (see Chapter 2 and Chapter 3), but found very little overlap between PBS and caerulein populations (Fig. 34a). As we had already determined that similar populations existed in these datasets (Fig. 31, 32, 33), it was likely this separation was due to batch effects. Therefore, we utilized canonical correlation analysis (CCA) to merge the two datasets (Fig. 34b-c). We found more overlap between the PBS and caerulein samples, although cells from either PBS or caerulein samples aggregated together within clusters. Based on the differential gene expression analysis of known markers described above,

we identified a ductal, six mesenchymal (M1-M6), two mesothelial (Meso1, Meso2), a mixed mesenchymal and mesothelial (M/Meso), two endothelial (Endo 1, Endo 2), two immune (Imm 1, Imm 2), a proliferating population, and an ambiguous population similar to that described before (Fig. 34c-d). To understand whether similar populations exist during homeostasis and pancreatitis, but change in frequency, we calculated the percentage of each population within each of the PBS and caerulein samples (Fig. 34e-f). Within the mesenchymal populations, there was a decrease in the frequency of the M1 population and concomitant increase in the M2 population under caerulein treatment (Fig. 34e). The mesothelial populations displayed a slight increase in the M/Meso population and decrease of Meso2 in the caerulein sample (Fig. 34f). These shifts suggest that caerulein treatment may favor specific subtypes of mesenchymal or mesothelial populations.

Discussion

While the mesenchyme is critical for the development, progression, and recovery from fibrotic diseases in multiple adult organs, the cellular populations within this compartment and their functions in the adult pancreas remain relatively unknown. There is already evidence for pancreatic mesenchymal heterogeneity during both homeostasis and disease states. For example, *Acta2* marks a subset of mesenchymal cells during pancreatitis, the activated PSCs, which are critical for turnover of ECM during disease states (Apte et al., 2012). However, it is unclear if all PSCs become activated and express *Acta2*, or only a subset, and whether *Acta2*-negative PSCs also contribute to disease progression. Additionally, knockout of *Wtl*, a gene expressed in the adult pancreatic mesothelium and a subset of PSCs during homeostasis, results in severe atrophy of the exocrine pancreas (Chau et al., 2011). Whether this phenotype is due to the loss of this

gene in the mesothelium and/or PSCs or in other tissues throughout the body remains unknown. Additionally, whether Wt1+ PSCs are functionally distinct from Wt1- PSCs has not been determined. An improved understanding of adult mesenchymal heterogeneity would allow for the study of cellular interactions and functions that contribute to disease progression.

In order to build a catalogue of mesenchymal subtypes, we utilized single-cell RNA-sequencing on dissociated whole adult pancreata after treatment with caerulein, a pancreatitis-inducing chemical, or PBS control. A major challenge in executing this technique is the dissociation of adult pancreas, a tissue with high production of digestive enzymes. Although we optimized multiple conditions of the dissociation, we were still unable to achieve cell-type proportions representative of an adult pancreas. While the pancreas is largely composed of epithelial exocrine cells, with only 4-7% of the total cellular mass composed of PSCs, our FACS analysis showed relatively low percentages (< 30%) of epithelial cells, and much higher percentages of mesenchymal cells (ranging from 10% - 50% depending on conditions). The results from our single-cell RNA-sequencing show even smaller percentages. Indeed, we were only able to capture a small ductal cluster in the PBS sample, while the majority of cells were mesenchymal and mesothelial. We hypothesize that this is due to the large amounts of epithelial, especially exocrine, cell death upon dissociation of the pancreas. Such a large degree of cell death not only results in loss of those particular cells, but likely affects the surrounding, surviving cells within the single-cell suspension. Therefore, these datasets must be interpreted with caution, and the gene expression profiles validated *in vivo* before making definitive conclusions.

Improvements in the protocol for dissociation of adult pancreata would be beneficial for the unbiased study of adult cellular heterogeneity. One of the key steps we introduced in our

protocol was the lysis of red blood cells (RBCs). The large number of RBCs required a removal step to enrich for all other cell types within the pancreas (data not shown). We utilized a common RBC lysis buffer that should selectively disrupt RBCs based on the osmolality of the solution. However, the specificity of this approach was not verified in our hands, and this lysis step may have 1) resulted in non-specific lysis of pancreatic cells or 2) caused indirect effects due to the creation of a large amount of cellular debris. We have now tested bead-based approaches, rather than lysis, for the removal of RBCs in late stage embryonic pancreata that have resulted in the removal of RBCs without major shifts in the pancreatic cellular proportions (data not shown). A similar approach could be taken for adult pancreata, in order to minimize the damage during the dissociation and improve the resulting cell type proportions.

Another alternative approach would be to perform single-cell RNA-sequencing on cellular nuclei, rather than live, intact cells. This methodology would not require maintaining digestive enzyme-producing acinar cells through a dissociation, FACS, and single-cell capture, which can take multiple hours. Instead, in nuclei sequencing, the cellular membranes are disrupted, the nuclei isolated and then loaded for single-cell capture. Therefore, nuclei single-cell RNA-sequencing could solve the problem of the high production of digestive enzymes either secreted by live acinar cells or released from dying acinar cells during dissociation, and potentially improve the quality of the resulting datasets.

Besides dissociation, this work highlighted the challenges of merging two independent datasets to identify differences between conditions. The separation of real biological differences from variation due to technical aspects of the methodology remains a major challenge for the entire field of single-cell RNA-sequencing (Yuan et al., 2017). Many batch correction methods, including linear regression, were developed for bulk sequencing approaches, and may not be

appropriate for single-cell datasets. Batch correction methods for single-cell datasets have recently been developed (Buettner et al., 2015; A. Butler et al., 2018), including the canonical correlation analysis (CCA) utilized in this study, but these methodologies are still actively being tested and an agreed upon gold standard has yet to be decided.

In our work, we found that the CCA batch correction methodology produced better overlap between the PBS and caerulein batches than linear regression. However, there were still groupings of batches within the larger mixed clusters, what is sometimes termed a “shadowing” effect. The segregation of cells from each sample in this approach may reflect true biological differences between the PBS and caerulein control. Indeed, histology and staining have demonstrated remarkable differences in pancreatic tissue *in vivo*. However, this shadowing may also be due to unresolved batch effects. The difficulty, therefore, is in determining where the line between true differences and technical differences lies, and likely, these differences will be intertwined. One way to combat this would be to include another biological replicate to measure the effectiveness of the batch correction method. In this case, one can expect complete overlap of the biological replicates, and the overlap of the sample representing another condition can distinguish true biological commonalities and differences. This approach worked well in our developmental datasets (Chapter 2 and Chapter 3) and could be applied to the adult pancreas as well. Another option is to multiplex samples in order to pool all cells for single-cell RNA-sequencing capture and library preparation, which would reduce batch effects associated with the single-cell methodology (McGinnis et al., 2018). The improvement of this key aspect of data analysis will help facilitate more robust downstream analyses, such as clustering and differential gene expression analysis.

Although these challenges exist for our current datasets, we were still able to find evidence of cellular and transcriptional heterogeneity in the adult pancreas. First, we found distinct transcriptomic signatures that segregated all mesothelial populations from all mesenchymal cell types. Identification of genes that can specifically mark the mesothelium will be critical for future lineage tracing and functional studies. This is especially important for the pancreas, where the marker most commonly used to study adult mesothelial layers, *Wt1*, is known to also be expressed in PSCs (Chau et al., 2011), and there have not been studies to demonstrate specific expression of other mesothelial markers. We verified specific expression of genes such as *Upk3b*, *Krt18*, *Krt19*, *Msln*, *Nkain4*, and *Gpm6a* in the adult pancreatic mesothelium, many of which have been described in other mesothelial layers (Kanamori-Katayama et al., 2011; Yuchang Li et al., 2013). Therefore, the development of tools utilizing these gene promoters could facilitate studies of the mesothelium in multiple tissues.

Within both the mesothelial and mesenchymal groups, we identified multiple subpopulations. These populations were segregated by differential expression of a variety of secreted factors and ECM-proteins, which implies that these cell types may also have functional differences. Given the difficulty of dissociation of the adult pancreas and the potential for gene expression patterns to be altered during this process, it is critical that the expression of these genes be verified *in vivo*. Indeed, there are reports of dissociation-induced gene expression changes in other systems that can influence single-cell RNA-sequencing results (van den Brink et al., 2017). The isolation and culture of PSCs *in vitro*, for example, is known to cause their activation and expression of *Acta2* (Apte et al., 1998; Bachem et al., 1998). Validation by immunostaining or *in situ* hybridization will clarify the influence of dissociation effects on these gene expression patterns.

With the transcriptional and cellular heterogeneity now catalogued in each of the homeostatic and diseased samples, we can now focus on understanding the transcriptional and cellular differences between PBS- and caerulein-treated pancreata. There may be multiple routes for obtaining disease-specific gene expression profiles, including the appearance of new disease-specific populations, disappearance of homeostatic populations, or shifts in transcription within a homeostatic population (Fig. 27). Upon treatment with caerulein, we noticed multiple shifts in both transcription and cellular populations. The expression of *Wt1*, for instance, was expanded in the caerulein treated animals. *Wt1* has been shown to be important for maintaining homeostasis of multiple organs, facilitating EMT processes during development, and regulating transcription either as a transcription factor or through the modulation of chromatin (Hastie, 2017), suggesting that the upregulation of this gene during pancreatitis may be functionally relevant.

Understanding the gene expression pattern of *Wt1* throughout pancreatitis development, progression and recovery will help determine its potential functional role. For example, is *Wt1* expression maintained throughout the recovery process or downregulated once the initial injury is cleared? The timing of *Wt1* expression may be particularly relevant given that *Wt1* regulates chromatin switching mechanisms depending on the cellular context (Essafi et al., 2011). The latter study demonstrated that *Wt1* acts as a repressor of the *Wnt4a* locus in epicardial cells, but activates the same locus in kidney cells, suggesting that *Wt1* function can change depending on the cellular context. Therefore, *Wt1* may play multiple roles in pancreatic mesothelial and mesenchymal cells, and these roles may be dynamic throughout the disease process. Targeted transcriptional profiling of *Wt1*⁺ populations during disease progression will help identify potential downstream functional targets of *Wt1*. Additionally, future experiments should

manipulate *Wtl* expression in specific populations at key points during disease progression in order to understand the potential various functions of this gene.

In addition to the transcriptional upregulation of *Wtl*, we also noticed shifting proportions of mesenchymal and mesothelial clusters in the caerulein sample. While the PBS sample contained near equal proportions of the M1 and M2 populations, this proportion was skewed in the caerulein sample, with the M2 population being the dominant contributor. The M2 population differentially-expressed the WNT inhibitor, *Sfrp4*, which is upregulated in mouse models of systemic sclerosis (Ssc), and in tissue from Ssc patients (Bayle et al., 2008), and has been demonstrated to reduce fibrosis after ischemia in the heart (Matsushima et al., 2010) or renal injury (Surendran, 2005). The M2 population also expressed higher levels of the ECM-glycoproteins *Mfap5* and *Mfap4*. *Mfap5* has been shown to increase the stability of *procollagen1* *in vitro* (R. Lemaire, Korn, Shipley, & Lafyatis, 2005) and *Mfap4* was identified as a biomarker for hepatic fibrosis (Bracht et al., 2016). This gene expression profile suggests the M2 population may be functioning as a caerulein-induced fibrosis-regulating population during pancreatitis.

In addition to the M2 population, the caerulein sample also contained a higher proportion of the M/Meso population. This population shared gene expression patterns of both mesothelial and mesenchymal cells, suggestive of an intermediate cell type or an intermediate cell state during the differentiation of a mesothelial cell towards a mesenchymal cell fate. This increase in M/Meso was concomitant with the decrease in the Meso1 population. The Meso1 population expressed the mesothelial markers found in the Meso2 population as well as additional mesothelial markers, such as *Krt19* and *Msln*, at higher levels than Meso2. Therefore, Meso1 may represent a more mature or stable mesothelial population, while Meso2 and M/MEso are more plastic or closer transcriptionally to a mesenchymal phenotype. In this model, caerulein

treatment could shift mesothelial cells towards a more plastic state, perhaps to facilitate a MMT process and contribute to mesenchymal cell types. Pseudotime ordering methods can be used to test these hypotheses *in silico*. The current challenge to this approach is the input of CCA batch corrected data, which is not supported by most pseudotime ordering algorithms, but will likely be incorporated soon. *In vivo* lineage tracing of the M1, M2, and M/Meso populations can also directly test this model but will require building additional genetic tools to specifically trace these cells. Nevertheless, our findings highlight multiple potential caerulein-shifted populations that may be functionally relevant for pancreatitis progression.

Our current datasets provide a resource for heterogeneity during a specific timepoint of caerulein-induced disease. Additional timepoints during caerulein treatment would allow for more robust detection of gene expression and cellular population shifts during disease. Earlier timepoints may help clarify the populations involved in immune cell recruitment, and the activation process of PSCs while later timepoints could target cell types involved in the recovery and regeneration process. Understanding how the acute injury is resolved would be especially informative for chronic pancreatitis, which may be a result from the failure of the pancreas to regenerate (Murtaugh & Keefe, 2015). Applying the approaches taken in this chapter to other models of pancreatitis, including those for chronic pancreatitis, will also shed light on key processes driving disease onset and progression. This current dataset provides a starting resource to add and compare additional timepoints and model systems.

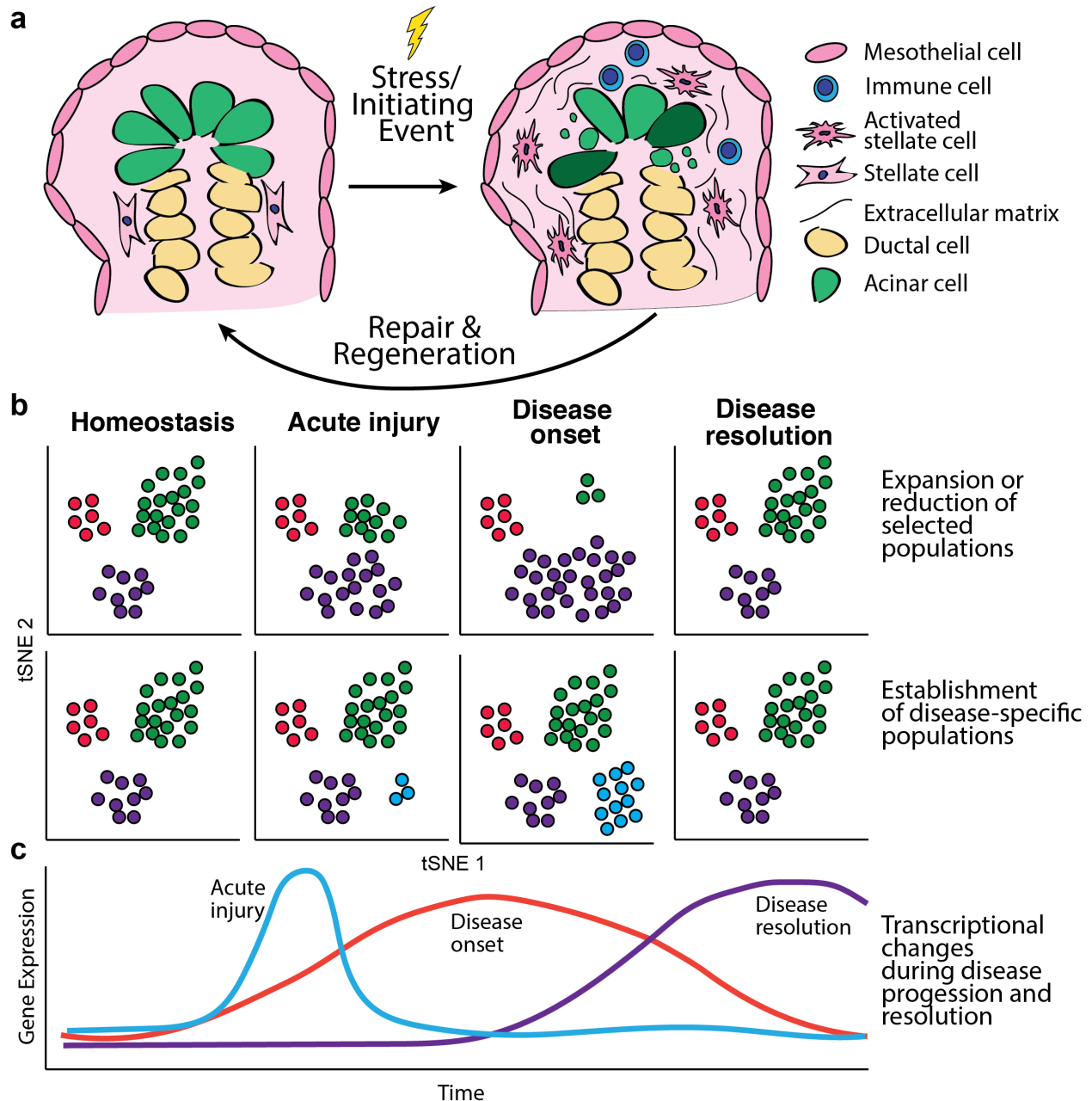


Figure 27. Acute pancreatitis model and potential alterations in cellular and transcriptional heterogeneity. a) Model of acute pancreatitis. Upon exposure to stress or an initiating event, the pancreas is characterized by acinar cell death, infiltration of immune cells, and activation of resident stellate cells. Activated stellate cells produce and secrete extracellular matrix components as part of the wound healing process. Over a few days to one week, the undergoes repair and regeneration to result in a histologically normal pancreas. b) Potential cellular shifts during disease progression and recovery. There may be expansion (purple population) or reduction (green population) of cellular populations present during homeostasis or establishment of disease-specific populations (blue population). c) Potential transcriptional shifts during disease progression and recovery. Genes may be upregulated during acute injury (blue line), disease onset (red line) or disease resolution (purple line).

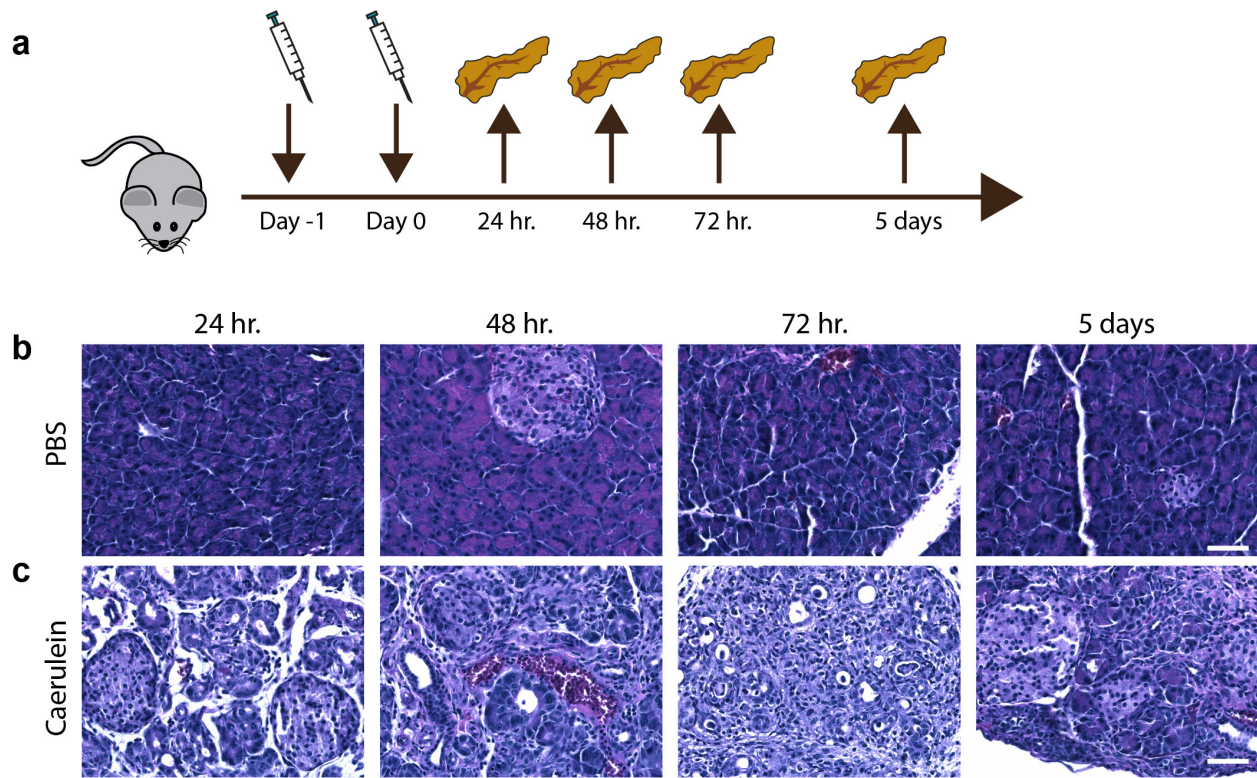


Figure 28. Caerulein injections result in acute pancreatitis in mice. a) Caerulein injection scheme. Mice were injected with 75 ug/kg caerulein or PBS once per hour for 8 hours on two consecutive days. Pancreata were collected at 24 hr, 48 hr, 72, hr, and 5 days post injections. (b-c) Hematoxylin and eosin (H&E) staining on pancreata from PBS injected (a) or caerulein injected (c) animals. Scale bars represent 200 um.

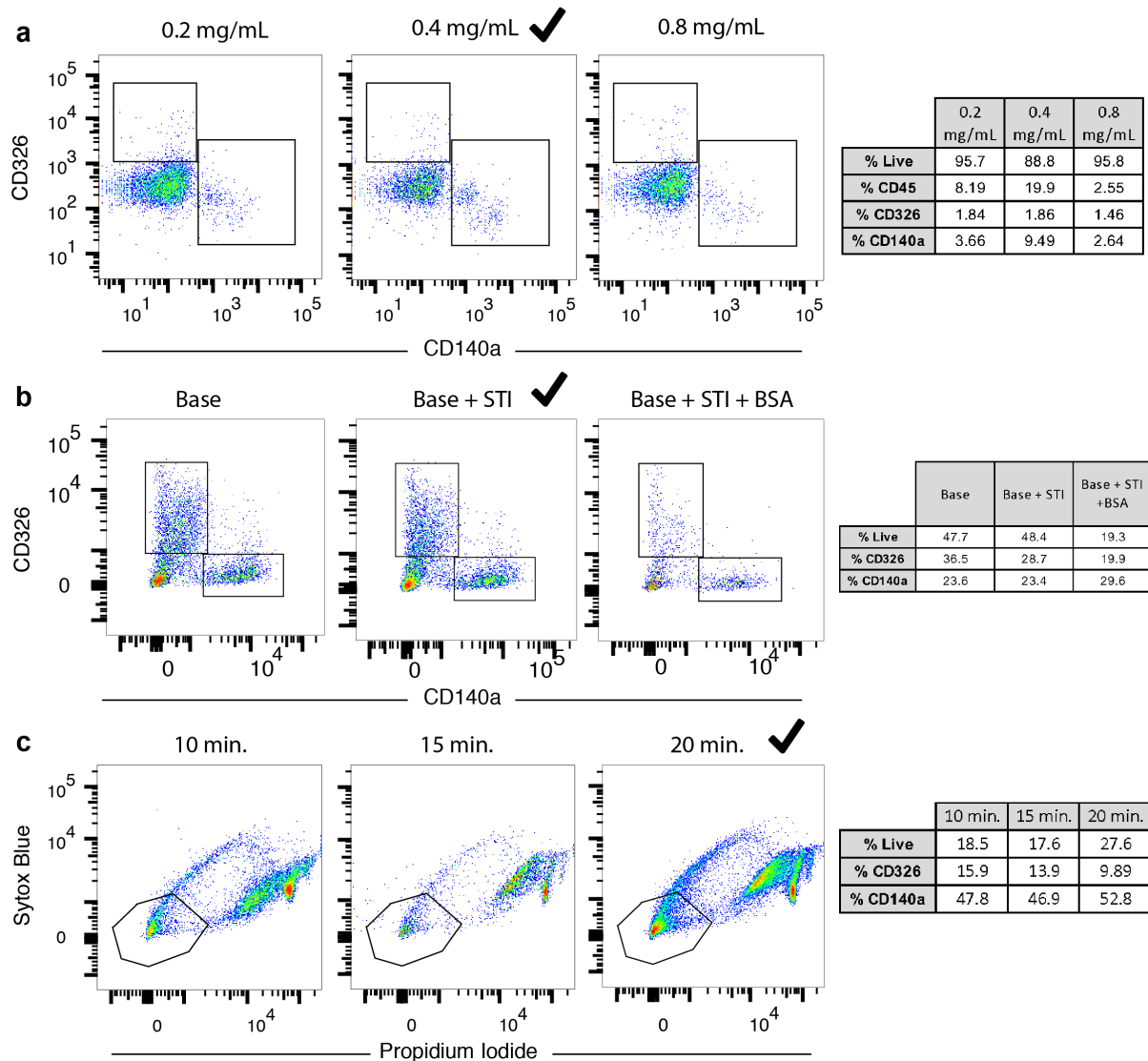


Figure 29. Optimization of adult pancreatic dissociation. a) FACS plots displaying CD140a and CD326 expression after dissociation of adult pancreata with varying concentrations of Collagenase P. b) FACS plots displaying CD140a and CD326 expression after dissociation of adult pancreata with the base dissociation buffer, 0.4 mg/mL Collagenase P and 1 ng/mL DNase1 (Base), the base buffer with 0.2 mg/mL soybean trypsin inhibitor (Base + STI), or the base buffer with 0.2 mg/mL soybean trypsin inhibitor and 10% bovine serum albumin (Base + STI + BSA). c) FACS plots displaying live/dead staining by both sytox blue and propidium iodide staining after dissociation for 10, 15, or 20 minutes with the base buffer with 0.2 mg/mL soybean trypsin inhibitor. (a-c) Percentages of live, CD326+, and CD140a+ of parent population for each condition (rightmost panel). Checkboxes represent conditions used in future experiments.

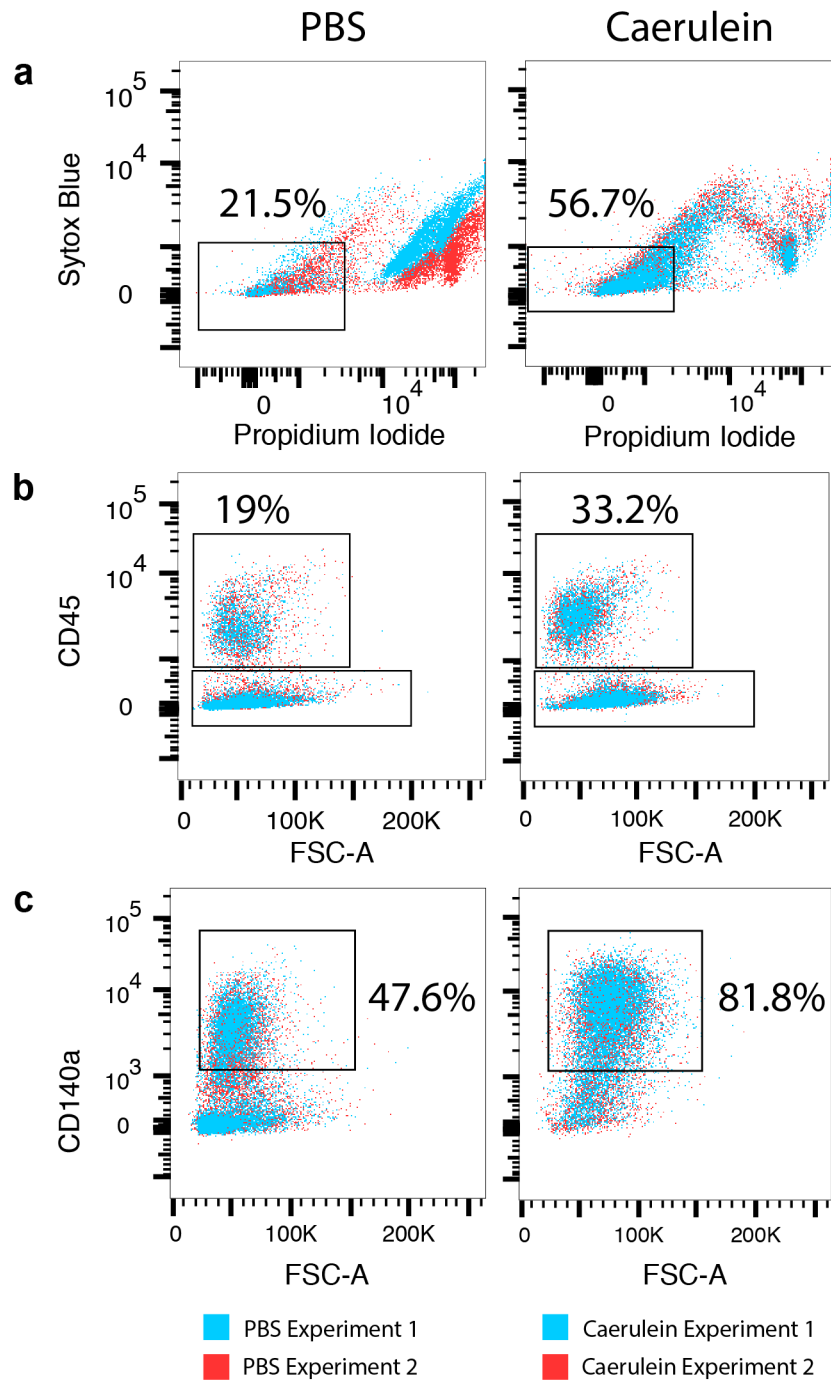


Figure 30. Dissociation of pancreata from PBS and caerulein injected animals. (a-c) FACS plots comparing (a) sytox blue and propidium iodide, (b) CD45, and (c) CD140a markers between dissociated pancreata from PBS (left panels) and caerulein (right panels) injected animals. Blue dots represent results from tube 1 of dissociated cells and red dots represent results from tube 2 of dissociated cells for each treatment. Percentages of each cell type are noted. In (c), cells are derived from the CD45-negative compartment in (b).

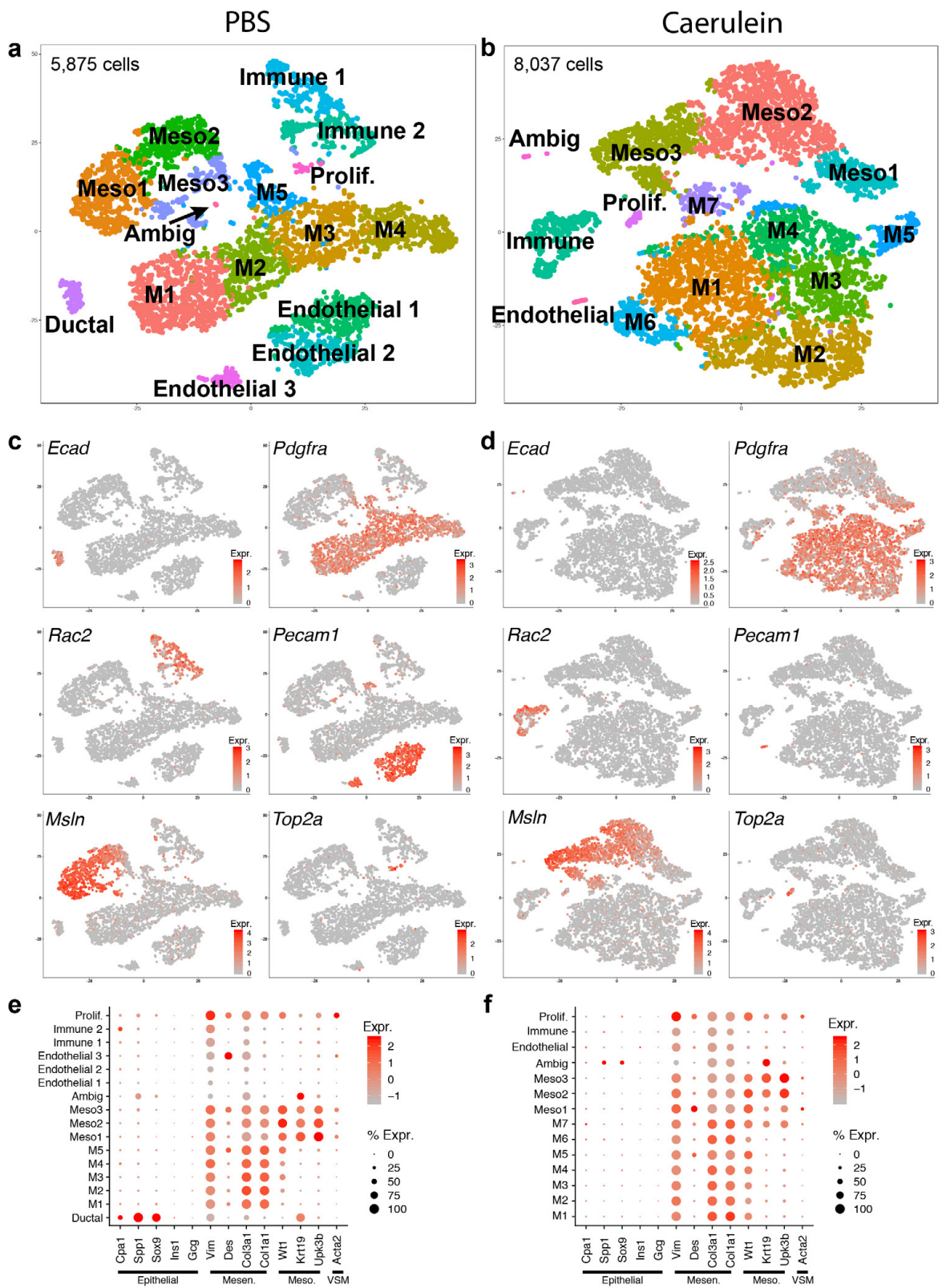


Fig. 31. Single-cell RNA-sequencing of adult pancreata from PBS- and caerulein-treated animals. (n=4 pooled pancreata from individual mice for each sample)(a-b) t-SNE representation

of cells from (a) PBS or (b) caerulein samples. (c-d) Expression of markers denoting major cellular categories in (c) PBS or (d) caerulein samples. Color indicates level of expression. (e-f) Expression of known markers of epithelial and mesenchymal subtypes. Size of the dot represents proportion of the population that expresses each specified marker. Color indicates level of expression. Mesen. = mesenchymal. Meso = mesothelial. VSM = vascular smooth muscle.

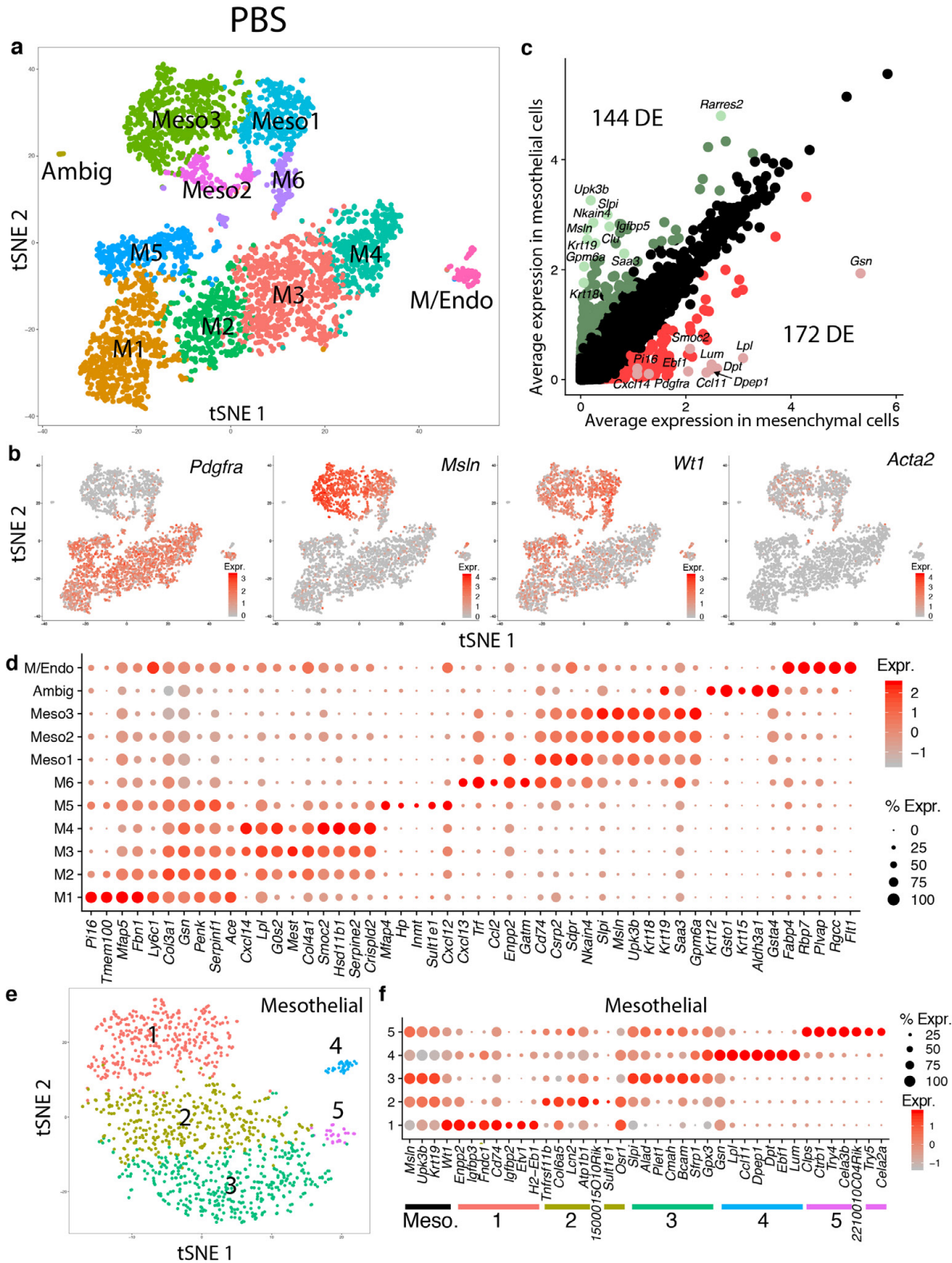


Figure 32. Mesenchymal and mesothelial heterogeneity during adult homeostasis. a) t-SNE representation of reclustered mesenchymal, mesothelial, and ambiguous populations from Fig.

30a. b) Expression of known mesenchymal (*Pdgfra*) and mesothelial (*Msln*) markers, and markers known to be important in the mesenchyme during pancreatic homeostasis or injury, (*Wt1*, *Acta2*). Color indicates level of expression. c) Comparison of grouped mesenchymal (M1-M6) and mesothelial (Meso1-Meso3) populations. Green and red dots represent genes that are greater than 2-fold differentially-expressed and have an adjusted pvalue < 0.05. Lighter shades of green and red dots highlight top differentially-expressed genes. d) Expression of top differentially-expressed genes for each cluster. e) t-SNE representation of reclustered mesothelial populations from (a) (Meso1-Meso3). f) Expression of differentially-expressed genes in mesothelial populations. Bars are colored to match cluster identity in (e). Black bar indicates known mesothelial markers. (d, f) Size of the dot represents proportion of the population that expresses each specified marker. Color indicates level of expression.

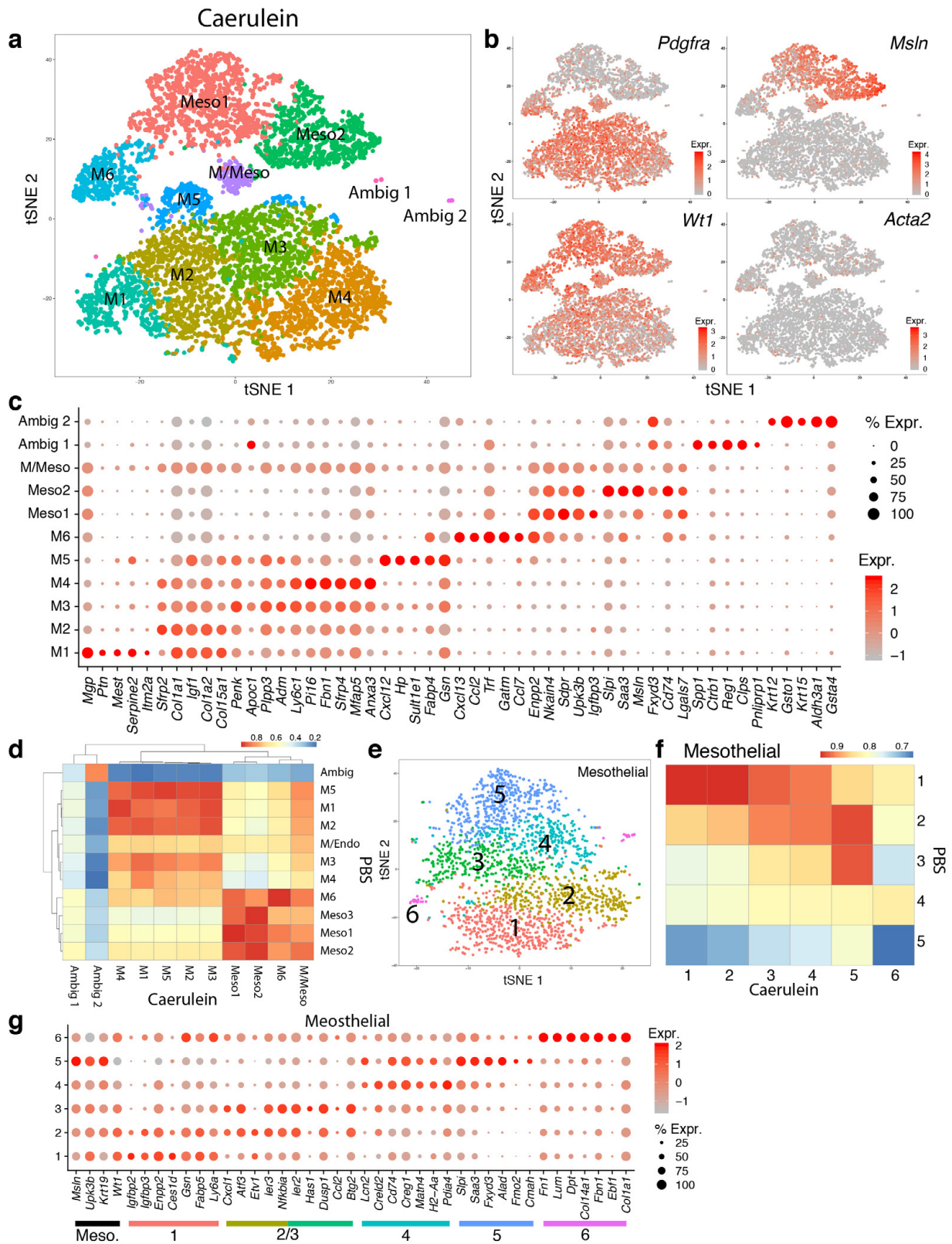


Figure 33. Mesenchymal and mesothelial heterogeneity during pancreatitis. a) t-SNE representation of reclustered mesenchymal, mesothelial, and ambiguous populations from Fig.

30b. b) Expression of known mesenchymal (*Pdgfra*) and mesothelial (*Msln*) markers, and markers known to be important in the mesenchyme during pancreatic homeostasis or injury, (*Wt1*, *Acta2*). Color indicates level of expression. c) Expression of top differentially-expressed genes for each cluster. d) Correlation of caerulein clusters from (a) with PBS clusters from Fig. 31a. Color indicates spearman correlation value. e) t-SNE representation of reclustered mesothelial populations from (a) (Meso1-Meso2). f) Correlation of caerulein clusters from (e) with PBS clusters from Fig. 31e. Color indicates spearman correlation value. g) Expression of differentially-expressed genes in mesothelial populations. Bars are colored to match cluster identity in (e). Black bar indicates known mesothelial markers. (c, g) Size of the dot represents proportion of the population that expresses each specified marker. Color indicates level of expression.

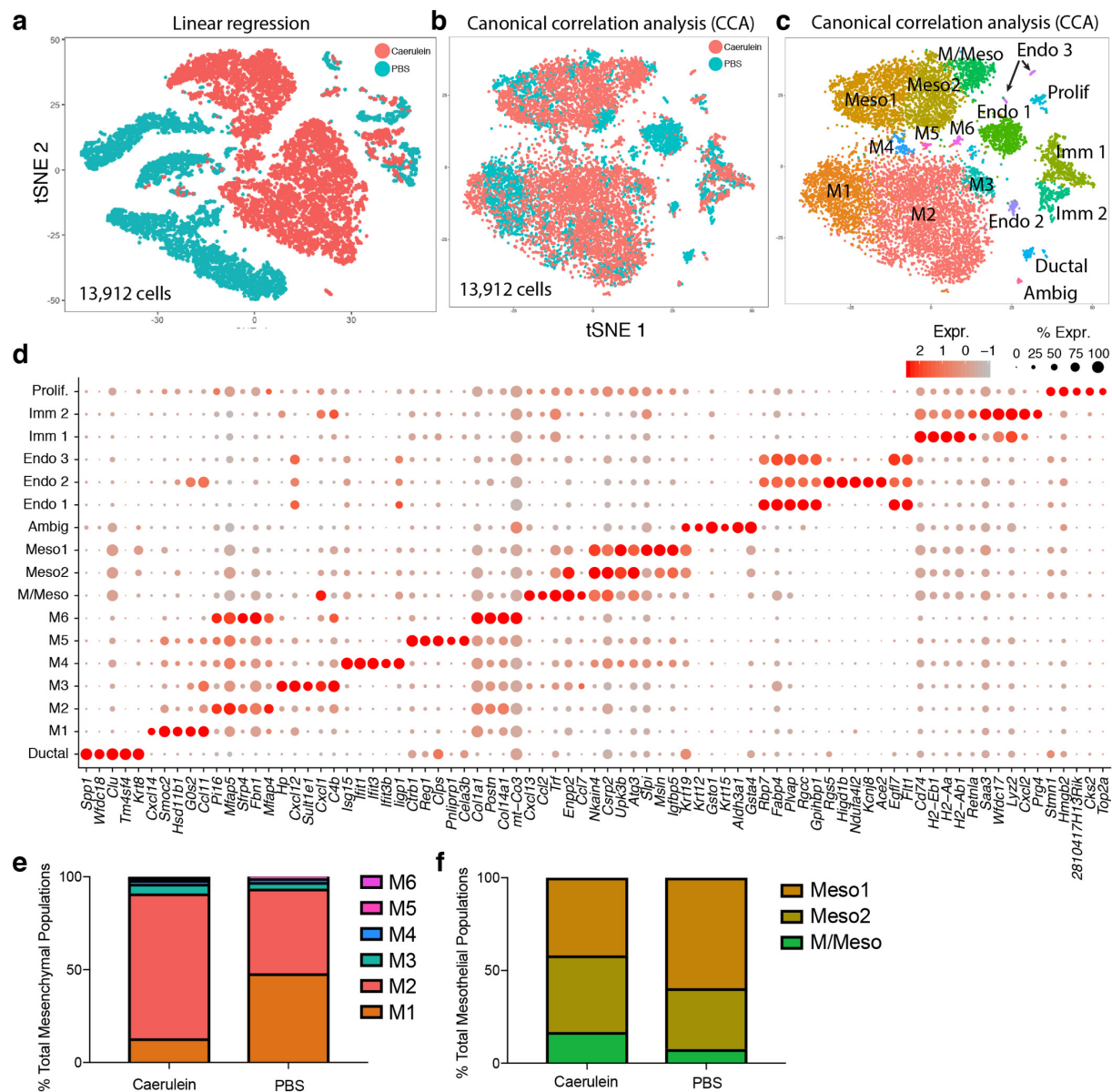


Figure 34. Merging PBS and caerulein single-cell RNA-sequencing datasets. a-b) t-SNE visualization of PBS and caerulein merged dataset with batch corrected by a) linear regression or b) canonical correlation analysis (CCA). Colors represent dataset cells are originally derived from before merging. c) t-SNE visualization of CCA merged dataset colored by cluster ID. t-SNE matches (b). d) Expression of top differentially-expressed genes in clusters shown in (c). Size of the dot represents proportion of the population that expresses each specified marker. Color indicates level of expression. e-f) Proportion of each (e) mesenchymal or (f) mesothelial merged cluster within the PBS and caerulein sample.

Chapter 6

Conclusions and Future Directions

In this work, we have identified novel transcriptional and cellular heterogeneity in both the epithelial and mesenchymal compartment of the pancreas during development, adult homeostasis, and adult fibrotic disease. The identification of a novel epithelial progenitor cell population and division of the mesenchyme into distinct subtypes in our developmental studies (Chapter 2, 3, and 4) impacts our understanding of endocrine differentiation, the development of the pancreatic mesenchyme, and the epithelial-mesenchymal interactions that guide pancreatic organogenesis. In Chapter 5, we provide critical first steps toward defining, cataloguing, and comparing the pancreatic mesenchymal cell types in adult homeostasis and disease. These findings facilitate future studies that aim to understand the cellular mechanisms regulating disease progression and regeneration and identify novel targets for potential therapies. Overall, the combination of single-cell RNA-sequencing technology with *in vivo* immunohistochemistry, *in situ* hybridization, and lineage tracing offers a powerful approach for the study of heterogeneity in the cell types that comprise different organs.

The relevance of mouse models to human pancreatic development

Much of the progress in the study of pancreatic biology has been through the use of mouse model systems. While these models offer many advantages, there are known species differences that can hinder the translation of findings in mouse models to human therapies. Studies have identified key differences during human and mouse pancreatic development (Nair & Hebrok, 2015). One major difference in human and mouse endocrine development is the expression pattern of *Neurogenein3* (*Ngn3*). In mice, *Ngn3* is expressed in two waves, with one early wave peaking at E10-E10.5, and a second later wave occurring after E12.5 (Villasenor et al., 2008). This expression pattern of *Ngn3* correlates with the two waves of endocrine

differentiation (Pictet, Clark, Williams, & Rutter, 1972). The majority of endocrine cells produced in the first wave of differentiation, from E9.5 – E12.5, are glucagon⁺ cells, with a smaller proportion of polyhormonal cells, which express insulin and an additional hormone (glucagon, pancreatic polypeptide, or peptide YY) (Herrera et al., 1991; Upchurch, Aponte, & Leiter, 1994). The second wave of differentiation, from E12.5 to E14.5, produces all the single-hormone endocrine cell types of adult islet. In contrast, during human development *NGN3* is expressed in a single wave during human pancreatic development, beginning at 8 week post conception (wpc) and peaking at 10-12 wpc (Salisbury et al., 2014). Also in contrast to findings in mice, beta cells are the earliest produced endocrine cell type in humans, rather than alpha cells, and there is an increased proportion of polyhormonal cells (20-30%) during human development (Jeon, Correa-Medina, Ricordi, Edlund, & Diez, 2009; K. A. Johansson et al., 2007; Piper et al., 2004). Finally, differences have been noted for key transcription factors, such as *Nkx2-2*, which marks pancreatic progenitor cells prior to *Ngn3* expression and endocrine commitment in mice, but is only present after *NGN3* expression in humans (Jennings et al., 2013). These studies suggest that there may be different mechanisms regulating differentiation of human endocrine progenitors to the various endocrine cell types of the mature pancreas.

The *Fev*⁺ endocrine progenitors identified in our mouse work were also detected in human fetal pancreata at 23 wpc, and in endocrine progenitor stage hESC-derived beta cells *in vitro*. As 23 wpc corresponds to a post-natal timepoint in mouse development (Nair & Hebrok, 2015), determining the presence of a *FEV*⁺ population throughout human pancreatic development can give insights into whether all humane endocrine populations are derived from a *FEV*⁺ progenitor. Additionally, co-expression analysis of *FEV* and genes that we identified as potentially promoting an alpha or beta cell fate in mice, *PEG10* and *GNG12*, should also be

analyzed in human tissue. Are FEV⁺ cells present during the differentiation of the first beta cells at 7 wpc in humans, and if so, is *GNG12* expressed in these FEV⁺ cells? Shortly after, when alpha cells first appear, is *PEG10* upregulated within a subset of FEV⁺ cells? Answers to these questions can provide evidence for the potential function of FEV⁺ cells during human endocrine differentiation.

Although lineage tracing experiments are not possible in fixed human tissue from embryos, the *in vitro* stem cell differentiations offer a platform for more direct lineage tracing of FEV⁺ cells during human endocrine differentiation. Combining a FEV⁺ lineage trace with knockdown or knockout of *PEG10* or *GNG12* will determine the function of these genes on cell fate decisions in the FEV⁺ population. Integration of a *Fev-Cre* into hESCs can trace *Fev*⁺ cells during a variety of differentiation conditions, including a viral- or CRISPR-mediated knockout of *PEG10* and *GNG12*. As differentiation protocols for other endocrine cell types are developed, we can also probe for the FEV⁺ population during differentiation of alpha, epsilon, gamma, and delta cells, and help clarify whether a FEV⁺ progenitor is required for all endocrine subtypes. In summary, while we provide evidence for the presence of a FEV⁺ population in humans, future experiment should focus on characterizing the appearance of this population and its function during endocrine differentiation in human systems.

Although recent work in human tissue and *in vitro* platforms have increased our knowledge of human pancreatic epithelial development, there are only a few studies focused on the development of the non-epithelial cells of the human pancreas. Differences in the timing of pancreatic islet innervation and vascularization have been noted between humans and mice. Human pancreatic islets are innervated starting at 12 wpc and fully vascularized by 20 wpc (Proshchina, Krivova, Barabanov, & Saveliev, 2014; Roost et al., 2014), while mouse islets are

innervated post-natally and fully vascularized at birth (Reinert et al., 2014). As innervation has been demonstrated to influence islet cytoarchitecture, these differences may reflect the structural differences between mature human and mouse islets (Proshchina et al., 2014).

Similar to mouse, the remaining loosely packed non-epithelial cell types in the developing human pancreas are broadly termed mesenchymal. Very little work has been done to understand the development and function of this compartment. One study demonstrated the expression of *FGF7* and *FGF10* in human pancreatic mesenchyme, and further showed that these factors could promote pancreatic epithelial progenitor proliferation, mirroring studies in mice (Bhushan et al., 2001; Ye, Duvilli, & Scharfmann, 2005). However, the mesenchymal cell types present during human pancreatic development remain completely unexplored.

Both the findings from this study and the approaches utilized can be applied to human tissue in order to study the cellular heterogeneity of the human pancreatic mesenchyme. First, a directed approach looking for the presence of the mesenchymal populations identified in mice can be performed by multiplexed immunohistochemistry and/or *in situ* hybridization. Second, an unbiased single-cell RNA-sequencing approach with human pancreatic tissue can be performed in order to more robustly characterize the cellular populations during development. Comparisons of these mouse and human datasets would allow for identification of key similarities or differences within this compartment.

In particular, the development of the human pancreatic mesothelium can be compared to our findings in mice. Although the adult human pancreas is known to contain a mesothelial layer, little is known regarding its development. Probing human tissue for expression of key mesothelial genes identified in our mouse dataset can help determine when and how this tissue arises during human development. Additionally, we can correlate the appearance of the human

mesothelial layer with the expression of genes expressed in the populations predicted to arise from the mouse mesothelial layer during development, such as *PITX2* and *STMN2*. Finally, determining the expression pattern of *FGF9* and other secreted factors in human pancreas can help determine if the human pancreatic mesothelium is likely to function as a source of secreted factors.

Giving back to the dish

One goal of this study was to inform current efforts to produce hESC-derived beta cells for cellular therapy. One component that has traditionally been left out of differentiation protocols are the supporting niche cells, including vascular, neuronal, and mesenchymal cells. Given the importance of these cell types in pancreatic epithelial development *in vivo*, both in mice and humans, the absence of these cells *in vitro* may hinder the differentiation process towards a beta cell fate. Indeed, co-culture of primary mesenchymal cells with hESC-derived definitive endoderm progenitor cells has been demonstrated to support pancreatic progenitor proliferation *in vitro* (Sneddon et al., 2012). The mesenchymal cell lines used for co-culture were derived by outgrowth of either human fetal or embryonic mouse pancreata. Therefore, the cellular identity of these cells remains unknown, making their mechanistic contribution to the differentiation difficult to determine. Additionally, there may be additional mesenchymal populations that are critical for beta cell differentiation but are not able to survive or proliferate in the outgrowth culture methodology.

Co-culture of the mesenchymal subtypes identified in this study with various stages of endocrine differentiation *in vitro* can help elucidate the function of these individual populations during development and potentially improve the differentiation efficiency or final product. By

testing defined populations, we can compare the differentiation outcome upon addition of different mesenchymal populations and correlate this back to the population's gene expression profile to identify mechanistic targets. Additionally, defined ratios and combinations of mesenchymal cells types can be tested and matched to the ratios present during developmental stages in both mouse and human pancreata. Understanding the impact of these individual populations may help improve *in vitro* differentiation platforms.

The datasets developed in this study can be probed for cell surface markers that can be used to isolate individual mesenchymal populations identified by this study. As the mesenchymal populations have highly overlapping transcriptomic signatures and the transcriptomic coverage in single-cell RNA-sequencing datasets is only 10-15%, it may be challenging to identify a panel of markers capable of separating each population. Deeper sequencing of these populations can be obtained by newer versions of commercially available single-cell RNA-sequencing kits (10X Genomics, version 2). Additionally, intracellular markers can be identified and used to sort mesenchymal populations and then bulk sequencing performed to screen for cellular surface molecules specific to that population (Hrvatin, Deng, O'Donnell, Gifford, & Melton, 2014).

Recapitulation of development in disease

An emerging theme in the study of disease, wound healing, and regeneration is reactivation of processes and pathways that regulate development (Cofre & Abdelhay, 2017; Fancy, Chan, Baranzini, Franklin, & Rowitch, 2011; Roxburgh, Murphy, Pollock, & Brazil, 2006; Shworak, 2004). For example, the progression of renal fibrosis highlights the reemergence of epithelial-to-mesenchymal transitions (EMT), and expression of genes that regulate this process during development (Roxburgh et al., 2006). Additionally, transcriptomic profiles of

various cancers have identified a “developmental” signature, suggesting that cancer cells could be considered cells undergoing aberrant or improper developmental processes (Borczuk et al., 2003; Cofre & Abdelhay, 2017; Kho, 2004). This hypothesis implies that developmental mechanisms of cellular differentiation and organization can be used as a guide to probe disease progression and may represent critical targets for disease therapies.

Within the pancreas, there is evidence for the return of mature pancreatic cells to a more “developmental” like state during injury conditions. Pancreatitis is characterized by the “dedifferentiation” of acinar cells, as evidenced by the re-expression of genes expressed in acinar progenitors during development, such as *Pdx1*, *Notch*, and *beta-catenin* (Jensen et al., 2005). After acute injury, these dedifferentiated cells then differentiate into acinar cells in order to regenerate the lost exocrine tissue, suggesting that dedifferentiation may be a protective mechanism (Jensen et al., 2005). Beta cells have also been shown to undergo dedifferentiation during stress conditions, upregulating genes normally expressed in progenitor cells, such as *Ngn3*, *Oct4*, *Nanog*, and *L-Myc* (Talchai, Xuan, Lin, Sussel, & Accili, 2012)}. This process of dedifferentiation has been proposed as the major factor leading to reduced beta cell mass in type 2 diabetes, and similar to acinar cell dedifferentiation, may be a protective mechanism to prevent cell death (Accili et al., 2016).

The reactivation of developmental programs during injury suggests that the findings from our developmental dataset may be relevant for the study of adult disease. Is the *Fev+* population present during adult homeostasis, or reactivated during a variety of disease conditions, such as obesity, diabetes, or fibrosis? The re-expression of *Ngn3* and subsequent re-differentiation into beta cells in diabetes (Z. Wang, York, Nichols, & Remedi, 2014) could mean that these cells also pass through a *Fev+* state. If that is true, is the re-differentiation process facilitated by similar

mechanisms as those in the development? Are the resulting beta cells equivalent to those produced during development, or does this re-differentiation process leave “scars”? Combining lineage tracing of these dedifferentiated cells with single-cell RNA-sequencing approaches can reveal the trajectory of de- and re-differentiation. Comparison of the gene expression patterns with the developmental trajectories in this work can identify the similarities and differences, and potentially inform therapeutics for regenerative medicine.

Although much emphasis has been placed on the recapitulation of developmental programs in the epithelial cells of the regenerating pancreas, it is currently unknown whether mesenchymal cells also revert to a developmental phenotype during injury. In the heart, the mesothelium has been described as undergoing a “reactivation” process that results in re-expression of developmental genes and reversion to its developmental function as a mesenchymal progenitor cell (Bin Zhou et al., 2011). Pancreatic mesenchymal cells undergo dynamic changes during pancreatitis (Apte et al., 2012), but given our lack of understanding of the mesenchymal cell types in either development or disease, it has been challenging to study these populations. With the datasets derived in this work, we can begin to compare the mesenchymal transcriptomic signatures in development and adult homeostasis and disease. Evidence of shifting populations in caerulein-treated pancreata suggests that multiple mesenchymal and mesothelial populations change transcriptionally during pancreatitis. Do these changes reflect reversions to a developmental population? If so, do they share functional roles in both development and disease progression or recovery? Future experiments aimed at characterizing the mesenchymal populations across the pancreatic timecourse will shed light on these questions and help drive progress in identifying new cellular or mechanistic targets for therapies.

Materials and Methods

Chapters 2 and 3

Mice

All mouse procedures were approved by the University of California, San Francisco (UCSF) Institutional Animal Care and Use Committee (IACUC). Mice were housed in a 12-hour light-dark cycle in a controlled temperature climate. Noon of the day of vaginal plug was considered embryonic day 0.5.

Timed-pregnant Swiss Webster mice were obtained from Charles River Laboratories. *Ngn3-Cre* (Schonhoff, Giel-Moloney, & Leiter, 2004) (a gift from Dr. Matthias Hebrok), *Fev-Cre* (Scott et al., 2005) (The Jackson Laboratory 012712), and *ROSA26mTmG* (Muzumdar et al., 2007) (the Jackson Laboratory 007676) mice were maintained in a C57BL/6J background. The Cre transgene was genotyped using the following primers: GGGCGGCATGGTGCAAGTT and CGGTGCTAACCAGCGTTTTC.

Human tissue procurement and isolation

Human fetal pancreata were harvested from post-mortem fetuses at 23 weeks of gestation with permission from the ethical committee of the University of California, San Francisco (UCSF). Tissue was fixed in 4% paraformaldehyde overnight at 4°C. After three washes in 1X PBS, tissue was either cryopreserved in 30% sucrose solution at 4°C overnight and embedded in OCT, or placed in 40% ethanol then 70% ethanol before paraffin embedding. 8 µm sections were cut on the cryostat or microtome. *In situ* hybridization and immunofluorescence were then performed as described below.

Adult human islets were isolated from cadaveric donor tissue by the UCSF Islet Production Core with permission from the UCSF ethical committee. Consented cadaver donor pancreata were provided by the nationally-recognized organization UNOS via local organ procurement agencies. The identifiers were maintained at the source only, and the investigators received de-identified specimens.

Informed consent was obtained for all human (fetal and adult) tissue collection, and protocols were approved by the Human Research Protection Program Committee on Human Research of the University of California, San Francisco (UCSF).

Embryonic stem cell culture and differentiation

The human embryonic stem cell (hESC) line HUES8 was obtained from Harvard University and used for the generation of hESC-derived beta-like cells (BLCs). Pluripotent HUES8 cells were maintained as spherical clusters in suspension in mTeSR-1 (StemCell Technologies) in 500mL spinner flasks (Corning, VWR) on a magnetic stir plate (Dura-Mag) within a 37°C incubator at 5% CO₂, 100% humidity, and a rotation rate of 70 rpm. Cells were screened for mycoplasma contamination using the MycoProbe Mycoplasma Detection Kit (R&D Systems), according to the manufacturer's instructions.

hESC-derived endocrine progenitor cells were generated as previously described (Pagliuca et al., 2014). In brief, HUES8 cells were seeded into a spinner flask at a concentration of 8×10^5 cells/mL in mTeSR-1 media with 10 μ M Rock inhibitor Y27632 (StemCell Technologies) to allow formation of spherical clusters. Differentiation was initiated 72 hours later. Differentiation was achieved in a step-wise fashion using the following growth factors and/or small molecules: definitive endoderm (Stage 1) (1 day of 100 ng/mL Activin A (R&D

Systems) and 14 µg/mL of CHIR99021 (Stemgent); 2 days of 100 ng/mL Activin A); gut tube endoderm (Stage 2) (3 days of 50 ng/mL KGF (Peprotech)); early pancreatic progenitors (Stage 3) (1 day of 200 nM LDN193189 (Fisher Scientific), 50 ng/mL KGF, 0.25 µM Sant-1 (Sigma), 2 µM Retinoic Acid (Sigma), 500 nM PdbU (EMD Biosciences); 1 day of 50 ng/mL KGF, 0.25 µM Sant-1, 2 µM Retinoic Acid, 500 nM PdbU); later pancreatic progenitors (Stage 4) (5 days of 50 ng/mL KGF, 0.25 µM Sant-1, 0.1 µM Retinoic Acid); endocrine progenitors (Stage 5) (4 days of 0.25 µM Sant-1, 0.1 µM Retinoic Acid, 1 µM XXI (EMD Millipore), 10 µM Alk5i (Axxora), 1 µM T3 (EMD Biosciences), 20 ng/mL Betacellulin (Fisher Scientific); 3 days of 25 nM Retinoic Acid, 1 µM XXI, 10 µM Alk5i, 1 µM T3, 20 ng/mL Betacellulin); BLCs (Stage 6) (6 days of 10 µM Alk5i; 1 µM T3). Successful differentiation was assessed at Stages 1, 3, 4, 5, and 6 via immunofluorescence or FACS for stage-specific marker genes.

To measure the expression of *FEV* at various stages of human endocrine differentiation, aliquots of clusters were removed from the flask and analyzed at several timepoints: after 5 days in Stage 5 (“mid-stage endocrine progenitors”), after 7 days in Stage 5 (“late-stage endocrine progenitors”), and after 5 days at the BLC stage. As a comparator, pluripotent, undifferentiated hESCs in mTeSR-1, as well as human adult islets, were also analyzed for *FEV* expression.

Immunofluorescence

Embryonic mouse pancreata were dissected in cold 1X PBS and fixed in zinc-buffered formalin (Anatech LTD) at room temperature (RT) for 30-90 minutes or overnight at 4°C. After three washes in 1X PBS, tissue was processed for either cryopreservation or paraffin embedding. Cryopreserved pancreata were placed in 30% sucrose solution at 4°C overnight before embedding in OCT. Paraffin-embedded pancreata were placed in 40% ethanol and 70% ethanol

before paraffin tissue processing. 8 um sections were cut on the cryostat or microtome. For immunofluorescence on paraffin sections, slides were baked at 55°C for 30 minutes, deparaffinized in xylene, and rehydrated in decreasing concentrations of ethanol. Heat-mediated antigen retrieval was performed using Antigen Retrieval Citra Solution (Biogenex Laboratories). Tissue sections were blocked in 5% normal donkey serum (NDS; Rockland Immunochemicals) and Mouse-on-Mouse IgG blocking reagent (Vector Laboratories) when appropriate in 0.2% Triton X-100 in PBS (PBT) for 1 hour and then stained overnight at 4°C using the following primary antibodies: Acta2 (1:200, Abcam ab21027), Cav1 (1:200, Abcam ab2910), Chromogranin A (1:100, Abcam ab15160), E-cadherin (1:200, BD Transduction Lab 610182), Glucagon (1:100, Abcam ab82270), Insulin (1:50, DAKO A0564), Vimentin (1:200, Abcam ab92547), and Wt1 (1:100, Abcam ab89901). All antibodies have been validated by the manufacturer. The next day, sections were washed three times in 0.1% Tween 20 in 1X PBS and then incubated with species-specific Alexa Fluor 488-, 594-, or 647-conjugated secondary antibodies (1:500, Jackson ImmunoResearch) and DAPI in 5% NDS in 0.2% PBT for 1 hour at RT. Sections were washed three times in 0.1% Tween 20 in 1X PBS, rinsed in 1X PBS, and then mounted in Fluoromount-G mounting medium (SouthernBiotech). Slides were stored at 4°C.

For immunofluorescence on cryosections, slides were removed from -80°C storage and allowed to reach RT. Sections were rinsed in 1X PBS three times and permeabilized in 0.5% PBT for 10 minutes at RT. Tissue sections were blocked in 5% NDS and, if needed, Mouse-on-Mouse IgG blocking reagent in 0.1% PBT for 1 hour and then stained overnight at 4°C using the following primary antibodies: CD326 (Epcam) (1:200, BD Transduction Lab 552370), Glucagon (1:2000, Millipore 4031-01F), Insulin (1:250, DAKO A0564), Somatostatin (1:500, Santa Cruz Biotechnology sc-7819), Ghrelin (1:1500, Santa Cruz Biotechnology sc-10368), Pancreatic

Polypeptide (PP; 1:250, Abcam ab77192), and Vimentin (1:200, Abcam ab92547). All antibodies have been validated by manufacturer. Sections were washed the next day three times in 1X PBS and then incubated with species-specific Alexa Fluor 488-, 555-, 594-, or 647-conjugated secondary antibodies and DAPI in 5% NDS in 0.1% PBT for 1 hour at RT. Sections were washed three times in 1X PBS and mounted in Fluoromount-G mounting medium. Slides were stored at 4°C.

Images were captured on a Zeiss Apotome Widefield microscope with optical sectioning capabilities or Leica confocal laser scanning SP8 microscope. Maximum intensity z-projections were then prepared using ImageJ, where brightness, contrast, and pseudo-coloring adjustments were applied equally across all images in a given series.

In situ hybridization

In situ hybridization was performed on 8 um sections using RNAscope technology (Advanced Cell Diagnostics)(F. Wang et al., 2012) according to the manufacturer's instructions. *In situ* probes against mouse *Ngn3* (422409-C2), *Fev* (413241-C3), *Isl1* (451931), *Ins1* (414661-C4), *Gcg* (400601), *Sst* (404631-C3), *Ghrl* (415301-C2), *Ppy* (482701), *Peg10* (512921-C4), *Gngl2* (462521-C2), *Nnat* (432631-C2), *Barx1* (414681), *Pitx2* (412841-C2), *Stmn2* (498391-C3), *Msln* (443241) and human *NGN3* (505791-C4), *FEV* (471421-C3), and *ISL1* (478591-C2) were used in combination with the RNAscope Multiplex Fluorescent Reagent Kit v2 for target detection. Following signal amplification of the target probes, sections were washed in 1X PBS three times and blocked in 5% NDS in 0.1% PBT for 1 hour at RT. Tissue sections were then stained with primary and secondary antibodies as described above in the "immunofluorescence" section.

For *in situ* hybridization of hESC-derived clusters, cells were fixed with 4% PFA for 15 minutes at RT, washed with PBS, and cryoprotected in 30% sucrose overnight. The next day, clusters were embedded in a small sphere of 1.5% low-melting temperature agarose; these were again cryoprotected in 30% sucrose overnight. The following day, the agarose spheres were soaked in OCT and frozen in a dry ice bath. *In situ* hybridization was then performed on 8 um sections using human *NGN3*, *FEV*, and *ISL1* RNAscope probes.

Quantification of cell proportions

Quantification of pancreata was performed by manual counting using ImageJ software. Cell populations present at less than 1% in *Ngn3*-lineage traced E14.5 replicates were deemed artifact and excluded from further analysis.

Quantitative RT-PCR

hESCs from various stages of directed differentiation were collected and RNA extracted with the RNeasy Mini Kit (Qiagen). Reverse transcription was performed with the Clontech RT-PCR kit. RT-PCR was run on a 7900HT Fast Real-Time PCR instrument (Applied Biosystems) with Taqman probes for *FEV* (assay ID: Hs00232733_m1) and *GAPDH* (assay ID: Hs02758991_g1) in triplicate. Data were normalized to *GAPDH*. Error bars represent standard deviation.

Dissociation and FACS of embryonic pancreas

Embryonic mouse pancreata were dissected and placed in 1X PBS on ice, then dissociated into single cells using TrypLE Express dissociation reagent (Thermo Fisher) at 37°C

with pipet trituration at 5-minute intervals during incubation. For v1 datasets, E12.5 pancreata were dissociated for 10 minutes, E14.5 pancreata for 15 minutes, and E17.5 pancreata for 30 minutes. For batch 1, we pooled 14 E14.5 pancreata from one litter. For batch 2, which was collected on a different day, we pooled tissue from each timepoint separately: 18 E12.5 pancreata from two litters, 11 E14.5 pancreata from one litter, and 8 E17.5 pancreata from one litter. Dissociations were neutralized with FACS buffer (10% FBS + 2mM EDTA in phenol-red free HBSS). Dissociated cells were passed through a 30 um cell strainer and stained with Sytox live/dead stain (Thermo Fisher). Stained cells were washed twice in FACS buffer and then sorted using a BD FACS Aria II. After size selection to remove doublets, all live cells were collected.

For version 2 10X datasets, we pooled tissue from each timepoint separately, each performed on a different day: 14 E12.5 pancreata from one litter, 13 E14.5 pancreata from one litter, and 13 E17.5 pancreata from one litter. For the E14.5 *Fev-Cre; ROSA26^{mTmG}* 10X sample, we pooled 3 pancreata from one litter. Dissociations were performed as described above. Cells undergoing a CD140a negative selection were stained with CD140a-APC (1:50; eBiosciences, cat. 17-1401-81; validated by manufacturer). Stained cells were washed twice in FACS buffer and then sorted using a BD FACS Aria II. After size selection to remove doublets, all live CD140a- cells were collected. For the E14.5 *Fev-Cre; mTmG* pancreata, live GFP+ cells and GFP-/TdTomato+ cells were collected. All 4,000 GFP+ (*Fev*-lineage traced) cells were loaded onto the 10X Genomics platform, supplemented with an additional 21,000 TdTomato+/GFP- (non-lineage traced).

Single-cell capture and sequencing

To capture individual cells, we utilized the Chromium Single Cell 3' Reagent Version 1 Kit (10X Genomics) (Zheng et al., 2017). For batch 1, 12,800 cells from E14.5 pancreata were loaded into one well of the 10X chip, while for batch 2, 18,000 cells per timepoint were each loaded into their own respective wells to produce Gel Bead-in-Emulsions (GEMs). GEMs underwent reverse transcription to barcode RNA before cleanup and cDNA amplification. Libraries were prepared with the Chromium Single Cell 3' Reagent Version 1 Kit. Each sample was sequenced on 2 (Batch 1) or 1 (Batch 2) lanes of the HiSeq2500 (Illumina) in Rapid Run Mode with paired-end sequencing parameters: Read1, 98 cycles; Index1, 14 cycles; Index2, 8 cycles; and Read2, 10 cycles.

The CD140a-depleted E12.5, E14.5, and E17.5 datasets and *Fev-Cre; ROSA26^{mTmG}* dataset were generated with Chromium Single Cell 3' Reagent Version 2 kits (10X Genomics). 27,000 cells were loaded onto their respective wells and underwent the same processing as the Version 1 kits, according to manufacturer instructions for Version 2 kits. Libraries were sequenced on the NovaSeq (Illumina) with the same sequencing parameters as above.

Single-cell analysis

For the v1 datasets, we utilized CellRanger v1.1.0 software for v1 datasets and v2.1.0 for v2 datasets with default settings for de-multiplexing, aligning reads to the mouse genome (10X Genomics pre-built mm10 reference genome) with STAR (Dobin et al., 2012) and counting unique molecular identifiers (UMIs) to build transcriptomic profiles of individual cells. For the v1 datasets, gene-barcode matrices were analyzed with the R package Seurat v1.4, using the online tutorial as a guide (R core team, 2016; Satija et al., 2015). We first performed a filtering

step, retaining only the cells that expressed a minimum of 200 genes and only the genes that were expressed in at least 3 cells. A large number of cells did not meet this threshold in the E17.5 timepoint and were determined to be red blood cells by the high expression of hemoglobin genes. Variable genes were determined by mean-variance relationship to identify highly-expressed and variable genes with the Seurat function MeanVarPlot with default settings. UMI counts were log-normalized, and linear regression was performed with RegressOut to account for differences in the number of UMIs between cells. Principal component analysis (PCA) was then utilized to determine sources of variability in the dataset with PCAfast. Significant PCs were determined based on the Scree plot and utilized for Seurat's graph-based clustering algorithm (function FindClusters) with default parameters, except for the resolution parameter. To vary cluster numbers, the resolution parameter in FindClusters was adjusted from 0.6 – 3.0, and resulting clusters analyzed as follows. Clusters were visualized with t-distributed stochastic neighbor embedding (t-SNE) with Seurat's RunTSNE function with default settings (Maaten & Hinton, 2008). Differentially-expressed genes were determined with the FindAllMarkers function, which uses a bimodal likelihood ratio test (McDavid et al., 2012). We confirmed differential gene expression analysis with the Wilcoxon rank sum test and MAST (Finak et al., 2015) utilizing Seurat v2's FindMarkers function with default settings. These tests calculate adjusted p-values for multiple comparisons. To determine the final number of clusters, clusters were required to have at least 9 significantly ($p < 0.05$) differentially-expressed genes with a 2-fold difference in expression in comparison to all other clusters. Clusters were manually curated for differential gene expression, and those that did not meet this threshold were manually merged with the nearest cluster based on the phylogenetic tree from Seurat's BuildClusterTree. In some cases, clusters met the 9-gene threshold but appeared to have very similar differentially-

expressed genes to another cluster. This is likely a result of the comparison of individual clusters against all other clusters in determining differentially-expressed genes. In these cases, a pairwise comparison between the two clusters was performed and the same 9-gene threshold applied. An exception to the 9-gene threshold was made to annotate the proliferating population in early stages of the cell cycle within the E14.5 mesenchymal analysis (Fig. 4, cluster 8). Additionally, cluster 10 in the E14.5 mesenchymal dataset did not meet the 9-gene threshold. Rather, clusters 1-9 had distinct transcriptomic signatures (with at least 9 differentially expressed genes) that distinguished them from cluster 10. Lists of at least 2-fold differentially-expressed genes for individual analyses are provided in Supplementary Data 1.

For v2 datasets, Seurat v2.2 and v2.3 was utilized to perform the analysis. Cells with less than 200 genes and genes expressed in fewer than 3 cells were removed, as above. UMI counts were normalized with `NormalizeData` using default settings. Variable genes were determined with `FindVariableGenes`, using the following cut-offs suggested by the online tutorial (`x.low.cutoff = 0.0125`, `x.high.cutoff = 3`, `y.cutoff = 0.5`). Data was scaled and UMI counts regressed out with the `ScaleData` function. Principal component analysis was performed with `RunPCA`, and significant PCs determined based on the Scree plot. t-SNE analysis and clustering was performed as described above for the v1 datasets. For the E12.5 exocrine dataset, the ductal population did not meet the 9-gene threshold. All other populations within this dataset could be distinguished from the ductal population by at least 9-differentially-expressed genes, therefore we still annotated this cluster. Some of the clusters depicted for the *Fev-Cre; ROSA26^{mTmG}* dataset do not meet the 9-gene threshold. We chose to visualize these clusters in order to better illustrate their placement along the pseudotime trajectory.

Custom genome build

The custom genome for alignment of reads to eGFP and TdTomato sequences from the mTmG mouse line was created according to instructions provided by 10X Genomics reference support (<https://support.10xgenomics.com/single-cell-gene-expression/software/pipelines/latest/advanced/references>). eGFP and TdTomato sequences were concatenated to the mm10-2.1.0 reference genome (FASTA file) provided by 10X Genomics. eGFP and TdTomato annotations were then concatenated to the mm10 annotations (GTF file) provided by 10X Genomics. The cellranger mkref command was then utilized with the genome and annotations with eGFP and TdTomato, as described in the above link.

Pathway analysis

Pathway analysis and calculation of associated p-values were performed using the ConsensusPathDB over-representation analysis for pathway-based sets category (<http://cpdb.molgen.mpg.de>) (Kamburov, Wierling, Lehrach, & Herwig, 2008).

Aggregating E17.5 v2 datasets

E17.5 technical replicates from the v2 dataset were aggregated with Cellranger v2.1, utilizing the aggr function with default settings. The aggregated dataset was used for analysis and merging with the E12.5 and E14.5 v2 datasets.

Sub-clustering and merging datasets

Sub-clustering was performed by isolating clusters of interest with the Seurat function SubsetData and reanalyzing as described above (identification of variable gene, regression, and determination of significant PCs). Cells were classified as epithelial based on the expression of

E-cadherin (*Cdh1*) and other known epithelial population markers. Cells that were *Cdh1*⁻, *Vim*⁺, and *collagen3a1* (*Col3a1*)⁺ were classified as mesenchymal. Multiple batches were merged with the MergeSeurat function. The merged dataset was reanalyzed as above, with batch included as a latent variable in the RegressOut function. The v1 E14.5 batch 1 and batch 2 clusters were robust to the sampling differences between batches as evidenced by the contribution of cells from both batches to each cluster (Supplementary Fig. 2b). We find high correlation of cell type proportion between batches in all populations except the exocrine compartment (acinar and ductal) (Supplementary Fig. 2c), possibly due to technical challenges of pancreatic dissociation. Within each cluster, batch 1 cells correlated most highly with those of batch 2 contained in the same cluster, indicating proper cluster calling with the merged datasets (Supplementary Fig. 2d).

For v2 datasets (E12.5, E14.5 and E17.5), multiple canonical correlation analysis (multiCCA) from Seurat v2.3 was utilized to merge the epithelial datasets (A. Butler et al., 2018). The top 1,000 most highly variable genes that were variable in at least 2 datasets were used for the alignment, as recommended in the Seurat tutorial. The shared correlation strength of each CC was measured with Seurat's MetageneBicorPlot, and those before the drop-off were used for alignment, analogous to the Scree plot in choosing significant PCs. We then aligned the datasets with AlignSubspace and ran an integrated t-SNE and clustering analysis, as outlined in the Seurat tutorial. Clusters were required to have 9 significantly differentially-expressed genes as described above. Clusters with similar differentially-expressed genes were verified with pairwise comparisons to the most related clusters (based on BuildClusterTree) and merged if they did not meet the pairwise 9-gene threshold. The Beta 2 cluster in the v2 endocrine merged timecourse data met the 9-gene threshold for 2 out of the 3 differential expression tests (Bimodal

likelihood ratio and Wilcoxon rank sum tests), but had only 8 differentially-expressed genes for the MAST test.

Doublets were identified based on co-expression of two mutually exclusive genes, such as both mesenchymal and epithelial genes, and removed from further analysis. In the v2 datasets, rare cells (4 cells in E12.5 and 13 cells in E14.5 endocrine datasets) with high levels of hemoglobin gene expression were removed from the analysis.

Downsampling analysis

To determine if the sequencing depth was sufficient for calling clusters, downsampling analysis was performed for the v1 E14.5 batch 1 dataset. Reads were randomly downsampled from the 10x Cellranger bam file output to a specified percentage, then grouped based on UMI to generate a count profile for each cell. The number of genes with greater than 0 counts was then calculated. UMI downsampling was performed with the SampleUMI function. A new Seurat object was created with the downsampled matrix and reanalyzed as above.

The number of UMIs/cell was downsampled from an average of 4,600 UMIs/cell in the full dataset to 200 UMIs/cell, and the median number of genes/cell and clustering robustness was then calculated. Clustering robustness was determined as the percentage of cells within the same cluster, with clusters required to maintain at least 9 genes with a 2-fold change in expression in comparison to all other clusters. Within this dataset, robust clustering was maintained all the way down to 500 UMIs/cell, when the percentage of cells in the same cluster began to climb, indicating collapsing of individual clusters. Both of these downsampling analyses indicate that sufficient sequencing depth was reached.

Pseudotemporal ordering

We utilized Monocle 2.6.4 (X. Qiu et al., 2017b) to order cells in pseudotime based on their transcriptomic similarity. For v1 timecourse datasets, batch-corrected values and variable genes from Seurat analysis were used as input, utilizing the gaussianff expressionFamily, and clusters were projected onto the minimum spanning tree after ordering.

For the *Fev*-lineage traced dataset, UMI counts and variable genes from the Seurat analysis were used as input, utilizing the negBinom expressionFamily. To find genes differentially-expressed across the branch point in the trajectory, we used monocle's internal BEAM analysis and selected genes with an FDR cutoff of 0.001. Gene expression patterns were plotted with `plot_genes_branched_heatmap` and `plot_multiple_branches_pseudotime`.

Data and code availability

The accession number for the raw data files of the single-cell RNA-sequencing analyses reported in this paper is GEO: GSE101099. Seurat and monocle R objects used for analysis are available, along with scripts, at Figshare, DOI: 10.6084/m9.figshare.c.4158458. Scripts are available at <https://github.com/sneddonucs/2018-Developmental-single-cell-RNA-sequencing>.

Chapters 4 and 5

Mice

All mouse procedures were approved by the University of California, San Francisco (UCSF) Institutional Animal Care and Use Committee (IACUC). *Wt1-Cre* (Bin Zhou et al., 2008), *Wt1-CreER* (Bin Zhou et al., 2008) (The Jackson Laboratory 010912), *Krt19-CreER* (Means, Xu, Zhao, Ray, & Gu, 2008) (a gift from Dr. Holger Willenbring), and *Krt18-CreER*

(Van Keymeulen et al., 2009) (a gift from Dr. Ophir Klein), and *Fgf9-LacZ* (Huh et al., 2015) (a gift from Dr. David Ornitz) mice were maintained on mixed backgrounds. Cre alleles were genotyped with primers listed in “Mice” for Chapters 2 and 3. *Fgf9* mice were genotyped with the following primers: WT 3’: CCGCGAATGCTGACCAGGCCCACTGCTAT, WT 5’: CATATACATGTACATGCTCACATACACACT, MUT 3’: TCTAGAGAATAGGAACTTCGGAATAGGA. WT 3’ and 5’ detected a 500 bp wild type allele and MUT 3’ and WT 5’ detected a 141 bp mutant allele.

Immunofluorescence

Embryonic mouse pancreata were dissected in cold 1X PBS and fixed 4% paraformaldehyde in 1X PBS at room temperature (RT) for 30-90 minutes or overnight at 4°C. After three washes in 1X PBS, tissue was processed for either cryopreservation or paraffin embedding. Cryopreserved pancreata were placed in 30% sucrose solution at 4°C overnight before embedding in OCT. 5-8 um sections were cut on a cryostat and immunostaining performed as stated in “Immunofluorescence” for Chapters 2 and 3. Additionally antibodies used in Chapters 4 and 5 include: WT1 (1:200, Abcam, ab89901), CAV1 (1:200, Abcam ab2910), EBP50 (1:200, Abcam, ab3452), CRYAB (1:200, Abcam, ab13496), GFP (1:200, Aves, GFP-1020), KRT19 (1:200, Abcam, ab133496), CD31 (1:200, BD Biosciences, 553370), CPA1 (1:200, R&D Systems, AF2765), and SMA (1:200, Abcam, ab21027).

Whole mount immunofluorescence

Embryonic mouse pancreata were dissected in cold 1X PBS and fixed with 4% PFA for 45 min. at RT. Pancreata were washed three times with 0.2% bovine serum albumin

(BSA) in 1X PBS for 10 min. at RT while shaking, and blocked in 2% BSA, 5% normal donkey serum (NDS), 0.1% Triton X-100 in 1X PBS for 3 hours at RT. Primary antibodies were diluted in the block buffer and pancreata stained overnight at 4°C while shaking. After four washes in 0.1% Triton X-100 in 1X PBS for 15 minutes each, pancreata were stained with species-specific Alexa 488-, 549-, or 647- secondary antibodies diluted in block buffer overnight at 4C while shaking. Pancreata were then washed three times with block buffer for 30 minutes each. Pancreata were dehydrated in a methanol series: 10 minutes each in 25%, 50%, 75%, and 100% methanol and one additional 10 minutes wash in 100% methanol before clearing in 50% benzyl alcohol and 50% benzyl benzoate (BABB). Imaging was performed on a Leica confocal laser scanning SP8 microscope and three dimensional reconstructions were performed with Imaris software.

Primary antibodies used for whole mount imaging include CD326 (Abcam 552370), CRYAB (1:100, Abcam ab13496), and EBP50 (1:100, Abcam, ab3452).

Lineage tracing

Wt1-Cre, Wt1-CreER, Krt19-CreER, and Krt18-CreER males were crossed to ROSA26^{mTmG} females. Tamoxifen was administered to pregnant dams via interperitoneal injection (Krt19-CreER) or oral gavage (Wt1-CreER, Krt18-CreER). ROSA26^{mTmG} crossed to Wt1-CreER males received two 2.5 mg doses of tamoxifen 8 hours apart at E12.5, and pancreata were collected at either E13.5 or E17.5. ROSA26^{mTmG} crossed to Krt19-CreER males received one 4.5 mg dose of tamoxifen at E12.5 and E13.5, and pancreata were collected at E17.5. ROSA26^{mTmG} crossed to Krt18-CreER males received one 3 mg dose of tamoxifen was given at E11.5 and E12.5, and pancreata collected at E13.5.

Hematoxylin and eosin (H&E) staining

Adult pancreata from PBS- and caerulein-injected animals were dissected and fixed in zinc-buffered formalin (Anatech LTD) overnight at 4C. Pancreata were washed three times in 1X PBS over the course of 4 hours, placed in 40% ethanol for 20 minutes at 4C and then stored in 70% ethanol at 4C until processing for paraffin embedding. 6 um sections were cut on the microtome. H&E staining was performed with the following immersion steps: HistoClear twice for 4 minutes, 100% ethanol twice for 2 minutes, 95% ethanol for 2 minutes, tap water for 3 minutes, hematoxylin (ThermoFisher) for 3 minutes, tap water for 3 minutes, 95% ethanol for 1 min, eosin (ThermoFisher) for 1 minute, 95% ethanol for 1 minute, 100% ethanol twice for 2 minutes, histoClear twice for 2 minutes. Slides were then mounted with Cytoseal (ThermoFisher) and imaged with the Zeiss Brightfield microscope.

Caerulein treatment

Acute pancreatitis was induced in 6-8 week old Swiss Webster mice. For the timecourse experiments, 2 ug Caerulein (Bachem) was injected by i.p hourly for 8 hours on two consecutive days in both male and female mice. For the single-cell RNA-sequencing experiments, 75 ug/kg caerulein was used per injection and only male mice was used.

Dissociation and FACS of adult pancreas

Adult pancreata were dissected in pairs and placed in cold 1X PBS. For the single-cell RNA-sequencing experiments, 2 PBS-treated and 4 caerulein-treated animals were dissected. Once all dissections were complete pancreata were placed in dissociation buffer (0.4 mg/mL

Collagenase P (Roche), 1 ng/mL DNase1 (Roche), 0.2 mg/mL soybean trypsin inhibitor (STI) or with modifications as outlined in results) at 37C for 20-25 minutes with pipet trituration at 5-minute intervals during incubation. Dissociations were neutralized with FACS buffer (10% FBS + 2mM EDTA in phenol-red free HBSS) and passed through a 30 um cell strainer twice. Red blood cell lysis buffer (High Yield Lyse, ThermoFisher) was diluted 1:10 in water and added to dissociations at a 10:1 ratio for 2 minutes at RT. Cells were stained with various combinations of sytox blue (1:2000), propidium iodide (1:1000), CD326-FITC (1:100, eBiosciences 115791), CD140a-APC (1:100, eBiosciences 171401), and CD45-PE (1:100, eBiosciences 120451). Stained cells were washed twice in FACS buffer and then sorted using a BD FACS Aria II. After size selection to remove doublets and live/dead selection of sytox blue and PI negative cells, cells were sorted into CD45+ and CD45-negative fractions.

Single-cell capture and sequencing

The PBS and caerulein datasets were generated with Chromium Single Cell 3' Reagent Version 2 kits (10X Genomics). 27,000 cells total, 15% of which was CD45+ and 85% of which was CD45-negative, from each of the PBS and caerulein dissociations were loaded onto separate wells of the 10X Chromium machine for single cell capture and libraries prepared according to manufacturer instructions for Version 2 kits. Libraries were sequenced on the NovaSeq (Illumina) with the same sequencing parameters outlined in “Single-cell capture and sequencing” for Chapters 2 and 3.

Single-cell analysis

PBS and caerulein datasets were processed as described in “Single-cell analysis” for Chapters 2 and 3. Seurat v2 was utilized for all downstream analysis following the same scripts as described for the v2 datasets in Chapters 2 and 3. For clustering, the default resolution of 0.8 was used without additional merging of clusters. Therefore, we did not apply the 9-gene threshold criteria used in Chapters 2 and 3. Differentially-expressed genes were determined using the Wilcoxon rank sum test from Seurat’s FindAllMarkers. Subclustering was performed as described in “Single-cell analysis” for Chapters 2 and 3, using mesenchymal (*Pdgfra*) and mesothelial (*Msln*) markers as inclusion or exclusion criteria.

References

- Accili, D., Talchai, S. C., Kim-Muller, J. Y., Cinti, F., Ishida, E., Ordelheide, A. M., et al. (2016). When β -cells fail: lessons from dedifferentiation. *Diabetes, Obesity and Metabolism*, *18*, 117–122. <http://doi.org/10.1111/dom.12723>
- Agha, El, E., Herold, S., Alam, Al, D., Quantius, J., MacKenzie, B., Carraro, G., et al. (2014). Fgf10-positive cells represent a progenitor cell population during lung development and postnatally. *Development (Cambridge, England)*, *141*(2), 296–306. <http://doi.org/10.1242/dev.099747>
- Aghdassi, A. A., Mayerle, J., Christochowitz, S., Weiss, F. U., Sendler, M., & Lerch, M. M. (2011). Animal models for investigating chronic pancreatitis. *Fibrogenesis & Tissue Repair*, *4*(1), 26. <http://doi.org/10.1186/1755-1536-4-26>
- Ahlgren, U., Pfaff, S. L., Jessell, T. M., Edlund, T., & Edlund, H. (1997). Independent requirement for ISL1 in formation of pancreatic mesenchyme and islet cells. *Nature*, *385*, 1–4.
- Ahnfelt-Rønne, J., Ravassard, P., Pardanaud-Glavieux, C., Scharfmann, R., & Serup, P. (2010). Mesenchymal Bone Morphogenetic Protein Signaling Is Required for Normal Pancreas Development. *Diabetes*, *59*(8), 1948–1956. <http://doi.org/10.2337/db09-1010>
- Alam, Al, D., Sala, F. G., Baptista, S., Galzote, R., Danopoulos, S., Tiozzo, C., et al. (2012). FGF9-Pitx2-FGF10 signaling controls cecal formation in mice. *Developmental Biology*, *369*(2), 340–348. <http://doi.org/10.1016/j.ydbio.2012.07.008>
- Andoh, A., Takaya, H., Saotome, T., Shimada, M., Hata, K., Araki, Y., et al. (2000). Cytokine regulation of chemokine (IL-8, MCP-1, and RANTES) gene expression in human pancreatic periacinar myofibroblasts. *Gastroenterology*, *119*(1), 211–219. <http://doi.org/10.1053/gast.2000.8538>
- Andrée, B., Hillemann, T., Kessler-Icekson, G., Schmitt-John, T., Jockusch, H., Arnold, H.-H., & Brand, T. (2000). Isolation and Characterization of the Novel Popeye Gene Family Expressed in Skeletal Muscle and Heart. *Developmental Biology*, *223*(2), 371–382. <http://doi.org/10.1006/dbio.2000.9751>
- Ang, S.-L., & Rossant, J. (1994). HNF-3 β is essential for node and notochord formation in mouse development. *Cell*, *78*(4), 561–574. [http://doi.org/10.1016/0092-8674\(94\)90522-3](http://doi.org/10.1016/0092-8674(94)90522-3)
- Angelo, J. R., & Tremblay, K. D. (2018). Identification and fate mapping of the pancreatic mesenchyme. *Developmental Biology*, *435*(1), 15–25. <http://doi.org/10.1016/j.ydbio.2018.01.003>
- Apelqvist, Å., Li, H., Sommer, L., Beatus, P., Anderson, D. J., Honjo, T., et al. (1999). Notch signalling controls pancreatic cell differentiation. *Nature Publishing Group*, *400*(6747), 877–881. <http://doi.org/10.1038/23716>
- Apte, M. V., Haber, P. S., Applegate, T. L., Norton, I. D., McCaughan, G. W., Korsten, M. A., et al. (1998). Periacinar stellate shaped cells in rat pancreas: identification, isolation, and culture. *Gut*, *43*(1), 128–133.
- Apte, M. V., Haber, P. S., Darby, S. J., Rodgers, S. C., McCaughan, G. W., Korsten, M. A., et al. (1999). Pancreatic stellate cells are activated by proinflammatory cytokines: implications for pancreatic fibrogenesis. *Gut*, *44*(4), 534–541. <http://doi.org/10.1136/gut.44.4.534>
- Apte, M. V., Phillips, P. A., Fahmy, R. G., Darby, S. J., Rodgers, S. C., McCaughan, G. W., et al. (2000). Does alcohol directly stimulate pancreatic fibrogenesis? Studies with rat pancreatic stellate cells. *Gastroenterology*, *118*(4), 780–794.

- Apte, M., Pirola, R., & Wilson, J. (2012). Pancreatic stellate cells: a starring role in normal and diseased pancreas. *Frontiers in Physiology*, 3. <http://doi.org/10.3389/fphys.2012.00344>
- Ariza, L., Cañete, A., Rojas, A., Chapuli, R. M., & Carmona, R. (2018). Role of the Wilms' tumor suppressor gene *Wt1* in pancreatic development. *Developmental Dynamics*, 247(7), 924–933. <http://doi.org/10.1002/dvdy.24636>
- Ariza, L., Carmona, R., Cañete, A., Cano, E., & Chapuli, R. M. (2016). Coelomic epithelium-derived cells in visceral morphogenesis. *Developmental Dynamics*, 245(3), 307–322. <http://doi.org/10.1002/dvdy.24373>
- Arnes, L., Hill, J. T., Gross, S., Magnuson, M. A., & Sussel, L. (2012). Ghrelin Expression in the Mouse Pancreas Defines a Unique Multipotent Progenitor Population. *PLoS ONE*, 7(12), e52026. <http://doi.org/10.1371/journal.pone.0052026>
- Asahina, K., Tsai, S. Y., Li, P., Ishii, M., Maxson, R. E., Jr., Sucov, H. M., & Tsukamoto, H. (2008). Mesenchymal Origin of Hepatic Stellate Cells, Submesothelial Cells, and Perivascular Mesenchymal Cells During Mouse Liver Development. *Hepatology (Baltimore, Md.)*, 49(3), 998–1011. <http://doi.org/10.1002/hep.22721>
- Asahina, K., Zhou, B., Pu, W. T., & Tsukamoto, H. (2011). Septum transversum-derived mesothelium gives rise to hepatic stellate cells and perivascular mesenchymal cells in developing mouse liver. *Hepatology (Baltimore, Md.)*, 53(3), 983–995.
- Asimakopoulou, A., Weiskirchen, S., & Weiskirchen, R. (2016). Lipocalin 2 (LCN2) Expression in Hepatic Malfunction and Therapy. *Frontiers in Physiology*, 7(33), 779. <http://doi.org/10.3389/fphys.2016.00430>
- Azizoglu, D. B., Chong, D. C., Villasenor, A., Magenheimer, J., Barry, D. M., Lee, S., et al. (2016). Vascular development in the vertebrate pancreas. *Developmental Biology*, 420(1), 67–78. <http://doi.org/10.1016/j.ydbio.2016.10.009>
- Bachem, M. G., Schneider, E., Groß, H., Weidenbach, H., Schmid, R. M., Menke, A., et al. (1998). Identification, culture, and characterization of pancreatic stellate cells in rats and humans. *Gastroenterology*, 115(2), 421–432.
- Barge, J. U., & Lopera, J. E. (2012). Vascular Complications of Pancreatitis: Role of Interventional Therapy. *Korean Journal of Radiology*, 13(Suppl 1), S45. <http://doi.org/10.3348/kjr.2012.13.S1.S45>
- Bayle, J., Fitch, J., Jacobsen, K., Kumar, R., Lafyatis, R., & Lemaire, R. (2008). Increased Expression of *Wnt2* and *SFRP4* in Tsk Mouse Skin: Role of Wnt Signaling in Altered Dermal Fibrillin Deposition and Systemic Sclerosis. *Journal of Investigative Dermatology*, 128(4), 871–881. <http://doi.org/10.1038/sj.jid.5701101>
- Becerril, B., Marangoni, S., & Possani, L. D. (1997). Toxins and genes isolated from scorpions of the genus *Tityus*. *Toxicon*, 35(6), 821–835. [http://doi.org/10.1016/S0041-0101\(96\)00198-5](http://doi.org/10.1016/S0041-0101(96)00198-5)
- Benitez, C. M., Qu, K., Sugiyama, T., Pauerstein, P. T., Liu, Y., Tsai, J., et al. (2014). An Integrated Cell Purification and Genomics Strategy Reveals Multiple Regulators of Pancreas Development. *PLOS Genetics*, 10(10), e1004645. <http://doi.org/10.1371/journal.pgen.1004645>
- Berna, M. J., Seiz, O., Nast, J. F., Benten, D., Bläker, M., Koch, J., et al. (2010). CCK1 and CCK2 receptors are expressed on pancreatic stellate cells and induce collagen production. *Journal of Biological Chemistry*, 285(50), 38905–38914. <http://doi.org/10.1074/jbc.M110.125534>

- Beucher, A., Martín, M., Spenle, C., Poulet, M., Collin, C., & Gradwohl, G. (2012). Competence of failed endocrine progenitors to give rise to acinar but not ductal cells is restricted to early pancreas development. *Developmental Biology*, *361*(2), 277–285. <http://doi.org/10.1016/j.ydbio.2011.10.025>
- Bhushan, A., Itoh, N., Kato, S., Thiery, J. P., Czernichow, P., Bellusci, S., & Scharfmann, R. (2001). Fgf10 is essential for maintaining the proliferative capacity of epithelial progenitor cells during early pancreatic organogenesis. *Development (Cambridge, England)*, *128*(24), 5109–5117. <http://doi.org/10.1038/385257a0>
- Bin Zhou, Honor, L. B., He, H., Ma, Q., Oh, J.-H., Butterfield, C., et al. (2011). Adult mouse epicardium modulates myocardial injury by secreting paracrine factors. *The Journal of Clinical Investigation*, *121*(5), 1894–1904. <http://doi.org/10.1172/JCI45529>
- Bin Zhou, Ma, Q., Rajagopal, S., Wu, S. M., Domian, I., Rivera-Feliciano, J., et al. (2008). Epicardial progenitors contribute to the cardiomyocyte lineage in the developing heart. *Nature*, *454*(7200), 109–113. <http://doi.org/10.1038/nature07060>
- Bockman, D. E., Boydston, W. R., & Anderson, M. C. (1982). Origin of tubular complexes in human chronic pancreatitis. *The American Journal of Surgery*, *144*(2), 243–249. [http://doi.org/10.1016/0002-9610\(82\)90518-9](http://doi.org/10.1016/0002-9610(82)90518-9)
- Boggs, K., Wang, T., Orabi, A. I., Mukherjee, A., Eisses, J. F., Sun, T., et al. (2018). Pancreatic gene expression during recovery after pancreatitis reveals unique transcriptome profiles. *Scientific Reports*, *8*(1), 1406. <http://doi.org/10.1038/s41598-018-19392-0>
- Bonner-Weir, S., Aguayo-Mazzucato, C., & Weir, G. C. (2016). Dynamic development of the pancreas from birth to adulthood. *Upsala Journal of Medical Sciences*, *121*(2), 155–158. <http://doi.org/10.3109/03009734.2016.1154906>
- Borcuk, A. C., Gorenstein, L., Walter, K. L., Assaad, A. A., Wang, L., & Powell, C. A. (2003). Non-Small-Cell Lung Cancer Molecular Signatures Recapitulate Lung Developmental Pathways. *The American Journal of Pathology*, *163*(5), 1949–1960.
- Bracht, T., Mölleken, C., Ahrens, M., Poschmann, G., Schlosser, A., Eisenacher, M., et al. (2016). Evaluation of the biomarker candidate MFAP4 for non-invasive assessment of hepatic fibrosis in hepatitis C patients. *Journal of Translational Medicine*, *14*(1), 201. <http://doi.org/10.1186/s12967-016-0952-3>
- Brade, T., Kumar, S., Cunningham, T. J., Chatzi, C., Zhao, X., Cavallero, S., et al. (2010). Retinoic acid stimulates myocardial expansion by induction of hepatic erythropoietin which activates epicardial *Igf2*. *Development (Cambridge, England)*, *138*(1), 139–148. <http://doi.org/10.1242/dev.054239>
- Brock, C. (2013). Pathophysiology of chronic pancreatitis. *World Journal of Gastroenterology*, *19*(42), 7231–7240. <http://doi.org/10.3748/wjg.v19.i42.7231>
- Buchholz, M., Biebl, A., Neeße, A., Wagner, M., Iwamura, T., Leder, G., et al. (2003). SERPINE2 (Protease Nexin I) Promotes Extracellular Matrix Production and Local Invasion of Pancreatic Tumors in Vivo. *Cancer Research*, *63*(16), 4945–4951. [http://doi.org/10.1016/S0378-1119\(99\)00045-1](http://doi.org/10.1016/S0378-1119(99)00045-1)
- Buettner, F., Natarajan, K. N., Casale, F. P., Proserpio, V., Scialdone, A., Theis, F. J., et al. (2015). 25599176. *Nature Biotechnology*, *33*(2), 155–160. <http://doi.org/10.1038/nbt.3102>
- Butler, A. E., Dhawan, S., Hoang, J., Cory, M., Zeng, K., Fritsch, H., et al. (2016). β -Cell Deficit in Obese Type 2 Diabetes, a Minor Role of β -Cell Dedifferentiation and Degranulation. *The Journal of Clinical Endocrinology & Metabolism*, *101*(2), 523–532. <http://doi.org/10.1210/jc.2015-3566>

- Butler, A., Hoffman, P., Smibert, P., Papalexi, E., & Satija, R. (2018). Integrating single-cell transcriptomic data across different conditions, technologies, and species. *Nature Biotechnology*, *36*(5), 411–420.
- Cai, C.-L., Martin, J. C., Sun, Y., Cui, L., Wang, L., Ouyang, K., et al. (2008). A myocardial lineage derives from Tbx18 epicardial cells. *Nature*, *454*(7200), 104–108. <http://doi.org/10.1038/nature06969>
- Cano, E., Carmona, R., & Munoz-Chapuli, R. (2013). Wt1-expressing progenitors contribute to multiple tissues in the developing lung. *American Journal of Physiology - Lung Cellular and Molecular Physiology*, *305*(4), L322–L332. <http://doi.org/10.1152/ajplung.00424.2012>
- Cao, H., Jheon, A., Li, X., Sun, Z., Wang, J., Florez, S., et al. (2013). The Pitx2:miR-200c/141:noggin pathway regulates Bmp signaling and ameloblast differentiation. *Development (Cambridge, England)*, *140*(16), 3348–3359. <http://doi.org/10.1242/dev.089193>
- Carmona, R., Cano, E., Mattiotti, A., Gaztambide, J., & Munoz-Chapuli, R. (2013). Cells Derived from the Coelomic Epithelium Contribute to Multiple Gastrointestinal Tissues in Mouse Embryos. *PLoS ONE*, *8*(2), e55890. <http://doi.org/10.1371/journal.pone.0055890>
- Cassiman, D., Barlow, A., Vander Borgh, S., Libbrecht, L., & Pachnis, V. (2006). Hepatic stellate cells do not derive from the neural crest. *Journal of Hepatology*, *44*(6), 1098–1104. <http://doi.org/10.1016/j.jhep.2005.09.023>
- Chau, Y.-Y., Brownstein, D., Mjoseng, H., Lee, W.-C., Buza-Vidas, N., Nerlov, C., et al. (2011). Acute Multiple Organ Failure in Adult Mice Deleted for the Developmental Regulator Wt1. *PLoS Genetics*, *7*(12), e1002404. <http://doi.org/10.1371/journal.pgen.1002404>
- Chiellini, C., Grenningloh, G., Cochet, O., Scheideler, M., Trajanoski, Z., Ailhaud, G., et al. (2008). Stathmin-like 2, a developmentally-associated neuronal marker, is expressed and modulated during osteogenesis of human mesenchymal stem cells. *Biochemical and Biophysical Research Communications*, *374*(1), 64–68. <http://doi.org/10.1016/j.bbrc.2008.06.121>
- Christoffels, V. M., Grieskamp, T., Norden, J., Mommersteeg, M. T. M., Rudat, C., & Kispert, A. (2009). Tbx18 and the fate of epicardial progenitors. *Nature*, *458*(7240), E8–E9. <http://doi.org/10.1038/nature07916>
- Cofre, J., & Abdelhay, E. (2017). Cancer Is to Embryology as Mutation Is to Genetics: Hypothesis of the Cancer as Embryological Phenomenon. *The Scientific World Journal*, *2017*(6), 1–17. <http://doi.org/10.1155/2017/3578090>
- Collombat, P. (2005). The simultaneous loss of Arx and Pax4 genes promotes a somatostatin-producing cell fate specification at the expense of the β - and δ -cell lineages in the mouse endocrine pancreas. *Development (Cambridge, England)*, *132*(13), 2969–2980. <http://doi.org/10.1242/dev.01870>
- Collombat, P., Mansouri, A., Hecksher-Sørensen, J., Serup, P., Krull, J., Gradwohl, G., & Gruss, P. (2003). Opposing actions of Arx and Pax4 in endocrine pancreas development. *Genes & Development*, *17*(20), 2591–2603. <http://doi.org/10.1101/gad.269003>
- Colvin, J. S., White, A. C., Pratt, S. J., & Ornitz, D. M. (2001). Lung hypoplasia and neonatal death in Fgf9-null mice identify this gene as an essential regulator of lung mesenchyme. *Development (Cambridge, England)*, *128*(11), 2095–2106. [http://doi.org/10.1002/\(SICI\)1097-0177\(199909\)216:1<2095::AID-DVDY9>3.0.CO;2-9](http://doi.org/10.1002/(SICI)1097-0177(199909)216:1<2095::AID-DVDY9>3.0.CO;2-9)

- Corish, P., & Tyler-Smith, C. (1999). Attenuation of green fluorescent protein half-life in mammalian cells. *Protein Engineering, Design and Selection*, 12(12), 1035–1040. <http://doi.org/10.1093/protein/12.12.1035>
- D'Amour, K. A., Agulnick, A. D., Eliazer, S., Kelly, O. G., Kroon, E., & Baetge, E. E. (2005). Efficient differentiation of human embryonic stem cells to definitive endoderm. *Nature Biotechnology*, 23(12), 1534–1541. <http://doi.org/10.1038/nbt1163>
- D'Amour, K. A., Bang, A. G., Eliazer, S., Kelly, O. G., Agulnick, A. D., Smart, N. G., et al. (2006). Production of pancreatic hormone-expressing endocrine cells from human embryonic stem cells. *Nature Biotechnology*, 24(11), 1392–1401. <http://doi.org/10.1038/nbt1259>
- Davis, M. R., Arner, E., Duffy, C. R. E., De Sousa, P. A., Dahlman, I., Arner, P., & Summers, K. M. (2016). Expression of FBN1 during adipogenesis: Relevance to the lipodystrophy phenotype in Marfan syndrome and related conditions. *Molecular Genetics and Metabolism*, 119(1-2), 174–185. <http://doi.org/10.1016/j.ymgme.2016.06.009>
- Dekel, B., Metsuyanin, S., Schmidt-Ott, K. M., Fridman, E., Jacob-Hirsch, J., Simon, A., et al. (2006). Multiple Imprinted and Stemness Genes Provide a Link between Normal and Tumor Progenitor Cells of the Developing Human Kidney. *Cancer Research*, 66(12), 6040–6049. <http://doi.org/10.1158/0008-5472.CAN-05-4528>
- del Monte, G., Casanova, J. C., Guadix, J. A., MacGrogan, D., Burch, J. B. E., Perez-Pomares, J.-M., & la Pompa, de, J. L. (2011). Differential Notch Signaling in the Epicardium Is Required for Cardiac Inflow Development and Coronary Vessel Morphogenesis. *Circulation Research*. <http://doi.org/10.1161/CIRCRESAHA.110.229062;pageGroup:string:Publication>
- Desai, B. M., Oliver-Krasinski, J., De Leon, D. D., Farzad, C., Hong, N., Leach, S. D., & Stoffers, D. A. (2007). Preexisting pancreatic acinar cells contribute to acinar cell, but not islet β cell, regeneration. *The Journal of Clinical Investigation*, 117(4), 971–977. <http://doi.org/10.1172/JCI29988>
- Desgraz, R., & Herrera, P. L. (2009). Pancreatic neurogenin 3-expressing cells are unipotent islet precursors. *Development (Cambridge, England)*, 136(21), 3567–3574. <http://doi.org/10.1242/dev.039214>
- Dettman, R. W., Denetclaw, W., Jr., Ordahl, C. P., & Bristow, J. (1998). Common Epicardial Origin of Coronary Vascular Smooth Muscle, Perivascular Fibroblasts, and Intermycocardial Fibroblasts in the Avian Heart. *Developmental Biology*, 193(2), 169–181. <http://doi.org/10.1006/dbio.1997.8801>
- Dichmann, D. S., Miller, C. P., Jensen, J., Scott Heller, R., & Serup, P. (2003). Expression and misexpression of members of the FGF and TGF β families of growth factors in the developing mouse pancreas. *Developmental Dynamics*, 226(4), 663–674. <http://doi.org/10.1002/dvdy.10270>
- Dimagno, M., Lee, S., Hao, Y., Zhou, S., McKenna, B., & Owyang, C. (2005). A Proinflammatory, Antiapoptotic Phenotype Underlies the Susceptibility to Acute Pancreatitis in Cystic Fibrosis Transmembrane Regulator (–/–) Mice. *Gastroenterology*, 129(2), 665–681. <http://doi.org/10.1016/j.gastro.2005.05.059>
- Dixit, R., Ai, X., & Fine, A. (2013). Derivation of lung mesenchymal lineages from the fetal mesothelium requires hedgehog signaling for mesothelial cell entry. *Development (Cambridge, England)*, 140(21), 4398–4406. <http://doi.org/10.1242/dev.098079>

- Dobin, A., Davis, C. A., Schlesinger, F., Drenkow, J., Zaleski, C., Jha, S., et al. (2012). STAR: ultrafast universal RNA-seq aligner. *Bioinformatics*, *29*(1), 15–21. <http://doi.org/10.1093/bioinformatics/bts635>
- Dorrell, C., Schug, J., Canaday, P. S., Russ, H. A., Tarlow, B. D., Grompe, M. T., et al. (2016). Human islets contain four distinct subtypes of β cells. *Nature Communications*, *7*, 11756. <http://doi.org/10.1038/ncomms11756>
- Duvillié, B., Attali, M., Bounacer, A., Ravassard, P., Basmaciogullari, A., & Scharfmann, R. (2006). The Mesenchyme Controls the Timing of Pancreatic β -Cell Differentiation. *Diabetes*, *55*(3), 582–589. <http://doi.org/10.2337/diabetes.55.03.06.db05-0839>
- Ebert, M., Yokoyama, M., Ishiwata, T., Friess, H., Büchler, M. W., Malfertheiner, P., & Korc, M. (1999). Alteration of fibroblast growth factor and receptor expression after acute pancreatitis in humans. *Pancreas*, *18*(3), 240–246.
- Eblaghie, M. C., Reedy, M., Oliver, T., Mishina, Y., & Hogan, B. L. M. (2006). Evidence that autocrine signaling through *Bmpr1a* regulates the proliferation, survival and morphogenetic behavior of distal lung epithelial cells. *Developmental Biology*, *291*(1), 67–82. <http://doi.org/10.1016/j.ydbio.2005.12.006>
- Epshtein, A., Sakhneny, L., & Landsman, L. (2017). Isolating and Analyzing Cells of the Pancreas Mesenchyme by Flow Cytometry. *Journal of Visualized Experiments*, (119), e55344–e55344. <http://doi.org/10.3791/55344>
- Erkan, M., Adler, G., Apte, M. V., Bachem, M. G., Buchholz, M., Detlefsen, S., et al. (2011). StellaTUM: current consensus and discussion on pancreatic stellate cell research. *Gut*, *61*(2), 172–178. <http://doi.org/10.1136/gutjnl-2011-301220>
- Erkan, M., Weis, N., Pan, Z., Schwager, C., Samkharadze, T., Jiang, X., et al. (2010). Organ-, inflammation- and cancer specific transcriptional fingerprints of pancreatic and hepatic stellate cells. *Molecular Cancer*, *9*(1), 88. <http://doi.org/10.1186/1476-4598-9-88>
- Ernst, M. C., & Sinal, C. J. (2010). Chemerin: at the crossroads of inflammation and obesity. *Trends in Endocrinology & Metabolism*, *21*(11), 660–667. <http://doi.org/10.1016/j.tem.2010.08.001>
- Esni, F., Johansson, B. R., Radice, G. L., & Semb, H. (2001). Dorsal Pancreas Agenesis in N-Cadherin- Deficient Mice. *Developmental Biology*, *238*(1), 202–212. <http://doi.org/10.1006/dbio.2001.0405>
- Essafi, A., Webb, A., Berry, R. L., Slight, J., Burn, S. F., Spraggon, L., et al. (2011). A Wt1-Controlled Chromatin Switching Mechanism Underpins Tissue-Specific Wnt4 Activation and Repression. *Developmental Cell*, *21*(3), 559–574. <http://doi.org/10.1016/j.devcel.2011.07.014>
- Fancy, S. P. J., Chan, J. R., Baranzini, S. E., Franklin, R. J. M., & Rowitch, D. H. (2011). Myelin Regeneration: A Recapitulation of Development? *Dx.Doi.org*, *34*(1), 21–43. <http://doi.org/10.1146/annurev-neuro-061010-113629>
- Fendrich, V., Esni, F., Garay, M. V. R., Feldmann, G., Habbe, N., Jensen, J. N., et al. (2008). Hedgehog Signaling Is Required for Effective Regeneration of Exocrine Pancreas. *Gastroenterology*, *135*(2), 621–631.e8. <http://doi.org/10.1053/j.gastro.2008.04.011>
- Figura, von, G., Morris, J. P., Wright, C. V. E., & Hebrok, M. (2014). Nr5a2 maintains acinar cell differentiation and constrains oncogenic Kras-mediated pancreatic neoplastic initiation. *Gut*, *63*(4), 656–664. <http://doi.org/10.1136/gutjnl-2012-304287>
- Finak, G., McDavid, A., Yajima, M., Deng, J., Gersuk, V., Shalek, A. K., et al. (2015). MAST: a flexible statistical framework for assessing transcriptional changes and characterizing

- heterogeneity in single-cell RNA sequencing data. *Genome Biology*, 16(1), 278.
<http://doi.org/10.1186/s13059-015-0844-5>
- Frank, P. G. (2003). Caveolin, Caveolae, and Endothelial Cell Function. *Arteriosclerosis, Thrombosis, and Vascular Biology*, 23(7), 1161–1168.
<http://doi.org/10.1161/01.ATV.0000070546.16946.3A>
- Fujitani, Y., Fujitani, S., Boyer, D. F., Gannon, M., Yoshiya, K., Ray, M., et al. (2006). Targeted deletion of a *cis*-regulatory region reveals differential gene dosage requirements for *Pdx1* in foregut organ differentiation and pancreas formation. *Genes & Development*, 20(2), 253–266. <http://doi.org/10.1101/gad.1360106>
- Fukuda, A., Morris, J. P., IV, & Hebrok, M. (2012). Bmi1 Is Required for Regeneration of the Exocrine Pancreas in Mice. *Gastroenterology*, 143(3), 821–831.e2.
<http://doi.org/10.1053/j.gastro.2012.05.009>
- Gaisano, H. Y., Lutz, M. P., Leser, J., Sheu, L., Lynch, G., Tang, L., et al. (2001). Supramaximal cholecystokinin displaces Munc18c from the pancreatic acinar basal surface, redirecting apical exocytosis to the basal membrane. *The Journal of Clinical Investigation*, 108(11), 1597–1611. <http://doi.org/10.1172/JCI9110>
- Gannon, M., Tweedie Ables, E., Crawford, L., Lowe, D., Offield, M. F., Magnuson, M. A., & Wright, C. V. E. (2008). *pdx-1* function is specifically required in embryonic β cells to generate appropriate numbers of endocrine cell types and maintain glucose homeostasis. *Developmental Biology*, 314(2), 406–417. <http://doi.org/10.1016/j.ydbio.2007.10.038>
- Gaudio, E., Rendina, E. A., Pannarale, L., Ricci, C., & Marinozzi, G. (1988). Surface Morphology of the Human Pleura: A Scanning Electron Microscopic Study. *Chest*, 93(1), 149–153. <http://doi.org/10.1378/chest.93.1.149>
- Geske, M. J., Zhang, X., Patel, K. K., Ornitz, D. M., & Stappenbeck, T. S. (2008). Fgf9 signaling regulates small intestinal elongation and mesenchymal development. *Development (Cambridge, England)*, 135(17), 2959–2968. <http://doi.org/10.1242/dev.020453>
- Gibson, M. A., Finnis, M. L., Kumaratilake, J. S., & Cleary, E. G. (2016). Microfibril-associated Glycoprotein-2 (MAGP-2) Is Specifically Associated with Fibrillin-containing Microfibrils but Exhibits More Restricted Patterns of Tissue Localization and Developmental Expression Than Its Structural Relative MAGP-1. *Journal of Histochemistry & Cytochemistry*, 46(8), 871–885. <http://doi.org/10.1177/002215549804600802>
- Gilbert, S. F. (2000). The Neural Crest. In *Developmental Biology*. 6th edition. Sinauer Associates.
- Gise, von, A., Stevens, S. M., Honor, L. B., Oh, J.-H., Gao, C., Bin Zhou, & Pu, W. T. (2016). Contribution of Fetal, but Not Adult, Pulmonary Mesothelium to Mesenchymal Lineages in Lung Homeostasis and Fibrosis. *American Journal of Respiratory Cell and Molecular Biology*, 54(2), 222–230. <http://doi.org/10.1165/rcmb.2014-0461OC>
- Golosow, N., & Grobstein, C. (1962). Epitheliomesenchymal interaction in pancreatic morphogenesis. *Developmental Biology*, 4(2), 242–255. [http://doi.org/10.1016/0012-1606\(62\)90042-8](http://doi.org/10.1016/0012-1606(62)90042-8)
- González-Rosa, J. M., Peralta, M., & Mercader, N. (2012). Pan-epicardial lineage tracing reveals that epicardium derived cells give rise to myofibroblasts and perivascular cells during zebrafish heart regeneration. *Developmental Biology*, 370(2), 173–186.
<http://doi.org/10.1016/j.ydbio.2012.07.007>

- Gorelick, F. S., & Lerch, M. M. (2017). Do Animal Models of Acute Pancreatitis Reproduce Human Disease? *Cellular and Molecular Gastroenterology and Hepatology*, 4(2), 251–262. <http://doi.org/10.1016/j.jcmgh.2017.05.007>
- Gouzi, M., Kim, Y. H., Katsumoto, K., Johansson, K., & Grapin-Botton, A. (2011). Neurogenin3 initiates stepwise delamination of differentiating endocrine cells during pancreas development. *Developmental Dynamics*, 240(3), 589–604. <http://doi.org/10.1002/dvdy.22544>
- Gradwohl, G., Dierich, A., LeMeur, M., & Guillemot, F. (2000). neurogenin3 is required for the development of the four endocrine cell lineages of the pancreas. *Proceedings of the National Academy of Sciences*, 97(4), 1607–1611. <http://doi.org/10.1073/pnas.97.4.1607>
- Grenningloh, G., Soehrman, S., Bondallaz, P., Ruchti, E., & Cadas, H. (2003). Role of the microtubule destabilizing proteins SCG10 and stathmin in neuronal growth. *Journal of Neurobiology*, 58(1), 60–69. <http://doi.org/10.1002/neu.10279>
- Gruessner, A. C., & Gruessner, R. W. G. (2016). Long-term outcome after pancreas transplantation. *Current Opinion in Organ Transplantation*, 21(4), 377–385. <http://doi.org/10.1097/MOT.0000000000000331>
- Gu, G., Dubauskaite, J., & Melton, D. A. (2002). Direct evidence for the pancreatic lineage: NGN3+ cells are islet progenitors and are distinct from duct progenitors. *Development (Cambridge, England)*, 129(10), 2447–2457.
- Gu, G., Wells, J. M., Dombkowski, D., Preffer, F., Aronow, B., & Melton, D. A. (2004). Global expression analysis of gene regulatory pathways during endocrine pancreatic development. *Development (Cambridge, England)*, 131(1), 165–179. <http://doi.org/10.1242/dev.00921>
- Gu, H., Werner, J., Bergmann, F., Whitcomb, D. C., Büchler, M. W., & Fortunato, F. (2013). Necro-inflammatory response of pancreatic acinar cells in the pathogenesis of acute alcoholic pancreatitis. *Cell Death & Disease*, 4(10), e816–e816. <http://doi.org/10.1038/cddis.2013.354>
- Gukovskaya, A. S., & Pandol, S. J. (2004). Cell death pathways in pancreatitis and pancreatic cancer. *Pancreatology*, 4(6), 567–586. <http://doi.org/10.1159/000082182>
- Gukovsky, I., & Gukovskaya, A. S. (2010). Impaired autophagy underlies key pathological responses of acute pancreatitis. *Autophagy*, 6(3), 428–429.
- Gukovsky, I., Pandol, S. J., Mareninova, O. A., Shalbuева, N., Jia, W., & Gukovskaya, A. S. (2012). Impaired autophagy and organellar dysfunction in pancreatitis. *Journal of Gastroenterology and Hepatology*, 27(3), 27–32. <http://doi.org/10.1111/j.1440-1746.2011.07004.x>
- Guo, T., Landsman, L., Li, N., & Hebrok, M. (2013). Factors Expressed by Murine Embryonic Pancreatic Mesenchyme Enhance Generation of Insulin-Producing Cells From hESCs. *Diabetes*, 62(5), 1581–1592. <http://doi.org/10.2337/db12-0167>
- Haber, P. S., Keogh, G. W., Apte, M. V., Moran, C. S., Stewart, N. L., Crawford, D. H. G., et al. (1999). Activation of Pancreatic Stellate Cells in Human and Experimental Pancreatic Fibrosis. *The American Journal of Pathology*, 155(4), 1087–1095. [http://doi.org/10.1016/S0002-9440\(10\)65211-X](http://doi.org/10.1016/S0002-9440(10)65211-X)
- Hart, A., Papadopoulou, S., & Edlund, H. (2003). Fgf10 maintains notch activation, stimulates proliferation, and blocks differentiation of pancreatic epithelial cells. *Developmental Dynamics*, 228(2), 185–193. <http://doi.org/10.1002/dvdy.10368>
- Hasegawa, M., Higashi, K., Matsushita, T., Hamaguchi, Y., Saito, K., Fujimoto, M., & Takehara, K. (2013). Dermokine inhibits ELR+CXC chemokine expression and delays early skin

- wound healing. *Journal of Dermatological Science*, 70(1), 34–41.
<http://doi.org/10.1016/j.jdermsci.2013.01.007>
- Hastie, N. D. (2017). Wilms' tumour 1 (WT1) in development, homeostasis and disease. *Development (Cambridge, England)*, 144(16), 2862–2872.
<http://doi.org/10.1242/dev.153163>
- Hebrok, M., Kim, S. K., & Melton, D. A. (1998). Notochord repression of endodermal Sonic hedgehog permits pancreas development. *Genes & Development*, 12(11), 1705–1713.
<http://doi.org/10.1101/gad.12.11.1705>
- Hecksher-Sørensen, J., Watson, R. P., Lettice, L. A., Serup, P., Eley, L., De Angelis, C., et al. (2004). The splanchnic mesodermal plate directs spleen and pancreatic laterality, and is regulated by Bapx1/Nkx3.2. *Development (Cambridge, England)*, 131(19), 4665–4675.
<http://doi.org/10.1242/dev.01364>
- Heeg, S., Das, K. K., Reichert, M., Bakir, B., Takano, S., Caspers, J., et al. (2016). ETS-Transcription Factor ETV1 Regulates Stromal Expansion and Metastasis in Pancreatic Cancer. *Gastroenterology*, 151(3), 540–553.e14.
- Heller, R. S., Dichmann, D. S., Jensen, J., Miller, C., Wong, G., Madsen, O. D., & Serup, P. (2002). Expression patterns of Wnts, Frizzleds, sFRPs, and misexpression in transgenic mice suggesting a role for Wnts in pancreas and foregut pattern formation. *Developmental Dynamics*, 225(3), 260–270. <http://doi.org/10.1002/dvdy.10157>
- Hernandez-Torres, F., Rodríguez-Outeiriño, L., Franco, D., & Aranega, A. E. (2017). Pitx2 in Embryonic and Adult Myogenesis. *Frontiers in Cell and Developmental Biology*, 5, 211.
<http://doi.org/10.3389/fcell.2017.00046>
- Herrera, P. L. (2000). Adult insulin- and glucagon-producing cells differentiate from two independent cell lineages. *Development (Cambridge, England)*, 127(11), 2317–2322.
- Herrera, P. L., Huarte, J., Sanvito, F., Meda, P., Orci, L., & Vassalli, J. D. (1991). Embryogenesis of the murine endocrine pancreas; early expression of pancreatic polypeptide gene. *Development (Cambridge, England)*, 113(4), 1257–1265.
- Hishida, T., Naito, K., Osada, S., Nishizuka, M., & Imagawa, M. (2007). peg10, an imprinted gene, plays a crucial role in adipocyte differentiation. *FEBS Letters*, 581(22), 4272–4278.
<http://doi.org/10.1016/j.febslet.2007.07.074>
- Hori, K., Nagai, T., Shan, W., Sakamoto, A., Taya, S., Hashimoto, R., et al. (2014). Cytoskeletal Regulation by AUTS2 in Neuronal Migration and Neuritogenesis. *CellReports*, 9(6), 2166–2179. <http://doi.org/10.1016/j.celrep.2014.11.045>
- Hrvatin, S., Deng, F., O'Donnell, C. W., Gifford, D. K., & Melton, D. A. (2014). MARIS: Method for Analyzing RNA following Intracellular Sorting. *PLoS ONE*, 9(3), e89459.
<http://doi.org/10.1371/journal.pone.0089459>
- Huang, C., Xiang, Y., Chen, S., Yu, H., Wen, Z., Ye, T., et al. (2017). Dermokine contributes to epithelial–mesenchymal transition through increased activation of signal transducer and activator of transcription 3 in pancreatic cancer. *Cancer Science*, 108(11), 2130–2141.
<http://doi.org/10.1111/cas.13347>
- Huh, S.-H., Warchol, M. E., & Ornitz, D. M. (2015). Cochlear progenitor number is controlled through mesenchymal FGF receptor signaling. *eLife*, 4, 1191.
<http://doi.org/10.7554/eLife.05921>
- Ijpenberg, A., Pérez Pomares, J. M., Guadix, J. A., Carmona, R., Portillo-Sánchez, V., Macías, D., et al. (2007). Wt1 and retinoic acid signaling are essential for stellate cell development

- and liver morphogenesis. *Developmental Biology*, 312(1), 157–170.
<http://doi.org/10.1016/j.ydbio.2007.09.014>
- Ikejiri, N. (1990). The vitamin A-storing cells in the human and rat pancreas. *The Kurume Medical Journal*, 37(2), 67–81.
- Jayewickreme, C. D., & Shivdasani, R. A. (2015). Control of stomach smooth muscle development and intestinal rotation by transcription factor BARX1. *Developmental Biology*, 405(1), 21–32. <http://doi.org/10.1016/j.ydbio.2015.05.024>
- Jennings, R. E., Berry, A. A., Kirkwood-Wilson, R., Roberts, N. A., Hearn, T., Salisbury, R. J., et al. (2013). Development of the Human Pancreas From Foregut to Endocrine Commitment. *Diabetes*, 62(10), 3514–3522. <http://doi.org/10.2337/db12-1479>
- Jensen, J. N., Cameron, E., Garay, M. V. R., Starkey, T. W., Gianani, R., & Jensen, J. (2005). Recapitulation of elements of embryonic development in adult mouse pancreatic regeneration. *Gastroenterology*, 128(3), 728–741.
<http://doi.org/10.1053/j.gastro.2004.12.008>
- Jensen, J., Pedersen, E. E., Galante, P., Hald, J., Heller, R. S., Ishibashi, M., et al. (2000). Control of endodermal endocrine development by Hes-1. *Nature Genetics*, 24(1), 36–44.
<http://doi.org/10.1038/71657>
- Jeon, J., Correa-Medina, M., Ricordi, C., Edlund, H., & Diez, J. A. (2009). Endocrine Cell Clustering During Human Pancreas Development. *Journal of Histochemistry & Cytochemistry*, 57(9), 811–824. <http://doi.org/10.1369/jhc.2009.953307>
- Johansson, K. A., Dursun, U., Jordan, N., Gu, G., Beermann, F., Gradwohl, G., & Grapin-Botton, A. (2007). Temporal Control of Neurogenin3 Activity in Pancreas Progenitors Reveals Competence Windows for the Generation of Different Endocrine Cell Types. *Developmental Cell*, 12(3), 457–465. <http://doi.org/10.1016/j.devcel.2007.02.010>
- Kamburov, A., Wierling, C., Lehrach, H., & Herwig, R. (2008). ConsensusPathDB—a database for integrating human functional interaction networks. *Nucleic Acids Research*, 37(suppl_1), D623–D628.
- Kanai-Azuma, M., Kanai, Y., Gad, J. M., Tajima, Y., Taya, C., Kurohmaru, M., et al. (2002). Depletion of definitive gut endoderm in Sox17-null mutant mice. *Development (Cambridge, England)*, 129(10), 2367–2379. [http://doi.org/10.1016/S0960-9822\(00\)80016-0](http://doi.org/10.1016/S0960-9822(00)80016-0)
- Kanamori-Katayama, M., Kaiho, A., Ishizu, Y., Okamura-Oho, Y., Hino, O., Abe, M., et al. (2011). LRRN4 and UPK3B are markers of primary mesothelial cells. *PLoS ONE*, 6(10), e25391. <http://doi.org/10.1371/journal.pone.0025391>
- Kang, H. S., Kim, Y.-S., ZeRuth, G., Beak, J. Y., Gerrish, K., Kilic, G., et al. (2009). Transcription Factor Glis3, a Novel Critical Player in the Regulation of Pancreatic β -Cell Development and Insulin Gene Expression. *Molecular and Cellular Biology*, 29(24), 6366–6379. <http://doi.org/10.1128/MCB.01259-09>
- Kapadia, C., Ghosh, M. C., Grass, L., & Diamandis, E. P. (2004). Human kallikrein 13 involvement in extracellular matrix degradation. *Biochemical and Biophysical Research Communications*, 323(3), 1084–1090. <http://doi.org/10.1016/j.bbrc.2004.08.206>
- Karki, S., Surolia, R., Hock, T. D., Guroji, P., Zolak, J. S., Duggal, R., et al. (2014). Wilms' tumor 1 (Wt1) regulates pleural mesothelial cell plasticity and transition into myofibroblasts in idiopathic pulmonary fibrosis. *The FASEB Journal*, 28(3), 1122–1131.
<http://doi.org/10.1096/fj.13-236828>
- Katz, T. C., Singh, M. K., Degenhardt, K., Rivera-Feliciano, J., Johnson, R. L., Epstein, J. A., & Tabin, C. J. (2012). Distinct Compartments of the Proepicardial Organ Give Rise to

- Coronary Vascular Endothelial Cells. *Developmental Cell*, 22(3), 639–650.
<http://doi.org/10.1016/j.devcel.2012.01.012>
- Keim, V., Bauer, N., Teich, N., Simon, P., Lerch, M. M., & Mössner, J. (2001). Clinical characterization of patients with hereditary pancreatitis and mutations in the cationic trypsinogen gene. *The American Journal of Medicine*, 111(8), 622–626.
- Keirstead, H. S., Nistor, G., Bernal, G., Totoiu, M., Cloutier, F., Sharp, K., & Steward, O. (2005). Human Embryonic Stem Cell-Derived Oligodendrocyte Progenitor Cell Transplants Remyelinate and Restore Locomotion after Spinal Cord Injury. *Journal of Neuroscience*, 25(19), 4694–4705. <http://doi.org/10.1523/JNEUROSCI.0311-05.2005>
- Kho, A. T. (2004). Conserved mechanisms across development and tumorigenesis revealed by a mouse development perspective of human cancers. *Genes & Development*, 18(6), 629–640. <http://doi.org/10.1101/gad.1182504>
- Kim, S. K., Hebrok, M., & Melton, D. A. (1997). Notochord to endoderm signaling is required for pancreas development. *Development (Cambridge, England)*, 124(21), 4243–4252.
- Kim, Y.-S., Kang, H. S., Takeda, Y., Hom, L., Song, H.-Y., Jensen, J., & Jetten, A. M. (2012). Glis3 Regulates Neurogenin 3 Expression in Pancreatic β -Cells and Interacts with Its Activator, Hnf6. *Molecules and Cells*, 34(2), 193–200. <http://doi.org/10.1007/s10059-012-0109-z>
- Kroon, E., Martinson, L. A., Kadoya, K., Bang, A. G., Kelly, O. G., Eliazar, S., et al. (2008). Pancreatic endoderm derived from human embryonic stem cells generates glucose-responsive insulin-secreting cells *in vivo*. *Nature Biotechnology*, 26(4), 443–452.
- Kumar, M. E., Bogard, P. E., Espinoza, F. H., Menke, D. B., Kingsley, D. M., & Krasnow, M. A. (2014). Defining a mesenchymal progenitor niche at single-cell resolution. *Science*, 346(6211), 1258810–1258810. <http://doi.org/10.1126/science.1258810>
- Kumar, M., Jordan, N., Melton, D. A., & Grapin-Botton, A. (2003). Signals from lateral plate mesoderm instruct endoderm toward a pancreatic fate, 1–14. [http://doi.org/10.1016/S0012-1606\(03\)00183-0](http://doi.org/10.1016/S0012-1606(03)00183-0)
- Kupffer, C. (1876). Ueber Sternzellen der Leber. *Link.Springer.com*.
- Kuroda, Y., Maruyama, K., Fujii, H., Sugawara, I., Ko, S. B. H., Yasuda, H., et al. (2016). Osteoprotegerin Regulates Pancreatic β -Cell Homeostasis upon Microbial Invasion. *PLoS ONE*, 11(1), e0146544. <http://doi.org/10.1371/journal.pone.0146544>
- Kurup, S., & Bhonde, R. R. (2002). Analysis and Optimization of Nutritional Set-up for Murine Pancreatic Acinar Cells. *Journal of the Pancreas*, 3(1), 8–15.
- Kusaka, M., Katoh-Fukui, Y., Ogawa, H., Miyabayashi, K., Baba, T., Shima, Y., et al. (2010). Abnormal Epithelial Cell Polarity and Ectopic Epidermal Growth Factor Receptor (EGFR) Expression Induced in Emx2 KO Embryonic Gonads. *Endocrinology*, 151(12), 5893–5904. <http://doi.org/10.1210/en.2010-0915>
- Kwapiszewska, G., Wygrecka, M., Marsh, L. M., Schmitt, S., Trosser, R., Wilhelm, J., et al. (2008). Fhl-1, a New Key Protein in Pulmonary Hypertension. *Circulation*, 118(11), 1183–1194. <http://doi.org/10.1161/CIRCULATIONAHA.107.761916>
- Lammert, E., Cleaver, O., & Melton, D. (2001). Induction of pancreatic differentiation by signals from blood vessels. *Science*, 294(5542), 564–567. <http://doi.org/10.1126/science.1064344>
- Lampel, M., & Kern, H. F. (1977). Acute interstitial pancreatitis in the rat induced by excessive doses of a pancreatic secretagogue. *Virchows Archiv. a, Pathological Anatomy and Histology*, 373(2), 97–117.

- Landsman, L., Nijagal, A., Whitchurch, T. J., VanderLaan, R. L., Zimmer, W. E., MacKenzie, T. C., & Hebrok, M. (2011). Pancreatic Mesenchyme Regulates Epithelial Organogenesis throughout Development. *PLOS Biology*, *9*(9), e1001143. <http://doi.org/10.1371/journal.pbio.1001143>
- Lankisch, P. G., Apte, M., & Banks, P. A. (2015). Acute pancreatitis. *The Lancet*, *386*(9988), 85–96. [http://doi.org/10.1016/S0140-6736\(14\)60649-8](http://doi.org/10.1016/S0140-6736(14)60649-8)
- Lardon, J., Rooman, I., & Bouwens, L. (2002). Nestin expression in pancreatic stellate cells and angiogenic endothelial cells. *Histochemistry and Cell Biology*, *117*(6), 535–540. <http://doi.org/10.1007/s00418-002-0412-4>
- LaRocca, P. J., & Rheinwald, J. G. (1984). Coexpression of simple epithelial keratins and vimentin by human mesothelium and mesothelioma in vivo and in culture. *Cancer Research*, *44*(7), 2991–2999.
- Larsen, B. M., Hrycaj, S. M., Newman, M., Li, Y., & Wellik, D. M. (2015). Mesenchymal Hox6 function is required for mouse pancreatic endocrine cell differentiation. *Development (Cambridge, England)*, *142*(22), 3859–3868. <http://doi.org/10.1242/dev.126888>
- Lavine, K. J. (2006). Fibroblast growth factor signals regulate a wave of Hedgehog activation that is essential for coronary vascular development. *Genes & Development*, *20*(12), 1651–1666.
- Lavine, K. J., & Ornitz, D. M. (2008). Fibroblast growth factors and Hedgehogs: at the heart of the epicardial signaling center. *Trends in Genetics*, *24*(1), 33–40. <http://doi.org/10.1016/j.tig.2007.10.007>
- Lavine, K. J., Yu, K., White, A. C., Zhang, X., Smith, C., Partanen, J., & Ornitz, D. M. (2005). Endocardial and Epicardial Derived FGF Signals Regulate Myocardial Proliferation and Differentiation In Vivo. *Developmental Cell*, *8*(1), 85–95. <http://doi.org/10.1016/j.devcel.2004.12.002>
- Lee, B., Zhao, Q., & Habtezion, A. (2017). Immunology of pancreatitis and environmental factors. *Current Opinion in Gastroenterology*, *33*(5), 383–389. <http://doi.org/10.1097/MOG.0000000000000387>
- Lemaire, K., Thorrez, L., & Schuit, F. (2016). Disallowed and Allowed Gene Expression: Two Faces of Mature Islet Beta Cells. *Annual Review of Nutrition*, *36*(1), 45–71. <http://doi.org/10.1146/annurev-nutr-071715-050808>
- Lemaire, R., Korn, J. H., Shipley, J. M., & Lafyatis, R. (2005). Increased expression of type I collagen induced by microfibril-associated glycoprotein 2: Novel mechanistic insights into the molecular basis of dermal fibrosis in scleroderma. *Arthritis & Rheumatism*, *52*(6), 1812–1823. <http://doi.org/10.1002/art.21059>
- Lerch, M. M., & Gorelick, F. S. (2013). Models of Acute and Chronic Pancreatitis. *Gastroenterology*, *144*(6), 1180–1193. <http://doi.org/10.1053/j.gastro.2012.12.043>
- Li, Peng, Cavallero, S., Gu, Y., Chen, T. H. P., Hughes, J., Hassan, A. B., et al. (2011). IGF signaling directs ventricular cardiomyocyte proliferation during embryonic heart development. *Development (Cambridge, England)*, *138*(9), 1795–1805. <http://doi.org/10.1242/dev.054338>
- Li, Yuchang, Lua, I., French, S. W., & Asahina, K. (2016). Role of TGF- β signaling in differentiation of mesothelial cells to vitamin A-poor hepatic stellate cells in liver fibrosis. *American Journal of Physiology - Gastrointestinal and Liver Physiology*, *310*(4), G262–G272. <http://doi.org/10.1152/ajpgi.00257.2015>

- Li, Yuchang, Wang, J., & Asahina, K. (2013). Mesothelial cells give rise to hepatic stellate cells and myofibroblasts via mesothelial–mesenchymal transition in liver injury. *Proceedings of the National Academy of Sciences of the United States of America*, *110*(6), 2324–2329. <http://doi.org/10.1073/pnas.1214136110>
- Li, Zhixing, Manna, P., Kobayashi, H., Spilde, T., Bhatia, A., Preuett, B., et al. (2004). Multifaceted pancreatic mesenchymal control of epithelial lineage selection. *Developmental Biology*, *269*(1), 252–263.
- Lindahl, P., Karlsson, L., Hellström, M., Gebre-Medhin, S., Willetts, K., Heath, J. K., & Betsholtz, C. (1997). Alveogenesis failure in PDGF-A-deficient mice is coupled to lack of distal spreading of alveolar smooth muscle cell progenitors during lung development. *Development*, *124*, 3943–3953.
- Lu, J., Chatterjee, M., Schmid, H., Beck, S., & Gawaz, M. (2016). CXCL14 as an emerging immune and inflammatory modulator. *Journal of Inflammation*, *13*(1), 1. <http://doi.org/10.1186/s12950-015-0109-9>
- Luttenberger, T., Schmid-Kotsas, A., Menke, A., Siech, M., Beger, H., Adler, G., et al. (2000). Platelet-derived growth factors stimulate proliferation and extracellular matrix synthesis of pancreatic stellate cells: implications in pathogenesis of pancreas fibrosis. *Laboratory Investigation*, *80*(1), 47–55.
- Maaten, L. V. D., & Hinton, G. (2008). Visualizing Data using t-SNE. *Journal of Machine Learning Research*, *9*(Nov), 2579–2605.
- Macosko, E. Z., Basu, A., Satija, R., Nemes, J., Shekhar, K., Goldman, M., et al. (2015). Highly Parallel Genome-wide Expression Profiling of Individual Cells Using Nanoliter Droplets. *Cell*, *161*(5), 1202–1214. <http://doi.org/10.1016/j.cell.2015.05.002>
- Majesky, M. W., Dong, X. R., Regan, J. N., Hognlund, V. J., & Schneider, M. (2011). Vascular Smooth Muscle Progenitor Cells. *Circulation Research*, *108*(3), 365–377. <http://doi.org/10.1161/CIRCRESAHA.110.223800>
- Majumder, S., & Chari, S. T. (2016). Chronic pancreatitis. *The Lancet*, *387*(10031), 1957–1966. [http://doi.org/10.1016/S0140-6736\(16\)00097-0](http://doi.org/10.1016/S0140-6736(16)00097-0)
- Mandalia, A., Wamsteker, E.-J., & DiMagno, M. (2018). Recent advances in understanding and managing acute pancreatitis. *F1000Research*, *7*, 959. <http://doi.org/10.12688/f1000research.14244.1>
- Manohar, M., Verma, A. K., Venkateshaiah, S. U., Sanders, N. L., & Mishra, A. (2017). Pathogenic mechanisms of pancreatitis. *World Journal of Gastrointestinal Pharmacology and Therapeutics*, *8*(1), 10–25. <http://doi.org/10.4292/wjgpt.v8.i1.10>
- Martín, M., Gallego-Llamas, J., Ribes, V., Keding, M., Niederreither, K., Chambon, P., et al. (2005). Dorsal pancreas agenesis in retinoic acid-deficient Raldh2 mutant mice. *Developmental Biology*, *284*(2), 399–411. <http://doi.org/10.1016/j.ydbio.2005.05.035>
- Matsushima, K., Suyama, T., Takenaka, C., Nishishita, N., Ikeda, K., Ikada, Y., et al. (2010). Secreted Frizzled Related Protein 4 Reduces Fibrosis Scar Size and Ameliorates Cardiac Function After Ischemic Injury. *Tissue Engineering Part A*, *16*(11), 3329–3341. <http://doi.org/10.1089/ten.tea.2009.0739>
- McCarroll, J. A., Phillips, P. A., Kumar, R. K., Park, S., Pirola, R. C., Wilson, J. S., & Apte, M. V. (2004). Pancreatic stellate cell migration: role of the phosphatidylinositol 3-kinase (PI3-kinase) pathway. *Biochemical Pharmacology*, *67*(6), 1215–1225. <http://doi.org/10.1016/j.bcp.2003.11.013>

- McCulley, D., Wienhold, M., & Sun, X. (2015). The Pulmonary Mesenchyme Directs Lung Development. *Current Opinion in Genetics & Development*, 32, 98–105. <http://doi.org/10.1016/j.gde.2015.01.011>
- McDavid, A., Finak, G., Chattopadhyay, P. K., Dominguez, M., Lamoreaux, L., Ma, S. S., et al. (2012). Data exploration, quality control and testing in single-cell qPCR-based gene expression experiments. *Bioinformatics*, 29(4), 461–467. <http://doi.org/10.1093/bioinformatics/bts714>
- McGinnis, C. S., Patterson, D. M., Winkler, J., Hein, M. Y., Srivastava, V., Conrad, D. N., et al. (2018). MULTI-seq: Scalable sample multiplexing for single-cell RNA sequencing using lipid-tagged indices. *bioRxiv*, 387241. <http://doi.org/10.1101/387241>
- Means, A. L., Xu, Y., Zhao, A., Ray, K. C., & Gu, G. (2008). A CK19 CreERTknockin mouse line allows for conditional DNA recombination in epithelial cells in multiple endodermal organs. *Genesis*, 46(6), 318–323. <http://doi.org/10.1002/dvg.20397>
- Mews, P., Phillips, P., Fahmy, R., Korsten, M., Pirola, R., Wilson, J., & Apte, M. (2002). Pancreatic stellate cells respond to inflammatory cytokines: potential role in chronic pancreatitis. *Gut*, 50(4), 535–541. <http://doi.org/10.1136/gut.50.4.535>
- Michailova, K. N. (2004). Mesothelial lamellar bodies in norm and experimental conditions. Transmission and scanning electron microscopic observations on the peritoneum, pleura and pericardium. *Anatomy and Embryology*, 208(4), 301–309. <http://doi.org/10.1007/s00429-004-0390-5>
- Michailova, K. N., & Usunoff, K. G. (2006). Serosal Membranes (Pleura, Pericardium, Peritoneum). Normal Structure, Development and Experimental Pathology (Vol. 183, pp. 1–151).
- Miralles, F., Czernichow, P., & Scharfmann, R. (1998). Follistatin regulates the relative proportions of endocrine versus exocrine tissue during pancreatic development. *Development (Cambridge, England)*, 125(6), 1017–1024.
- Miyamoto, Y., Maitra, A., Ghosh, B., Zechner, U., Argani, P., Iacobuzio-Donahue, C. A., et al. (2003). Notch mediates TGF alpha-induced changes in epithelial differentiation during pancreatic tumorigenesis. *Cancer Cell*, 3(6), 565–576.
- Miyatsuka, T., Kosaka, Y., Kim, H., & German, M. S. (2011). Neurogenin3 inhibits proliferation in endocrine progenitors by inducing Cdkn1a. *Proceedings of the National Academy of Sciences*, 108(1), 185–190. <http://doi.org/10.1073/pnas.1004842108>
- Miyatsuka, T., Li, Z., & German, M. S. (2009). Chronology of Islet Differentiation Revealed By Temporal Cell Labeling. *Diabetes*, 58(8), 1863–1868. <http://doi.org/10.2337/db09-0390>
- Mizunuma, T., Kawamura, S., & Kishino, Y. (1984). Effects of Injecting Excess Arginine on Rat Pancreas. *The Journal of Nutrition*, 114(3), 467–471. <http://doi.org/10.1093/jn/114.3.467>
- Molotkov, A., Molotkova, N., & Duester, G. (2005). Retinoic acid generated by Raldh2 in mesoderm is required for mouse dorsal endodermal pancreas development. *Developmental Dynamics*, 232(4), 950–957. <http://doi.org/10.1002/dvdy.20256>
- Morris, J. P., IV, Cano, D. A., Sekine, S., Wang, S. C., & Hebrok, M. (2010). b-catenin blocks Kras-dependent reprogramming of acini into pancreatic cancer precursor lesions in mice. *The Journal of Clinical Investigation*, 120(2), 508–520. <http://doi.org/10.1172/JCI40045>
- Moulson, C. L., Li, C., & Miner, J. H. (2001). Localization of Lutheran, a novel laminin receptor, in normal, knockout, and transgenic mice suggests an interaction with laminin $\alpha 5$ in vivo. *Developmental Dynamics*, 222(1), 101–114. <http://doi.org/10.1002/dvdy.1169>

- Muraro, M. J., Dharmadhikari, G., Grün, D., Groen, N., Dielen, T., Jansen, E., et al. (2016). A Single-Cell Transcriptome Atlas of the Human Pancreas. *Cell Systems*, 3(4), 385–394.e3. <http://doi.org/10.1016/j.cels.2016.09.002>
- Murtaugh, L. C. (2008). The what, where, when and how of Wnt/ β -catenin signaling in pancreas development. *Organogenesis*, 4(2), 81–86.
- Murtaugh, L. C., & Keefe, M. D. (2015). Regeneration and Repair of the Exocrine Pancreas. *Dx.Doi.org.Ucsf.Idm.Oclc.org*, 77(1), 229–249. <http://doi.org/10.1146/annurev-physiol-021014-071727>
- Mutsaers, S. E., & Wilkosz, S. (2007). Structure and Function of Mesothelial Cells, (134), 1–19.
- Mutsaers, S. E., Birnie, K., Lansley, S., Herrick, S. E., Lim, C.-B., & Prêle, C. M. (2015). Mesothelial cells in tissue repair and fibrosis. *Frontiers in Pharmacology*, 6(Suppl. 3), 279730. <http://doi.org/10.3389/fphar.2015.00113>
- Muzumdar, M. D., Tasic, B., Miyamichi, K., Li, L., & Luo, L. (2007). A global double-fluorescent Cre reporter mouse. *Genesis*, 45(9), 593–605. <http://doi.org/10.1002/dvg.20335>
- Nair, G., & Hebrok, M. (2015). Islet formation in mice and men: lessons for the generation of functional insulin-producing β -cells from human pluripotent stem cells. *Current Opinion in Genetics & Development*, 32, 171–180. <http://doi.org/10.1016/j.gde.2015.03.004>
- Neuschwander-Tetri, B., Burton, F., Presti, M., Bitton, R., Janney, C., Garvin, P., et al. (2000). Repetitive Self-Limited Acute Pancreatitis Induces Pancreatic Fibrogenesis in the Mouse, 1–10.
- Niederrau, C., Ferrell, L. D., & Grendell, J. H. (1985). Caerulein-induced acute necrotizing pancreatitis in mice: protective effects of proglumide, benzotript, and secretin. *Gastroenterology*, 88(5), 1192–1204.
- Ohlsson, H., Karlsson, K., & Edlund, T. (1993). IPF1, a homeodomain-containing transactivator of the insulin gene. *The EMBO Journal*, 12(11), 4251–4259.
- Ohmuraya, M., Hirota, M., Araki, K., Baba, H., & Yamamura, K.-I. (2006). Enhanced Trypsin Activity in Pancreatic Acinar Cells Deficient for Serine Protease Inhibitor Kazal Type 3. *Pancreas*, 33(1), 104–106. <http://doi.org/10.1097/01.mpa.0000226889.86322.9b>
- Ohmuraya, M., Hirota, M., Araki, M., Mizushima, N., Matsui, M., Mizumoto, T., et al. (2005). Autophagic Cell Death of Pancreatic Acinar Cells in Serine Protease Inhibitor Kazal Type 3—Deficient Mice. *Gastroenterology*, 129(2), 696–705. <http://doi.org/10.1016/j.gastro.2005.05.057>
- Ohta, Y., Kosaka, Y., Kishimoto, N., Wang, J., Smith, S. B., Honig, G., et al. (2011). Convergence of the Insulin and Serotonin Programs in the Pancreatic β -Cell. *Diabetes*, 60(12), 3208–3216. <http://doi.org/10.2337/db10-1192>
- Ohuchi, H., Hori, Y., Yamasaki, M., Harada, H., Sekine, K., Kato, S., & Itoh, N. (2000). FGF10 Acts as a Major Ligand for FGF Receptor 2 IIIb in Mouse Multi-Organ Development. *Biochemical and Biophysical Research Communications*, 277(3), 643–649. <http://doi.org/10.1006/bbrc.2000.3721>
- Olivey, H. E., & Svensson, E. C. (2010). Epicardial–Myocardial Signaling Directing Coronary Vasculogenesis. *Circulation Research*, 106(5), 818–832. <http://doi.org/10.1161/CIRCRESAHA.109.209197>
- Omary, M. B., Lugea, A., Lowe, A. W., & Pandol, S. J. (2007). The pancreatic stellate cell: a star on the rise in pancreatic diseases. *Journal of Clinical Investigation*, 117(1), 50–59. <http://doi.org/10.1172/JCI30082>

- Ornitz, D. M., & Itoh, N. (2015). The Fibroblast Growth Factor signaling pathway. *Wiley Interdisciplinary Reviews: Developmental Biology*, 4(3), 215–266. <http://doi.org/10.1002/wdev.176>
- Pagliuca, F. W., & Melton, D. A. (2013). How to make a functional β -cell. *Development (Cambridge, England)*, 140(12), 2472–2483. <http://doi.org/10.1242/dev.093187>
- Pagliuca, F. W., Millman, J. R., Gürtler, M., Segel, M., Van Dervort, A., Ryu, J. H., et al. (2014). Generation of Functional Human Pancreatic β Cells In Vitro. *Cell*, 159(2), 428–439. <http://doi.org/10.1016/j.cell.2014.09.040>
- Pan, F. C., & Wright, C. (2011). Pancreas organogenesis: From bud to plexus to gland. *Developmental Dynamics*, 240(3), 530–565. <http://doi.org/10.1002/dvdy.22584>
- Parton, R. G., & Simons, K. (2007). The multiple faces of caveolae. *Nature Reviews Molecular Cell Biology*, 8(3), 185–194. <http://doi.org/10.1038/nrm2122>
- Peery, A. F., Dellon, E. S., Lund, J., Crockett, S. D., McGowan, C. E., Bulsiewicz, W. J., et al. (2012). Burden of Gastrointestinal Disease in the United States: 2012 Update. *Gastroenterology*, 143(5), 1179–1187.e3. <http://doi.org/10.1053/j.gastro.2012.08.002>
- Peng, T., Tian, Y., Boogerd, C. J., Lu, M. M., Kadzik, R. S., Stewart, K. M., et al. (2013). Coordination of heart and lung co-development by a multipotent cardiopulmonary progenitor. *Nature*, 500(7464), 589–592. <http://doi.org/10.1038/nature12358>
- Perez-Pomares, J.-M., Carmona, R., Gonzalez-Iriarte, M., Atencia, G., Wessels, A., & Munoz-Chapuli, R. (2002). Origin of coronary endothelial cells from epicardial mesothelium in avian embryos. *International Journal of Developmental Biology*, 46(8), 1005–1013. <http://doi.org/10.1387/ijdb.12533024>
- Petri, A., Ahnfelt-Ronne, J., Frederiksen, K. S., Edwards, D. G., Madsen, D., Serup, P., et al. (2006). The effect of neurogenin3 deficiency on pancreatic gene expression in embryonic mice. *Journal of Molecular Endocrinology*, 37(2), 301–316. <http://doi.org/10.1677/jme.1.02096>
- Pérez Pomares, J. M., Carmona, R., González Iriarte, M., Macías, D., Guadix, J. A., & Muñoz Chápuli, R. (2004). Contribution of mesothelium-derived cells to liver sinusoids in avian embryos. *Developmental Dynamics*, 229(3), 465–474. <http://doi.org/10.1002/dvdy.10455>
- Pham, A., & Forsmark, C. (2018). Chronic pancreatitis: review and update of etiology, risk factors, and management. *F1000Research*, 7, 607. <http://doi.org/10.12688/f1000research.12852.1>
- Phillips, P. A., McCarroll, J. A., Park, S., Wu, M.-J., Pirola, R., Korsten, M., et al. (2003). Rat pancreatic stellate cells secrete matrix metalloproteinases: implications for extracellular matrix turnover. *Gut*, 52(2), 275–282. <http://doi.org/10.1136/gut.52.2.275>
- Phillips, P. A., Yang, L., Shulkes, A., Vonlaufen, A., Poljak, A., Bustamante, S., et al. (2010). Pancreatic stellate cells produce acetylcholine and may play a role in pancreatic exocrine secretion. *Proceedings of the National Academy of Sciences*, 107(40), 17397–17402. <http://doi.org/10.1073/pnas.1000359107>
- Piccand, J., Meunier, A., Merle, C., Jia, Z., Barnier, J.-V., & Gradwohl, G. (2014). Pak3 Promotes Cell Cycle Exit and Differentiation of β -Cells in the Embryonic Pancreas and Is Necessary to Maintain Glucose Homeostasis in Adult Mice. *Diabetes*, 63(1), 203–215. <http://doi.org/10.2337/db13-0384>
- Pictet, R. L., Clark, W. R., Williams, R. H., & Rutter, W. J. (1972). An ultrastructural analysis of the developing embryonic pancreas. *Developmental Biology*, 29(4), 436–467. [http://doi.org/10.1016/0012-1606\(72\)90083-8](http://doi.org/10.1016/0012-1606(72)90083-8)

- Pilecki, B., Holm, A. T., Schlosser, A., Moeller, J. B., Wohl, A. P., Zuk, A. V., et al. (2016). Characterization of Microfibrillar-associated Protein 4 (MFAP4) as a Tropoelastin- and Fibrillin-binding Protein Involved in Elastic Fiber Formation. *Journal of Biological Chemistry*, 291(3), 1103–1114. <http://doi.org/10.1074/jbc.M115.681775>
- Piper, K., Brickwood, S., Turnpenny, L. W., Cameron, I. T., Ball, S. G., Wilson, D. I., & Hanley, N. A. (2004). Beta cell differentiation during early human pancreas development. *The Journal of Endocrinology*, 181(1), 11–23.
- Posselt, A. M., Szot, G. L., Frassetto, L. A., Masharani, U., Tavakol, M., Amin, R., et al. (2010). Islet Transplantation in Type 1 Diabetic Patients Using Calcineurin Inhibitor-Free Immunosuppressive Protocols Based on T-Cell Adhesion or Costimulation Blockade. *Transplantation*, 90(12), 1595–1601. <http://doi.org/10.1097/TP.0b013e3181fe1377>
- Potter, S. S. (2018). Single-cell RNA sequencing for the study of development, physiology and disease. *Nature Reviews Nephrology*, 14(8), 479–492. <http://doi.org/10.1038/s41581-018-0021-7>
- Prado, C. L., Pugh-Bernard, A. E., Elghazi, L., Sosa-Pineda, B., & Sussel, L. (2004). Ghrelin cells replace insulin-producing beta cells in two mouse models of pancreas development. *Proceedings of the National Academy of Sciences*, 101(9), 2924–2929. <http://doi.org/10.1073/pnas.0308604100>
- Proshchina, A. E., Krivova, Y. S., Barabanov, V. M., & Saveliev, S. V. (2014). Ontogeny of Neuro-Insular Complexes and Islets Innervation in the Human Pancreas. *Frontiers in Endocrinology*, 5(9), 143. <http://doi.org/10.3389/fendo.2014.00057>
- Qiu, W.-L., Zhang, Y.-W., Feng, Y., Li, L.-C., Yang, L., & Xu, C.-R. (2017a). Deciphering Pancreatic Islet β Cell and α Cell Maturation Pathways and Characteristic Features at the Single-Cell Level. *Cell Metabolism*, 25(5), 1194–1205.e4. <http://doi.org/10.1016/j.cmet.2017.04.003>
- Qiu, X., Mao, Q., Tang, Y., Wang, L., Chawla, R., Pliner, H. A., & Trapnell, C. (2017b). Reversed graph embedding resolves complex single-cell trajectories. *Nature Methods*, 14(10), 979–982. <http://doi.org/10.1038/nmeth.4402>
- Que, J., Wilm, B., Hasegawa, H., Wang, F., Bader, D., & Hogan, B. L. M. (2008). Mesothelium contributes to vascular smooth muscle and mesenchyme during lung development. *Proceedings of the National Academy of Sciences of the United States of America*, 105(43), 16626–16630. <http://doi.org/10.1073/pnas.0808649105>
- R core team. (2016). R: A language and environment for statistical computing. *R Foundation for Statistical Computing*. Retrieved from <http://www.R-project.org/>
- Reese, D. E., Zavaljevski, M., Streiff, N. L., & Bader, D. (1999). bves: A Novel Gene Expressed during Coronary Blood Vessel Development. *Developmental Biology*, 209(1), 159–171. <http://doi.org/10.1006/dbio.1999.9246>
- Reinert, R. B., Cai, Q., Hong, J. Y., Plank, J. L., Aamodt, K., Prasad, N., et al. (2014). Vascular endothelial growth factor coordinates islet innervation via vascular scaffolding. *Development (Cambridge, England)*, 141(7), 1480–1491. <http://doi.org/10.1242/dev.098657>
- Rezania, A., Bruin, J. E., Arora, P., Rubin, A., Batushansky, I., Asadi, A., et al. (2014). Reversal of diabetes with insulin-producing cells derived *in vitro* from human pluripotent stem cells. *Nature Biotechnology*, 32(11), 1121–1133. <http://doi.org/10.1038/nbt.3033>
- Rhim, A. D., & Stanger, B. Z. (2010). Molecular Biology of Pancreatic Ductal Adenocarcinoma Progression: Aberrant Activation of Developmental Pathways. *Progress in Molecular*

- Biology and Translational Science*, 97, 41–78. <http://doi.org/10.1016/B978-0-12-385233-5.00002-7>
- Rinkevich, Y., Mori, T., Sahoo, D., Xu, P.-X., Bermingham, J. R., & Weissman, I. L. (2012). Identification and prospective isolation of a mesothelial precursor lineage giving rise to smooth muscle cells and fibroblasts for mammalian internal organs, and their vasculature. *Nature Cell Biology*, 14(12), 1251–1260. <http://doi.org/10.1038/ncb2610>
- Roost, M. S., van Iperen, L., de Melo Bernardo, A., Mummery, C. L., Carlotti, F., de Koning, E. J., & Chuva de Sousa Lopes, S. M. (2014). Lymphangiogenesis and angiogenesis during human fetal pancreas development. *Vascular Cell*, 6(1), 22. <http://doi.org/10.1186/2045-824X-6-22>
- Roskams, T., Cassiman, D., De Vos, R., & Libbrecht, L. (2004). Neuroregulation of the Neuroendocrine Compartment of the Liver. *The Anatomical Record*, 280A(1), 910–923. <http://doi.org/10.1002/ar.a.20096>
- Roxburgh, S. A., Murphy, M., Pollock, C. A., & Brazil, D. P. (2006). Recapitulation of Embryological Programmes in Renal Fibrosis – The Importance of Epithelial Cell Plasticity and Developmental Genes. *Nephron Physiology*, 103(3), p139–p148. <http://doi.org/10.1159/000092453>
- Rudat, C., & Kispert, A. (2012). Wt1 and Epicardial Fate Mapping. *Circulation Research*. <http://doi.org/10.1161/CIRCRESAHA.112.273946;wgroup:string:AHA>
- Rudat, C., Grieskamp, T., Röhr, C., Airik, R., Wrede, C., Hegermann, J., et al. (2014). Upk3b Is Dispensable for Development and Integrity of Urothelium and Mesothelium. *PLoS ONE*, 9(11), e112112. <http://doi.org/10.1371/journal.pone.0112112>
- Russ, H. A., Landsman, L., Moss, C. L., Higdon, R., Greer, R. L., Kaihara, K., et al. (2016). Dynamic Proteomic Analysis of Pancreatic Mesenchyme Reveals Novel Factors That Enhance Human Embryonic Stem Cell to Pancreatic Cell Differentiation. *Stem Cells International*, 2016(1), 1–9. <http://doi.org/10.1155/2016/6183562>
- Russ, H. A., Parent, A. V., Ringler, J. J., Hennings, T. G., Nair, G. G., Shveygert, M., et al. (2015). Controlled induction of human pancreatic progenitors produces functional beta-like cells *in vitro*. *The EMBO Journal*, 34(13), 1759–1772. <http://doi.org/10.15252/embj.201591058>
- Saga, Y., Miyagawa-Tomita, S., Takagi, A., Kitajima, S., Miyazaki, J. I., & Inoue, T. (1999). MesP1 is expressed in the heart precursor cells and required for the formation of a single heart tube. *Development (Cambridge, England)*, 126(15), 3437–3447.
- Salisbury, R. J., Blaylock, J., Berry, A. A., Jennings, R. E., De Krijger, R., Piper Hanley, K., & Hanley, N. A. (2014). The window period of NEUROGENIN3 during human gestation. *Islets*, 6(3), e954436. <http://doi.org/10.4161/19382014.2014.954436>
- Saluja, A. K., & Bhagat, L. (2003). Pathophysiology of Alcohol-Induced Pancreatic Injury. *Pancreas*, 27(4), 327–331.
- Sander, M., Sussel, L., Connors, J., Scheel, D., Kalamaras, J., Cruz, Dela, F., et al. (2000). Homeobox gene Nkx6.1 lies downstream of Nkx2.2 in the major pathway of beta-cell formation in the pancreas. *Development (Cambridge, England)*, 127(24), 5533–5540. <http://doi.org/10.1101/gad.12.12.1763>
- Satija, R., Farrell, J. A., Gennert, D., Schier, A. F., & Regev, A. (2015). Spatial reconstruction of single-cell gene expression data. *Nature Biotechnology*, 33(5), 495–502. <http://doi.org/10.1038/nbt.3192>

- Satoh, K., Shimosegawa, T., Hirota, M., Koizumi, M., & Toyota, T. (1998). Expression of transforming growth factor beta1 (TGFbeta1) and its receptors in pancreatic duct cell carcinoma and in chronic pancreatitis. *Pancreas*, *16*(4), 468–474.
- Schaffer, A. E., Freude, K. K., Nelson, S. B., & Sander, M. (2010). Nkx6 Transcription Factors and Ptf1a Function as Antagonistic Lineage Determinants in Multipotent Pancreatic Progenitors. *Developmental Cell*, *18*(6), 1022–1029. <http://doi.org/10.1016/j.devcel.2010.05.015>
- Schneider, E., Schmid-Kotsas, A., Zhao, J., Weidenbach, H., Schmid, R. M., Menke, A., et al. (2001). Identification of mediators stimulating proliferation and matrix synthesis of rat pancreatic stellate cells. *American Journal of Physiology-Cell Physiology*, *281*(2), C532–C543. <http://doi.org/10.1152/ajpcell.2001.281.2.C532>
- Schonhoff, S. E., Giel-Moloney, M., & Leiter, A. B. (2004). Neurogenin 3-expressing progenitor cells in the gastrointestinal tract differentiate into both endocrine and non-endocrine cell types. *Developmental Biology*, *270*(2), 443–454.
- Scott Heller, R., Stoffers, D. A., Liu, A., Schedl, A., Crenshaw, E. B., III, Madsen, O. D., & Serup, P. (2004). The role of Brn4/Pou3f4 and Pax6 in forming the pancreatic glucagon cell identity. *Developmental Biology*, *268*(1), 123–134. <http://doi.org/10.1016/j.ydbio.2003.12.008>
- Scott, M. M., Wylie, C. J., Lerch, J. K., Murphy, R., Lobur, K., Herlitze, S., et al. (2005). A genetic approach to access serotonin neurons for in vivo and in vitro studies. *Proceedings of the National Academy of Sciences*, *102*(45), 16472–16477. <http://doi.org/10.1073/pnas.0504510102>
- Selig, L., Sack, U., Gaiser, S., Klöppel, G., Savkovic, V., Mössner, J., et al. (2006). Characterisation of a transgenic mouse expressing R122H human cationic trypsinogen. *BMC Gastroenterology*, *6*(1), 30. <http://doi.org/10.1186/1471-230X-6-30>
- Sendler, M., Beyer, G., Mahajan, U. M., Kauschke, V., Maertin, S., Schurmann, C., et al. (2015). Complement Component 5 Mediates Development of Fibrosis, via Activation of Stellate Cells, in 2 Mouse Models of Chronic Pancreatitis. *Gastroenterology*, *149*(3), 765–776.e10. <http://doi.org/10.1053/j.gastro.2015.05.012>
- Seymour, P. A., Freude, K. K., Dubois, C. L., Shih, H. P., Patel, N. A., & Sander, M. (2008). A dosage-dependent requirement for Sox9 in pancreatic endocrine cell formation. *Developmental Biology*, *323*(1), 19–30. <http://doi.org/10.1016/j.ydbio.2008.07.034>
- Shang, Y., Yoshida, T., Amendt, B. A., Martin, J. F., & Owens, G. K. (2008). Pitx2 is functionally important in the early stages of vascular smooth muscle cell differentiation. *The Journal of Cell Biology*, *181*(3), 461–473. <http://doi.org/10.1083/jcb.200711145>
- Shannon, J. M., Nielsen, L. D., Gebb, S. A., & Randell, S. H. (1998). Mesenchyme specifies epithelial differentiation in reciprocal recombinants of embryonic lung and trachea. *Developmental Dynamics*, *212*(4), 482–494. [http://doi.org/10.1002/\(SICI\)1097-0177\(199808\)212:4<482::AID-AJA2>3.0.CO;2-D](http://doi.org/10.1002/(SICI)1097-0177(199808)212:4<482::AID-AJA2>3.0.CO;2-D)
- Shapiro, A. M. J., Lakey, J. R. T., Ryan, E. A., Korbitt, G. S., Toth, E., Warnock, G. L., et al. (2000). Islet Transplantation in Seven Patients with Type 1 Diabetes Mellitus Using a Glucocorticoid-Free Immunosuppressive Regimen. *New England Journal of Medicine*, *343*(4), 230–238.
- Shapiro, A. M. J., Pokrywczynska, M., & Ricordi, C. (2016). Clinical pancreatic islet transplantation. *Nature Reviews Endocrinology*, *13*(5), 268–277. <http://doi.org/10.1038/nrendo.2016.178>

- Shek, F. W.-T., Benyon, R. C., Walker, F. M., McCrudden, P. R., Pender, S. L. F., Williams, E. J., et al. (2002). Expression of Transforming Growth Factor- β 1 by Pancreatic Stellate Cells and Its Implications for Matrix Secretion and Turnover in Chronic Pancreatitis. *The American Journal of Pathology*, *160*(5), 1787–1798. [http://doi.org/10.1016/S0002-9440\(10\)61125-X](http://doi.org/10.1016/S0002-9440(10)61125-X)
- Shiba, Y., Fernandes, S., Zhu, W.-Z., Filice, D., Muskheli, V., Kim, J., et al. (2012). Human ES-cell-derived cardiomyocytes electrically couple and suppress arrhythmias in injured hearts. *Nature*, *489*(7415), 322–325.
- Shih, H. P., Kopp, J. L., Sandhu, M., Dubois, C. L., Seymour, P. A., Grapin-Botton, A., & Sander, M. (2012). A Notch-dependent molecular circuitry initiates pancreatic endocrine and ductal cell differentiation. *Development (Cambridge, England)*, *139*(14), 2488–2499. <http://doi.org/10.1242/dev.078634>
- Shih, H. P., Wang, A., & Sander, M. (2013). Pancreas Organogenesis: From Lineage Determination to Morphogenesis. *Annual Review of Cell and Developmental Biology*, *29*(1), 81–105. <http://doi.org/10.1146/annurev-cellbio-101512-122405>
- Shworak, N. W. (2004). Angiogenic modulators in valve development and disease: does valvular disease recapitulate developmental signaling pathways? *Current Opinion in Cardiology*, *19*(2), 140–146.
- Singh, S., Bhardwaj, U., Verma, S. K., Bhalla, A., & Gill, K. (2016). Hyperamylasemia and acute pancreatitis following anticholinesterase poisoning. *Human & Experimental Toxicology*, *26*(6), 467–471. <http://doi.org/10.1177/0960327107076814>
- Siveke, J. T., Lubeseder Martellato, C., Lee, M., Mazur, P. K., Nakhai, H., Radtke, F., & Schmid, R. M. (2008). Notch Signaling Is Required for Exocrine Regeneration After Acute Pancreatitis. *Gastroenterology*, *134*(2), 544–555.e3. <http://doi.org/10.1053/j.gastro.2007.11.003>
- Slack, J. M. (1995). Developmental biology of the pancreas. *Development (Cambridge, England)*, *121*(6), 1569–1580.
- Sleightholm, R. L., Neilsen, B. K., Li, J., Steele, M. M., Singh, R. K., Hollingsworth, M. A., & Oupicky, D. (2017). Emerging roles of the CXCL12/CXCR4 axis in pancreatic cancer progression and therapy. *Pharmacology & Therapeutics*, *179*, 158–170. <http://doi.org/10.1016/j.pharmthera.2017.05.012>
- Smith, J. P., & Solomon, T. E. (2014). Cholecystokinin and pancreatic cancer: the chicken or the egg? *American Journal of Physiology - Gastrointestinal and Liver Physiology*, *306*(2), G91–G101. <http://doi.org/10.1152/ajpgi.00301.2013>
- Sneddon, J. B., Borowiak, M., & Melton, D. A. (2012). Self-renewal of embryonic-stem-cell-derived progenitors by organ-matched mesenchyme. *Nature Publishing Group*, *491*(7426), 765–768. <http://doi.org/10.1038/nature11463>
- Sneddon, J. B., Tang, Q., Stock, P., Bluestone, J. A., Roy, S., Desai, T., & Hebrok, M. (2018). Stem Cell Therapies for Treating Diabetes: Progress and Remaining Challenges. *Cell Stem Cell*, *22*(6), 810–823. <http://doi.org/10.1016/j.stem.2018.05.016>
- Solar, M., Cardalda, C., Houbracken, I., Martín, M., Maestro, M. A., De Medts, N., et al. (2009). Pancreatic Exocrine Duct Cells Give Rise to Insulin-Producing β Cells during Embryogenesis but Not after Birth. *Developmental Cell*, *17*(6), 849–860. <http://doi.org/10.1016/j.devcel.2009.11.003>

- Sosa-Pineda, B., Chowdhury, K., Torres, M., Oliver, G., & Gruss, P. (1997). The Pax4 gene is essential for differentiation of insulin-producing beta cells in the mammalian pancreas. *Nature*, 386.
- Speer, M. Y., Yang, H.-Y., Brabb, T., Leaf, E., Look, A., Lin, W.-L., et al. (2009). Smooth Muscle Cells Give Rise to Osteochondrogenic Precursors and Chondrocytes in Calcifying Arteries. *Circulation Research*, 104(6), 733–741. <http://doi.org/10.1161/CIRCRESAHA.108.183053>
- Spencer, W. C., & Deneris, E. S. (2017). Regulatory Mechanisms Controlling Maturation of Serotonin Neuron Identity and Function. *Frontiers in Cellular Neuroscience*, 11, 302. <http://doi.org/10.3389/fncel.2017.00215>
- Stanescu, D. E., Yu, R., Won, K.-J., & Stoffers, D. A. (2017). Single Cell Analysis: Single cell transcriptomic profiling of mouse pancreatic progenitors. *Physiological Genomics*, 49(2), 105–114. <http://doi.org/10.1152/physiolgenomics.00114.2016>
- Strobel, O., Dor, Y., Alsina, J., Stirman, A., Lauwers, G., Trainor, A., et al. (2007). In Vivo Lineage Tracing Defines the Role of Acinar-to-Ductal Transdifferentiation in Inflammatory Ductal Metaplasia. *Gastroenterology*, 133(6), 1999–2009. <http://doi.org/10.1053/j.gastro.2007.09.009>
- Su, K. H., Cuthbertson, C., & Christophi, P. C. (2006). Review of experimental animal models of acute pancreatitis. *HPB : the Official Journal of the International Hepato Pancreato Biliary Association*, 8(4), 264–286. <http://doi.org/10.1080/13651820500467358>
- Sugiyama, T., Rodriguez, R. T., McLean, G. W., & Kim, S. K. (2007). Conserved markers of fetal pancreatic epithelium permit prospective isolation of islet progenitor cells by FACS. *Proceedings of the National Academy of Sciences*, 104(1), 175–180. <http://doi.org/10.1073/pnas.0609490104>
- Surendran, K. (2005). Wnt-Dependent β -Catenin Signaling Is Activated after Unilateral Ureteral Obstruction, and Recombinant Secreted Frizzled-Related Protein 4 Alters the Progression of Renal Fibrosis. *Journal of the American Society of Nephrology*, 16(8), 2373–2384. <http://doi.org/10.1681/ASN.2004110949>
- Sussel, L., Kalamaras, J., Hartigan-O'Connor, D. J., Meneses, J. J., Pedersen, R. A., Rubenstein, J. L., & German, M. S. (1998). Mice lacking the homeodomain transcription factor Nkx2.2 have diabetes due to arrested differentiation of pancreatic beta cells. *Development (Cambridge, England)*, 125(12), 2213–2221.
- Sylvestersen, K. B., Herrera, P. L., Serup, P., & Rescan, C. (2011). Fgf9 signalling stimulates Sprad and Sprouty expression in embryonic mouse pancreas mesenchyme. *Gene Expression Patterns*, 11(1-2), 105–111. <http://doi.org/10.1016/j.gep.2010.10.001>
- Talchai, C., Xuan, S., Lin, H. V., Sussel, L., & Accili, D. (2012). Pancreatic β Cell Dedifferentiation as a Mechanism of Diabetic β Cell Failure. *Cell*, 150(6), 1223–1234.
- Tremblay, K. D. (2010). Formation of the Murine Endoderm: Lessons from the Mouse, Frog, Fish, and Chick. *Progress in Molecular Biology and Translational Science*, 96, 1–34. <http://doi.org/10.1016/B978-0-12-381280-3.00001-4>
- Tusi, B. K., Wolock, S. L., Weinreb, C., Hwang, Y., Hidalgo, D., Zilionis, R., et al. (2018). Population snapshots predict early haematopoietic and erythroid hierarchies. *Nature Publishing Group*, 555(7694), 54–60. <http://doi.org/10.1038/nature25741>
- Upchurch, B. H., Aponte, G. W., & Leiter, A. B. (1994). Expression of peptide YY in all four islet cell types in the developing mouse pancreas suggests a common peptide YY-producing progenitor. *Development (Cambridge, England)*, 120(2), 245–252.

- Urbaschek, R., McCuskey, R. S., Rudi, V., Becker, K. P., Stickel, F., Urbaschek, B., & Seitz, H. K. (2001). Endotoxin, Endotoxin-Neutralizing-Capacity, sCD14, sICAM-1, and Cytokines in Patients With Various Degrees of Alcoholic Liver Disease. *Alcoholism: Clinical and Experimental Research*, 25(2), 261–268. <http://doi.org/10.1111/j.1530-0277.2001.tb02207.x>
- Valle, M. T., Degl'Innocenti, M. L., Bertelli, R., Facchetti, P., Perfumo, F., Fenoglio, D., et al. (1995). Antigen-presenting function of human peritoneum mesothelial cells. *Clinical and Experimental Immunology*, 101(1), 172–176.
- van den Brink, S. C., Sage, F., Vértesy, Á., Spanjaard, B., Peterson-Maduro, J., Baron, C. S., et al. (2017). Single-cell sequencing reveals dissociation-induced gene expression in tissue subpopulations. *Nature Methods*, 14(10), 935–936. <http://doi.org/10.1038/nmeth.4437>
- Van Keymeulen, A., Mascré, G., Youseff, K. K., Harel, I., Michaux, C., De Geest, N., et al. (2009). Epidermal progenitors give rise to Merkel cells during embryonic development and adult homeostasis. *The Journal of Cell Biology*, 187(1), 91–100. <http://doi.org/10.1083/jcb.200907080>
- Villasenor, A., Chong, D. C., & Cleaver, O. (2008). Biphasic Ngn3 expression in the developing pancreas. *Developmental Dynamics*, 237(11), 3270–3279. <http://doi.org/10.1002/dvdy.21740>
- Vonlaufen, A., Xu, Z., Daniel, B., Kumar, R. K., Pirola, R., Wilson, J., & Apte, M. V. (2007). Bacterial Endotoxin: A Trigger Factor for Alcoholic Pancreatitis? Evidence From a Novel, Physiologically Relevant Animal Model. *Gastroenterology*, 133(4), 1293–1303. <http://doi.org/10.1053/j.gastro.2007.06.062>
- Wang, F., Flanagan, J., Su, N., Wang, L.-C., Bui, S., Nielson, A., et al. (2012). A Novel *In Situ* RNA Analysis Platform for Formalin-Fixed, Paraffin-Embedded Tissues. *The Journal of Molecular Diagnostics*, 14(1), 22–29. <http://doi.org/10.1016/j.jmoldx.2011.08.002>
- Wang, J., Karra, R., Dickson, A. L., & Poss, K. D. (2013). Fibronectin is deposited by injury-activated epicardial cells and is necessary for zebrafish heart regeneration. *Developmental Biology*, 382(2), 427–435. <http://doi.org/10.1016/j.ydbio.2013.08.012>
- Wang, L.-L., Gu, H., Fan, Y., Zhang, Y., Wu, D., Miao, J.-N., et al. (n.d.). Up-regulated FHL1 Expression Maybe Involved in the Prognosis of Hirschsprung's Disease. *International Journal of Medical Sciences*, 11(3), 262–267. <http://doi.org/10.7150/ijms.7287>
- Wang, Z., York, N. W., Nichols, C. G., & Remedi, M. S. (2014). Pancreatic β Cell Dedifferentiation in Diabetes and Redifferentiation following Insulin Therapy. *Cell Metabolism*, 19(5), 872–882. <http://doi.org/10.1016/j.cmet.2014.03.010>
- Watari, N., Hotta, Y., & Mabuchi, Y. (1982). Morphological studies on a vitamin A-storing cell and its complex with macrophage observed in mouse pancreatic tissues following excess vitamin A administration. *Okajimas Folia Anatomica Japonica*, 58(4-6), 837–858.
- Weaver, M., Batts, L., & Hogan, B. L. M. (2003). Tissue interactions pattern the mesenchyme of the embryonic mouse lung. *Developmental Biology*, 258(1), 169–184. [http://doi.org/10.1016/S0012-1606\(03\)00117-9](http://doi.org/10.1016/S0012-1606(03)00117-9)
- Weinreb, C., Wolock, S., & Klein, A. M. (2018). SPRING: a kinetic interface for visualizing high dimensional single-cell expression data. *Bioinformatics*, 34(7), 1246–1248. <http://doi.org/10.1093/bioinformatics/btx792>
- Weinstein, D. C., Ruiz i Altaba, A., Chen, W. S., Hoodless, P., Prezioso, V. R., Jessell, T. M., & Darnell, J. E., Jr. (1994). The winged-helix transcription factor HNF-3 β is required for notochord development in the mouse embryo. *Cell*, 78(4), 575–588. [http://doi.org/10.1016/0092-8674\(94\)90523-1](http://doi.org/10.1016/0092-8674(94)90523-1)

- Wessels, A., van den Hoff, M. J. B., Adamo, R. F., Phelps, A. L., Lockhart, M. M., Sauls, K., et al. (2012). Epicardially derived fibroblasts preferentially contribute to the parietal leaflets of the atrioventricular valves in the murine heart. *Developmental Biology*, *366*(2), 111–124. <http://doi.org/10.1016/j.ydbio.2012.04.020>
- Whitcomb, D. C., Gorry, M. C., Preston, R. A., Furey, W., Sossenheimer, M. J., Ulrich, C. D., et al. (1996). Hereditary pancreatitis is caused by a mutation in the cationic trypsinogen gene. *Nature Genetics*, *14*(2), 141–145.
- White, A. C., Lavine, K. J., & Ornitz, D. M. (2007). FGF9 and SHH regulate mesenchymal Vegfa expression and development of the pulmonary capillary network. *Development (Cambridge, England)*, *134*(20), 3743–3752. <http://doi.org/10.1242/dev.004879>
- White, A. C., Xu, J., Yin, Y., Smith, C., Schmid, G., & Ornitz, D. M. (2006). FGF9 and SHH signaling coordinate lung growth and development through regulation of distinct mesenchymal domains. *Development (Cambridge, England)*, *133*(8), 1507–1517. <http://doi.org/10.1242/dev.02313>
- White, P., May, C. L., Lamounier, R. N., Brestelli, J. E., & Kaestner, K. H. (2008). Defining Pancreatic Endocrine Precursors and Their Descendants. *Diabetes*, *57*(3), 654–668. <http://doi.org/10.2337/db07-1362>
- Wilm, B., Ipenberg, A., Hastie, N. D., Burch, J. B. E., & Bader, D. M. (2005). The serosal mesothelium is a major source of smooth muscle cells of the gut vasculature. *Development (Cambridge, England)*, *132*(23), 5317–5328. <http://doi.org/10.1242/dev.02141>
- Wilson, M. E., Scheel, D., & German, M. S. (2003). Gene expression cascades in pancreatic development. *Mechanisms of Development*, *120*(1), 65–80. [http://doi.org/10.1016/S0925-4773\(02\)00333-7](http://doi.org/10.1016/S0925-4773(02)00333-7)
- Winters, N. I., Thomason, R. T., & Bader, D. M. (2012). Identification of a novel developmental mechanism in the generation of mesothelia. *Development (Cambridge, England)*, *139*(16), 2926–2934. <http://doi.org/10.1242/dev.082396>
- Winters, N. I., Williams, A. M., & Bader, D. M. (2014). Resident progenitors, not exogenous migratory cells, generate the majority of visceral mesothelium in organogenesis. *Developmental Biology*, *391*(2), 125–132. <http://doi.org/10.1016/j.ydbio.2014.04.003>
- Winters, N., & Bader, D. (2013). Development of the Serosal Mesothelium. *Journal of Developmental Biology*, *1*(2), 64–81. <http://doi.org/10.3390/jdb1020064>
- Wyler, S. C., Spencer, W. C., Green, N. H., Rood, B. D., Crawford, L., Craige, C., et al. (2016). Pet-1 Switches Transcriptional Targets Postnatally to Regulate Maturation of Serotonin Neuron Excitability. *Journal of Neuroscience*, *36*(5), 1758–1774. <http://doi.org/10.1523/JNEUROSCI.3798-15.2016>
- Yadav, D., & Lowenfels, A. B. (2013). The Epidemiology of Pancreatitis and Pancreatic Cancer. *Gastroenterology*, *144*(6), 1252–1261. <http://doi.org/10.1053/j.gastro.2013.01.068>
- Yamaguchi, H., Kimura, T., Mimura, K., & Nawata, H. (1989). Activation of Proteases in Cerulein-Induced Pancreatitis. *Pancreas*, *4*(5), 565.
- Yáñez-Mó, M., Lara-Pezzi, E., Selgas, R., Ramírez-Huesca, M., Domínguez-Jiménez, C., Jiménez-Heffernan, J. A., et al. (2003). Peritoneal Dialysis and Epithelial-to-Mesenchymal Transition of Mesothelial Cells. *New England Journal of Medicine*, *348*(5), 403–413. <http://doi.org/10.1056/NEJMoa020809>
- Ye, F., Duvilli, B., & Scharfmann, R. (2005). Fibroblast growth factors 7 and 10 are expressed in the human embryonic pancreatic mesenchyme and promote the proliferation of embryonic

- pancreatic epithelial cells. *Diabetologia*, 48(2), 277–281. <http://doi.org/10.1007/s00125-004-1638-6>
- Yin, Y., Wang, F., & Ornitz, D. M. (2011). Mesothelial- and epithelial-derived FGF9 have distinct functions in the regulation of lung development. *Development (Cambridge, England)*, 138(15), 3169–3177. <http://doi.org/10.1242/dev.065110>
- Yoshitomi, H. (2004). Endothelial cell interactions initiate dorsal pancreas development by selectively inducing the transcription factor Ptf1a. *Development (Cambridge, England)*, 131(4), 807–817. <http://doi.org/10.1242/dev.00960>
- Yuan, G.-C., Cai, L., Elowitz, M., Enver, T., Fan, G., Guo, G., et al. (2017). Challenges and emerging directions in single-cell analysis. *Genome Biology*, 18(1), 84. <http://doi.org/10.1186/s13059-017-1218-y>
- Zang, G., Sandberg, M., Carlsson, P.-O., Welsh, N., Jansson, L., & Barbu, A. (2015). Activated pancreatic stellate cells can impair pancreatic islet function in mice. *Upsala Journal of Medical Sciences*, 120(3), 169–180. <http://doi.org/10.3109/03009734.2015.1032453>
- Zeng, C., Mulas, F., Sui, Y., Guan, T., Miller, N., Tan, Y., et al. (2017). Pseudotemporal Ordering of Single Cells Reveals Metabolic Control of Postnatal b Cell Proliferation. *Cell Metabolism*, 25(5), 1160–1175.e11. <http://doi.org/10.1016/j.cmet.2017.04.014>
- Zheng, G. X. Y., Terry, J. M., Belgrader, P., Ryvkin, P., Bent, Z. W., Wilson, R., et al. (2017). Massively parallel digital transcriptional profiling of single cells. *Nature Communications*, 8, 14049. <http://doi.org/10.1038/ncomms14049>
- Zhong, B., Zhou, Q., Toivola, D. M., Tao, G.-Z., Resurreccion, E. Z., & Omary, M. B. (2004). Organ-specific stress induces mouse pancreatic keratin overexpression in association with NF-κB activation. *Journal of Cell Science*, 117(9), 1709–1719. <http://doi.org/10.1242/jcs.01016>
- Zhou, Q., Law, A. C., Rajagopal, J., Anderson, W. J., Gray, P. A., & Melton, D. A. (2007). A Multipotent Progenitor Domain Guides Pancreatic Organogenesis. *Developmental Cell*, 13(1), 103–114. <http://doi.org/10.1016/j.devcel.2007.06.001>
- Zhu, S., Russ, H. A., Wang, X., Zhang, M., Ma, T., Xu, T., et al. (2016). Human pancreatic beta-like cells converted from fibroblasts. *Nature Communications*, 7, 10080. <http://doi.org/10.1038/ncomms10080>
- Zimmermann, A., Gloor, B., Kappeler, A., Uhl, W., Friess, H., & Büchler, M. W. (2002). Pancreatic stellate cells contribute to regeneration early after acute necrotising pancreatitis in humans. *Gut*, 51(4), 574–578.

Publishing Agreement

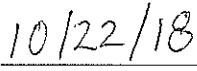
It is the policy of the University to encourage the distribution of all theses, dissertations, and manuscripts. Copies of all UCSF theses, dissertations, and manuscripts will be routed to the library via the Graduate Division. The library will make all theses, dissertations, and manuscripts accessible to the public and will preserve these to the best of their abilities, in perpetuity.

Please sign the following statement:

I hereby grant permission to the Graduate Division of the University of California, San Francisco to release copies of my thesis, dissertation, or manuscript to the Campus Library to provide access and preservation, in whole or in part, in perpetuity.



Author Signature



Date